Stellingen

behorend bij het proefschrift *Piezo-driven stages for nanopositioning with extreme stability*

1 Het benoemen van het inertial sliding mechanisme met de term stick-slip mechanisme wekt ten onrechte de suggestie dat de werking van dit mechanisme gebaseerd zou zijn op een verschil in de statische en de dynamische wrijvingskracht.

2 Actieve trillingsisolatie in het nanometergebied is niet mogelijk met behulp van praktisch uitvoerbare capacitieve sensoren. (n.a.v. dit proefschrift)

3 Bij het streven naar een snelle beeldstabilisatie in een transmissie electronenmicroscoop vormt de interne preparaatdrift een belangrijke belemmering. (n.a.v. dit proefschrift)

4 De relatief lage contactstijfheid tussen een object en zijn lagering vormt een obstakel in het streven naar een hoge mechanische resonantiefrequentie. (dit proefschrift)

5 Voor het zinvol doen van onderzoek in het (sub)nanometergebied zijn geen bijzondere of extreem nauwkeurige fabricagetechnieken vereist. (dit proefschrift)

6 Geadsorbeerde waterlagen hebben grote invloed op de positiestabiliteit van objecten in het nanometergebied, wanneer deze worden ondersteund door een relatief 'groot' schijnbaar contactoppervlak (H. van der Wulp et al., J. of Vac. Sci & Technol. B 15).

7 Sensoren zullen de meest kritische componenten vormen in de verbrandingsmotoren van de 21ste eeuw.

8 Mechatronisch opgeleide ingenieurs kunnen een spilfunctie vervullen bij concurrent engineering aangezien deze methode naast specialisten om personen met kundigheid op verschillende technische terreinen vraagt.

9 Sociaal-economische gezondheidsverschillen zijn niet noodzakelijkerwijs kleiner in landen met een traditie van egalitair sociaal-economisch beleid en gezondheidsbeleid (Cavelaars et al, J. Epidemiol. Community Health (in press)).

10 De waarde van een produkt wordt alleen bepaald door de eindgebruiker.

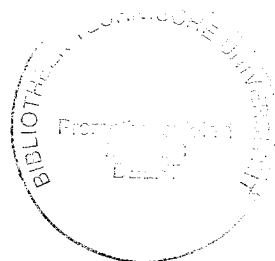# Piezo-driven stages for nanopositioning with extreme stability

theoretical aspects and practical design considerations

Piezo-driven stages for nanopositioning with extreme stability

theoretical aspects and practical design considerations

PROEFSCHRIFT

ter verkrijging van de graad van doctor

aan de Technische Universiteit Delft,

op gezag van de Rector Magnificus Prof.dr.ir. J. Blaauwendraad,

in het openbaar te verdedigen ten overstaan van een commissie,

door het College van Dekanen aangewezen,

op maandag 8 december 1997 te 16.00 uur

door Hendrik VAN DER WULP

werktuigbouwkundig ingenieur

geboren te Middelburg

Dit proefschrift is goedgekeurd door de promotor:
Prof.dr.ir. H.F. van Beek

Samenstelling promotiecommissie:

Rector Magnificus,	voorzitter
Prof.dr.ir. H.F. van Beek,	TU Delft, promotor
Prof.dr.ir. P. Kruit,	TU Delft
Prof.dr.ir. M.P. Koster,	U-Twente
Prof.dr. J.F. van der Veen,	U-Amsterdam
Prof.dr.ir. S. Radelaar,	TU Delft
Ir. P.V. Pistecky,	TU Delft
Dr. R. Fastenau,	Philips Electron Optics, Eindhoven

Table of contents

List of symbols

a	= capacitor electrode width	[m]
a	= radius of a (elliptical) contact area	[m]
$\hat{a}$	= amplitude of floor vibrations	[m]
A	= overlapping electrode area of a parallel plate capacitive transducer	[m^2]
A_a	= apparent contact area	[m^2]
A_r	= real contact area	[m^2]
b	= capacitor electrode length	[m]
b	= radius of a (elliptical) contact area	[m]
B	= magnetic field density	[T]
c	= damping constant	[N·s/m]
c	= specific heat	[J/kg·K]
C	= capacitance	[F]
C_0	= nominal capacitance	[F]
C_{ip}	= capacitance of an in-plane transducer	[F]
C_{pd}	= capacitance of a plate-distance transducer	[F]
C_p	= parasitic capacitance	[F]
C_r	= reference capacitance	[F]
C_x	= capacitance to be measured	[F]
d_0	= nominal plate distance between capacitor plates	[m]
d_{ij}	= piezoelectric charge constant	[m/V]
d_{in}	= inner diameter of a piezo tube	[m]
d_{out}	= outer diameter of a piezo tube	[m]
D	= dielectric displacement (amount of charge on a piezo per unit of area)	[C/m^2]

$D_{\dot{x}_r}$	= velocity deadband	[m/s]
e	= capacitor electrode width	[m]
E	= electric field strength	[V/m]
E	= modulus of elasticity	[N/m^2]
E_e	= equivalent modulus of elasticity	[N/m^2]
f	= frequency	[Hz]
f_0	= resonance frequency	[Hz]
F	= force	[N]
F_C	= Coulomb friction force	[N]
F_f	= friction force	[N]
$F_{f_{max}}$	= maximum friction force	[N]
F_g	= gravity force	[N]
F_L	= Lorentz force	[N]
F_n	= normal force	[N]
F_p	= preload force	[N]
F_t	= tangential force	[N]
g	= acceleration of the gravity field	[m/s^2]
G	= shear modulus of elasticity	[N/m^2]
h	= height	[m]
h_p	= desired piezo actuator position enforced by an electric field	[m]
H_V	= Vickers hardness	[HV]
I	= current	[A]
I_d	= detector current	[A]
k	= stiffness	[N/m]
k_c	= tangential contact stiffness	[N/m]
k_{epoxy}	= stiffness of an epoxy layer	[N/m]
k_p	= stiffness of a piezo actuator	[N/m]
k_s	= stiffness of a support	[N/m]
K	= heat transfer coefficient for conduction	[W/m^2·K]
K_{ij}^T	= relative permittivity or dielectric constant of a piezo ceramic at constant stress	[-]
l	= length of a conductor	[m]

L	= length of a piezo actuator	[m]
L_t	= length of a piezo tube	[m]
m_{eff}	= effective mass	[kg]
m_i	= impact mass	[kg]
m_p	= mass of a piezo	[kg]
m_s	= mass of a support	[kg]
m_t	= mass of a table	[kg]
P	= polarization of a piezoelectric ceramic	[C/m^2]
P_r	= remanent polarization of a piezoelectric ceramic	[C/m^2]
P_s	= saturation polarization of a piezoelectric ceramic	[C/m^2]
$\dot{Q}_c$	= conductive heat transfer rate	[W]
$\dot{Q}_{cg}$	= conductive heat transfer rate in a gas	[W]
$\dot{Q}_r$	= radiative heat transfer rate	[W]
$\dot{Q}_s$	= heat transfer rate due to sliding	[W]
R_0	= resistance representing dielectric loss	[Ω]
R_l	= resistance representing mechanical loss	[Ω]
R_a	= roughness	[m]
R_e	= equivalent radius of two bodies in contact	[m]
R_i	= parasitic resistances	[Ω]
s_{ij}	= mechanical compliance of a piezoelectric ceramic	[m^2/N]
s_t	= table step size	[m]
S	= strain of a piezoelectric ceramic	[-]
t	= thickness of a piezo actuator	[m]
t_i	= numerical integration step size	[s]
T	= applied stress	[N/m^2]
T_{high}	= highest temperature	[K]
T_{low}	= lowest temperature	[K]
U_0	= amplitude of a sine wave voltage	[V]
U_{out}^{dc}	= output voltage of a synchronous detector	[V]
U_p	= driving voltage of a piezo actuator	[V]
$U_{p_{min}}$	= minimum driving voltage over a piezo drive	[V]

V	= volume or occupied space	[m^3]
w	= width	[m]
x	= displacement	[m]
$\dot{x}_r$	= relative velocity	[m/s]
x_t	= table displacement in a direction perpendicular to the gravity field	[m]
z_p	= pole piece displacement	[m]
z_t	= table displacement in a direction parallel to the gravity field	[m]
α	= linear expansion coefficient	[K^{-1}]
α_i	= heat transfer coefficient for convection	[W/m^2·K]
β	= relative damping	[-]
β	= molecular accomodation factor	[-]
δ	= approach of two bodies in contact	[m]
δ_i	= initial displacent due to gravity forces	[m]
δ_t	= tangential deformation of a contact area	[m]
ε	= dielectric permittivity	[F/m]
ε	= position error	[m]
ε_0	= permittivity of vacuum	[F/m]
ε_r	= relative permittivity or dielectric constant	[-]
ε_r'	= real part of permittivity which represents storage	[-]
ε_r''	= imaginairy part of permittivity which represents loss	[-]
ϕ	= parasitic rotation	[rad]
λ	= conductivity	[W/m·K]
Λ	= free molecular thermal conductivity coefficient	[W/m^2]/[K·Pa]
μ_d	= coefficient of dynamic friction	[-]
μ_r	= relative permeability	[-]
μ_{st}	= coefficient of static friction	[-]
v	= Poisson constant	[-]
ρ	= density	[kg/m^3]
σ_e	= yield stress	[N/m^2]
$tan\,\delta$	= loss angle of a material	[-]

1 Introduction

1.1 Nanopositioning

As a result of miniaturization trends in fundamental and applied research, in technology, in product design and in fabrication processes, the need for sophisticated devices for controlled motion at the (sub)micrometer level and beyond is high. Such devices can be found in high quality consumer products (e.g. compact disc players and data storage facilities), in production machines (e.g. wafer steppers, diamond turning machines), in robots and instruments for biological, physical and chemical research (e.g. high resolution microscopes), and various others [1,2,3,4,5]. The requirements regarding range of operation, positioning resolution, velocity, maximum accelerations, the number of degrees of freedom, environmental conditions, and price vary substantially between these positioning devices.

A particular class of positioning devices can, for instance, be found in high resolution microscopes such as (calibrated) scanning probe microscopes (SPM) and electron microscopes (EM). These devices can be called *nanopositioning* devices. As high resolution microscopes offer nanometer and subnanometer (atomic) image resolution, nanopositioning devices are used to position the specimen relative to the electron beam or mechanical probe with very high accuracy and stability.

In this thesis, nanopositioning is defined as moving and positioning objects in one or several degrees of freedom with nanometer displacement resolution and nanometer positioning repeatability with stroke to resolution ratios of 10^5 up to 10^6. Nanopositioning devices as meant here differ from other classes of positioning devices by their compact configuration, by their maximum stroke which is in the order of millimeters, by the (sometimes large) number of degrees of freedom, and by the fact that they are almost always driven by high electric fields only. Besides high resolution positioning, some applications ask for nanometer position *repeatability* of the object that must be positioned relative to a reference. In order to achieve this, the object's position must normally be accurately controlled. An additional requirement often made to these positioning devices is position *stability* of the object relative to a reference. This especially applies to transmission electron microscopes (TEM) in which the specimen's stability relative to the objective lens determines, among other things, the image stability and the image resolution.

The field of nanopositioning is relatively new. Important progress was made as a result of the invention of the SPM by Binnig and Rohrer [6] and by the development of different *piezoelectric*

drives [7,8]. Nanopositioning devices ask for a different approach in construction, material selection, general control, and treatment in order to achieve the required nanometer positioning repeatability and mechanical stability at the picometer level, as compared to the class of devices that require (sub)micrometer positioning repeatability and stability.

1.2   Goal and approach of this research

This research was conducted at the Laboratory for Micro Engineering, Faculty of Mechanical Engineering and Marine Technology of the Delft University of Technology. At the Laboratory, it was the first project in the complex field of nanopositioning. Throughout this research, the specimen stage in a TEM was used as an important example of a nanopositioning device. The wish of both the Research Group for Particle Optics of the Delft University of Technology and of the Philips Electron Optics department for improved positioning repeatability and position stability of the specimen relative to the objective lens in a transmission electron microscope was the starting point for this research. The device that positions the specimen, i.e. the specimen stage or goniometer stage in combination with a specimen holder, plays a key role with respect to this positioning repeatability and position stability.

The aims of this research were formulated in close co-operation between the three groups mentioned. The first aim was to investigate a new concept of the specimen positioning device in a transmission electron microscope as an alternative for the conventional side-entry goniometer stage. At the moment, the side-entry goniometer stage is the widest applied device for specimen positioning in a TEM. It is already a very sophisticated positioning device which enables specimen motion in up to five degrees of freedom over large strokes in combination with high level specimen stability after positioning. However, demands for higher specimen positioning repeatability and position stability require improvement of the goniometer stage. Unfortunately, further improvement of the side-entry goniometer stage performance is extremely difficult to achieve while maintaining the side-entry concept and maintaining specimen positioning in five degrees of freedom. This can be explained by the complex configuration of the side-entry goniometer. It only allows indirect position measurement of the specimen relative to the objective lens resulting in a low positioning repeatability. Also, the design of the specimen holder limits its resonance frequency and hence its stability relative to the objective lens. Therefore, a different approach for specimen positioning was studied which may be an alternative for some applications of the side-entry goniometer stage. This approach is called the *nano stage concept*.

Depending on the application, the nano stage must fulfill the following tasks or functions:

- translation of the specimen over millimeter strokes with nanometer positioning repeatability, perpendicular and parallel to the gravity field,
- tilt of the specimen over almost 180° with micro radian positioning repeatability[1], and
- contribute to the specimen stability relative to the objective lens.

---

[1] Specimen tilt is defined as rotation about an axis perpendicular to the microscope's electron beam. Specimen rotation is defined as rotation about an axis parallel to the electron beam. Specimen rotation was not considered during this research.

The nano stage has to operate inside the small vacuum chamber of a TEM. Therefore, it must be high vacuum (HV) or even ultrahigh vacuum (UHV) compatible, it must not cause disturbance of the electron beam or the magnetic lenses, and it must not be influenced by the high magnetic fields applied in a TEM.

The second aim was to gain knowledge which can support the design of nano stages for application as a specimen positioning device in a TEM or for application in other types of microscopes, in straightness motion systems or in robotics.

The strict demands made on the application of a nano stage as a specimen positioning device in a TEM substantially limits design freedom. For instance, the number and type of actuators and sensors which can be used in a TEM nano stage is small. On the other hand, the characteristic properties, the advantages and disadvantages of suitable actuators and sensors should be extensively discussed in order to be able to design for maximum performance. Due to the complexity of the field of nanopositioning, a strong synergy between theoretical analysis and practical experience was required. Practical experience was gained by the design and realization of test setups.

1.3   The transmission electron microscope

The most common instrument for studying small specimen parts is an optical microscope. Unfortunately, its spatial resolution is limited by the wavelength of the light source used. As a result of an enormous theoretical and experimental effort in the field of quantum mechanics since the end of the 19th century, De Broglie [9] proposed in 1924 that, analogous to the dual nature of light, particles such as electrons have the nature of a wave as well. This means that electrons obey diffraction laws similar to light. As electrons are charged particles, they can be deflected by means of a magnetic or electrostatic field. It was Busch [10] who used this fact to build the first magnetic electron lens. In 1931, Knoll and Ruska [11] built the first magnetic lens electron microscope. This was a break-through. Since electrons can have wavelengths in the order of a few
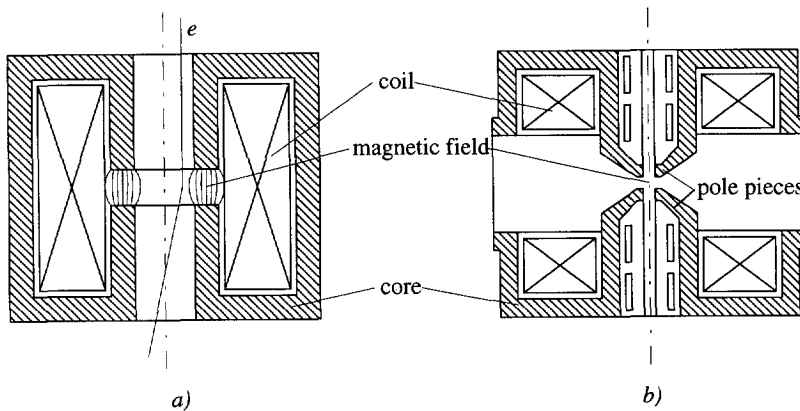
Fig. 1.1   a) An electromagnetic lens consists of a coil and a soft iron core which has a small gap. In this gap a high magnetic field is obtained. b) Through the years, the specially shaped parts of the core near the gap developed into the special shaped lens pole pieces.

picometers, depending on their acceleration voltage, the resolution of this electron microscope was far better than the resolution of any optical microscope.

An electromagnetic lens consists of a coil which is surrounded by a soft iron core, having a small gap (see figure 1.1a). In this gap a strong magnetic field is obtained. Through the years, the ends of the cores were given a special shape in order to obtain the optimum shape of the magnetic field in the gap (see figure 1.1b). These core ends are called the lens pole pieces. In a TEM, the specimen is placed in between the pole pieces of the objective lens.

A major advantage of electromagnetic lenses is that its focal length can be adjusted by changing the current through the coil(s) of the lens. This makes mechanical lens adjustment superfluous. Like common lenses for visible light, magnetic lenses cause the usual aberrations. Through the years, an enormous effort was made to minimize these aberrations in order to gain image resolution. This was, among other things, achieved by maximizing the magnetic field strength in the lens. Since the magnetic field strength is inversely proportional to the gap width between the pole pieces, the gap width was made small. As a result, there is extremely little space for specimen manipulation.

Nowadays, different companies offer a variety of transmission electron microscopes enabling subnanometer image resolution. Electron energies range from 0.08 up to 1.2 MeV and magnifications up to $1.5 \cdot 10^6$ are achieved. Figure 1.2 shows a cross section of a modern high resolution TEM [12]. The microscope consists of a long column, which is isolated from the floor by a vibration isolation system. The column consists of an electron gun, a number of lenses, a goniometer stage including a specimen holder, a set of apertures, an image or fluorescent screen, and a CCD camera for image recording. Besides the specimen holder, some other instruments are present in the proximity of the objective lens pole pieces. Depending on the application, these are: an aperture holder, an X-ray detector, and detectors for secondary and backscattered electrons. In case of *in-situ* experiments, the diversity in the composition of instruments near the specimen becomes even larger [13].

An important condition for the electrons to reach the specimen and to reach the fluorescent screen is to avoid electron collisions with particles in the electron beam

Fig. 1.2   Cross section of a modern JEOL TEM 1010.

path. Therefore, electron microscopes can not work without a vacuum. In fact, ultrahigh vacuum ($<10^{-5}$ Pa) is extremely important with regard to a low specimen contamination.

The specimen changes either the amplitude or the phase of the incoming electron waves, thus allowing for image formation gathering about the specimen. As the electron interaction with atoms in the specimen is strong, the specimen for transmission electron microscopy must be thin in order to achieve transmission of most electrons through the specimen. The specimen thickness t ranges from 5 to 500 nm. Due to the interaction with the specimen, electrons loose about 0.02% of their energy on average [14].

The most critical mechanical part of a TEM is undoubtedly the specimen stage. Features such as repeatability of translational positioning and tilting, and absence of drift and vibrations must be achieved if the ultimate performance of the microscope is not to be compromised. The maximum achievable image resolution is the most important specification of a TEM. Besides that this resolution is limited by the lens aberrations and the electron wavelength, it also largely depends on the drift and the vibration amplitude of the specimen relative to the lower pole piece of the objective lens, because the lower part of the objective lens creates the first specimen image. In that respect, the requirement on the mutual position stability of the objective lens and the first projector lens is less strict. Compared to the requirement on the specimen stability, the require-ment on the latter stability is relaxed by the magnification M of the objective lens. Generally, the magnification of an electromagnetic lens is about 50. As a result, the lower pole piece is the only correct position reference for the specimen.

In order to obtain atomic resolution, the vibration amplitude of the specimen holder must be smaller than 0.1 nm and the drift rate must be low, normally smaller than a few hundred pico-meters per minute. Often, the combination of the drift rate and the vibration amplitude is sum-marized in one characteristic term: *stability*.

1.4   Existing specimen stage concepts

1.4.1   Introduction

In a modern TEM, a large number of experiments and observations can be carried out, each type of experiment requiring a different range of specimen treatments and manipulations. Hence, a number of different specimen stages and specimen holders were developed, each one designed for a special task, like translating, rotating or tilting of a specimen, but also for heating, cooling and stretching specimens [14,15,16,17]. During the first three decades after the invention of the electron microscope, its resolution increased continuously. By 1960, the first prototypes of high resolution electron microscopes (resolution ≤ 1 nm) were developed [18]. At the same time, the necessity for accurate specimen positioning, tilting in particular, became clear and a start was made on the development of a goniometer stage. With the improvement of the resolution, the requirements on the specimen (holder) stability increased accordingly.

Traditionally, two types of goniometer stages can be distinguished: the top-entry and the side-entry goniometer stage. Both goniometer stages have advantages and disadvantages with regard

to specimen manipulation and treatment, which can strongly differ with the application. With regard to future developments (this research), it is useful to discuss the general advantages and disadvantages of the top-entry and the side-entry goniometer stages.

1.4.2 The top-entry goniometer stage

Figure 1.3 shows the concept of the top-entry goniometer stage. The specimen stage is mounted on top of the upper pole piece of the objective lens. The specimen is loaded by a special transfer mechanism that places the specimen via the small bore onto the specimen holder. The specimen stage can be moved in the X and the Y direction; the specimen holder enables (double) specimen tilt. Top-entry stages do often not facilitate specimen motion in the Z direction.

The major advantage of the top-entry concept is its high intrinsic stability. This results from its compact configuration and the possibility to decouple the stage from its drivers [19]. Also, in the top-entry concept there is a lot of space available on top of the objective lens for specimen treatment chambers [20]. Disadvantages of the top-entry concept are the lack of eucentric tilting[2], the complex specimen insertion system, and the limited displacements in the X and Y direction ($\pm$ 2 mm). A large number of different types of top-entry stages was described by Glauert [14].
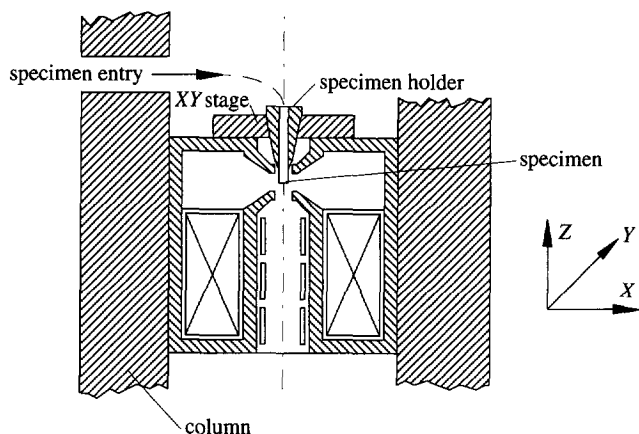
Fig. 1.3 *The existing concept of a top-entry goniometer stage. The specimen is inserted on the top-side of the specimen holder. The specimen stage is placed on top of the upper pole piece and enables specimen translations in the X and the Y direction. The specimen holder enables double tilt.*

1.4.3 The side-entry goniometer stage

A side-entry goniometer is a relatively large device consisting of several drives. It is mounted on the outside of the microscope column (see figure 1.4) [21]. A specimen holder is inserted from the side. One or several specimens are placed at the tip of the specimen holder. The specimen

---

[2] Eucentric specimen tilt means that the specimen remains focussed when it is tilted. Eucentric tilting is discussed in chapter 7.

holder is positioned in the center of the vacuum chamber in between the objective lens pole pieces. The typical design of the side-entry goniometer stage/specimen holder configuration results from the requirements of having to have to position the specimen in up to five degrees of freedom given the small gap between both pole pieces.
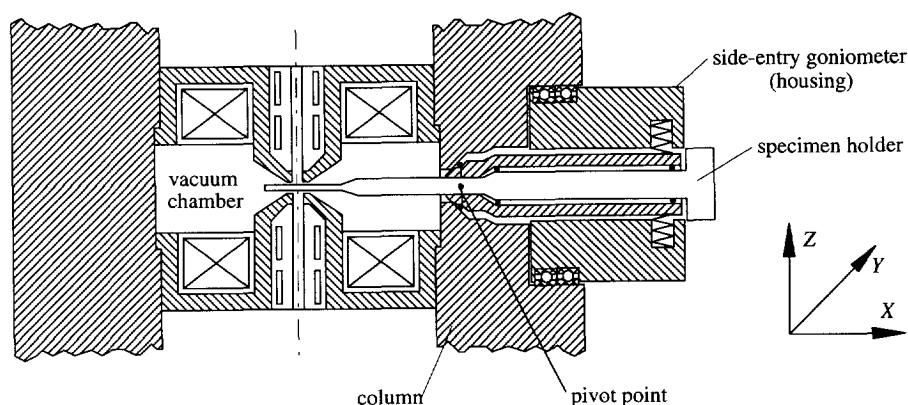
Fig. 1.4   The existing concept of the side-entry goniometer stage and the specimen holder.

Nowadays, side-entry goniometer stages enable computer controlled five degrees of freedom positioning of the specimen (holder) with 0.5 mm stroke in the Z direction up to 4 mm in the XY plane and tilts about the X and Y axis ranging from 10° up to 60°. The combination of such large strokes and nanometer positioning resolutions resulted in complex and large positioning devices. The specimen holder is supported by a V-shaped groove in the goniometer stage, allowing translation along the X axis. Specimen translations in the Y and the Z direction are achieved by rotation of the specimen holder around a pivot point, tens of millimeters away from the specimen. Eucentric tilt about the X axis (α) is achieved by tilting the whole translation system relative to the microscope wall. Specimen tilt about the Y axis can be achieved by means of a special double tilt holder [19].

The position of the specimen is measured by various transducers. Directly or indirectly, these transducers measure the specimen holder position relative to its housing, not to the lower pole piece of the objective lens. This means that the specimen position relative to the lower pole piece is measured through a large mechanical loop consisting of a number of components. It is due to this large measurement loop, due to the large dimensions of the specimen holder and the goniometer stage, and due to the direct connection of the specimen holder with the environment that high positioning accuracy and position stability of the specimen are not (always) obtained [22]. They conflict with the required specimen strokes and with the required number of degrees of freedom. At the moment, specimen positioning repeatability is in the order of 500 nm and the specimen drift rate directly after moving the specimen to a new position is typical tenths of nanometers per minute [23]. The specimen vibration amplitude can be in the order of 0.1 nm, depending on the quality of the vibration isolation. In the near future, specimen position repeatability and stability must be improved.

1.4.4   Concluding remarks and future requirements

Compared to top-entry goniometer stages, side-entry goniometer stages have a wider range of application due to their positioning capabilities. On the other hand, top-entry goniometer stages generally enable higher specimen stability. The nano stage concept may become a special designed specimen stage that is advantageous if specimen position stability at the nanometer level and positioning repeatability at the nanometer level in combination with large strokes in several degrees of freedom must be obtained. In that case, it may become an alternative for some applications of top-entry and side-entry goniometer stages.

As an example, the demands made by the Philips Electron Optics department on its next generation specimen stages are listed below in table 1.1 [23]. Implicitly, future specimen stages should meet these requirements.

	X,Y translation	Z translation	α, β tilt	
stroke	± 1.5	± 0.5	± 80	[mm] or [°]
repeatability	50	100	0.02	[nm] or [°]
max. velocity	0.2	0.05	10	[mm/sec.] or [°/sec]
min. velocity	0.5	1	0.1	[nm/sec.] or [°/sec]
drift rate[1]	0.1	0.2	[2]	[nm/min.]
vibration amplitude	0.01	0.02	[2]	[nm]

[1] Values should be reached within 10 seconds after positioning.
[2] Tilt axis stability is defined as 100 nm at 45° tilt.

Table 1.1   Requirements on future specimen stages for Philips TEMs.

1.5   Improved specimen positioning and stability

1.5.1   Introduction

As there are many applications of the TEM, the range of specimen positioning and stability requirements for these applications is accordingly large. Depending on the application, there will be different solutions to improve specimen positioning repeatability and position stability. For some applications, the solution may be to use the nano stage concept. For other applications, solutions may be to use a side-entry or top-entry goniometer and to use the image position information available from the CCD camera or to use the position information of additional position transducers in the proximity of the specimen and the lower pole piece.

1.5.2   Feedback of image information

A very direct solution to obtain nanometer positioning repeatability and/or subnanometer specimen stability is to use the momentary specimen position information available from the CCD camera in a feedback loop [22]. Unfortunately, this method has severe practical handicaps. For

some TEM experiments, the CCD camera is not available for position control. Apart from this, the bandwidth of this image feedback loop is limited to about 1 Hz as a result of the necessary complex cross correlation calculations between images. Consequently, the CCD camera resolution is limited by specimen vibrations which limit the accuracy of this feedback method. This means that image feedback can only be used for the compensation of quasi-static changes in the specimen position in the plane perpendicular to the optical axis and could possibly also be used to increase the positioning repeatability of the specimen within the field of view of the CCD camera. At the moment, this feedback method is not a general solution to increase specimen stability. However, with increasing computational power, this method may suit a customer microscope in the future.

1.5.3 Additional transducers

A second solution to increase specimen positioning repeatability is to add position transducers which are placed inside the vacuum chamber and to use the lower pole piece as their position reference. The specimen position should be measured as close as possible to the electron beam illumination spot on the specimen. Unfortunately, this method has certain limitations. As far as specimen positioning repeatability is concerned, it is extremely difficult to measure the specimen position with nanometer resolution over large strokes in up to five degrees of freedom within the limited space between the pole pieces. Therefore, this method can only be used in applications where the number of degrees of freedom or the stroke of the specimen (holder) in some degrees of freedom (especially tilts) can be reduced. If specimen stability is to be obtained by stability control, position transducers with picometer displacement resolution are required. There are very few types of transducers which have such resolutions and can be used in the vacuum chamber of the TEM. At the moment, capacitive displacement transducers are the only practical option. A major disadvantage of high resolution capacitive displacement transducers is that they would have to be mounted very close to the specimen holder, in that way drastically limiting the specimen holder stroke in most of its degrees of freedom. Consequently, a combination of large specimen holder strokes and controlled stability is, in principle, only possible for one or two translations. In that case, the performance of the transducer must be extremely high: picometer resolution over millimeter strokes and a sufficiently high bandwidth to measure specimen holder vibrations. Furthermore, the transducer must also be small to fit in the limited space near the pole piece.

An alternative way to obtain nanometer positioning repeatability and/or to obtain subnanometer specimen stability in several degrees of freedom is by stacking position transducers on a moveable position reference. This reference should be placed on the lower pole piece and should follow the specimen holder displacements. In this way, the stroke of the specimen holder is not limited by the presence of transducers. Such a configuration may be suitable for stability control if the stability of the tracking system is sufficient. However, the space available for such a configuration is limited. Furthermore, it does not guarantee full specimen holder motion in up to five degrees of freedom.

It should be noted from the former overview that additional position transducers in the proximity of the specimen holder of traditional goniometer stages may improve specimen positioning in one or two degrees of freedom or may improve specimen position stability in up to six degrees of

freedom. However, a combination of a high level of positioning repeatability and position sta-
bility of the specimen in up to five degrees of freedom while maintaining large specimen (holder)
strokes is not possible by means of this method.

1.5.4   A new concept: the nano stage

A way to improve specimen positioning repeatability and position stability in as many as possible
degrees of freedom is by developing a completely different specimen holder concept: the nano
stage. Due to its compact design, the nano stage can be placed inside the vacuum chamber of the
TEM. The concept is shown in figure 1.5 and it is based on the following principles:

- the nano stage is attached to the pole piece of the lower objective lens,
- the lower pole piece is used as the position reference of the specimen holder (or table),
- position transducers assure specimen holder positioning repeatability at the nanometer
  level,
- the nano stage has no mechanical connections to the outside of the vacuum chamber, and
- the specimen position stability can be obtained by stability control by means of position
  transducers with high resolution or by relying on the high intrinsic stability of the nano
  stage which results from its compact design.

Figure 1.5 shows the application of a nano stage in a TEM. A nano stage consists of five main
element groups: a position reference frame, several actuators, support elements, a table that has
to be moved, and several position transducers which measure the table's position relative to the
reference frame. In case of positioning in more than one degree of freedom, it may be necessary
to stack an additional set of actuators, support elements, position transducers, and a table on top
of the first table. The upper table in the stack at the same time is the specimen holder. The com-
bination of a table and the actuator(s), and the support element(s) which support the table is
called a *drive*.
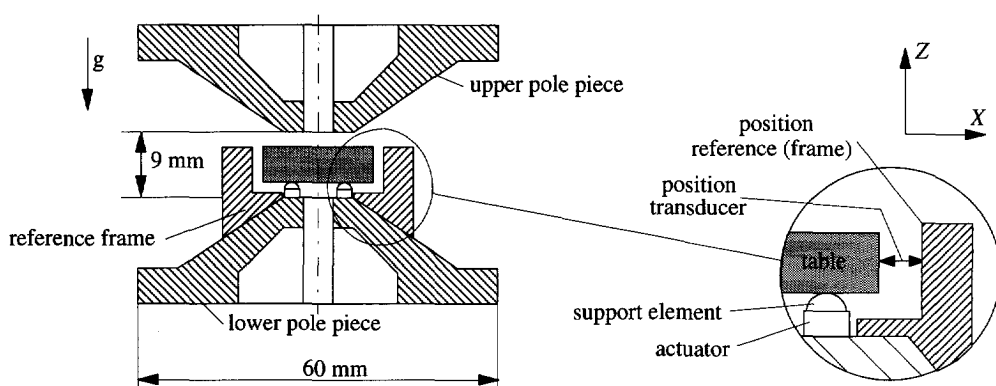
*Fig. 1.5   The nano stage concept in a TEM. The nano stage dimensions are such that the nano stage can
be placed between the pole pieces of the objective lens. A nano stage consists of five main ele-
ment groups: a position reference frame, one or several actuators, support elements, a table
that has to be moved, and a few position transducers.*

An advantage of the nano stage concept over the side-entry goniometer stage is the considerably smaller measurement loop between the specimen and the lower pole piece. A second advantage is that the small dimensions of the nano stage automatically decrease its sensitivity to internal and external disturbances resulting in a high intrinsic stability of the nano stage table. Intrinsic stability is the maximum stability that can be obtained without applying feedback control. An advantage of a high intrinsic stability of the nano stage is that feedback control of the table position may become superfluous. This implies that the stroke and the number of degrees of freedom of the nano stage table will not be limited by such a control. Also, by applying suitable drive mechanisms, the table strokes can be sufficiently large and positioning in up to five degrees of freedom becomes possible. Consequently, the nano stage concept may suit applications requiring a large number of degrees of freedom, large strokes, and a high specimen stability. The nano stage concept may also be a compact alternative when nanopositioning in a limited number of degrees of freedom must be combined with feedback control. Compared to conventional top-entry goniometer stages, the nano stage concept will have better positioning repeatability. The table stability is expected to be at least comparable, if not better, than the specimen holder stability of top-entry goniometers.

The advantages mentioned make the nano stage concept a promising alternative for some applications of the side-entry and top-entry goniometer stages. Also, it may create new applications.

1.6   The nano stage concept

1.6.1   Scope of the problem

The main problems concerning specimen positioning with a nano stage in a TEM are:

- the number of degrees of freedom in relation to the available space in the vacuum chamber,
- the number of degrees of freedom in relation to the strokes,
- the level of positioning repeatability in relation to the strokes,
- the level of position stability in relation to the strokes and the nano stage dimensions, and
- the UHV compatibility.

Although these problems show some resemblance with the problems concerning nanopositioning devices in (calibrated) scanning probe microscopes (SPM) or scanning electron microscopes (SEM), there are substantial differences. The problem similarity concerns the ratio of the positioning stroke of the actuators and the resolution, which is in the order of 10^6, and the application of many of these positioning devices in vacuum. The differences, however, are numerous. The available space in SPM or SEM applications is generally larger than the space within a TEM. As a result of the presence of both objective lens pole pieces, the vacuum chamber has a very special shape, making the design process even more complex. The number of degrees of freedom of the specimen motion in SPM applications is rarely more than three, in SPM applications often divided into two separate positioning devices, one to position the specimen and the other to position the scanning probe. Another difference concerns the positioning repeatability. In SPMs, finding a special spot on a specimen is mainly achieved by finding special markers, not by means of additional transducers. In calibrated SPMs, position transducers must possess a high displace-

ment *accuracy* in contrast to position repeatability in a TEM. Also, the specimen holder strokes in a TEM are generally one order of magnitude larger than in SPMs. A last point of difference is the explicit demand on the specimen stability concerning drift and vibration amplitude. Up till now, open-loop or closed-loop stability of nano stages at the picometer level has not been a major topic in research.

Operation of the nano stage in vacuum has the advantage of the absence of air turbulence and changes in the characteristic air properties like humidity and the relative dielectric constant, which could disturb the stability of a nano stage and the stability or the positioning repeatability of the transducers applied. On the other hand, heat transfer in vacuum is limited to conduction by mechanical contact and to radiation, which may lead to undesirable heat storage in critical nano stage elements, resulting in an expansion of these elements and an increase of nano stage drift.

The TEM nano stage asks for completely different position transducers and actuators as compared to the conventional goniometer stages. Both the transducers and the actuators have to be small, extremely stable, (U)HV compatible and have to possess a large ratio of range of operation and resolution. Furthermore, they must not influence or be influenced by the strong magnetic field density (~2 tesla) between the pole pieces and must not be influenced by the electron beam (100 keV, 1 nA).

1.6.2 Actuators

Examples of nano actuators are (electro)magnetic actuators, piezoelectric actuators, electrostrictive and magnetostrictive actuators, electrostatic actuators and friction drives. As a result of the requirements for the actuators in the TEM nano stage, only a few types need to be seriously considered. As a matter of fact, one type was clearly favorable: the piezoelectric actuator. Therefore, no comprehensive comparison between different actuators was made. The choice for piezoelectric actuators was based on:

- the common approach to use piezo actuators in 'comparable' positioning devices like SPMs,
- the variety of piezo actuators commercially available,
- the possible small size,
- the possible picometer positioning resolution,
- the low heat production in low frequency, low voltage applications,
- the amount of knowledge available in literature, and
- the knowledge that several, non space consuming *piezo drives* exist to overcome the small deformations of single piezo actuators.

1.6.3 Transducers

Like for actuators, only a limited number of transducer types are available which enable displacement measurement over millimeter ranges with nanometer resolution. Examples of possible transducers are laser or fibre interferometers and other optical transducers, capacitive transducers and inductive transducers. Unfortunately, the volume of most of the transducers mentioned is relatively large compared to the space available in the TEM. Capacitive displacement transducers are clearly favorable as far as displacement measurements with picometer resolution are con-

cerned. Besides that, they can also be applied to obtain nanopositioning over millimeter ranges. Although a fibre interferometer may be a suitable alternative for this latter application, in this experimental phase it was advantageous to use only one type of transducer. Therefore, capacitive displacement transducers were used throughout the experiments to perform position measurements at the nanometer and picometer level. They have the following features:

- a high design flexibility as far as range of operation and resolution are concerned,
- picometer resolution is possible,
- a large ratio of the range of operation and the resolution,
- a small volume,
- a relatively large transducer area over which position measurements are averaged, in that way smoothing surface irregularities in the transducer area,
- a contactless measurement principle, and
- a low heat production.

1.6.4   First order nano stage design

Figure 1.5 is used to indicate some of the design problems and design parameters of the TEM nano stage. The distance between the pole pieces of the objective lens is typical in the order of 10 mm. The space between the pole pieces is reduced by the presence of an aperture holder and a backscattered electron detector. The volume of the table of the nano stage will therefore have a maximum in the order of 3 cm^3. As a high number of degrees of freedom in combination with large table strokes can often not be obtained by means of a single drive, drives have to be stacked. Consequently, the space for transducers and actuators is even more limited and therefore their volume should be minimized. Also, the stacking order of drives will have a strong influence on the performance of a nano stage.

In order to obtain nanopositioning over large strokes, the maximum deformation of single piezo actuators, which is in the order of a few tenths of a micrometer, must be converted into millimeter translations and unlimited rotations or tilts by means of compact piezo drives. The design and the drive mechanisms of piezo drives determine the resonance frequency of the drive which is important with regard to the nano stage sensitivity to pole piece vibrations and with regard to the performance of the piezo drive. Other important piezo drive parameters are its displacement resolution and minimum driving voltage. As there are several drive mechanisms for piezo drives, their performance should be compared.

Besides the use of piezo drives, capacitive displacement transducers are required to obtain nanopositioning. The maximum transducer area is limited by the space between the objective lens pole pieces and is estimated to be about 100 mm^2. In view of a small nano stage volume, the transducer dimensions should be considered as a function of range of operation and resolution, and as a function of parasitic motion.

If table stability is to be obtained by intrinsic means or by open-loop control, the intrinsic stability of the piezo actuators and of the contact area between the table and the support elements directly after moving the table to a new position, must be high. In that respect, drift in the piezo actuators and creep in the contact area should be considered. In order to verify the table stability relative to the position reference, the (electronic) stability of the capacitive transducers must be

sufficient. In order to obtain or monitor subnanometer position stability of the specimen, a reasonable target resolution for the capacitive transducer is 10 pm.

The selection of a piezoelectric ceramic material is a very important aspect of a stable nano stage. Attention should be paid to both piezoelectric and mechanical properties of piezo ceramics. The table and the reference frame material must be non magnetic, must have a high ratio of the modulus of elasticity and the density (E/ρ), and must have a low ratio of the linear expansion coefficient and the conductivity (α/λ). Such materials are, for instance, aluminium, beryllium or beryllium-copper. The table mass will therefore be in the order of $7.5 \cdot 10^{-3}$ kg. Depending on the direction of motion, either parallel or perpendicular to the gravity field and depending on the magnitude of the coefficient of friction, the preload forces on the supports are then in the order of 10^{-2} up to 1 N. With a support stiffness in the order of 10^6 N/m in the direction of motion, the first resonance frequency of the nano stage is expected to be in the order of 2 up to 5 kHz.

1.7   Layout of this thesis

Chapter 2 gives an overview of the theoretical backgrounds on piezo actuators required for this research. It describes the effects of piezo hysteresis and drift in a different way compared to the common viewpoint in the literature. This was needed to understand and describe their influence on the nano stage stability. Furthermore, chapter 2 concentrates on the differences in subsequent piezoelectric ceramics and on different types of piezo actuators.

In chapter 3, the application of piezoelectric actuators in vacuum compatible piezo drives with a large ratio of stroke and resolution is considered. Three different drive mechanisms are presented to achieve translations and rotations: inertial sliding motion (ISM), impact drive motion (IDM) and frictional stepping motion (FSM). These drive mechanisms are compared extensively on the basis of their configuration and by means of electromechanical models. Each model consists of a model for the piezo hysteresis, a model for friction, and a model of the contact areas between the table and the support. From the analytic models follow some design considerations for these piezoelectric drive mechanisms.

Chapter 4 gives a short theoretical overview of capacitive position transducers. It compares two types of capacitive displacement transducers with regard to the application in a nano stage and it discusses the influence of guarding electrodes with regard to positioning repeatability and crosstalk. The characteristic properties of the measuring electronics used throughout this research are described. By means of some experiments, the stability of the measuring electronics as well as the stability of standard and precision capacitors used, is determined. The design of practical transducers for nanopositioning applications is discussed.

Chapter 5 discusses the nano stage stability both in theory and in practice. The influence of various quasi-static and dynamic disturbances affecting the stability performance of a nano stage is described. Through experiments, the influence of drift in the piezo actuators and creep in the supports on the drift rate of the nano stage table and on the settling time to reach a sufficient level of stability are investigated.

Chapter 6 describes four different experimental nano stage setups. It discusses the nanopositioning and stability performance on the basis of the knowledge and the considerations presented in chapters 2 to 5. The ISM model is evaluated by computer simulations and experiments. One of the four setups is a one degree of freedom nano stage placed on the lower objective lens pole piece in a TEM. Special attention is paid to the stability of the nano stage and the image.

Chapter 7 discusses the practical design of TEM nano stages on the basis of the positioning tools for translations and rotations that have to be incorporated. Examples of 'impossible' configurations as well as examples of possible configurations are given.

Chapter 8 draws conclusions of this research and gives recommendations for further research on nano stages.

2 Piezoelectric actuators

2.1 Piezoelectricity

In 1880, the French brothers Curie discovered that certain crystals became electrically polarized when they were subjected to mechanical strain. This effect was called the *piezoelectric effect*. The reciprocal effect is used in piezoelectric actuators: the *inverse piezoelectric effect*. By applying an electric field over a piezoelectric material, the material deforms.

In order to exhibit the piezoelectric effect, the crystal structure of a material must not have a center of symmetry. This means that such materials have built-in highly oriented dipoles and thus intrinsically possess polarity. When piezoelectric materials are subjected to mechanical strain or an electric field, the distance between the positive and negative dipole charge sites changes, leading to a netto polarization at the material surface and to material deformation.

Both the piezoelectric effect and the inverse piezoelectric effect are proportional and linear to the applied mechanical strain and the applied electric field, respectively. Linearity implies that electric fields generated by compressive and tensile stresses have opposite polarity. A thorough review of the early history of piezoelectric crystals can be found in the work by W.G. Cady [24].

At this moment, piezoelectric ceramics are the widest applied piezoelectric materials as opposed to the traditional crystallines. However, it took 60 years before piezoelectricity in ceramics was discovered. During World War II, scientists realized that the unusual dielectric properties of piezoelectric ceramics were caused by *ferroelectricity* (analogous with ferromagnetics). Ferroelectricity is the ability of an electric dipole to change orientations between two or more preferred crystallographic directions by means of an external applied electric field. Piezoelectric ceramics are all ferroelectric.

The dielectric material properties are represented by two parameters: the relative permittivity or dielectric constant $K = \varepsilon_r = \varepsilon / \varepsilon_0$ and the dielectric loss $tan\,\delta = \varepsilon_r^{''} / \varepsilon_r^{'}$, where ε_0 is the permittivity of vacuum and ε is the permittivity of the piezoelectric ceramic. The dielectric constant K indicates the ratio of the maximum charge that can be stored on an electroded piece of material and on the same electrodes separated by vacuum. The dielectric loss factor $tan\,\delta$ gives the ratio of the amount of energy lost, represented by the imaginary part $\varepsilon_r^{''}$, and the amount of energy stored, represented by the real part of the relative permittivity $\varepsilon_r^{'}$, in a material subjected to an external electric field. Compared to crystallines like quartz ($\varepsilon_r = 4.3$), the dielectric constant of

modern piezoelectric ceramics is high, between several hundred and several thousand. This high charge storage capability indirectly leads to a much stronger piezoelectric effect in ceramics.

The piezoelectric effect strongly depends on the temperature of the ceramic and its application is limited by the Curie point. Above this temperature, the polycrystalline structure of piezoelectric ceramics is symmetric, which means that the centers of the positive and negative charge sites coincide so that piezoelectric effects cannot occur. When the temperature of the ceramic drops below the Curie point, a phase transition at the Curie point causes a change to a non-symmetric crystal structure in which the centers of the positive and negative charge sites no longer coincide. The Curie point of piezoelectric ceramics (150-400°C) is generally much higher than for traditional crystallines.

There are several possible preferred directions for the polarization axis in a ceramic. This gives rise to a combination of rather complicated twinning patterns, called domains. Due to the random orientation of the dipoles, there is no netto polarization in the ceramic. In order to obtain the (inverse) piezoelectric effect, piezoelectric ceramics have to be polarized by a strong external electric field at a temperature slightly below the Curie point. As a result, the dipoles orientate along the electric field leaving a remnant polarization when the field is removed. The remnant polarization can be explained by the dielectric hysteresis loop *abcda* in figure 2.1, which shows the relation between the polarization P and the electric field strength E. During the polarization process, the path $0cd$ is followed. Dipole alignment increases with increasing electric field until the saturation polarization P_s is reached. Reducing the field to zero leaves the dipoles in one of their preferred directions, in this case the one closest aligned to the former electric field. The polarization does not go back to zero but to a remnant polarization P_r. Point d becomes the operating point of the piezoelectric ceramic. During normal operation, only lower electric field strengths are used (no saturation), resulting in minor loops like *defgd*.

A good approximation of the interaction between the electrical and mechanical behavior of piezoelectric ceramics is the following set of coupled equations:
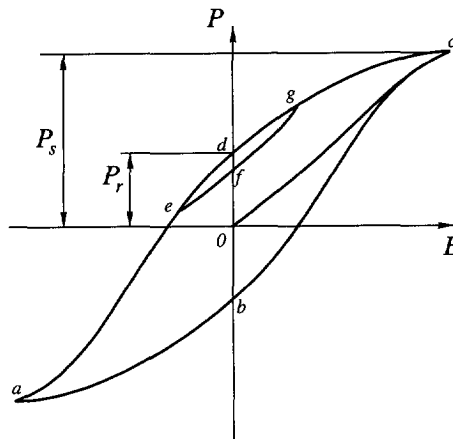
Fig. 2.1   The dielectric hysteresis loop of a piezoelectric ceramic, showing the polarization P as a function of the electric field strength E.

$$D = d_{ij}T + \varepsilon_{ij}^{T}E$$

$$(2.1)$$

$$S = s_{ij}^{E}T + d_{ij}E$$

where: D is the dielectric displacement (or amount of charge on the piezo per unit of area),

S is the strain in the piezo,

T is the applied stress,

E is the electric field strength,

d_{ij} is the piezoelectric charge constant,

s_{ij} is the mechanical compliance of the ceramic, and

ε_{ij} is the permittivity of the ceramic.

Since piezoelectric ceramics are anisotropic, their physical constants are tensor quantities. They are related to both the direction of the applied stress or the electric field and to the directions perpendicular to these. The physical constants are generally given two subscript indexes and a superscript index. The subscripts refer to the direction of the two related quantities, the superscript is used to indicate the quantity that is kept constant. The piezoelectric ceramic most often used is lead zirconate titanate (PZT). An extensive review on piezoelectric ceramics can be found in the work by Jaffe [25]. A brief general overview on piezoelectric ceramic actuators can be found in [26] and [27]. Section 2.2 discusses the properties of piezo actuators with regard to application in a nano stage. Section 2.3 discusses the properties of piezo ceramics and pays attention to the choice of a ceramic. The different deformation modes and the different types of piezo actuators are discussed in section 2.4, while section 2.5 considers possible side effects of the application of piezo actuators in a TEM.

2.2   Actuator properties

2.2.1   Introduction

Piezo actuators use the inverse piezoelectric effect to convert electrical energy into mechanical energy. The input is a driving voltage or current and the output is a deformation or displacement. Piezoelectric actuators have some fundamental characteristics and practical limitations which affect their application in nano stages. The maximum piezo actuator deformation is important with regard to the application in piezo drives, whereas the piezo actuator displacement resolution is important with regard to accurate control of the position of the table (section 2.2.3). However, the main subject of this section is the quasi-static stability of piezo actuators, which is influenced by hysteresis, drift, and heat dissipation. These stability properties will be discussed in section 2.2.4. Before that, the electromechanical model of a piezo actuator is considered.

2.2.2   The electromechanical model

The electromechanical model of a piezo actuator can be divided in three parts: an electrical equivalent circuit of the actuator input, an electromechanical transducer part, and a mechanical output. Traditionally, the electrical equivalent circuit is given by the diagram as in figure 2.2. For

quasi-static operation up to a few hertz, the series resonance circuit, parallel to the main capacitance C_0 and the resistance R_0, which represents the dielectric losses, is cancelled out and the piezo actuator is mainly a capacitor.
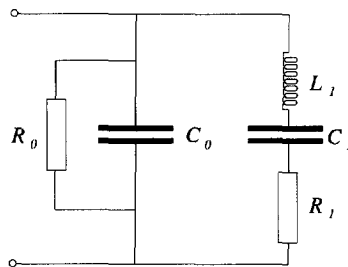
Fig. 2.2   The equivalent circuit of a piezoelectric actuator, where:
   C_0 is the piezo capacitance far below resonance,
   R_0 is the resistance representing the dielectric loss,
   R_1 is the resistance representing the mechanical loss,
   C_1 is the capacitance of the mechanical circuit, and
   L_1 is the inductance of the mechanical circuit.

As far as the electromechanical transducer part is concerned, it is known that ferroelectric materials are nonlinear in their response to electric fields, showing hysteresis and drift. However, it is generally assumed that the relation between polarization and piezoelectric strain and therefore between dielectric displacement and piezoelectric strain is free of hysteresis. The relation between the piezo deformation and the applied electric field as a function of various parameters was earlier investigated by Basedow [28], Holman [29], Hues [30], and Van de Leemput [31].
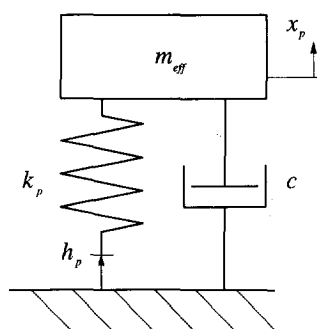
Fig. 2.3   The equivalent of the mechanical output of a piezo actuator, where:
   k_p is the stiffness of the piezo actuator,
   c is the damping constant of the piezo actuator,
   m_{eff} is the effective mass of the piezo actuator,
   h_p is the desired piezo actuator position enforced by the electric field, and
   x_p is the real position of the piezo actuator.

The mechanical output of a piezo actuator can be represented by a mass-spring-damper system having a stiffness k_p and a damping constant c (see figure 2.3). The mechanical output can be described by the following equation:

$$m_{eff}\ddot{x}_p = k_p(h_p - x_p) - c\dot{x}_p \tag{2.2}$$

2.2.3   Positioning properties

Piezo actuators are normally driven by applying a voltage difference. The maximum piezo *deformation* is limited by the saturation polarization. It is also limited by the maximum negative field strength at which (partial) depolarization occurs (see figure 2.1). Normally, the maximum allowable field strength is in the order of 1000 V/mm, the maximum negative field strength is generally much smaller. Besides these maximum field strengths, the maximum piezo deformation is determined by the ceramic material composition, the type of piezo used and its dimensions. As the piezoelectric charge constant for piezoelectric ceramics ranges from 0.1 up to 1 nm/V, it should be noted that the maximum piezo strain at zero stress is generally smaller than 10^{-3}. The maximum deformation of piezo actuators with typical dimensions in the millimeter range is therefore in the order of 1 μm, which is clearly insufficient with regard to the required specimen strokes in many nano stage applications.

In theory, there is no limit to the deformation *resolution* of a piezo actuator, although the smoothness of the piezo deformation is determined by discrete switches of domain walls in the ceramic. The deformation velocity of a piezoelectric actuator is limited by its first resonance frequency f_0. In practical applications, the deformation velocity is limited by the first resonance frequency of the setup. Generally, the frequency of the driving voltage over the piezo should preferably be lower than this resonance frequency.

The piezo *sensitivity* (the amount of piezo deformation per volt) depends not only on the magnitude of the voltage change, but also on the voltage change rate. The piezo sensitivity decreases with increasing frequency of an alternating driving voltage but increases when the magnitude of the voltage change increases. Some authors have shown measurements on this effect at low voltage change rates [29,31]. Figure 2.4 shows the piezo sensitivity measured as a function of voltage change rates up to 10^5 V/s.

The polarization process introduces mechanical stresses in the ceramic. These stresses cause a slow return of the ceramic to the disordered state of the dipoles before polarization. This *ageing*
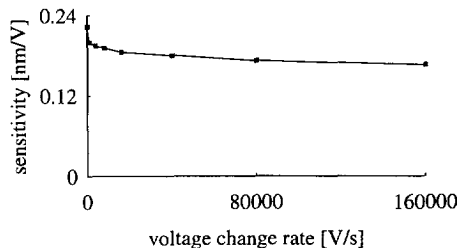
Fig. 2.4   Piezo sensitivity as a function of the voltage change rate.

process is a logarithmic function of time which in general practice can be neglected.

2.2.4 Piezo hysteresis and drift

It is generally agreed that piezo actuator hysteresis is caused by delayed domain wall switching. A sudden change in the electric field over a piezo causes an immediate and a time dependent change in the strain of the piezo actuator. The time dependent change of the strain is called drift. Piezo drift can have a strong influence on the stability of the table of a nano stage. This drift is a direct result of hysteresis and follows any electric field change. The dipoles within a domain follow a change in the electric field instantly. It is assumed that this causes stress in the ceramic, especially between the domain walls. This stress induces the delayed switching of domain walls to a different preferred crystallographic direction. This means that although the electric field is kept constant, a follow-up deformation to a desired end-position occurs. The amount of switches is proportional to the amount of stress and it decreases logarithmically with time. Hysteresis is defined as the maximum difference between the upper and the lower branch of the hysteresis loop. The drift rate is defined as the amount of (piezo) deformation per unit of time. Hysteresis increases with increasing piezo deformation. The amount of drift is often estimated from the voltage change.

During this research, the following practical point of view on hysteresis and drift of piezo actuators was developed. It considers the piezo deformation with regard to position stability directly after a voltage change has been applied. At a certain offset voltage V_{os}, a piezo actuator has certain nominal dimensions. These are reached long after the last voltage change was applied, when drift no longer substantially affects the piezo dimensions. The piezo has then reached its virginal dimensions, represented by the *zero point* H_0. The absolute values of the piezo dimensions depend on the (dynamic) deformation history and on transient effects such as quasi-static changes in temperature. It is, however, of no direct interest to nano stages.

The zero point can be used to explain the amount and direction of piezo drift. Figure 2.5 shows an experimental hysteresis loop. The hysteresis loop starts at the zero point H_0 at an offset
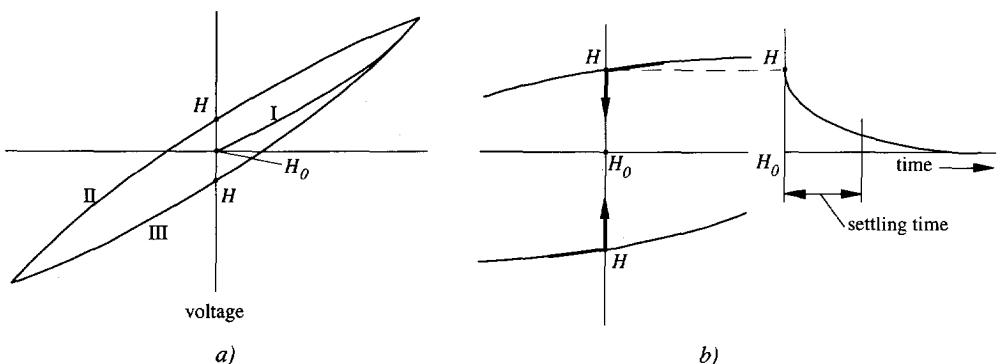
Fig. 2.5 a) The hysteresis loop of a piezo actuator. Branch I is the virginal curve after a relative long period of rest. Branches II and III form the real hysteresis loop. b) From one of the points H, the piezo drifts back in the direction of the zero point H_0, following a logarithmic curve in time.

voltage V_{os}. Next, the piezo follows branches II and III. At the end of branch III, the hysteresis loop is closed. Branches II and III cross the vertical line through the zero point in the hysteresis points H. The distance of these points changes relative to the zero point with the magnitude of the voltage change and slightly with the change rate of the driving voltage. After a deformation loop, the value for the piezo actuator deformation ends, for instance, in one of the points H. From this point, the piezo actuator drifts back in the direction of the zero point, following a logarithmic curve in time. This means that the starting point of a next hysteresis loop depends on the time between loops. The distance of a point H relative to the zero point determines the amount of drift and the drift rate of the piezo actuator. However, the prediction of the amount of the drift directly after a voltage change is complicated by the fact that a voltage change, changes the position of the zero point along the vertical axis.

If the voltage change is repeated instantly, the piezo actuator will again follow branches II and III. This means that the distance between the points H and the zero point H_0, in theory, does not change with repeated loops if the voltage loop width is constant. In theory, the amount of piezo drift after repeated loops is the same as after a single loop. In practice, the piezo drift is also influenced by heat produced in the piezo. As will be shown later in chapter 5, this effect is small for small voltage changes and low frequencies.
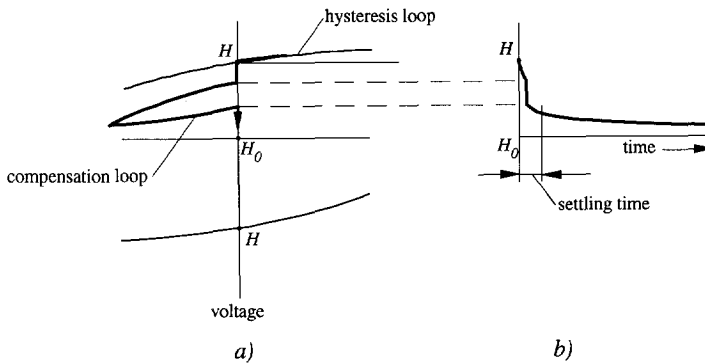
Fig. 2.6   Effect of a compensation voltage loop on the drift rate of a piezo actuator. After a voltage loop (a), the piezo starts to drift from point H towards H_0 (b). If a compensation loop is applied (a), the piezo deformation will be shifted towards the new zero point H_0 (b). After such a loop, the piezo drift rate is much lower.

With regard to the TEM nano stage, it is important to minimize the *settling time* to reach a certain minimum drift rate. This can be done by means of closed-loop position control, but it can also be done by applying only small driving voltages, in that way keeping the drift rate small. Another method is the use of open-loop control, either by knowledge about the drift rate or by shifting the point H closer to its (new) zero point by means of a small voltage change in the direction opposite to the last voltage change. Figure 2.6 shows the effect of such a voltage change on the drift rate of a piezo actuator. Both open-loop control methods will be considered in chapter 5.

Figure 2.7a shows the effect of a repeated triangular voltage loop on the piezo deformation and the position of the points H.

a)   b)
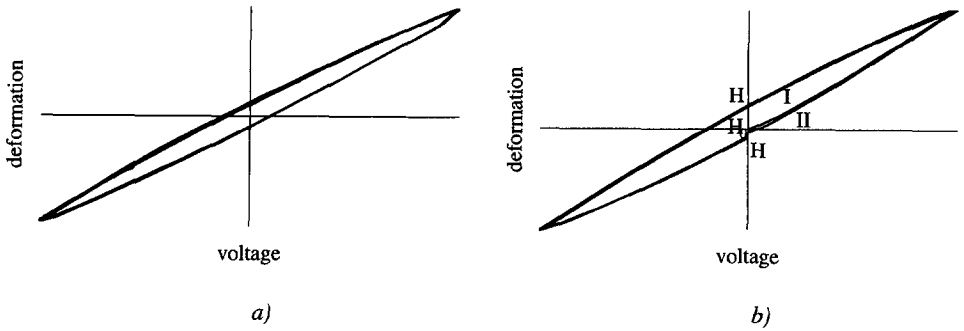
Fig. 2.7 a) Repeated experimental hysteresis loops (25 mHz). The position of the points H relative to the zero point H_0 does not depend on the number of cycles. Only for the first few cycles (not shown) a small shift of the complete hysteresis curve in the upper direction was found. b) Two successive hysteresis loops with 1 minute delay between them. The starting point of the second (II) hysteresis loop depends on the time between the loops.

2.2.5   Heat production

Heat production in a piezo can be explained by a small loss of energy during charging and discharging. When a piezo actuator with capacitance C_p is subjected to a voltage U_p, a small amount of energy is converted into heat due to the hysteresis behavior. The heat production rate $\dot{Q}_p$ in the piezo actuator can be estimated by:

$$\dot{Q}_p \approx f C_p U_p^2 \tan \delta \tag{2.3}$$

where f is the driving frequency of the piezo.

2.2.6   Limitations of the driving electronics

Although there is no theoretical limit to the deformation resolution of a piezo actuator, it is in practice limited by the noise level of the driving electronics. A practical limit to the piezo deformation is the maximum voltage range of the high voltage amplifiers (HVA).

The electronics limit the deformation velocity of the piezo actuator in two ways. The slew rate as well as the maximum output current I_{max} of the HVA are limited. For sine waves, the maximum driving frequency f_{max} can be calculated by:

$$f_{max} = \frac{I_{max}}{2\pi C_p U_p} \tag{2.4}$$

For triangle waves, this frequency is increased by a factor of π. The bandwidth of the amplifier used in this research was 450 kHz. With a maximum current of 150 mA, a piezo capacitance of typically 1 nF, and a maximum voltage loop width of 400 V, the maximum driving frequency is about 60 kHz. This frequency is sufficient because it is much higher than the resonance frequency of practical setups. The slew rate of the high voltage electronics was limited by the arbitrary waveform generator used to generate the drive signals to 200 V/µs.

2.2.7 Concluding remarks

It should be noted that the deformation of piezoelectric actuators as a function of the driving voltage is hard to describe due to its dependence on the deformation history of the piezo. Prediction of the piezo deformation at the nanometer level is therefore extremely difficult. As a result, accurate positioning at the nanometer level with piezoelectric actuators is only possible by means of closed-loop position control.

In order to obtain a high quasi-static stability of the piezo actuator, either closed-loop positioning by means of position transducers or open-loop control methods can be applied to reduce the settling time to reach picometer stability. Another method is to use small driving voltages, in that way minimizing piezo drift.

2.3 Properties of piezoelectric materials

2.3.1 An overview

At this moment, many companies offer many different types of piezoelectric materials or ceramics, which differ in their chemical composition and ferroelectric properties [26,27,32,33,34]. In order to be able to choose the best ceramic for nano stage applications, an overview of the major properties of ceramics is given. These properties can be divided in three groups: piezoelectric properties, mechanical properties, and thermal properties. Although the dividing line is no longer clear, piezoelectric ceramics can in general be divided in two groups: hard and soft ceramics. Compared to soft piezoelectric ceramics, hard piezoelectric ceramics have:

- a higher Curie point,
- less hysteresis (approximately 5% full scale),
- a better linearity (approximately 5% full scale),
- a smaller loss factor $tan\,\delta$,
- a smaller ageing rate,
- smaller dielectric constants K_{ij}^{T}, and
- smaller charge constants d_{ij}.

Typical hard piezoelectric ceramics have much smaller charge constants d_{ij} which means that they have a smaller displacement at given driving voltage change. However, in case of accurate, low frequency positioning applications, it may be advantageous to use hard instead of soft piezoelectric ceramics because closed-loop position control is more straightforward with a more linear actuator having smaller hysteresis. Also, a small loss factor $tan\,\delta$ and small dielectric constants K_{ij}^{T} result in less heat production and therefore in an intrinsically more stable positioning system.

In order to obtain an impression of the values and the relation between the characteristic properties of piezoelectric ceramics, table 2.1 lists six different ceramics supplied by Physik Instrumente GmbH [26]. Dynamic material properties like coupling factors, Q factor and frequency constants have been omitted.

ceramic properties[1]		PIC 131	PIC 140	PIC 141	PIC 151	PIC 155	PIC 163	
density	ρ	7.85	7.60	7.80	7.80	7.70	7.75	$[\cdot 10^3 \ \mathrm{kg/m^3}]$
Curie point		265	330	275	250	320	240	[°C]
$K_{33}^T = \varepsilon_{33}^T/\varepsilon_0$		600	1200	1300	2000	1700	1200	[-]
$K_{11}^T = \varepsilon_{11}^T/\varepsilon_0$		1300	680	1500	1980	1500	-	[-]
angle of loss	$tan\,\delta$	10	10	5	15	15	10	$[\cdot 10^{-3}]$
charge constant	d_{31}	-70	-60	-115	-170	-140	-113	$[\cdot 10^{-12} \ \mathrm{m/V}]$
	d_{33}	200	200	330	450	310	260	$[\cdot 10^{-12} \ \mathrm{m/V}]$
	d_{15}	440	265	475	580	450	425	$[\cdot 10^{-12} \ \mathrm{m/V}]$
mod. of elasticity[2]	E_{33}^E	92.5	85.5	79.4	66.7	75.8	-	$[\cdot 10^9 \ \mathrm{N/m^2}]$
	E_{11}^E	100	85.5	76.9	52.6	53.5	-	$[\cdot 10^9 \ \mathrm{N/m^2}]$
lin. expansion coeff.	α	5	5	5	5	3	5	$[\cdot 10^{-6}]$
specific heat	c	400	400	400	400	400	400	[J/kg·K]
conductivity	λ	2.5	2.5	2.5	2.5	2.5	2.5	[W/m·K]
hysteresis		12	11	12	15	13	15	[%]
aging rate		0.02	0.03	0.03	-	-	-	[%/dec.]

[1] Most values given in this table can vary strongly with temperature, driving voltage and frequency.

[2] There is a considerable difference between the open circuit (E_{ij}^D) and short circuit (E_{ij}^E) modulus of elasticity. Piezo actuators are normally used in 'open circuit'. Generally, open circuit values are about 20% higher. Unfortunately, only short circuit values were available.

Table 2.1   Values of the characteristic properties of six piezoelectric ceramics (from [26]).

2.3.2   The choice of a piezoelectric ceramic

The optimum choice for a piezoelectric ceramic does not depend on its material properties only. It partly depends on the type of actuators used. For instance, the sensitivity of a piezo actuator depends not only on the piezoelectric charge constants, but also on the type of actuator and its dimensions. The same applies for the actuator dissipation; it depends not only on the dielectric constant and the dielectric loss factor, but also on the amplitude and the frequency of the driving voltage and on the piezo capacitance ($\cong$ actuator dimensions). During this research the following criteria for the choice of a piezoelectric ceramic in a nano stage were formulated.

The first criterion of importance is that the materials of a nano stage used as a specimen stage in a TEM must be nonmagnetic in order not to disturb the magnetic field between the pole pieces of the objective lens. Piezoelectric ceramics are nonmagnetic and piezo actuators do not create a magnetic field.

A second criterion of importance is the ratio of the ceramic sensitivity in the relevant directions and the hysteresis. It should be as high as possible. In this respect, it should be noted that the hysteresis for the range of ceramics of table 2.1 is relatively high. Besides that, there is not much difference in the magnitude of the hysteresis.

The ratio of the modulus of elasticity E in the relevant direction and the density ρ (E/ρ) should be as high as possible in order to obtain high resonance frequencies of the piezo actuator. Besides that, the product of the piezo sensitivity and its modulus of elasticity in the relevant direction(s) should be as high as possible. In this respect, it should be noted that the data of table 2.1 show a strong relation between the magnitude of the dielectric constant K_{ij}^T, the magnitude of the charge constant d_{ij}, and the magnitude of the modulus of elasticity E_{ij}^E. Although, there is no large difference in the ceramic density, there is a considerable difference in the factor E/ρ.

Insensitivity of the piezoelectric ceramic to changes in the overall temperature or in the temperature gradients is important with regard to position stability. Thermal properties of a ceramic are the linear thermal expansion α, the specific heat c, and the thermal conductivity λ. With regard to stability, it is important to choose a ceramic with a low ratio of its linear expansion and its conductivity (α/λ) and a high thermal diffusivity $(\lambda/c\rho)$ [35,36]. Normally, the thermal ceramic properties do not differ substantially from one ceramic to another (see table 2.1). Therefore, this criterion has generally little influence on the choice of a piezoelectric ceramic. However, it should be noted that all piezoelectric material constants are temperature dependent. This may complicate the choice of a ceramic. For instance, the charge constant decreases with decreasing temperature by about 0.2% per kelvin. This effect can be neglected at room temperatures, but it reduces the piezo sensitivity at cryogenic temperatures to about 25% of the room temperature value [37]. Hopefully, recent developments on piezoelectric ceramics may solve this problem in the future [38].

The heat production in a piezo actuator must be as low as possible. Equation 2.3 showed that the heat production rate in the actuator is proportional to some ceramic properties, while it is also proportional to the amplitude of the applied driving voltage squared and proportional to the frequency of the driving voltage. In order to minimize the heat production, the factors $tan\,\delta\cdot C_p$ and $f\cdot U_p^2$ should be minimized. For low frequency (<5 kHz) and low electric field (<200 V/mm) applications, the angle of loss can be considered constant [39]. The piezo capacitance, however, does not only depend on the dielectric constant of the piezo ceramic and its dimensions but also on the driving voltage and its frequency [26,40]. Depending on the type of ceramic, the capacitance at fields of 1000 V/mm is about 30% larger than the capacitance at less strong fields. However, piezo capacitance decreases with increasing driving frequency. In order to obtain a low piezo capacitance, the dielectric constant and the driving voltage should be kept low. The piezo electrode areas should be small, while the electrode distance should be large. Investigation of piezo drives has shown that the adjustment range of the factor $f\cdot U_p^2$ is much wider than the adjustment range of the factor $tan\,\delta\cdot C_p$. Therefore, a low dielectric loss factor and a low dielectric constant are of less importance for a low heat production than the amplitude and the frequency of the driving voltage.

A last and simple criterion concerns the Curie point. It is a generally accepted rule that the Curie point of the ceramic must be at least twice the maximum temperature in the application. For UHV application, the Curie point of the ceramic must be about 300°C, owing to the bakeout temperature of 150°C required to obtain UHV. The data show a considerable variety in the Curie point. There appears to be no strong relation between the Curie point and other important ceramic properties. Piezoelectric ceramics are chemically inert and their properties are immune to humidity and other atmospheric conditions (except temperature). However, when they are used in UHV, they have to be provided with a special coating with a low outgassing rate.

From the former review, it should be concluded that the choice of the optimum piezoelectric ceramic can be rather complicated due to the conflicting interests with regard to the mechanical, the thermal and the piezoelectric properties. Therefore, the choice of a piezoelectric ceramic is almost always a compromise.

2.4   Actuator types

2.4.1   An overview

Piezo actuators have three basic deformation modes (see figure 2.8): the axial mode, the transversal mode, and the shear mode. The vectors E, P and x indicate the direction of the electric field, the polarization and the deformation, respectively. The parameters L, w, and t are the length, the width, and the thickness of the piezo actuator, respectively. The numbers along the axes correspond with the subscript indices for some piezoelectric parameters, where the 3-axis is often parallel to the polarization direction. The three basic deformation modes result in just as much piezo actuator types: the axial actuator, the transversal actuator and the shear actuator. Besides that, three additional types were developed: the stack actuator (axial mode), the bimorph actuator (transversal mode), and the tube actuator (transversal mode), see figure 2.9.
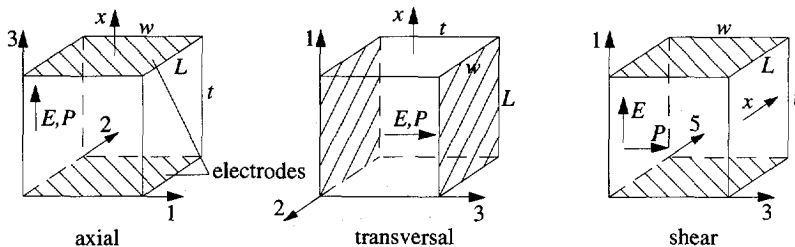
Fig. 2.8   The three basic deformation modes of piezoelectric actuators. The E vector indicates the electric field direction, the P vector indicates the polarization direction, and the x vector indicates the direction of the piezo deformation.

The main advantage of the piezo stack and the bimorph is their relatively large maximum deformation compared to single actuators. A piezo stack consists of n axial actuator plates, increasing the deformation of a single actuator n times. The bimorph actuator is a combination of two transversal actuators which deform oppositely, resulting in a relatively large bending. The maximum deformation of a piezo stack or a bimorph can range from several micrometers up to tens of micrometers. In spite of these deformations, the strain remains low. Therefore, both actuator types are relatively large, which results in relatively low resonance frequencies compared to shear and tube actuators.

A piezo tube is a radially polarized, transversal actuator [41]. If the outer electrode is divided in four segments it bends when one of the electrodes is subjected to an electric field, or two opposite electrodes to opposite electric fields (bending mode). The piezo tube deforms vertically when

all electrodes are subjected to the same electric field (transversal mode). The piezo tube is in fact a three degrees of freedom actuator.
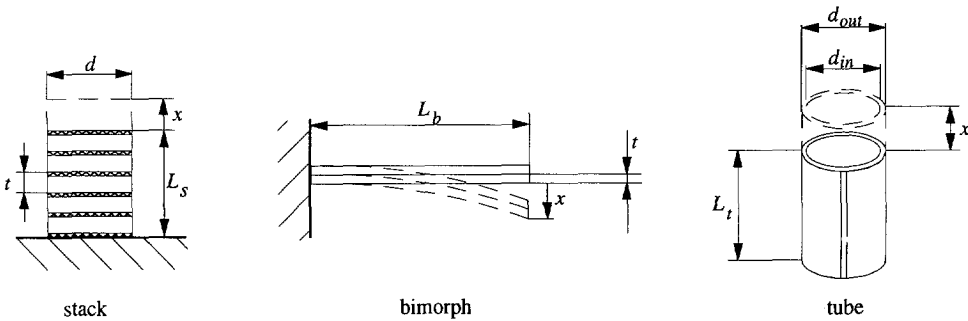
Fig. 2.9   *Three additional actuator configurations. The piezo stack consists of several axial actuators. The bimorph actuator is a combination of two transversal actuators. The tube actuator is a radially polarized, transversal actuator.*

Table 2.2 gives equations describing the linearized deformation and the capacitance of the piezo actuator types presented. These equations are true only for quasi-static deformations and for small changes of the electric field and are based on equation 2.1. If the actuators are free of mechanical preload forces, equation 2.1 is simplified to:

$$S = d_{ij} E \qquad (2.5)$$

From equation 2.5 the piezo displacement δ can be written as a function of the driving voltage:

	deformation	capacitance
axial	$\delta = d_{33} U_p$	$C_p = K_{33}^T \varepsilon_0 \dfrac{Lw}{t}$
transversal	$\delta = \dfrac{L}{t} d_{31} U_p$	$C_p = K_{33}^T \varepsilon_0 \dfrac{Lw}{t}$
shear	$\delta = d_{15} U_p$	$C_p = K_{33}^T \varepsilon_0 \dfrac{Lw}{t}$
stack	$\delta = n d_{33} U_p$	$C_p = n K_{33}^T \varepsilon_0 \dfrac{\pi d^2}{4t}$
bimorph	$\delta = 3 \dfrac{L_b^2}{t^2} d_{31} U_p$	$C_p = K_{33}^T \varepsilon_0 \dfrac{2 L_b w}{t}$
tube[1]	$\delta = \dfrac{2 L_t}{d_{out} - d_{in}} d_{31} U_p$	$C_p = K_{33}^T \varepsilon_0 \dfrac{2\pi L_t}{ln(d_{out}/d_{in})}$
tube[2]	$\delta = \dfrac{2\sqrt{2} L_t^2}{\pi d_{out}(d_{out} - d_{in})} d_{31} U_p$	$C_p = K_{33}^T \varepsilon_0 \dfrac{2\pi L_t}{ln(d_{out}/d_{in})}$

[1]   Transversal mode.

[2]   Tube in bending mode. The bending of the piezo tube is calculated for application of the voltage U_p on a single electrode only. See also literature reference [42].

Table 2.2   *The deformation and the capacitance of six different types of piezo actuators.*

$$\delta = \alpha d_{ij} U_p \tag{2.6}$$

where α is a geometry factor depending on the type of actuator. This geometry factor α can be derived from the equations for the deformation given in table 2.2, just as the piezo sensitivity.

2.4.2 A comparison

In order to be able to choose the best piezo actuator type for a nano stage application, a comparison was made during this research between shear and tube actuators with regard to stiffness, sensitivity, occupied space, resonance frequency, and capacitance. Shear actuators and tube actuators in bending mode will most likely be applied in nano stages. They are compared by means of figures 2.10 and 2.11. For the shear actuators, only the static stiffness k_p in the deformation direction was calculated because a pure shear resonance frequency does not occur in practice, as a result of the ratio of the shear actuator dimensions. The values for the tube actuator's bending stiffness and bending resonance frequency become inaccurate when the ratio of the tube length L_t and the outer diameter d_{out} becomes smaller than 1. Therefore, these values have been omitted in figure 2.11. In the comparison, the ceramic PIC155 was used. The piezo dimension are standard catalogue values, which are given in table 2.3.

shear		tube	
L [mm]	w [mm]	d_{out} [mm]	d_{in} [mm]
4	4	2.2	1.0
5	6	3.2	2.2
10	10	6.4	5.2

Table 2.3   Standard catalogue values of shear and tube actuator dimensions.

In practical applications, the piezo actuator has to be connected to a base. The construction of this base must be compact and rigid to avoid resonance frequencies below the actuator resonance frequency. In the comparison between the shear and the tube actuator, neither the influence of the base nor the influence of the connection between the piezo actuator and the base (often an epoxy layer) is taken into account. Examples of the influence of the epoxy connections and the base on the piezo actuator performance are given in chapter 6.

In combination with the selection criteria given in section 2.3.2 and the data of table 2.1, figures 2.10 and 2.11 enable the optimum choice of the piezoelectric ceramic and the type of piezo actuator for application in a nano stage.

Figure 2.10 shows that the length and the width of a shear actuator can be reduced without influencing the sensitivity. In this way, the space occupied by the actuator and the capacitance can be minimized. However, below a certain ratio of the shear actuator area and its thickness, the actuator deformation can no longer be regarded as pure shear deformation. This threshold value is assumed to be 2.

Using figures 2.10 and 2.11, the relative advantages and disadvantages of shear and tube actuators with regard to sensitivity, stiffness, volume and capacitance can be determined for applications having only one degree of freedom. However, regarding the number of degrees of freedom

of a tube actuator, it is more fair to compare a tube actuator with two stacked shear actuators, whose mutual polarization directions are rotated 90 degrees. This results in a two degrees of freedom actuator. The volume of this shear actuator stack is doubled, while the sensitivity stays the same. The total capacitance of the shear actuator stack increases a factor of 2, while the stiffness decreases a factor of 2. A disadvantage of this stack of shear actuators is the epoxy layer needed between both actuators to attach them. This epoxy layer will decrease the stiffness and thus the resonance frequency of the stack.
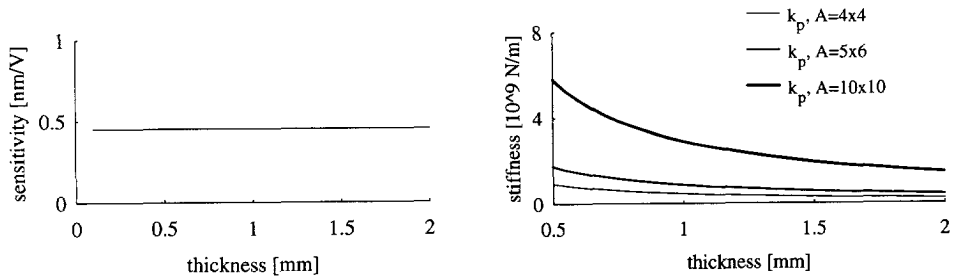
Fig. 2.10a   Calculated sensitivity and stiffness k_p in the direction of the deformation of a shear piezo as a function of its dimensions.
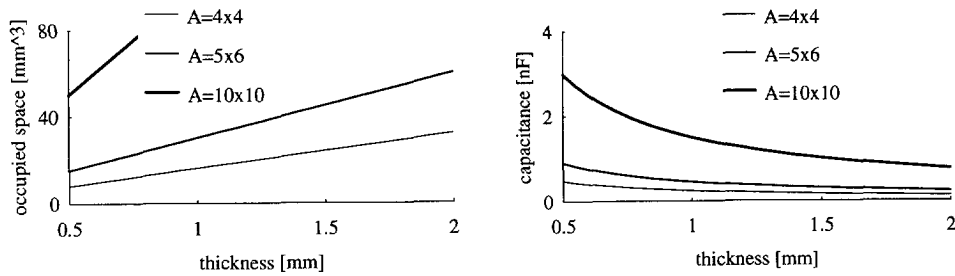
Fig. 2.10b   Calculated occupied space and capacitance of a shear piezo as a function of its dimensions.

The choice for either shear or tube actuators strongly depends on the application. A decisive parameter for this choice seems to be the number of degrees of freedom required in the application.
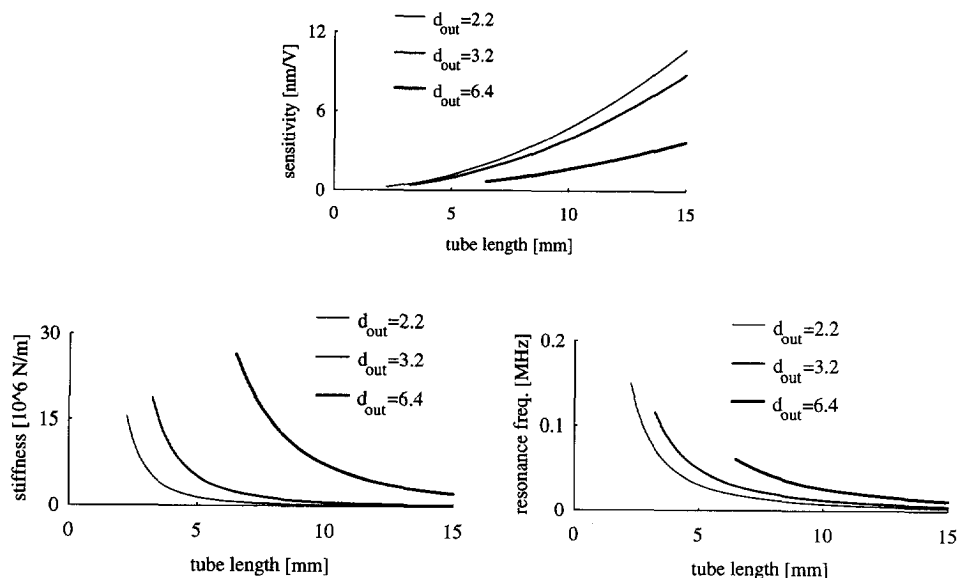
Fig. 2.11a *Calculated sensitivity, stiffness and resonance frequency of a piezo tube in bending mode as a function of its dimensions.*
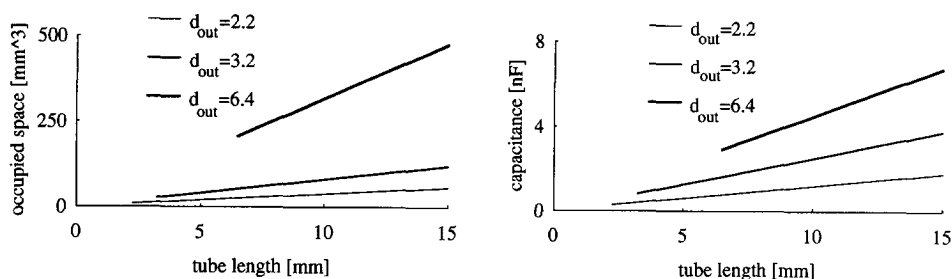
Fig. 2.11b *Calculated occupied space and capacitance as a function of the dimensions of a piezo tube in bending mode.*

2.5   Piezo actuators in a TEM: side effects

Interference of the electron beam or the magnetic field in-between the objective lens pole pieces and the piezoelectric actuators or vice versa is considered here. The magnetic induction between the pole pieces may be high (~2 tesla), but it is static. The magnetic field stability depends on the TEM voltage sources (dc), whose stability is in the order of 1 ppm per minute. The electrodes of a piezoelectric actuator need to be connected to the HV driving electronics outside the vacuum by means of thin leads. In a magnetic field, the electrons in these leads experience a Lorentz force which is perpendicular to the plane through the local magnetic induction vector $\overline{B}$ and the

electron velocity vector $e\overline{v}$ and proportional to the sine of the angle between the magnetic induction vector and this electron velocity:

$$F_L = \overline{B}\overline{v}e\sin\alpha = e\overline{v} \times \overline{B} \tag{2.7}$$

This force has no netto effect on the current through the leads to the piezoelectric actuator and thus no effect on the transducer accuracy. It results, however, in a netto force acting on the leads, which is proportional to the current I_p running through the leads. At this point, one should distinguish between a piezo actuator which is used in piezoelectric drives (see chapter 4), continuously driven at high driving voltages (100 V_{pp}) and frequencies in the order of 500 Hz and a piezo actuator integrated in a control loop for picometer position corrections. During the continuous drive, the stability of the object that is moved is not important and thus the effect of the Lorentz force (0.1 mN) on the leads can be neglected. During closed-loop control, the current running through the leads is estimated to be in the order of 1 µA (f_{max} = 5 kHz, C = 1 nF and U_p = 0.1 V). The Lorentz force acting on a lead with length l can be written as:

$$F_L = \overline{B}I_p l \tag{2.8}$$

With l = 50 mm, the force amplitude is no larger than 100 nN. It could however cause vibrations near the resonance frequency of the nano stage. Therefore, the leads should be fixed to the reference frame.

Piezoelectric actuators do not create a magnetic field. However, the current running through the leads induces a magnetic field. The order of magnitude of the magnetic induction can be estimated by:

$$\overline{B} = \frac{\mu_0 I_p}{2R} \tag{2.9}$$

where μ_0 is the permeability of vacuum ($\mu_0 = 4\pi \cdot 10^{-7}$) and R is the distance to the lead. The magnetic induction at 1 mm distance would be in the order of 10^{-10} T, which can be neglected. The driving electrodes of the piezo actuators must be electrically insulated from the electron beam, which requires some constructive measures.

3 Piezoelectric drives

3.1 Introduction

The maximum deformation of single piezo actuators is clearly insufficient to achieve nanopositioning over large strokes. Piezo stacks, bimorph actuators or piezo actuators in combination with stroke enlargement systems like flexible hinges are too bulky to achieve a compact, highly stable nano stage for specimen positioning in a TEM. Besides that, such actuators have a relatively low stiffness and a relatively low first resonance frequency. In a nano stage, alternative drive mechanisms have to be used.

In section 3.2, four drive mechanisms which enable nanopositioning are presented. They use piezo actuators and are therefore called *piezo drives*. Nevertheless, these drive mechanisms may also be applied with different actuators like electrostrictive or magnetostrictive actuators. The problem of the small piezo deformations is generally solved by using one of the three following drive mechanisms: clamp step motion (CSM), inertial sliding motion (ISM), or impact drive motion (IDM) [43,7,44]. More recently, frictional stepping motion (FSM) was presented [45]. One of the aims of this chapter is to compare these piezo drives in order to be able to make the best choice for a certain application. There are several parameters that should be looked at in this comparison. They are formulated below taking into account the positioning requirements given in table 1.1.

A piezo drive must enable nanopositioning in vacuum providing either translational or rotational motion. It must also be possible to move its table in a direction parallel to the gravity field. The required maximum specimen holder velocity makes demands on the driving voltage and frequency. They are bound to a maximum by the piezo actuator and the resonance frequency of the drive. Positioning with nanometer repeatability can be achieved by making steps of nanometer size or by applying a dc voltage over the piezo actuators. In order to avoid large dc voltages on the piezo actuators (avoiding unnecessary piezo drift), the minimum step size of the piezo drive should preferably be smaller than the positioning repeatability required. Also, the minimum step size must be such that 'continuous' and smooth low velocity motion is possible. As the step size is strongly coupled to the magnitude of the driving voltage, the minimum driving voltage must be equally low.

In case of stability control, the displacement resolution of the specimen holder must be in the order of picometers. If specimen holder stability is to be obtained by intrinsic means, a low piezo drift is favorable in most drive mechanisms. As was mentioned in chapter 2, this can be achieved by using a low driving voltage and frequency. A low vibration amplitude of the table is supported by a high resonance frequency of the piezo drive. This makes demands on its stiffness and mass.

The four drive mechanisms mentioned are presented in section 3.2. Three of them are further described in sections 3.3 to 3.6 in which, among other things, an analytic electromechanical model for these drives is derived. Section 3.7 describes the drive signals for the drives, while section 3.8 discusses some possible piezo rotor configurations. Section 3.9 describes the choice of the materials in the contact zone between table and supports and section 3.10 discusses scaling laws.

3.2   Drive mechanisms

3.2.1   Introduction

All four drive mechanisms described in this section consist of three main parts (see figure 3.1): one or more piezo actuators, a table which must be moved, and elements which support the table. Two important directions can be discerned: the *direction of motion* and the *direction of the pre-load force*. Each drive mechanism moves a table, which has a certain mass, in the 'direction of motion'. The table is preloaded by preload forces.

Piezo drives can have a number of different configurations. For instance, the piezo actuators can be connected to the table or to the base and the number and types of piezo actuators and the number and type of support elements can be different.
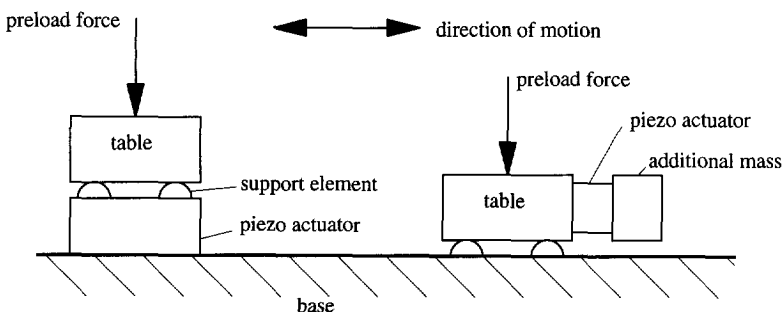
Fig. 3.1   The drive mechanisms consist of piezo actuators, a table, and support elements. There is a number of possible configurations for the drive mechanisms.

3.2.2   Clamp step motion

A clamp step motion (CSM) drive uses a combination of (a) piezoelectric actuator(s) and a set of clamps [46] or feet [47] to realize translation [43] or rotation [48]. Clamping is either realized by

elastic [49], electrostatic [50] or magnetic [51] forces. Figure 3.2 gives an example of a CSM drive configuration and explains its way of operation. In case of elastic clamping, piezoelectric actuators are often used to generate the clamping force. In some cases, piezo stacks or lever mechanisms are used to amplify the displacement of the feet in order to compensate for the small deformation of the clamping actuators [52,53]. The most well known CSM drive is the Burleigh Inchworm®.

CSM drives often require a number of (active) elements, some of them have to be very precisely machined. In general, CSM drives will be relatively large compared to other piezo drives because more space is needed to achieve a sufficient clamping force or foot deformation. In case of elastic or electrostatic clamping, the clamping voltages range from several volts up to several hundred volts, depending on the application, the smoothness of the surfaces and the direction of motion. The driving voltage of the main piezoelectric actuator ranges from 50 up to 1000 V, depending on the application. Compared to elastic or electrostatic clamping, the maximum magnetic clamping forces are larger, which facilitates vertical motion. Unfortunately, because of possible electron beam disturbance, magnetic clamping is not convenient in a TEM, unless parasitic magnetic fields can be properly shielded. Because the nominal step size at constant driving voltage varies from 5 up to 20%, displacement control is required to achieve nanometer positioning repeatability. Depending on its configuration, the translation stroke of a CSM drive is either limited by the dimensions of the drive or the base. By means of CSM, translations as well as rotations have been achieved both perpendicular and parallel to the gravity field.

Fig. 3.2 Motion of a clamp step drive is achieved by repeated run of the cycle: a) clamp foot 1, b) unclamp foot 2, c) extend piezo, d) clamp foot 2, e) unclamp foot 1 and f) contract piezo. The direction of motion can be changed by inverted run of this cycle.

3.2.3 Inertial sliding motion

Inertial sliding motion (ISM) drives have a very simple drive mechanism. This results in compact devices with generally only one precise machined component: the bearing surface. This means that an ISM drive can

be compact and stiff, having a high resonance frequency. One of the first ISM drives was described by Pohl [7]. Nowadays, it is frequently used for specimen and probe positioning in SPMs [54,55,56,57]. Especially the tube actuator has enabled a number of extremely simple and compact two and three degrees of freedom ISM drives [55,58,59]. By means of ISM, translations [60] as well as rotations [56] have been achieved in directions perpendicular and parallel to the gravity field. ISM has proven to work in ambient conditions as well as in UHV. The stroke of ISM drives is limited by the dimensions of the table or the base.
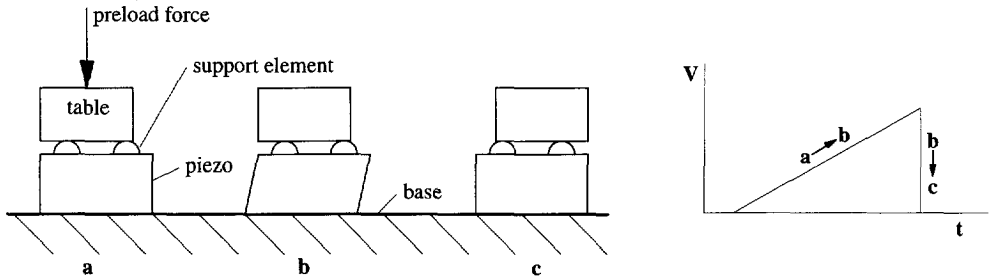
Fig. 3.3   The drive mechanism of inertial sliding motion (ISM) drives. During the slow piezo deforma-
tion (a→b), the table sticks to its supports and follows the deformation of the piezo. Due to its
large inertia, the table cannot follow the fast piezo deformation change back to its original
position and therefore moves relative to the supports and the base (b→c).

Figure 3.3 shows the drive mechanism of ISM. Motion by ISM is based on friction between the support of the table and the table itself and on the high ratio of the table inertia and the inertia of the piezo actuator(s). The piezoelectric actuator is driven by sawtoothlike or sinusoidal voltages. By varying the amplitude and frequency of the driving voltage, the step size and the velocity of the table can be varied. Driving voltages ranging from 30 up to 300 V, frequencies up to several kHz, and minimum step sizes ranging from 1 up to 50 nm have been reported. Step sizes at constant driving voltage and frequency vary about 10% of the nominal step size. Therefore, ISM drives require displacement control to achieve nanometer positioning repeatability.

3.2.4   Impact drive motion

The third drive mechanism is impact drive motion (IDM). For IDM, a piezo actuator and an impact mass are attached to the table (see figure 3.4). The table is supported by support elements. The table can be moved by fast extension or contraction of the piezo actuator. In that case, the impact force on the table becomes larger than the maximum friction force between the table and its supports so that slip occurs. IDM can be used for motion perpendicular and parallel to the gravity field.

The stroke of IDM drives depends on the dimensions of the supporting base. This means that IDM drives can, for instance, walk through thin and long pipes. The step size and the velocity of the table can be varied by varying the amplitude and the frequency of the driving voltage. Driving voltages ranging from 5 up to 300 V, driving frequencies up to several kHz, and minimum step sizes in the order of a few nanometers have been reported. Like CSM and ISM drives, IDM drives require displacement control to obtain nanometer positioning repeatability. The number of

degrees of freedom of an IDM drive is only limited by the configuration of the table supports and the base and by the number of degrees of freedom of the piezo actuators. It should further be noted that the impact mass may also be used as the table.
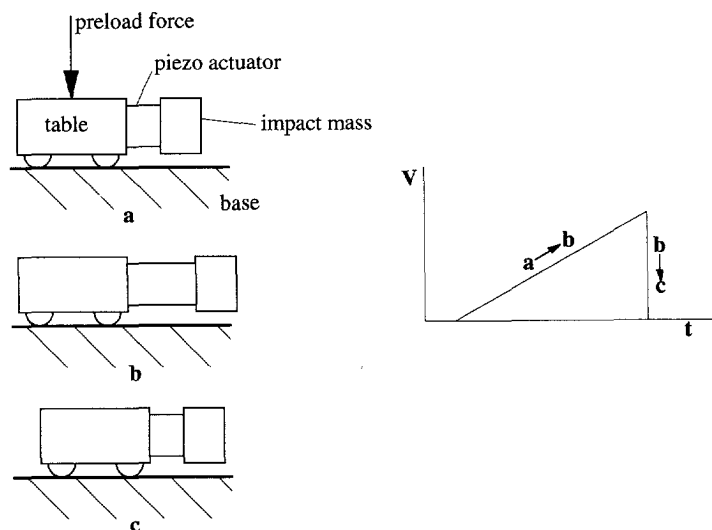
Fig 3.4   The drive mechanism of impact drive motion (IDM). If the impact force generated by fast extension or contraction of the piezo actuator becomes larger than the maximum friction force between the table and the support, the table is moved.

3.2.5   Frictional stepping motion

The name *frictional stepping motion* (FSM) was created during this research for a drive mechanism that was not yet given a general name in literature. Like ISM and IDM drives, FSM drives have a simple drive mechanism. It is explained in figure 3.5. In contrast to ISM, FSM is not based on the high ratio of inertia between the table and the piezo actuators, but only on friction forces. This means that tables of very low mass can be moved.

FSM drives can be used for positioning perpendicular and parallel to the gravity field. The stroke of the FSM drive of figure 3.5 depends on the dimensions of the table. However, if the piezo actuators are attached to the base, the stroke of the FSM drive depends on the dimensions of the base. Compared to ISM drives, there is only little information on the performance of FSM drives. Since their first application, FSM drives were only applied in low temperature STMs as a course positioning mechanism. Up to now, driving voltages ranging from 100 up to 600 V, driving frequencies up to 1 kHz, and minimum step sizes in the order of 100 nanometer have been reported [61]. Like the other drives, FSM drives require displacement control to achieve nanometer positioning repeatability.
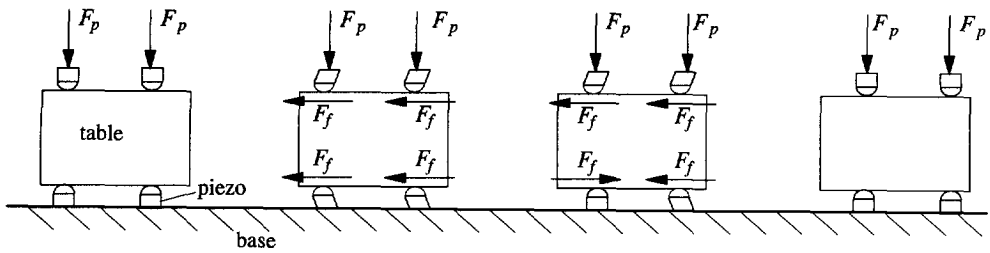
Fig. 3.5 The drive mechanism of frictional stepping motion (FSM). The preload forces and thus the maximum friction forces between each of the support elements and the table are assumed to be equal. The table is moved by applying a voltage to all piezo actuators. Next, the voltage on one piezo actuator is released resulting in a force on the table. If this force exceeds the maximum friction force, the piezo actuator deforms back while exerting a friction force on the table in the direction of the piezo deformation. The table is kept in place by the friction forces of the other three support elements. Subsequently, the other three piezo actuators are sequentially deformed, back to their starting position.

3.2.6 Concluding remarks

The relative characteristic properties of the four piezo drives described are summarized in table 3.1. It was already known from literature that all four drive mechanisms enable nanopositioning in vacuum for translational motion as well as for tilting, with a minimum step size in the nanometer and nanoradian range. For all four drive mechanisms, a high level of positioning repeatability of the table must be achieved by displacement control. The table velocity is determined by the step size multiplied by the driving frequency. For all four drive mechanisms maximum velocities in the order of millimeters per second have been reported.

The following remarks can be made with regard to the relative disadvantages of the mutual piezo drives. The displacement resolution of an IDM drive depends on whether the table is used as the impact mass or not. If so, the displacement resolution depends on the displacement resolution of the piezo actuator. If not, it depends on the minimum step size of the drive. For the IDM drive configuration of figure 3.4, the quasi-static position stability of the table relative to its base can be high because piezo drift will not influence the table position. On the other hand, its total mass may be relatively high due to the presence of the impact mass. The stability of a CSM drive is estimated to be relatively low due to the relatively large dimensions of the clamping actuators. This results in a relatively low stiffness, a relatively high volume, a possible higher mass, and hence a relatively lower resonance frequency. Due to the possible low mass of the FSM drive, its stability is expected to be relatively high.

Considering the four drive mechanisms, ISM, IDM and FSM seem the most promising. Their drive mechanisms are relatively simple, the number of (precise machined) components is low and they can be compact. This is not always the case for CSM. Therefore, CSM was not investigated during this research. However, this does not imply that CSM cannot be used for specimen positioning in a TEM. For some nano stage applications, it may be a useful alternative.

According to table 3.1 and the requirements summarized in section 3.1, ISM, IDM and FSM drives should be compared with regard to their minimum step size and driving voltage, with regard to their resonance frequency, and with regard to the space they consume. In general, it will be difficult to compare them with regard to resonance frequency and volume because of the enormous amount of possible configurations.

	CSM	ISM	IDM	FSM
picometer resolution	+	+	+/-	+
nanometer step size	+	+	+	+
stability	+/-	+	++	++
stiffness	-	+	+	+
mass	+/-	+	+/-	++
volume	-	+	+	+

Table 3.1   Representation of the relative properties of the four piezo drives.

Since the first STM [6] and since the development of the first piezo drives, much attention has been paid to the performance of the piezo drives but only little to the basic design concepts. In order to develop design recommendations, in order to optimize the drive performance, and in order to create a support in the design process of new ISM, IDM and FSM drives, analytic models are of interest. Two analytic electromechanical models for ISM and IDM were developed (sections 3.4 and 3.5). This way, a better understanding of the mechanisms of motion can be obtained and some drive parameters can be compared. The analytic ISM model was also implemented in a computer program in order to simulate ISM.

Before modelling ISM and IDM, piezo hysteresis, friction, and the influence of the contact area between the table and the support elements have to be discussed (section 3.3).

3.3   Models

3.3.1   Model for a piezo actuator

The electromechanical relation between the piezo deformation and the driving voltage is complicated. Some researchers have tried to describe piezo hysteresis analytically [62], but unfortunately such a description is so complicated that prediction of the piezo actuator deformation with nanometer accuracy is not possible. Prediction of the piezo deformation is important with regard to the computer simulation of ISM, which will be discussed on the basis of an experimental setup in chapter 6. In case of ISM, IDM and FSM, the following assumptions make prediction of the piezo deformation easier:

- the driving voltage has a constant shape,
- often, the waveform is instantly repeated many times,

- the waveform frequency is constant,
- the maximum driving voltage is 150 V (no saturation effects),
- the offset voltage is constant, and
- drift and ageing effects are neglected.

Using these assumptions, the piezo actuator behavior can be predicted by recording a hysteresis curve of the piezo actuator used in a setup. Recently, Holman [29] proved that the piezoelectric hysteresis curve, which is not affected by saturation effects, can be well described by a third order polynome. For the electromechanical transformation of the piezo voltage U_p to the piezo displacement h_p, this third order polynomial description was used.

3.3.2   Model for friction

Friction is present in all systems incorporating parts in mutual mechanical contact. Because friction often limits system accuracy, much research is done on this topic. One of the major problems with friction is the transition of sliding motion into stick and vice versa. For piezo drivers, continuous change between these phases is essential. In their extensive survey on tools for the control of systems with friction, Armstrong-Hélouvry et al. [63] reported many efforts by many different authors to model friction. These models are based on a combination of Coulomb forces and static friction forces.

The friction force F_f is equal to the Coulomb friction force F_C when there is relative motion between the two objects in contact; the relative velocity $\dot{x}_r$ between the objects is not zero. The friction force F_f depends on other forces in the system when there is no or very small relative motion between the two objects in contact. In that case, the friction force is called the *static* friction force. The Coulomb force F_C always opposes relative motion and is proportional to the normal force of contact F_n:

$$F_C = \mu |F_n| sign(\dot{x}_r) \qquad (3.1)$$

where μ is the coefficient of friction. The main problem of modelling friction is the discontinuity of the friction force at zero relative velocity. A general approach to this problem is to replace the discontinuity by a curve of finite slope, illustrated in figure 3.6a. However, this model causes physical and numerical problems. It does not provide true stick, meaning that the system creeps
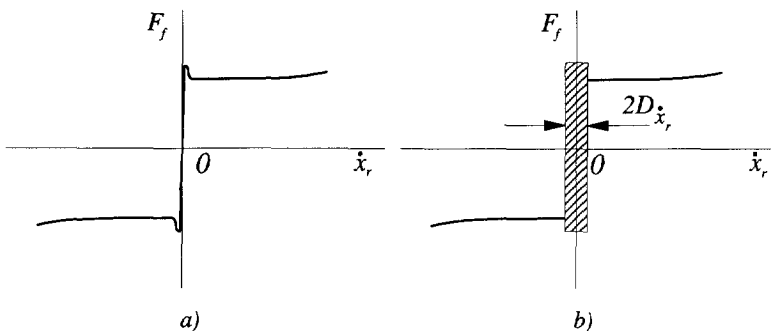
Fig. 3.6 a) Modelling friction by a finite slope curve causes physical and numerical problems. b) Karnopp's friction-velocity model. Stick is allowed in the $\pm D_{\dot{x}_r}$ interval (from [64]).

through zero relative velocity instead of sticking. Moreover, large slopes need small simulation step sizes, slowing the calculations.

Karnopp [64] developed a friction model with minimum algorithm complexity especially for numerical use. It gives useful results without needing excessively short simulation time steps. If very small displacements are to be accurately simulated, this model could be more accurate than the finite slope model [63]. A region of small relative velocity is defined as $-D_{\dot{x}_r} < \dot{x}_r < D_{\dot{x}_r}$, where $D_{\dot{x}_r}$ is called the velocity deadband. Outside this region, the friction force is a function of the relative velocity (see figure 3.6b). It was assumed that the Coulomb friction force was constant over the full relative velocity range. Inside this region, $\dot{x}_r$ is set to zero and the friction force is determined by other forces in the system in such a way that $\dot{x}_r$ remains in this region until the maximum static friction force $F_{f_{max}}$ is reached. A finite deadband is necessary since the exact value of zero will not be computed. The Karnopp model can be described by (see fig. 3.7):

$$F_f(\dot{x}_r, F_t) = \begin{cases} F_C & |\dot{x}_r| > D_{\dot{x}_r} \\ -sign(F_t) max(F_t, F_{f_{max}}) & |\dot{x}_r| \le D_{\dot{x}_r} \end{cases} \qquad (3.2)$$

where F_t is the tangential driving force,
$\quad\ F_{f_{max}}$ is the maximum static friction force, and
$\quad\ max(F_t, F_{f_{max}})$ equals F_t with a maximum of $F_{f_{max}}$.

The maximum friction force $F_{f_{max}}$ on the mass is ruled by the coefficient of *static* friction μ_{st}. The maximum friction force is given by:

$$F_{f_{max}} = \mu_{st}(F_p + mg \cos \alpha) \qquad (3.3)$$

For finite values of $D_{\dot{x}_r}$, the object has exactly zero velocity until the friction force F_f has reached the maximum level $F_{f_{max}}$. If such, slip occurs and the Coulomb friction force is assumed constant with increasing relative velocity:

$$F_C = \mu_d(F_p + mg \cos \alpha) \qquad (3.4)$$

where μ_d is the coefficient of dynamic friction,
$\quad\ F_p$ is the preload force on the object, and
$\quad\ \alpha$ is the angle of the setup relative to the gravity field.

The Karnopp friction model was used to convert the analytic ISM model into a suitable model for computer simulation.
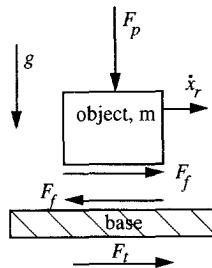
Fig. 3.7   Friction between an object with mass m and a base.

3.3.3 Effective masses

In order to be able to simulate the dynamic behavior of a piezo drive properly, the effective mass m_{eff} of the piezo and the supports must be estimated. The first resonance frequency of a system can be approximated by:

$$f_0 = \frac{1}{2\pi}\sqrt{\frac{k}{m_{eff}}} \tag{3.5}$$

where k is the system's stiffness. In case of an ISM or an FSM drive, the effective mass can be taken equal to the table mass, since the table mass is often much larger than the mass of the piezo and the supports. The effective mass of the IDM drive in the direction of motion can, by approximation, be taken equal to the sum of the table, the piezo and the impact mass.

The estimation of the first resonance frequency in the direction of the piezo deformation of a *piezo support* or of a piezo that has a small mass attached to it is more difficult. A piezo support is a combination of a piezo and a support element, as is shown in figure 3.8a. The direction of motion is indicated by the deformation x. Such systems may be modelled by a homogeneous beam, fixed at one end, its mass proportionally distributed over its length and a point mass at the end of the beam, as shown in figure 3.8b.
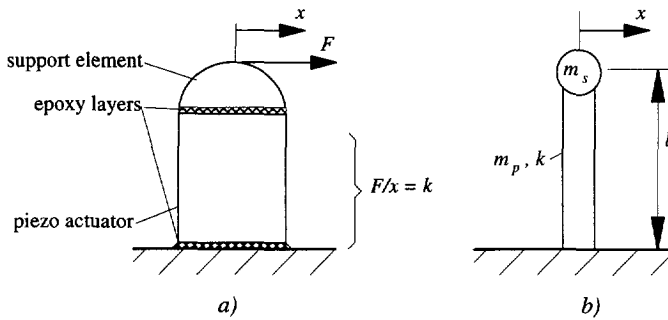
Fig. 3.8   a) A piezo support is a combination of a piezo and a support element. The stiffness k is a series connection of the piezo actuator stiffness, the support element stiffness, and the stiffness of the epoxy layers. b) Model of a piezo support or a piezo that has a mass m_s attached to it.

The resonance frequency of the piezo support model depends on the type of piezo actuator used. In case of an axial, transversal or shear piezo actuator, this resonance frequency can be approximated by [65]:

$$f_0 = \frac{1}{2\pi}\sqrt{\frac{3k}{m_p + 3m_s}} \tag{3.6}$$

resulting in $m_{eff} = m_p / 3 + m_s$, where m_p is the piezo mass and m_s is the mass of the support element. In case of a piezo tube (bending mode), the resonance frequency of the piezo support can be approximated by [65]:

$$f_0 = \frac{1}{2\pi}\sqrt{\frac{12.36k}{m_p + 12.36m_s}} \tag{3.7}$$

resulting in $m_{eff} = m_p / 12.36 + m_s$.

The stiffness k represents a series connection of three stiffnesses: the piezo actuator stiffness k_p, the stiffness of the support element k_s, and the combined stiffness of the epoxy layers k_{epoxy} between the base and the piezo actuator, between the piezo actuator and the support, or between the piezo actuator and the impact mass (see figure 3.8a).

Apart from the support stiffness k, the tangential contact stiffness k_c between the table and its supports must be taken into account when the stiffness of a piezo drive is considered.

3.3.4 Model for the contact area

The tables of piezoelectric drives are supported by a limited number of support elements resulting in a set of small contact areas. Investigation of the contact area behavior under normal and tangential forces is important with regard to the tangential contact stiffness k_c and with regard to the minimum voltage required to achieve stepping. Investigation of the contact area is also important with regard to the estimation of the maximum allowable normal load in order to avoid plastic deformation and with regard to estimation of the influence of surface coatings.

The deformation of the table and the support elements at their contact areas can be described by means of Hertz theory on contact mechanics. This theory assumes that the shape of each body in contact can be characterized by two radii, R_i' and R_i'', in accordance with their principle axes. The contact area and the deformation of the two bodies can be described by a set of simple equations when $R_i' = R_i''$. In that case, the contact area is circular having a radius a. Description of the contact area and the deformation of the bodies becomes much more difficult when $R_i' \neq R_i''$ for one of the bodies. This is extensively described by Johnson, in his book on contact mechanics [66]. Here, only the case $R_i' = R_i'' = R_i$ will be considered.

Figure 3.9a shows the configuration of the contact area between two bodies: a flat table and a spherical support. The contact area is loaded by the normal force F_n. If there is no tangential force, the deformation of both bodies is symmetric relative to the Z axis, resulting in a relative approach δ. The contact area is a circle with diameter $2a$. The relative approach δ can be calculated by:

$$\delta = \frac{a^2}{R_e} = \sqrt[3]{\frac{9}{16} \frac{F_n^2}{R_e E_e^2}} \qquad (3.8)$$

where R_e is the equivalent radius of the contact area and E_e is the equivalent modulus of elasticity. The equivalent radius is given by:

$$\frac{1}{R_e} = \frac{1}{R_t} + \frac{1}{R_s} \qquad (3.9)$$

where R_t is the radius of the table ($R_t \rightarrow \infty$) and R_s is the radius of the spherical support. The equivalent modulus of elasticity is given by:

$$\frac{1}{E_e} = \frac{1 - v_t^2}{E_t} + \frac{1 - v_s^2}{E_s} \qquad (3.10)$$

where v_s, v_t, E_s and E_t are the Poisson ratios and the moduli of elasticity of the sphere and the table. If the bodies are loaded by a tangential force F_t, the deformation of the bodies is no longer symmetric compared to the Z axis (see figure 3.9b). This results in an additional tangential displacement δ_t.
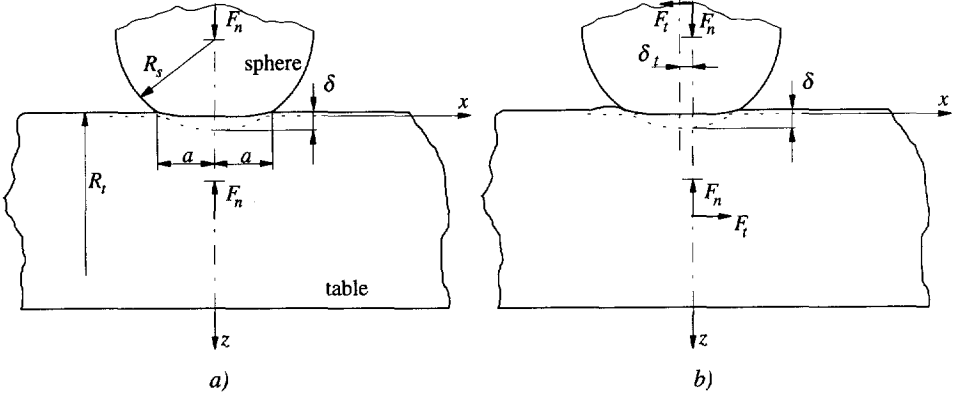
Fig. 3.9   *a) Contact point between a table and a spherical support loaded by a normal force F_n. b) The same contact point loaded both by a normal force F_n and a tangential force F_t.*

For nonconformal contact, the contact area is very small compared to the dimensions of the two bodies ($a \cong 10\text{-}20\ \mu m$). The penetration depth of significant contact stresses into both bodies extends over two up to ten times the size of the contact area. The magnitude of the tangential deformation δ_t is determined by the tangential contact stiffness k_c. As long as the tangential force is smaller than the maximum friction force $\mu_{st} F_n$, there will be no sliding motion. For a contact between a sphere and a flat, δ_t can be calculated by:

$$\delta_t = \frac{3\mu_{st}F_n}{16a}\left(\frac{2-v_s}{G_s} + \frac{2-v_t}{G_t}\right)\left\{1 - \left(1 - \frac{F_t}{\mu_{st}F_n}\right)^{\frac{2}{3}}\right\} \tag{3.11}$$

where G_s and G_t are the shear moduli of elasticity of both bodies in contact. From equation 3.11, the tangential contact stiffness can be calculated:

$$k_c = \frac{dF_t}{d\delta_t} = \frac{8a}{\left(\dfrac{2-v_s}{G_s} + \dfrac{2-v_t}{G_t}\right)}\left(1 - \frac{F_t}{\mu_{st}F_n}\right)^{\frac{1}{3}} \tag{3.12}$$

For small values of F_t, the tangential contact stiffness is independent of the tangential force. The tangential contact stiffness decreases with increasing tangential force, even to zero when $F_t = \mu_{st}F_n$. For a contact between a ruby sphere of 5 mm diameter ($E_s = 3.2 \cdot 10^{11}$ N/m²) and a flat aluminum table, loaded by a normal force of 0.1 N, k_c has a maximum of $1.5 \cdot 10^6$ N/m, according to equation 3.12. The tangential contact stiffness of this configuration was also calculated by means of FEA [67]. According to this finite element analysis, the penetration depth of the stresses corresponded well to the expected theoretical value. The tangential contact stiffness calculated by FEA was $1.9 \cdot 10^6$ N/m, which is in reasonable correspondence with the theoretical value.

In case of a circular contact area, the tangential contact stiffness can be maximized by choosing materials with a high modulus of elasticity, because k_c is proportional to $E_e^{2/3}$. The increase of k_c for a stainless steel table instead of aluminum is a factor of 1.7, resulting in $k_c = 2.5 \cdot 10^6$ N/m. If both the table and the spherical support would be made of ruby, this increase is a factor of two, which is about the maximum value possible for this configuration. It was found by Van der Schaft [68] that the tangential contact stiffness can be increased by applying a noncircular contact area. The tangential contact stiffness can also be increased by increasing the radius of the spherical support or the normal force. However, the stiffness gain is less compared to increasing the equivalent modulus of elasticity, since the contact stiffness is proportional to $R_e^{1/3}$ and $F_n^{1/3}$. Also, a strong increase of R_e does not result in an increase of the contact area defined by a. Moreover, an increase of F_n is unfavorable with regard to the table stability directly after stepping (see chapter 5) and with regard to the minimum driving voltage as will be shown hereafter.

The tangential contact stiffness directly affects the stiffness and hence the resonance frequency of a piezo drive in the direction of motion. In case of a circular contact area, k_c is relatively low compared to, for instance, the stiffness of the shear and tube actuators.

The tangential displacement δ_t influences the performance of piezoelectric drives. As a result of the (fast) drop of the piezo voltage, slip should occur between the supports and the table if the tangential force exceeds the maximum friction force. However, the tangential force deforms the contact area in the direction of motion. It is expected that this deformation keeps up with the fast deformation of the piezo actuator because of the magnitude of the contact stiffness k_c and the extremely low mass which is coupled to the deformation in the contact area. In that way, slip is prevented as long as the piezo deformation is smaller than the maximum tangential deformation. This means that the minimum driving voltage to achieve stepping is not only determined by the maximum friction force, but also by the contact stiffness k_c. In this respect, the double maximum tangential deformation $2\delta_t$ of the contact area was called the *elastic buffer*. For a ruby sphere and a stainless steel table, loaded by a normal force of 0.1 N, the elastic buffer is about 18 nm ($\mu_{st} \approx$ 0.15). Apart from that, the magnitude of the contact stiffness or the elastic buffer says nothing about the minimum achievable step size with a piezo drive.

Surface coatings in piezo drives are used in order to avoid abrasive wear in the contact points. Surface coatings are thin ($\pm$ 1 μm) layers with a high wear resistance. The influence of surface coatings can be estimated by calculating the approach δ in the contact area. For the example mentioned, this approach ranges between 80 and 400 nm for preload forces up to 1 N. This means that contact area deformation is determined by the elastic properties of the coating and the bulk material of the table. Unfortunately, the equivalent modulus of elasticity of a bulk material provided with a surface coating is difficult to determine.

Up to now, the contact area between the spherical support and the table was described on a macroscopic scale. In theories on friction, the macroscopic contact area described by the radius a is called the apparent contact area A_a. On a microscopic scale, the contact area is determined by the sum of the contact areas A_r' between sets of surface asperities of both bodies in contact. This sum is called the real contact area A_r ($A_r = \Sigma A_r'$). The real contact area is smaller than the apparent contact area (see figure 3.10). It is assumed [69] that the maximum friction force that can be applied between the two bodies in contact is proportional to the size of the real contact

area. The size of this real contact area increases with increasing normal load and with increasing (apparent) contact area A_a, which is in accordance with equation 3.12.
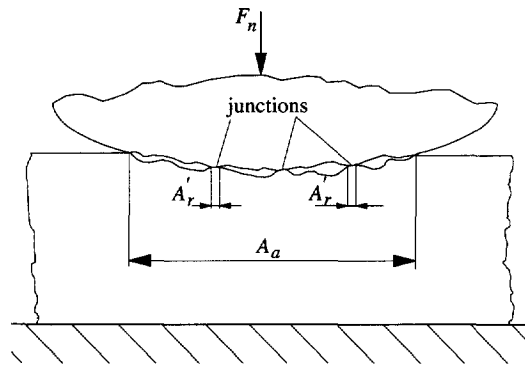
Fig. 3.10   Schematic view of two bodies in contact, showing the apparent area A_a. The real contact area A_r is formed by the sum of the areas A_r' of all the junctions.

The maximum allowable normal load applied at a contact point is determined by the tensile and shear stresses developed in both bodies. These stresses must be lower than the yield stress σ_y in order to avoid plastic deformation. For a contact between a sphere and a flat, the maximum allowable preload force is given by:

$$F_{n_{max}} = 372 \frac{\sigma_y^3 R_e^2}{E_e^2} \tag{3.13}$$

In case of a stainless steel table (σ_y = 400 N/mm^2) and a ruby sphere (σ_y = 2000 N/mm^2), this maximum load is about 8 N. The maximum allowable load is generally not a problem for piezo drives.

From the former overview, it is concluded that the minimum driving voltage for piezo drives is determined by the size of the elastic buffer and by the magnitude of the maximum friction force. The tangential contact stiffness can considerably decrease the stiffness of piezo drives if no special attention is paid to the shape of the contact area between table and supports and the materials in the contact zone.

3.4   Model for inertial sliding motion

The electromechanical models for ISM and IDM are based on the configurations given in figures 3.3 and 3.4. In the analytic models which describe ISM and IDM, some simplifications are used. The base the piezo actuator is attached to and the table are assumed to have infinite stiffness. It is assumed that the piezo actuator and the support elements have the same velocity and are subjected to the same forces. The elastic behavior of the piezo and other elastic elements in the construction can be described by Hooke's law.

The combination of these assumptions implies that the influence of the elastic buffer is not taken into account at this point. Taking the elastic buffer into account would have complicated the analytic model unnecessarily, while its influence can also be estimated by simple calculations. Besides that, it is assumed that the elastic buffer has no direct influence on the basic driving principle. In addition to the analytic model of piezoelectric drives, the elastic buffer is used to explain the minimum piezo voltage required to achieve stepping. In the analytic model derived, the table is assumed to have only one degree of freedom. As rotational ISM can be derived from the same model, only translations are discussed.

3.4.1 Horizontal motion

Figure 3.11 shows a mass-spring-damper representation for ISM in the X direction, where m_t is the mass of the table and m_{ps} is the effective mass of the piezo support. The equations of motion for the table and the piezo support are given by:

$$m_t \ddot{x}_t = F_f \tag{3.14}$$

$$m_{ps} \ddot{x}_{ps} = k\left(\alpha d_x U_p(t) - x_{ps}\right) - c\dot{x}_{ps} - F_f \tag{3.15}$$

where x_t is the table displacement,
x_{ps} is the piezo support displacement,
k is the stiffness of the piezo support,
c is the damping constant of the piezo support,
α is the geometry factor of the piezo, and
d_x is the piezoelectric charge constant valid for piezo displacements in the X direction.

The table is accelerated by friction forces. In case of stick, the coefficient of friction is μ_{st}. In case of slip, the coefficient of friction is μ_d.

The accelerations and the velocities of the piezo support and the table are equal in case of stick, $\ddot{x}_{ps} = \ddot{x}_o$, $\dot{x}_{ps} = \dot{x}_t$, and thus the equation of motion changes into:

$$\ddot{x}_{ps} = \ddot{x}_t = \frac{k\left(\alpha d_x U_p(t) - x_{ps}\right) - c\dot{x}_{ps}}{m_{ps} + m_t} \tag{3.16}$$

where $k\left(\alpha d_x U_p(t) - x_{ps}\right)$ is the piezo hold force. The friction force of the piezo support on the
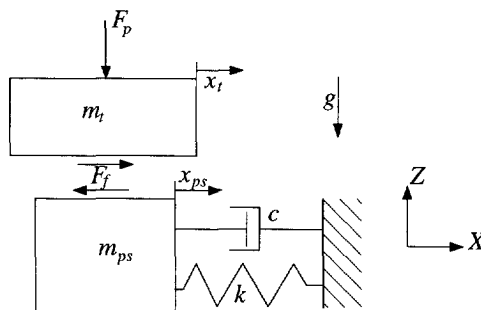
Fig. 3.11   Mass-spring-damper representation used to model ISM in the X direction.

table is given by:

$$F_f = \frac{m_t}{m_{ps} + m_t}\left(k\left(\alpha d_x U_p(t) - x_{ps}\right) - c\dot{x}_{ps}\right)$$
(3.17)

Slip between the supports and the table will occur when the friction force on the table exceeds the maximum friction force:

$$F_{f_{max}} = \mu_{st}\left(m_t g + F_p\right)$$
(3.18)

and thus the condition for slip is:

$$\left|\frac{m_t}{m_{ps} + m_t}\left(k\left(\alpha d_x U_p(t) - x_{ps}\right) - c\dot{x}_{ps}\right)\right| > \mu_{st}\left(m_t g + F_p\right)$$
(3.19)

where F_p is an additional preload force on the table. The direction of the friction force is always opposite to the direction of the table velocity relative to the piezo support velocity.

During the slip period, the friction force on the table is equal to:

$$F_{f_{slip}} = sign[\dot{x}_{ps} - \dot{x}_t]\mu_d\left(m_t g + F_p\right)$$
(3.20)

The table motion can be derived by dividing equation 3.20 by m_t:

$$\ddot{x}_t = sign[\dot{x}_{ps} - \dot{x}_t]\mu_d\left(g + \frac{F_p}{m_t}\right)$$
(3.21)

The equation of motion of the piezo support during slip is given by:

$$\ddot{x}_{ps} = \frac{k\left(\alpha d_x U_p(t) - x_{ps}\right) - c\dot{x}_{ps} - sign[\dot{x}_{ps} - \dot{x}_t]\mu_d\left(m_t g + F_p\right)}{m_{ps}}$$
(3.22)

The displacements of the table and the piezo support during a slip period are calculated by double integration of their accelerations. Sticking occurs when the relative velocity $\dot{x}_{ps} - \dot{x}_t$ between support and table drops back into the deadband defined by the Karnopp model.

The maximum step size that can be achieved by ISM strongly depends on the amplitude of the driving piezo voltage and the dynamic behavior of the system. Especially the dynamic friction force is an important parameter. By means of calculations on the energy in the piezoelectric drive, the maximum ISM step size can be estimated. For relatively large driving voltages, the maximum ISM step size can theoretically be almost as large as $2\alpha d_{ij} U_p$.

At this stage, especially equations 3.18 to 3.20 are important because they indirectly describe the conditions for the design and driving of ISM drives, as will be discussed in section 3.4.3.

3.4.2   Vertical motion

In case of vertical motion parallel to the gravity field, one of the solutions to prevent the table from vertically sliding away is to preload it horizontally. Figure 3.12 shows a mass-spring-damper representation for ISM in the Z direction.
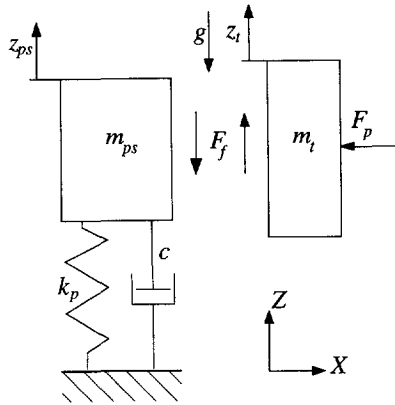
Fig. 3.12   Mass-spring-damper representation used to model ISM in the Z direction.

The equations of motion for the table and the piezo support are given by:

$$m_t \ddot{z}_t = F_f - m_t g \tag{3.23}$$

$$m_{ps} \ddot{z}_{ps} = k\left(\alpha d_z U_p(t) - z_{ps}\right) - c\dot{z}_{ps} - F_f - m_{ps} g \tag{3.24}$$

In case of stick, $\ddot{x}_{ps} = \ddot{x}_t$, $\dot{x}_{ps} = \dot{x}_t$ applies and thus:

$$\ddot{z}_{ps} = \ddot{z}_t = \frac{k\left(\alpha d_z U_p(t) - z_{ps}\right) - c\dot{z}_{ps}}{m_{ps} + m_t} - g \tag{3.25}$$

The friction force of the piezo support on the table is given by:

$$F_f = \frac{m_t}{m_{ps} + m_t}\left(k\left(\alpha d_z U_p(t) - z_{ps}\right) - c\dot{z}_{ps}\right) \tag{3.26}$$

and the condition for slip is:

$$\left|\frac{m_t}{m_{ps} + m_t}\left(k\left(\alpha d_z U_p(t) - z_{ps}\right) - c\dot{z}_{ps}\right)\right| > F_{f_{max}} = \mu_{st} F_p \tag{3.27}$$

During the slip period, the table motion can be written as:

$$\ddot{z}_t = sign[\dot{z}_{ps} - \dot{z}_t]\mu_d \frac{F_p}{m_t} - g \tag{3.28}$$

The piezo support equation of motion during slip is given by:

$$\ddot{z}_{ps} = \frac{k\left(\alpha d_z U_p(t) - z_{ps}\right) - c\dot{z}_{ps} - sign[\dot{z}_{ps} - \dot{z}_t]\mu_d F_p}{m_{ps}} - g \tag{3.29}$$

3.4.3   Design considerations

If it is assumed that the ISM step size is proportional to and of the same order as the maximum piezo deformation caused by the drive signal, the step size can be minimized by minimizing the amplitude of the drive signal $U_p(t)$ at which there is no slip between the table and the piezo support. Apart from minimizing the step size, it is important to minimize the applied piezo voltage for two other reasons: the amount of piezo drift is proportional to the amplitude of the driving voltage and low driving voltages require cheaper driving electronics.

The lowest obtainable driving voltage determined by the elastic buffer $2\delta_t$ is approximated by:

$$U_{p_{min}} = \frac{\delta_t}{\alpha d_x} \qquad (3.30)$$

In case of the example given in section 3.3.4, where the elastic buffer $2\delta_t$ is 18 nm, and assuming the piezo actuator sensitivity to be equal to 1 nm/V, the minimum driving voltage $U_{p_{min}}$ is 9 V.

In practice, however, the minimum driving voltage is also determined by the piezo actuator, the driving electronics, the ratio of the table mass and the effective mass of the piezo support, and the preload force as is shown by equation 3.19. If damping is neglected, this equation changes into:

$$\left| \frac{m_t}{m_{ps} + m_t} k \left(\alpha d_x U_p(t) - x_{ps} \right) \right| > \mu_{st} \left(m_t g + F_p \right) \qquad (3.31)$$

The factor $\left| \alpha d_x U_p(t) - x_{ps} \right|$ gives the difference between the desired and the actual position of the piezo support. It determines, in combination with the piezo support stiffness k, the piezo force on the table. The magnitude of this factor depends on the slew rate of the driving electronics and the resonance frequency of the piezo support. The amplitude of the driving voltage U_p can be minimized by maximizing the piezo sensitivity αd_x, by maximizing the factor $m_t k / (m_{ps} + m_t)$, by minimizing the coefficient of static friction, and by avoiding preloading. This implies that the piezo support mass relative to the table mass should be minimized. In combination with the maximization of the piezo support stiffness, this means that the resonance frequency of the piezo support is maximized.

The minimum driving voltage required according to equation 3.31 can be calculated as follows. The ratio of the time needed by the driving electronics to make a voltage step and the response time needed by the piezo support to reach the corresponding position determines the maximum of the factor $\left| \alpha d_x U_p(t) - x_{ps} \right|$. This ratio can be estimated from the slew rate of the driving electronics and from the step response of a mass spring damper system with relative damping β and resonance frequency f_0. With a slew rate of 200 V/μs, with $\beta = 0.03$ and with f_0 ranging from 10 to 30 kHz, $\left| \alpha d_x U_p(t) - x_{ps} \right|$ can be approximated by $\alpha d_x U_{p_{min}}$. If the table is not preloaded by an additional preload force F_p, the minimum piezo voltage to achieve stepping is then:

$$U_{p_{min}} = \frac{\mu_{st} g (m_{ps} + m_t)}{k \alpha d_x} \qquad (3.32)$$

Using the example given in section 3.3.4 (the table is supported by three piezo supports) and using real values for the parameters in equation 3.32 ($\mu_{st} = 0.15$, $m_{ps} = 5 \cdot 10^{-4}$ kg, $m_t = 3 \cdot 10^{-2}$ kg, $k = 1 \cdot 10^7$ N/m ($f_0 = 20$ kHz)), $U_{p_{min}}$ is 4.7 V. This value should be compared to the minimum

value determined by the elastic buffer given in equation 3.30. This means that, in this case, the minimum driving voltage would be determined by the elastic buffer.

Calculation of the minimum driving voltage for ISM parallel to the gravity field is not completely similar to motion perpendicular to the gravity field. The main difference is that the preload force F_p cannot be zero, but should at least be equal to $m_t g / \mu_{st}$. In order to accelerate the table upwards, the preload force must be even larger: $F_p = \gamma m_t g / \mu_{st}$, with $\gamma > 1$. A practical value for γ is 2.

Although equations 3.26 and 3.27 indicate otherwise, in case of ISM parallel to the gravity field, one should distinguish between stepping upwards and downwards. The increase of the normal force on the contact area between table and piezo support compared to motion perpendicular to the gravity field results in a much larger elastic buffer. Another difference is the continuously present tangential deformation at the contact points as a result of the gravity force on the table. This is illustrated in figure 3.13. For upward motion, the piezo actuator (which is in this case connected to the support) is fast retracted downwards. In that case, the piezo actuator must overcome the initial tangential deformation δ_i and half the elastic buffer δ_t in order to obtain slip. For downward motion, the piezo actuator must overcome the difference between half the elastic buffer and the initial tangential deformation δ_i. This implies a difference in the minimum driving voltages for upward and downward motion.
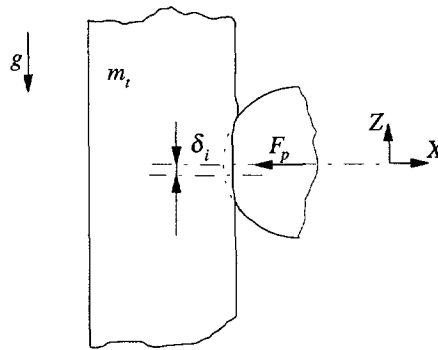
Fig. 3.13   *The initial tangential deformation δ_i and the elastic buffer $2\delta_t$ cause a difference in the minimum piezo voltage needed for stepping upwards and downwards.*

The theoretical minimum piezo voltage for upward motion can thus be estimated by:

$$U_{p_{min}}^{up} = \frac{\delta_t + \delta_i}{\alpha d_x} \tag{3.33}$$

and the theoretical minimum piezo voltage for downward motion by:

$$U_{p_{min}}^{down} = \frac{\delta_t - \delta_i}{\alpha d_x} \tag{3.34}$$

In order to minimize these minimum driving voltages, the elastic buffer should be minimized. The best way to obtain this is to minimize the table mass. If the table is preloaded by four piezo

supports and if the table mass m_t is $3 \cdot 10^{-2}$ kg, the minimum preload force F_p is 1 N ($\mu_{st} = 0.15$, $\gamma = 2$). If a ruby sphere and a stainless steel table are applied, the elastic buffer $2\delta_t$ can be calculated from equations 3.8 up to 3.11 to be 82 nm. The initial tangential deformation δ_t is 15 nm. This means that the minimum voltage to move upwards would be 67 V, while the minimum voltage to move downwards would be 26 V. This is both clearly larger than the minimum driving voltages for horizontal motion.

The minimum driving voltage is also determined by the condition for slip. If damping is neglected, equation 3.27 can be rewritten into:

$$\left| \frac{m_t}{m_{ps} + m_t} k \left(\alpha d_z U_p(t) - z_{ps} \right) \right| > \mu_{st} F_p \tag{3.35}$$

It is trivial that it is not useful to lower the static coefficient of friction or the preload force in order to minimize the minimum driving voltage. Compared to motion perpendicular to the gravity field, the piezo force must be about one order of magnitude higher in order to cause slip ($\mu_{st} \sim 0.15$). From equation 3.35, the minimum driving voltage can be written as:

$$U_{p_{min}} = \frac{\gamma \left(m_{ps} + m_t \right) g}{k \alpha d_z} \tag{3.36}$$

For the example defined before, the minimum driving voltage is 60 V, which would be almost equal to the influence of the elastic buffer for upward motion.

3.5   Model for impact drive motion

3.5.1   Horizontal motion

Figure 3.14 shows the schematic setup for IDM in the X direction, where m_t is the table mass, m_p the effective mass of the piezo, and m_i the impact mass.
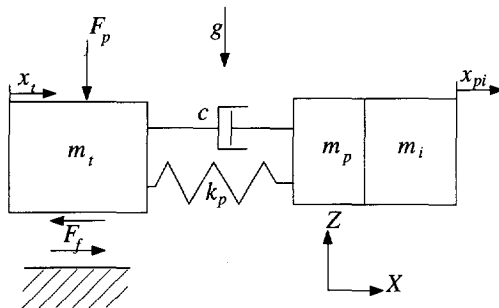
Fig. 3.14   Mass-spring-damper representation for IDM in the X direction.

The equations of motion for the table and the impact mass are given by:

$$m_t\ddot{x}_t = k\left(x_{pi} - x_t - \alpha d_x U_p(t)\right) + c\left(\dot{x}_{pi} - \dot{x}_t\right) - F_f \tag{3.37}$$

$$\left(m_p + m_i\right)\ddot{x}_{pi} = -k\left(x_{pi} - x_t - \alpha d_x U_p(t)\right) - c\left(\dot{x}_{pi} - \dot{x}_t\right) \tag{3.38}$$

If there is no relative motion between the table and the base ($\ddot{x}_t = \dot{x}_t = x = 0$), the friction force between them is given by:

$$F_f = \left(k\left(x_{pi} - \alpha d_x U_p(t)\right) + c\dot{x}_{pi}\right) \tag{3.39}$$

Slip between the table and the base will occur when the impact force on the table exceeds the maximum friction force $F_{f_{max}}$:

$$F_{f_{max}} = \mu_{st}\left(\left(m_t + m_p + m_i\right)g + F_p\right) \tag{3.40}$$

and thus the condition for slip is:

$$\left|\left(k\left(x_{pi} - \alpha d_x U_p(t)\right) + c\dot{x}_{pi}\right)\right| > \mu_{st}\left(\left(m_t + m_p + m_i\right)g + F_p\right) \tag{3.41}$$

where F_p is an additional preload force on the table. During slip, the table motion is described by:

$$m_t\ddot{x}_t = k\left(x_{pi} - x_t - \alpha d_x U_p(t)\right) + c\left(\dot{x}_{pi} - \dot{x}_t\right) - sign[\dot{x}_t]\mu_d\left(\left(m_t + m_p + m_i\right)g + F_p\right) \tag{3.42}$$

When the influence of the friction force is neglected, the maximum step size x for a voltage step U_p can be estimated by using the impulse equation $m_t\dot{x}_t = (m_p + m_i)\dot{x}_{pi}$ and the relation $(\dot{x}_t + \dot{x}_{pi})t = \alpha d_x U_p(t)$ as follows:

$$x = \alpha d_x U_p\left(\frac{m_p + m_i}{m_t + m_p + m_i}\right) \tag{3.43}$$

3.5.2 Vertical motion

Figure 3.15 shows the schematic setup for IDM in the Z direction.

The equations of motion for the table and the piezo support are given by:

$$m_t\ddot{z}_t = k\left(z_{pi} - z_t - \alpha d_z U_p(t)\right) + c\left(\dot{z}_{pi} - z_t\right) - F_f - \left(m_t + m_p + m_i\right)g \tag{3.44}$$

$$\left(m_p + m_i\right)\ddot{z}_{pi} = -k\left(z_{pi} - z_t - \alpha d_z U_p(t)\right) - c\left(\dot{z}_{pi} - z_t\right) - \left(m_p + m_i\right)g \tag{3.45}$$

Slip between the table support and the base will occur when the impact force on the table exceeds the maximum friction force $\mu_{st}F_p$:

$$\left|\left(k\left(z_{pi} - \alpha d_z U_p(t)\right) + c\dot{z}_{pi}\right) - \left(m_t + m_p + m_i\right)g\right| > \mu_{st}F_p \tag{3.46}$$

During the slip period, the table motion is described by:

$$m_t\ddot{z}_t = k\left(z_{pi} - z_t - \alpha d_z U_p(t)\right) + c\left(\dot{z}_{pi} - z_t\right) - sign[\dot{z}_t]\mu_d F_p - \left(m_t + m_p + m_i\right)g \tag{3.47}$$
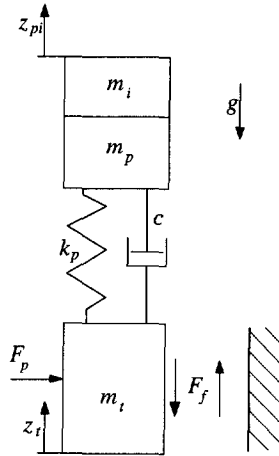
Fig. 3.15   Mass-spring-damper representation for IDM in the Z direction.

3.5.3   Design considerations

For horizontal motion, the minimum step size and the minimum piezo voltage of an IDM drive are determined by the elastic buffer, the piezo actuator, the drive electronics, the masses involved, and the preload force. As far as the elastic buffer is concerned, the minimum driving voltage can be estimated from equation 3.43:

$$U_{p_{min}} = \frac{m_t + m_p + m_i}{m_p + m_i} \frac{\delta_t}{\alpha d_x} \tag{3.48}$$

The minimum driving voltage is also determined by the factor $k(x_{pi} - \alpha d_x U_p(t))$, by the mass of the impact drive $(m_t + m_p + m_i)$ and by the preload force. Like for ISM, the factor $k(x_{pi} - \alpha d_x U_p(t))$ should be maximized, which implies a high slew rate of the driving electronics and a high stiffness k. In combination with a low impact drive mass, this implies a high resonance frequency of the system of the impact mass, the piezo and the table mass in the direction of motion. The amplitude of the piezo voltage $U_p(t)$ should be minimized. This is achieved by maximizing the piezo sensitivity αd_x and the resonance frequency of the piezo support. Preload forces should be as low as possible. In order to optimize the stepping efficiency, the ratio of the step size and the maximum piezo deformation, the table mass should be minimized relative to the impact mass.

Like for ISM, the minimum driving voltage is different for upward and downward motion. In order to minimize these minimum driving voltages, the impact drive mass should be minimized. At the same time, this minimizes the required preload force and the elastic buffer.

3.6   Frictional stepping motion

Compared to ISM and IDM, FSM is relatively new. It was used in the research group of Güntherodt as an approach mechanism in a low temperature STM [45] and it was applied in a low temperature STM by Altfeder and Volodin [61].

The important advantage of FSM over ISM and IDM is that the ratio of the masses involved does not influence its performance. In theory, infinitely small masses can be moved by FSM. This is especially advantageous in low temperature applications where the piezo sensitivity is lower and the friction forces are often difficult to adjust. Another advantage is that FSM does not need high piezo accelerations to achieve stepping. This is advantageous with regard to the repression of several modes of oscillation.

The schematic model of the ISM drive given in figures 3.11 and 3.12 also applies for FSM devices, although the number of piezo actuators may differ. It is expected that the performance of FSM drives with regard to the minimum drive voltage and the minimum step size does not significantly differ from the performance of ISM drives. In case of horizontal motion, the piezo force must still be larger than the maximum static friction force in order to cause slip between the table and the piezo support. Moreover, the piezo voltage must be large enough to overcome the elastic buffer. The same applies for vertical motion. Of course, the preload force and hence the elastic buffer can be much smaller in FSM drives due to the possible low table mass.

3.7   Drive signals

In order to achieve ISM or IDM, sudden changes in the voltage change rate must be a part of the drive signal. A possible drive signal is a sawtooth. Sometimes, the sudden change in the voltage change rate at the end of the steep voltage drop is considered as a disadvantage of a sawtooth drive signal (see figure 3.16a). This second sudden direction change of the sawtooth signal is sometimes thought to cause a large acceleration on the piezo actuator, influencing the ISM or IDM step size negatively. This is, however, only partly true. The acceleration of the piezo actuator is determined by the difference between the actual piezo actuator deformation and the deformation according to the applied piezo voltage. This difference has a large maximum directly after the steep voltage drop. In the period between two steep voltage drops, this difference is always smaller and thus the piezo acceleration has its maximum directly after the voltage drop. Nevertheless, the acceleration on the piezo at the start of the voltage slope can cause "negative" slip between the piezo support and the table, especially where upward motion is concerned, in that way decreasing the step size. This negative slip may be avoided by applying a drive signal with a smooth or rounded shape at the end of the voltage drop. However, the piezo acceleration to overcome the maximum friction force must still be achieved by a steep voltage drop. Any addition to

the simple shape of a sawtooth signal to avoid negative slip therefore causes an increase of the minimum driving voltage.
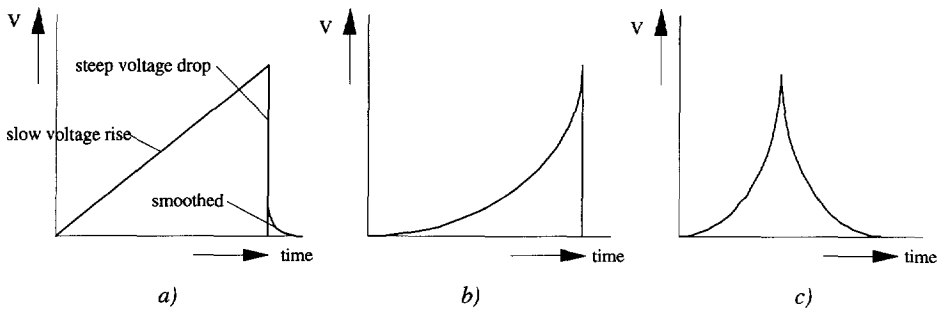
Fig. 3.16   Example of three different drive signals: a) sawtooth, b) parabola and c) cycloid.

Instead of the linear slope of the sawtooth, Wildoër [70] proposed a voltage increase proportional with time squared (see figure 3.16b). In that way, the piezo support and the table velocity can be maximized before the steep voltage drop. In some applications, especially for motion parallel to the gravity field, this may decrease the minimum driving voltage, although the elastic buffer must also be taken into account. Compared to applying a sawtooth voltage, it will certainly affect the step size, but the result completely depends on the system dynamics. An example of another drive signal was given by Renner [54] and later also by Blackford [71]. They used cycloid drive signals to move parallel to the gravity field. In order to get the maximum result of this type of signals, it is important to use smooth, analog drive signals. In that case, low drive voltages (< 30 V_{pp}) may become possible, especially for translations parallel to the gravity field if the elastic buffer can be made low enough.

In case of FSM, steep voltage drops are not necessary. However, in order to obtain a reasonable table velocity, the sequential retraction of the piezo actuators must be fast. The time between mutual retraction of the piezo actuators is probably limited by the resonance frequency of the FSM drive.

The influence of the drive signal shapes was not investigated extensively during this research.

3.8   Piezo rotors

Since the development of the SPM, not many compact, vacuum compatible piezo drives for tilting have been reported. Hatsuzawa [52] and Tojo [48] reported an Inchworm-like piezo drive for use in a scanning electron microscope and in lithography systems. Higuchi *et al.* [72] reported an impact driven robot with six degrees of freedom. All these *piezo rotors* have the disadvantage of being relatively large. Only Howald [59] has presented a compact piezo rotor. In this section, a couple of compact piezo rotor configurations will be described, which are originally based on ISM and IDM drives.

The first piezo rotor configuration is based on the rotation of a sphere by means of ISM with six shear piezo actuators or three piezo tubes and was developed by Howald (see figure 3.17). This piezo rotor configuration has three degrees of freedom and unlimited strokes. However, when applied in a TEM, the strokes will be limited by the fact that the electron beam must pass the sphere via a hole in the sphere.
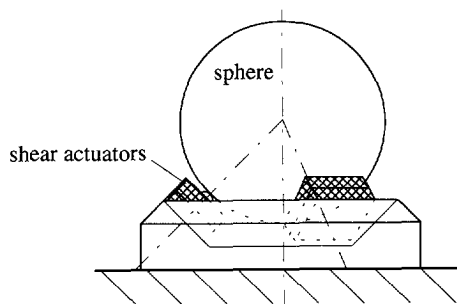
Fig. 3.17   Piezo rotor configuration with three degrees of freedom and unlimited strokes (from [59]).

The second piezo rotor configuration was developed during this research. It has only a single degree of freedom (see figure 3.18). The piezo rotor configuration is based on an ISM drive with shear piezo actuators. A two degrees of freedom piezo rotor can simply be obtained by stacking two of these piezo rotors.
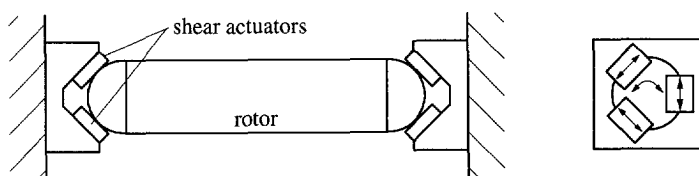
Fig. 3.18   ISM driven piezo rotor configuration with one degree of freedom and unlimited stroke.

A proposal for another piezo rotor configuration is given in figure 3.19. This piezo rotor has one degree of freedom, unlimited stroke and is based on an IDM drive.
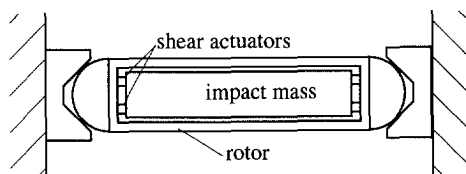
Fig. 3.19   IDM driven piezo rotor configuration with one degree of freedom and unlimited stroke.

A fourth piezo rotor configuration is based on an ISM drive (see figure 3.20). The rotor is driven by a shear piezo actuator and a leaf spring, which is pressed against the rotor. This configuration

was successfully applied in a double tilt holder of a Philips TEM by Van Voorst [73]. This implies that the piezo rotor was integrated in a volume of 6 x 3 x 2 mm^3.
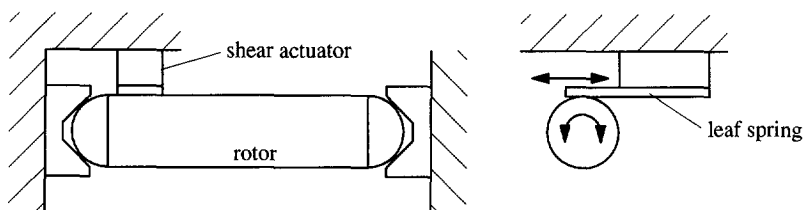
Fig. 3.20   ISM driven piezo rotor configuration with one degree of freedom and unlimited stroke.

3.9   Contact zone materials

An important problem that must be dealt with in piezo drives is wear in the contact zone between the table and the support(s). Wear can diminish the piezo drive performance and even prevent slip between the table and the support(s) to occur. Besides that, abrasive particles must be avoided in vacuum. The most common way to solve this problem is to use wear resistant coatings. It was assumed that the choice of contact zone materials for HV and UHV applications of nano stages is not a bottle neck for their design. This was based on the experiment with the TEM nano stage described in section 6.5 and on the experiments of others [70,74,75].

During this research, the combination of a ruby bulk material and a thin coating of either TiCN on stainless steel or aluminum oxide on aluminum was used to avoid wear. A general rule that can be applied for the materials choice in the contact zone is that a combination of a hard and stiff bulk ceramic against a thin layer with a high wear-resistance on a bulk material with a lower modulus of elasticity than the bulk ceramic suits the application in piezo drives very well. The layer material should preferably be different from the bulk ceramic material in order to prevent vacuum welding in the contact areas. The route to choose the optimum material combination for the contact zone between the table and its support has not been extensively investigated.

3.10   Scaling laws for piezo drives

Description of scaling laws for piezo drives is interesting with regard to low volume applications of nano stages like in a TEM. By means of scaling laws, the dependence of various physical magnitudes on the size of a system, defined by a length parameter L, can be examined, assuming that all shape parameters and material properties are constant. For a description of the scaling laws for an electromechanical system like a piezo drive, it was chosen to keep the stresses and the field strengths in the system constant. This implies scale independent elastic deformation and hence scale independent shape [76].

Given constantness of stress and material strength, the strength of a structure and the force it exerts scale with its cross-sectional area and hence with L^2. This implies that shear and bending

stiffness are proportional to L and that deformation is proportional to L. This is confirmed by considering the piezo deformation at constant mechanical stress described by equation 2.6. At constant electric field and for a constant electric charge constant, the piezo deformation scales with L. The assumption of constant density makes mass scale with volume (L^3). Application of Newton's law shows that acceleration is proportional to L^{-1}. The same applies for frequency, because it is proportional to the square root of the ratio of stiffness and mass.

Considering these scaling laws and the order of magnitude of general piezo drive dimensions, it is expected that downscaling the dimensions (L) with one order of magnitude will not prevent a piezo drive from working. It is true that the maximum allowable driving voltage is proportional to the piezo dimensions, but so is the minimum driving voltage. The latter is caused by a decrease of the elastic buffer which is proportional to L, the increase of the resonance frequency (L^{-1}), and the decrease of the friction forces (L^{-2}).

In general, scaling laws must be applied with care to friction forces, especially where the influence of lubricant layers is concerned (for instance water layers). When the driving speed is constant, shear stresses in these lubricant layers depend on the layer thickness. In case of downscaling, the question arises what influence this layer will have. Another point of attention concerns the wear-resistant layers. The equivalent modulus of elasticity at the surface approaches the modulus of elasticity of the bulk material if the thickness of the layer decreases. Besides that, the wear life of a wear-resistant layer is proportional to its thickness if the erosion rate is assumed to be constant.

3.11   Concluding remarks

Because of the large number of different applications and the large number of different configurations of CSM, ISM, IDM and FSM piezo drives, a best drive mechanism does not exist. Each new application of piezo drives requires consideration of all the advantages and disadvantages of the available principles before a choice is made. This chapter is a guide to find the best drive mechanism for a certain application and a help to optimize the performance of a piezo drive. In this respect, it should be concluded that the choice for a drive cannot be based just on its positioning performance. This is due to the fact that all four drive mechanisms offer a sufficiently large ratio of stroke and displacement resolution, the minimum table step size that can be obtained is in the order of a few nanometer for all four drives, and they all offer low driving voltages for motion perpendicular to gravity.

In general, it can be stated that during the design process and during actual positioning one will have to deal with the opposite interests between table velocity and open loop stability, between minimum driving voltage and tangential contact stiffness, and between a high piezo sensitivity and a high resonance frequency of a piezo drive. It should further be noted that the elastic buffer and hence the contact stiffness seem to have a considerable influence on the performance of piezo drives. The tangential contact stiffness should preferably be maximized by maximizing the equivalent modulus of elasticity of the contact area, by optimizing the shape of the contact area,

not by maximizing the preload force. The elastic buffer determines, among other things, the minimum driving voltage of a piezo drive. This especially applies for motion parallel to gravity. In order to minimize the minimum driving voltage, the preload force and thus the mass of the table should be minimized. Finally, it seems that piezo drive dimensions can be scaled down one order of magnitude without seriously affecting the performance of the drives.

The main advantage of an FSM drive compared to an ISM drive is the possibility to move tables with a very low mass. This is advantageous with regard to the first resonance frequency of the drive and with regard to table stability directly after stepping. A second advantage is the possibility to drive the table with low dynamic forces compared to an ISM drive. This may be advantageous with regard to the stability of the table after positioning and it was claimed to be advantageous with regard to positioning at temperatures down to 0.4 K [61]. When an FSM drive is used for positioning in the XY plane, it generally needs more piezo actuators and/or preloaded supports, compared to an ISM drive in order to avoid large parasitic motion. This may have a negative effect on the table stability after stepping.

The main advantage of an IDM drive over an ISM or a FSM drive is that piezo actuator drift occurring after stepping does not influence the table position stability relative to its supports. This is advantageous with regard to the table stability after stepping. Another advantage over the ISM drive is that a high ratio of the inertia of the table and the impact mass is no condition for stepping to occur. This means that the sum of the table mass, the impact mass and the piezo mass can be relatively low, which can result in a relatively high first resonance frequency, provided that the stiffness of the IDM drive is not limited by the contact stiffness. A disadvantage of an IDM drive is that stability control of the table at the picometer level relative to its base is not possible without stacking an additional drive on the table. Of course, the impact mass can also be used as the table, thus solving the latter problem. Another disadvantage of the IDM drive is the presence of the impact mass which must be connected to the table. It consumes a certain amount of space. This complicates the design of an IDM drive. Moreover, an IDM drive needs electrical connections to the table in order to drive the piezo actuator. This may cause stability problems when the mass of the IDM drive is low.

The main advantage of an ISM drive is its potential compact configuration as a result of a minimum number of driver elements. The major disadvantage of an ISM drive is the need for a relatively large ratio of the table inertia and the piezo inertia.

4 Capacitive displacement transducers

4.1 Introduction

Accurate positioning of objects at the nanometer level and beyond requires sophisticated displacement control. A major part of displacement control is the determination of the object's position or displacement relative to its position reference by means of displacement transducers. Nanopositioning of objects over millimeter strokes requires transducers with nanometer displacement resolution and a ratio of range and resolution of 10^6. In order to verify object stability, displacement transducers with picometer resolution over submicrometer ranges are required. One should also distinguish between displacement transducers for translation and rotation. Although other transducers may perform better on some of the required transducer specifications, in this experimental phase, capacitive displacement transducers were chosen for all the tasks. Capacitive transducers have excellent measurement properties, have a simple configuration and have an enormous flexibility in both design and application.

Various configurations of capacitive displacement transducers and a variety of capacitive measurement electronics have been developed and described in the literature. It strongly depends on the application of the nano stage which capacitive transducer configuration is the best. Therefore, it is useful to compare these configurations with regard to transducer sensitivity and with regard to their ratio of range and resolution and their sensitivity to parasitic motion as a function of their size. This sensitivity to parasitic motion should preferably be low for the sake of the controllability of the position of the nano stage table in different degrees of freedom. The size of TEM nano stage transducers should be minimized. After a comparison of different transducer configurations in section 4.3, section 4.4 discusses the electronic capacitance measurement system used. Section 4.5 discusses the transducer stability. In order to understand the working principle of capacitive displacement transducers, the concept of capacitance will be explained first.

4.2 The concept of capacitance

The original definition of capacitance was given in 1873 by Maxwell [77]. However, it was only in the second half of the 20$^{\text{th}}$ century that, as a result of a better understanding of the principles of

guarding, reliable and accurate capacitive transducers could be designed. Especially the contributions of Jones and Richards [78] and Heerens [79] gave rise to experimental and industrial applications of capacitive transducers. The basic theory on capacitance and the properties of different capacitive transducer configurations have been extensively discussed by Heerens and will therefore not be repeated here. Only those properties which are of specific importance to the use of capacitive transducers in nano stages will be shortly explained.

By definition, the capacitances between different electrodes of a (multi-terminal) electrode configuration are determined by the electrode existence and geometry, not by their potential. This means that the capacitance of homogeneously filled capacitors depends on the size and the shape of the electrodes, on their relative positions and on the medium in between the electrodes. Therefore, the capacitance C can be described as:

$$C = \varepsilon \, f(G) \tag{4.1}$$

where ε is the dielectric permittivity of the medium in between the electrodes of the capacitor and $f(G)$ is a geometry factor which depends on the size and shape of the electrodes and their relative positions. The permittivity of the medium can be written as:

$$\varepsilon = \varepsilon_0 \varepsilon_r \tag{4.2}$$

where ε_0 is the permittivity of vacuum, a physical constant ($\varepsilon_0 = 8.854187817 \cdot 10^{-12}$ F/m), and ε_r is the relative permittivity of the medium filling the capacitor. Capacitive transducers can measure capacitance changes as a result of changes in a variety of parameters, either mechanical, chemical or physical. In this research, the parameter of interest is the displacement or the position of an object relative to its position reference. This implies variation of the geometry factor $f(G)$.

4.3   Transducer configurations

4.3.1   The parallel plate transducer

Figure 4.1 shows the electrode configuration of a parallel plate displacement transducer. The capacitor is formed by both shaded electrodes, which are surrounded by guard electrodes. The electrodes are positioned at a nominal distance d_0, having an overlapping area $A = 2a \cdot 2b$. The capacitance of the parallel plate capacitor can be calculated exactly by [79]:

$$C = \frac{2\varepsilon_0 \varepsilon_r b}{\pi} \cdot ln\left(\frac{cosh\left(\frac{\pi}{2d_0}(x_3 - x_0) \right) \cdot cosh\left(\frac{\pi}{2d_0}(x_2 - x_1) \right)}{cosh\left(\frac{\pi}{2d_0}(x_2 - x_0) \right) \cdot cosh\left(\frac{\pi}{2d_0}(x_3 - x_1) \right)} \right) \tag{4.3}$$

assuming that the dimension of the lower electrode in the Y direction as well as the dimensions of the guard electrodes in the Y direction go to ∞ and to $-\infty$. If the dimensions of the guard electrodes in the X direction go to ∞ and to $-\infty$, the capacitance of the parallel plate capacitor can be exactly determined by:

$$C = \varepsilon_0 \varepsilon_r \frac{A}{d_0} \qquad (4.4)$$
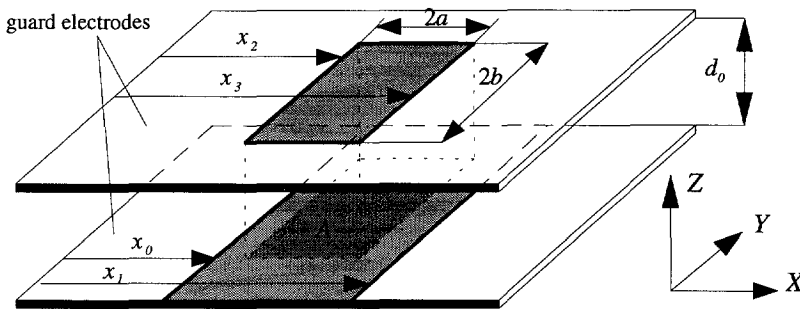
Fig. 4.1   Basic electrode configuration of a parallel plate capacitor surrounded by guard electrodes.

In practice, the electrode dimensions in both the X and the Y direction will be limited. It means that fringe effects, which occur at the borders of the electrodes have to be taken into account. Fringe effects are side effects caused by the limited electrode dimensions and the shape of the electrodes at their borders which directly influence the capacitance. The influence of fringe effects can be calculated analytically in one direction as was demonstrated by equation 4.3. Calculation of their influence in both the X and the Y direction simultaneously is extremely complex. Comparison of equations 4.3 and 4.4 indicates the influence of finite electrode dimensions in the X direction on the predictability of the capacitance. The extension of the electrodes in the Y direction is than still infinite, but it is assumed that the effect of electrode limitations in the Y direction are similar to the effect in the X direction. For the TEM nano stage transducers, the approximation of the transducer capacitance by equation 4.4 is mostly sufficient.

When comparing different capacitive displacement transducer configurations, one has to consider several design parameters: the size of the transducer and the space available in the application, the influence of parasitic motion on the transducer accuracy, the measuring bandwidth, the transducer range and resolution, the transducer sensitivity, and the medium filling the capacitor. The maximum available space for the transducer and its guard electrodes determines the maximum overlapping electrode area A. The measuring bandwidth is determined by a low pass filter at the detector output. The output noise of the capacitance detector determines the transducer resolution ΔC. The maximum ratio of range and resolution is determined by the maximum output voltage of the detector.

As the geometry factor $f(G)$ is uniquely defined by the electrode dimensions and the distance between them, a capacitive transducer is very well suitable to obtain nanopositioning if the mechanical and the electronical stability of the transducer is sufficient, if the mechanical stability of the position reference is sufficient, and if the dielectric permittivity of the medium filling the capacitor is constant. In many applications where capacitive displacement transducers were used, it was calculated or assumed that the mechanical stability of the capacitor plates was sufficient to obtain nanometer positioning repeatability [80,81,82]. However, in order to obtain position control or verify position stability at the picometer level this plate stability becomes much more critical.

For the measurement of displacements, there are two principal ways to achieve capacitance changes. The capacitance of a so called *plate-distance* transducer is changed by changing d_0. The capacitance of a so called *in-plane* transducer is changed by changing the overlapping area A. Recently, Holman [29] extensively discussed various configurations of both the in-plane and the plate-distance transducer and their characteristics with regard to application in a calibrated STM. Nevertheless, it is important to discuss the (dis)advantages of in-plane and plate-distance transducers from the viewpoint of the TEM application because there are many differences between these two applications.

As a result of the two principal ways to achieve capacitance changes, capacitive displacement transducers suffer from the influence of parasitic motion. The relative capacitance change of a transducer as a function of the parasitic motion is called crosstalk. The crosstalk δ can therefore be written as:

$$\delta = \frac{C(x,y,z,\phi_x,\phi_y) - C(x)}{C(x)} \tag{4.5}$$

For a number of configurations, the amount of crosstalk is determined by the size of the guard electrodes. In order to calculate the influence of the guard electrode size on the transducer crosstalk, equation 4.3 can be used.

In order to make a comparison between the two transducer configurations with regard to *translations*, the following design parameters are used as an example of the TEM application:

- the transducer range in the X, the Y and the Z direction is 1 mm,
- the required displacement resolution is 1 nm,
- the resolution of the measurement electronics ΔC is $1 \cdot 10^{-6}$ pF (at 2 Hz bandwidth),
- the maximum allowable capacitance change due to crosstalk is 1%,
- the minimum plate distance, as a result of production tolerances, is 0.1 mm, and
- the maximum plate dimensions are 10x10 mm^2.

In case of stability control at the picometer level, the minimum nominal plate distance may be reduced in order to gain resolution, but this will certainly complicate plate alignment and will make strict demands on in plane translations. The target resolution for control or verification of the position stability is 10 pm.

4.3.2 Plate-distance transducers

4.3.2.1 Single plate-distance transducers

Figure 4.2 shows the general configuration of a single plate-distance capacitive displacement transducer. When $2e$ is the width of the infinite strip of the lower electrode and when the upper electrode is placed symmetrically relative to the lower strip electrode, the capacitance of the plate-distance transducer can be rewritten from equation 4.3 as:

$$C_{pd} = \frac{4\varepsilon_0\varepsilon_r b}{\pi} \cdot ln\left(\frac{cosh\left(\frac{\pi}{2d_0}(e+a)\right)}{cosh\left(\frac{\pi}{2d_0}(e-a)\right)}\right) \tag{4.6}$$

If z is the displacement in the Z direction and d_0 is the plate distance when $z = 0$, the capacitance of the single plate-distance transducer can be approximated by:

$$C_{pd} = 4\varepsilon_0\varepsilon_r \frac{ab}{d_0 + z} = \varepsilon_0\varepsilon_r \frac{A}{d_0 + z} \tag{4.7}$$

The accuracy of this approximation depends on the electrode width $2e$. For instance, if $e - a = 2d_0$ and $a / d_0 = 1$, the error of this approximation is 0.06%.
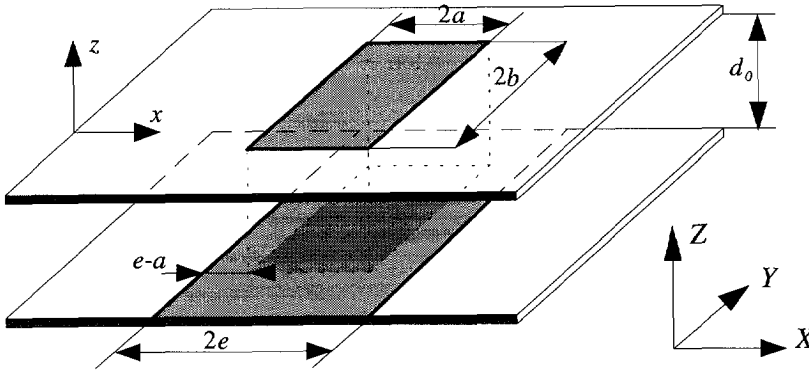
Fig. 4.2 Configuration of the single plate-distance transducer including its relevant dimensional parameters.

The sensitivity of a single plate-distance transducer can be approximated by:

$$\frac{dC_{pd}}{dz} = -\varepsilon_0\varepsilon_r \frac{A}{(d_0 + z)^2} \tag{4.8}$$

Both equations 4.7 and 4.8 show that the relation between the displacement z and the transducer capacitance is nonlinear. This is an important disadvantage of this transducer type. Also, the transducer sensitivity decreases with increasing plate distance.

According to the design parameters of the example, the nominal plate distance d_0, which is the plate distance at $z = 0$, has a minimum of half the required transducer range plus the minimum achievable plate distance of 0.1 mm resulting in $d_0 = 0.6$ mm. If the overlapping area A is maximized to 100 mm^2, the transducer sensitivity at $z = 0$ is approximately $2.4 \cdot 10^3$ pF/m, while the sensitivity at $z = 0.5$ is only $7.3 \cdot 10^2$ pF/m, which would be too low to have 1 nm resolution. Hence, the range of the single plate-distance transducer is limited by the maximum overlapping area A in combination with the required displacement resolution.

The plate-distance transducer capacitance is not only influenced by displacements in the Z direction, but also by parasitic translations in the X and the Y direction, and by out of plane rotations about the X and the Y axis. In case of parasitic in plane translations in the X direction, crosstalk can be calculated by rewriting equation 4.3. When the displacement of the upper electrode is given by x, the capacitance of the plate-distance transducer becomes:

$$C_{pd} = \frac{2\varepsilon_0\varepsilon_r b}{\pi} \cdot ln\left(\frac{cosh\left(\frac{\pi}{2(d_0+z)}(a+e+x)\right) \cdot cosh\left(\frac{\pi}{2(d_0+z)}(-a-e+x)\right)}{cosh\left(\frac{\pi}{2(d_0+z)}(-a+e+x)\right) \cdot cosh\left(\frac{\pi}{2(d_0+z)}(a-e+x)\right)}\right) \qquad (4.9)$$

The crosstalk δ can be written as:

$$\delta = \frac{C_{pd}(x,z) - C_{pd}(z)}{C_{pd}(z)} \qquad (4.10)$$
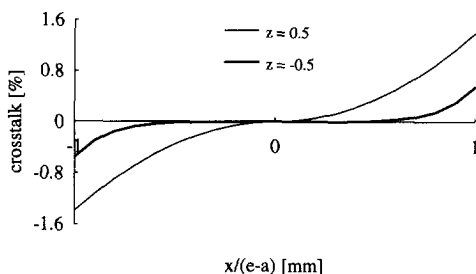
Fig. 4.3 Crosstalk for a single plate-distance transducer as a result of parasitic translations in the X direction for $d_0 = 0.6$ mm, $a = b = 4$ mm and for $z = 0.5$ and $z = -0.5$.

In a TEM nano stage, the width of the guard electrodes of a transducer should be minimized. In a practical configuration, the guard electrode around the largest of the two electrodes is omitted, so that the guard electrode width of the smallest electrode is equal to $e - a$. The amount of crosstalk can be influenced by the width of the guard electrode $e - a$, as is shown in figure 4.3. The influence of the parasitic in plane translation was calculated over a range of $x = -(e - a)$ to $x = (e - a)$. From figure 4.3, it should be noted that in order to keep crosstalk smaller than 1%, the ratio of the maximum parasitic displacement and the guard electrode width $e - a$ should be smaller than 0.85. For the example, the range in the X direction equals the range in the Z direction. This implies that a considerable part of the transducer area is required for the guard electrodes. This influences the maximum obtainable transducer sensitivity and resolution. As a matter of fact, crosstalk decreases strongly when the plate distance is decreased.

The plate-distance transducer capacitance is also influenced by parasitic tilts about the X and the Y axis. The plate-distance transducer capacitance can be written as a function of the parasitic tilts ϕ_x and ϕ_y, with $z = 0$, as follows [29]:

$$C_{pd}(\phi_x,\phi_y) = 4\varepsilon_0\varepsilon_r \frac{A}{d_0}\left(1 + \left(\frac{b^2}{3d_0^2} - \frac{1}{2}\right)\phi_x^2 + \left(\frac{a^2}{3d_0^2} - \frac{1}{2}\right)\phi_y^2 + \left(\frac{1}{4} - \frac{a^2+b^2}{6d_0^2} + \frac{2a^2b^2}{3d_0^4}\right)\phi_x^2\phi_y^2\right) + O\left[(\phi_x,\phi_y)^4\right]$$

$$(4.11)$$

This equation shows that the influence of parasitic tilts on the capacitance of the plate-distance transducer is of second order.

The displacement resolution required for feedback control of the quasi-static nano stage table stability was assumed to be 10 pm. If the transducer is only used for stability control, guard elec-

trodes are superfluous. In that case, the minimum required nominal plate-distance for $A = 100$ mm^2 is calculated to be 0.094 mm, which is small. Taking into account the size of the transducer area, such a plate distance asks for accurate plate alignment.

4.3.2.2 Differential plate-distance transducers

The characteristics of the single plate-distance transducer can be improved by use of a differential configuration. In general, an important argument to use differential capacitor configurations over single capacitor configurations is the possibility to design electronical and mechanical symmetric setups so that first order disturbances, like overall temperature changes, can be compensated for. Besides that, differential configurations allow zero-point measurements so that small changes in the capacitance difference can be measured on top of an electronical offset equal to zero. That way, the capacitance difference can be amplified to gain sensitivity. A differential plate-distance transducer configuration is shown in figure 4.4.
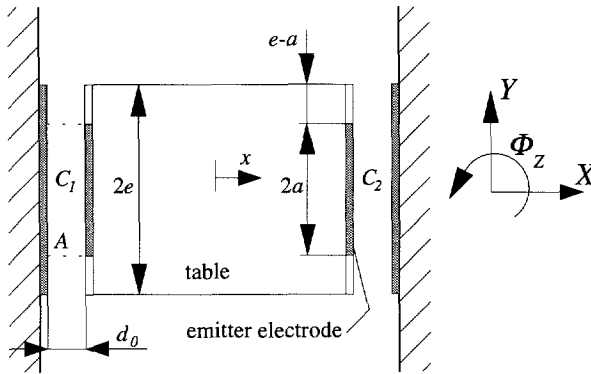
Fig. 4.4 Schematic configuration of a differential plate-distance transducer.

When parasitic tilts are neglected and the electrode dimensions for both capacitors are equal, the capacitance difference $C_{pd,diff}$ of a differential plate-distance transducer can be approximated by:

$$C_{pd,diff} = C_2 - C_1 = 2\varepsilon_0\varepsilon_r A \frac{x}{d_0^2 - x^2} \tag{4.12}$$

where d_0 is the plate distance when $x = 0$. The sensitivity of the differential plate-distance transducer follows from equation 4.12:

$$\frac{dC_{pd,diff}}{dx} = 2\varepsilon_0\varepsilon_r A \frac{d_0^2 + x^2}{\left(d_0^2 - x^2\right)^2} \tag{4.13}$$

This sensitivity has a minimum for $x = 0$, which is twice the sensitivity of a single plate-distance transducer for equal overlapping area and plate distance. This means that the transducer sensitivity is large enough to have 1 nm resolution over the full transducer range. Equation 4.13 also shows that the transducer linearity over a small part of the transducer range about $x = 0$ is improved compared to the single transducer. The minimum overlapping area A needed to achieve a displacement resolution Δx is calculated by:

$$A = \frac{1}{2} \frac{d_0^2}{\varepsilon_0 \varepsilon_r} \frac{\Delta C}{\Delta x} \tag{4.14}$$

Using the values from the example, this minimum overlapping area would be 21 mm^2. The range of a differential plate-distance transducer is limited by the nominal plate distance d_0.

Compared to the single plate-distance transducer, crosstalk is reduced for the differential configuration. Crosstalk can be calculated by substituting equation 4.9 into equation 4.12 (substituting $z = x$ and $x = y$) and by comparing the capacitance difference resulting from parasitic in plane translations to the capacitance difference when $y = 0$. The result is shown in figure 4.5. The effect of the parasitic displacements was calculated over a range of $y = -(e-a)$ to $y = (e-a)$. Figure 4.5 shows that a guard electrode width $e-a$ equal to the maximum parasitic in plane translation is sufficient to keep crosstalk smaller than 1%. Crosstalk was also evaluated by means of finite element analyses (FEA) using Maxwell finite element software [83]. This was done in order to compare the accuracy of the numerical and the finite element calculations. The results are included in figure 4.5. The analytic calculations and the finite element analysis correspond very well.
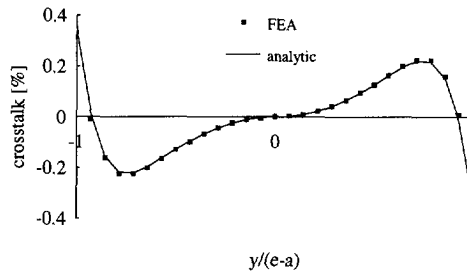
Fig. 4.5   Calculated crosstalk for a differential plate-distance transducer as a function of parasitic in plane Y translations for $d_0 = 0.6$ mm, $a = b = 4$ mm and $x = 0.5$ mm.

Subsequently, as crosstalk of combined parasitic translations and rotations in the XY plane on the capacitance difference is difficult to describe analytically, this crosstalk was calculated by means
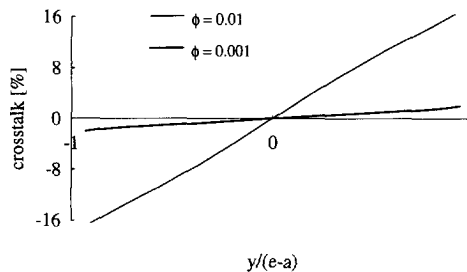
Fig. 4.6   Crosstalk calculated by FEA for a differential transducer as a function of parasitic rotations ϕ_z and parasitic translations in the Y direction for $x = 0.5$ mm.

of FEA. Figure 4.6 gives the results, for $x = 0.5$ mm, for $\phi_z = 0.01$ rad and for $\phi_z = 0.001$ rad. The nominal plate distance d_0 is 0.6 mm, and $a = b = 4$ mm. The effect of the parasitic translations was calculated over a range of $y = -(e - a)$ to $y = (e - a)$.

By comparing figures 4.5 and 4.6, it can be concluded that crosstalk strongly depends on changes in the angle ϕ_z. According to figure 4.6, crosstalk can be minimized by choosing large guard electrode widths. However, in volume critical applications like a TEM, it is not possible to have such large guard electrode widths. Therefore, the angle ϕ_z has to be kept smaller than $5 \cdot 10^{-4}$ rad. Finite element analysis also showed that accurate measurement of the angle ϕ_z is very well possible independent of the table position in the XY plane. If, by means of a convenient measurement and control protocol, the angle ϕ_z can be kept smaller than $5 \cdot 10^{-4}$ rad (for small angles, crosstalk is assumed to be linear dependent on the angle ϕ_z), crosstalk can be kept smaller than 1% even at a guard electrode width $e - a$.

If the differential transducer is only applied for control of the quasi-static stability, guard electrodes are not required. In that case, the minimum nominal plate distance d_0 can be a factor $\sqrt{2}$ larger compared to the single plate-distance transducer: 0.13 mm. This eases the demands on the plate flatness and alignment accuracy.

4.3.3   Differential in-plane transducers

It would not be useful to discuss the *single* in-plane transducer configuration, because its performance is exceeded by the *differential* in-plane transducer configuration, without consuming more space. A general configuration of the differential in-plane transducer is given in figure 4.7. Displacement measurements in the X direction are based on the capacitance difference $C_{ip,diff}$ between the capacitances C_1 and C_2.
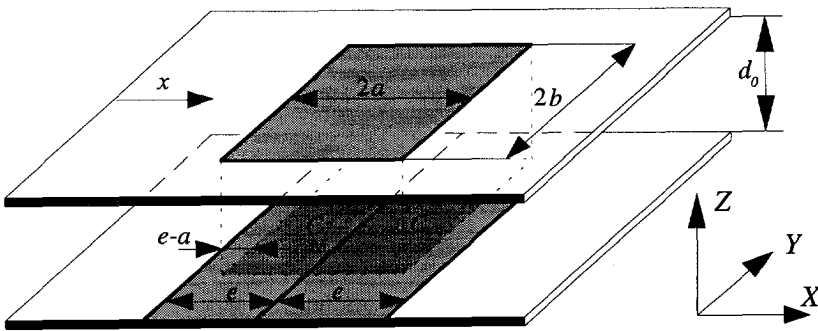
Fig. 4.7   Differential in-plane transducer including its relevant dimensional parameters.

Using equation 4.3 this differential capacitance can be written as:

$$C_{ip,diff} = C_2 - C_1 = \frac{2\varepsilon_0\varepsilon_r b}{\pi} \cdot ln\left(\left(\frac{cosh\left(\frac{\pi}{2d}(x+a)\right)}{cosh\left(\frac{\pi}{2d}(x-a)\right)}\right)^2\right.$$

$$\left.\times\frac{cosh\left(\frac{\pi}{2d}(x-e-a)\right)\cdot cosh\left(\frac{\pi}{2d}(x+e-a)\right)}{cosh\left(\frac{\pi}{2d}(x-e+a)\right)\cdot cosh\left(\frac{\pi}{2d}(x+e+a)\right)}\right)$$

(4.15)

where x is the displacement in the X direction. From figure 4.7, it can be concluded that the electrode width $2a$ must at least be equal to the transducer range. The electrode width e must at least be twice the width of the opposite electrode, $e \geq 2a$, but about 10% additional electrode width is preferred to keep the transducer sensitivity constant over its full range within 0.1%. The maximum electrode width e and hence the transducer range are determined by the space in the application.

Under the conditions mentioned above and if parasitic tilts are neglected, the capacitance difference of an in-plane transducer can be approximated by:

$$C_{ip,diff} = C_2 - C_1 = 4\varepsilon_0\varepsilon_r \frac{b}{d_0}x \qquad (4.16)$$

where d_0 is the nominal plate distance. The sensitivity of the transducer is constant:

$$\frac{dC_{ip,diff}}{dx} = 4\varepsilon_0\varepsilon_r \frac{b}{d_0} \qquad (4.17)$$

This means that the in-plane transducer is linear over its full range, which is an advantage of this transducer configuration. According to the example, the transducer sensitivity must be 10^3 pF/m. In order to achieve this, the factor b/d_0 must be larger than 28 ($\varepsilon_{r,air} \cong 1$). Consequently, the nominal plate distance d_0 has a maximum given by the maximum electrode length $2b$ allowed by the application.

The major disadvantage of differential in-plane transducers is that their capacitance depends on the plate distance. Parasitic motion in this direction strongly influences the transducer's behavior in the X direction. A solution to this problem is to measure the sum capacitance $C_1 + C_2$ in order to estimate the plate distance. A second form of parasitic motion is tilt about the Y axis, ϕ_y. The influence of this parasitic tilt for $\phi_x = 0$ and $x = 0$ can be written as follows [29]:

$$C_{ip}(\phi_y) = \frac{2\varepsilon_0\varepsilon_r b}{\phi_y} ln\left(\frac{(d_0 + a\sin(\phi_y))(d_0 - a\sin(\phi_y))}{d_0^2}cos^2(\phi_y)\right) \qquad (4.18)$$

This equation shows that the influence of parasitic tilt about the Y axis on the capacitance difference is of the first order, which is a clear disadvantage compared to the plate-distance transducer configuration. In order to achieve a high level of positioning repeatability, parasitic tilts must be measured and controlled or compensated for. Due to crosstalk, it is not possible to obtain accurate position information about the displacements in the X direction from a single differential in-plane transducer which suffers from parasitic displacements. Solutions to this problem ask for extra in-plane and/or plate-distance transducers, which would be very space consuming. Also, a

parallel coupling of in-plane transducers still has to deal with the inaccuracy of cross correlation calculations required to take parasitic motion into account. Nevertheless, because the in-plane transducer configuration does not limit (in first order) in plane translations, it may be a very interesting solution for some applications [84]. For other applications it is the only possible way to obtain the required positioning repeatability.

In case of stability control, the ratio b/d_0 must be larger than $2.8 \cdot 10^3$ in order to have 10 pm displacement resolution. If $d_0 = 0.1$ mm, a comparable alignment problem as for plate-distance transducers results. This leaves $b = 280$ mm, which asks for a relatively large plate area, even with a number of in-plane transducers in parallel. Reduction of the plate distance increases the sensitivity, increasing the manufacturing tolerances and plate alignment accuracy accordingly. Therefore, the in-plane transducer is less suitable for stability control at the picometer level than the plate-distance transducer.

4.3.4 Measurement of rotations

In a TEM nano stage, two types of rotations can be distinguished: small (parasitic) rotations which must be controlled to obtain a high level of positioning repeatability and large rotations for specimen tilting. A doubled plate-distance transducer configuration can be used to measure small rotations (see figure 4.8a). The angle ϕ is measured by subtracting the capacitances C_1 and C_2, while the plate distance is measured by summing these capacitances. The nonlinearity of this plate-distance configuration depends on the size of the overlapping electrode area. For $a = 2$ mm, $b = 4$ mm, $d_0 = 0.6$ mm, and $e - a = d_0$, the nonlinearity is smaller than 1% when ϕ is smaller than 0.02 rad.

a)   *b)*
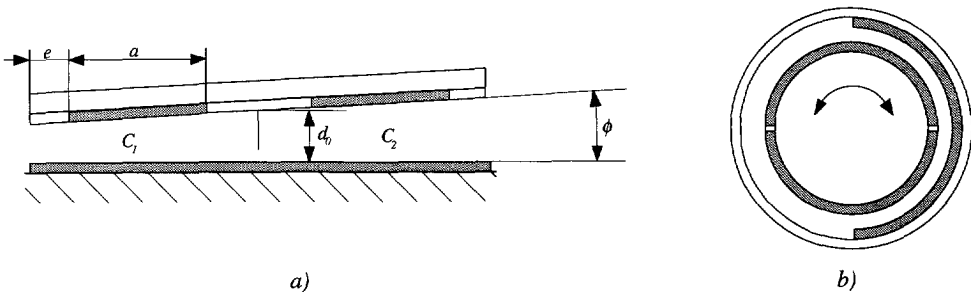
Fig. 4.8 a) A doubled plate-distance transducer can be used to measure small (parasitic) rotations. b) An in-plane transducer can be used to measure large rotations.

The only suitable capacitive transducer configuration for the control of large rotations is the differential in-plane transducer (see figure 4.8b). Since there are many variants for the standard configuration of figure 4.8b, they will not be discussed here. Besides that, they were not used during this research. The design of capacitive in-plane tilt transducers should be subject of further investigation during the development of a practical nano stage.

4.3.5 Concluding remarks

The differential in-plane transducer is linear over its full range, the plate-distance transducer is not. The in-plane transducer is very sensitive to parasitic changes in the electrode distance and to parasitic out of plane tilts, while the plate-distance transducer sensitivity to parasitic in-plane translations and parasitic tilts is only of second order, as long as the overlapping area A is kept constant. The sensitivity to parasitic motion of the in-plane transducers is a severe disadvantage with regard to displacement control. The overlapping area A can be kept constant by making one of the electrodes larger than the other. This means that the size of the overlapping area A is not only determined by the required transducer range, but also by the guard electrode width, which determines the amount of crosstalk as a result of motion in other degrees of freedom. For practical reasons, the plate-distance transducer sensitivity can often be higher than the in-plane transducer sensitivity. This is caused by the strong dependence of the in-plane transducer sensitivity on the electrode width $2b$, whose size is limited by the space within the application. Although strongly dependent on the application, in case of translations in one or two degrees of freedom, the maximum range of in-plane transducers can generally be larger than the range of plate-distance transducers. In general, the nominal plate distance of an in-plane transducer is smaller than the nominal plate distance of a plate-distance transducer. In single degree of freedom applications, this is not a problem. However, in applications with more than one degree of freedom, a small plate distance can become a limitation of the table stroke in one of the other degrees of freedom.

As far as nanopositioning is concerned, the differential plate-distance capacitive transducer is the most convenient configuration for measuring translations. In some practical applications, there may be no space for a differential configuration. In that case, a single plate-distance transducer is preferred to a differential in-plane transducer for the same reasons as mentioned in the former paragraph. Of course, for measurements of large tilt angles in-plane transducers must be used.

As far as position control at the picometer level is concerned, plate-distance transducers are preferred for their much simpler implementation and much lower sensitivity to parasitic motion. Nevertheless, in some applications in-plane transducers or a combination of in-plane and plate-distance transducers will be the better alternative. The nominal plate distance can in theory be decreased until the electric field strength in the capacitor caused by the measuring voltage exceeds the breakdown field strength. The practical minimum plate distance is determined by the flatness of the transducer plates and the accuracy of the plate alignment. Practical minimum plate distances will range between 10 and 100 µm, depending on the dimensions of the capacitor plates.

An indication of the relative properties of the single and differential plate-distance transducer and the differential in-plane transducer configuration are summarized in table 4.1.

	range	linearity	sensitivity	parasitic motion	multi DoF	translations	rotations
Single pl-dis	+	-	+	+	+	+	+
Diff. pl-dis	-	+	++	++	++	++	+
Diff. in-plane	++	++	+/-	--	+/-	+/-	++

Table 4.1   Relative properties of the three capacitive displacement transducer configurations discussed.

It should be noted that the overall dimensions of nano stages described in this work strongly depend on the dimensions of the capacitive transducer plates and much less on the dimensions of the piezo drives.

4.4   Measurement of capacitance

The accuracy of the capacitance measurement of a capacitive (displacement) transducer completely depends on the electronic measurement configuration used. This configuration has to deal with the relatively large parasitic capacitances of the measurement terminals to ground. Generally, the nominal capacitance of a capacitive displacement transducer is very small and ranges from 0.1 pF to several pF to be compared with measurement resolutions down to the order of 10^{-6} pF, whereas the parasitic capacitances are in the order of several pF up to several hundreds of pF, depending on the measurement configuration.

A number of capacitance measurement configurations have been described by Heerens [79], Zhu [85], de Jong [86] and Huang [87] and will therefore not be discussed here. The choice for one of these configurations was obvious: the alternating current bridge (ac-bridge). Although the ac-bridge has been known for a long time, it is still the most accurate measurement configuration. This is due to its large rejection to parasitic capacitances to ground. By means of the ac-bridge, resolutions down to 10^{-19} F (= 0.1 aF) can be achieved [88]. The ac-bridge was used throughout this work to measure capacitances. A very detailed description of the ac-bridge was given by Hague and Foord [89].
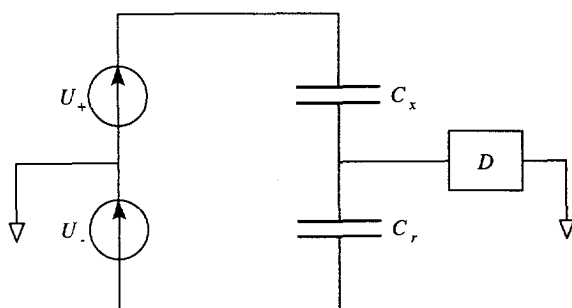
Fig. 4.9   A simple ac-bridge circuit.

A simple ac-bridge circuit is shown in figure 4.9. Two excitation signal sources, U_+ and U_-, a reference capacitor C_r, and the unknown capacitor C_x are placed in a symmetric circuit. The capacitance difference is detected by the detector D. The capacitor electrodes at the side of the signal sources are called *emitter* electrodes, the electrodes at the side of the detector are called *detector* electrodes. The equivalent circuit is given in figure 4.10, where C_{pe1} and C_{pe2} are stray capacitances of the leads and of the emitter electrodes to ground, C_{pd} is the stray capacitance of the lead and the detector electrode to ground. The resistances R_{p1} to R_{p4} represent the transformer, the lead and the electrode resistances. The excitation signal sources can, for instance, be replaced by a single sine wave voltage source and a ratio transformer.
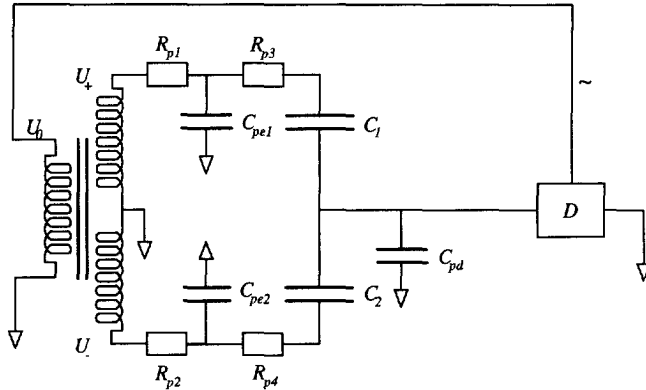
Fig. 4.10   The equivalent ac-bridge including parasitic capacitors and resistances.

The large rejection ratio for parasitic capacitances is based on the 90° phase shift of the current and voltage output signals of the ac-bridge with regard to the first order disturbances produced by the parasitic capacitances and the resistances of the leads. This phase shift can be used to reduce the influences of parasitic capacitances and resistances by means of synchronous or phase sensitive detection (PSD).

The principle of the ac-bridge is shortly explained as follows. The synchronous detector produces a sine wave which is fed into the ratio transformer. This produces a detector current I_d which equals:

$$I_d = 2\pi f (C_r - C_x) U_0 \cos(2\pi f t) \tag{4.19}$$

where $U_0 \cos(2\pi f t)$ is the sine wave voltage on the electrodes. The detector input current is zero when the capacitances in both ratio arms are equal. The detection circuit consists of a current to voltage preamplifier A_p in combination with the synchronous detector D. The dc output voltage U_{out}^{dc} of the synchronous detector is given by [29]:

$$U_{out}^{dc} = \frac{2U_0 G_s A_p \cos(\varphi_0)}{\pi} \tag{4.20}$$

where G_s is the attenuation of the sine wave amplitude by the capacitive system and φ_0 the phase difference between the reference and the unknown signal.

The electronical stability of the output voltage U_{out}^{dc} is important with regard to position control of the nano stage table. According to equation 4.20, the output voltage stability depends on the amplitude stability of the sine wave voltage, on the stability of the current to voltage conversion, and on the phase drift and the phase jitter between the reference and the unknown signal. This is not the case for zero point measurements $(C_r - C_x = 0)$. Therefore, displacement control should preferably be performed when the ac-bridge is balanced. In an off-balance situation, the measurement stability decreases linearly with the oscillator amplitude and the phase drift, and the ratio of the capacitances in the measurement arms. In case of a differential capacitive displacement transducer, this off-balance can become large for large stroke applications. For instance, suppose the capacitance difference is perfectly constant and the amplitude stability of the voltage source is 10^{-5}. If the detector resolution is 10^{-6}, the capacitive off-balance must be smaller than 10% of the nominal capacitance in order to detect no significant change in the detector output.

For large stroke applications, the off-balance problem can be solved either by inserting a variable offset capacitor or by use of a variable ratio transformer. From equation 4.20, the conclusion can be drawn that the detector sensitivity may be increased by increasing the sine wave amplitude.

The synchronous detectors used during this research were commercial instruments [90]. The detector output had several amplification settings (0.1, 1, 10, 100, 1000) and the dc output voltage ranged from -10 up to 10 Volt. The detector output was fed through a low pass filter. Three cut-off frequencies were available: 20 Hz, 2 kHz and 12 kHz. The sine wave frequencies of the three synchronous detectors used were 62.5 kHz, 92 kHz and 125 kHz. The three terminal ratio transformer was made from a high quality magnetic core provided with 3 sets of windings.

4.5   Transducer stability

4.5.1   Introduction

Positioning repeatability at the nanometer level and measurement and control of the nano stage table stability with capacitive displacement transducers requires a stable measurement setup. This concerns the environmental stability, the stability of the mechanical reference frame of the nano stage, and the stability of the capacitance measurement configuration. This section deals with, the stability performance of a typical measurement setup. Other important measurement properties which were investigated are the resolution and the bandwidth of the synchronous detectors used.

4.5.2   Stability

4.5.2.1   Environmental stability

The capacitance of a capacitive transducer is influenced by environmental conditions in two ways. The relative dielectric permittivity of air ε_r and the geometry factor $f(G)$ are not constant. The relative dielectric permittivity is influenced by changes in temperature, relative humidity (RH) and pressure. Table 4.2 gives the relative effects of these three parameters at 20°C temperature, 50% RH and $1.013 \cdot 10^5$ Pa pressure [80]. The geometry factor $f(G)$ is mainly influenced by temperature changes.

$\dfrac{\partial \varepsilon_r}{\partial T}$	2	[ppm/K]
$\dfrac{\partial \varepsilon_r}{\partial RH}$	2	[ppm/%]
$\dfrac{\partial \varepsilon_r}{\partial P}$	50	[ppm/Pa]

Table 4.2   The relative influence of temperature, humidity and pressure on the relative dielectric permittivity.

Most experimental setups described in this thesis were used in air, in a conditioned environment with 20°C as nominal temperature and 50% as nominal relative humidity. Within 24 hours, only

small changes of temperature (<0.2 K) and relative humidity (2-4 %) occurred. Changes in air pressure were up to $6 \cdot 10^3$ Pa. Nevertheless, these changes neither significantly influenced the short term (3 minutes) nor the middle-long term (1 hour) stability measurements, because changes occurred very slowly. Some experiments were performed under vacuum conditions. In that case, changes in the dielectric permittivity can be neglected.

4.5.2.2 Electrode stability

As far as the stability of the geometry factor $f(G)$ is concerned, temperature changes are a factor of major importance. Changes in the environmental temperature affect the size of the electrodes and thus affect the output of the capacitive displacement transducer. If linear expansion is assumed, the error in the measured electrode distance is proportional to the linear expansion coefficient of the substrate material applied and the magnitude of the temperature change: $2\alpha\Delta T$. The influence of this error can be minimized by choosing a substrate material with a low linear expansion coefficient and by avoiding large temperature changes. In a differential situation, the influence of temperature changes is of the second order when the setup is fully symmetric, when both capacitances in the measurement circuit are equal and when both capacitor plates are made from the same material and have equal dimensions. In practice, changes in the electrode dimensions are often overruled by changes in the plate distance due to heat up of the setup.

4.5.2.3 Electronic stability

According to equation 4.20, the sine wave voltage amplitude stability influences the stability of the detector output voltage. The sine wave amplitude stability of the commercial synchronous detectors used was measured to be 30 ppm/hour. The amplitude difference between both arms of the ratio transformer was also measured. This resulted in a middle-long term stability of 2 ppm/hour. Short term stability was better than 0.5 ppm/min.

The zero point stability of a capacitance measurement setup was determined by balancing the ac-bridge with two 1 pF reference capacitors. The short term stability was better than $1 \cdot 10^{-6}$ pF and the middle-long term stability (1 hour) was better than 10^{-5} pF. This is sufficient for the TEM nano stage application. Next, one of the reference capacitors was replaced by a variable precision capacitor [91]. The capacitance of this capacitor can be adjusted from 0.01 up to 11 pF. The short term zero-point stability of this configuration was $1 \cdot 10^{-6}$ pF. The middle-long term zero-point stability of this configuration was better than 10^{-5} pF. The variable precision capacitor had no significant influence on the setup stability. As expected, ac-bridge stability decreased when the ratio arms are no longer balanced. For 1 pF off balance, the short term stability dropped to $1 \cdot 10^{-5}$ pF and the middle-long term stability to $4 \cdot 10^{-5}$ pF. This short term stability is not sufficient for nano stage applications and therefore bridge balancing is very important. It is assumed that the repeatability of a capacitive transducer is completely determined by the transducer stability.

4.5.2.4 Detector resolution and bandwidth

The resolution of the synchronous detector at low bandwidth was measured by balancing the ac-bridge by means of two 1 pF reference capacitors [91]. At 20 Hz bandwidth and at amplification gain 1 (1 V $\cong$ 1 pF), the noise level was less than 5 μV ($5 \cdot 10^{-6}$ pF), resulting in a range to resolution ratio of $4 \cdot 10^6$. For a 2 Hz bandwidth, the resolution increases to better than 1 μV, resulting in a range to resolution ratio of $2 \cdot 10^7$. For nanopositioning in the TEM, a 2 Hz bandwidth was

assumed to be sufficient. For position control at high velocities in the order of tenths of milli-meters per second, the displacement resolution can be low and thus the measurement bandwidth can be increased. At a 2 kHz bandwidth, the detector resolution is in the order of 5 mV.

In case of stability control, displacements in the order of 10 pm will correspond to capacitance changes in the order of 10^{-6} pF because the plate distance is usually between 10 and 100 μm and the nominal capacitance is usually around 1 pF. As a consequence of this ratio of range and resolution, only quasi-static position changes at the picometer level can be detected. Hence, sup-pression of table vibrations with amplitudes in this range is not possible in an active way. Thus, passive means must be applied.

The bandwidth of the synchronous detector with sine wave frequency 125 kHz was measured by applying a sine wave of swept frequency to the current to voltage converter. The bandwidth was measured to be 6 kHz.

4.5.2.5 Influences of imperfections

Although air capacitors are nearly ideal capacitors, their imperfections can become important at radio frequencies [89]. As the measurement frequencies used here are at the border of audio and radio frequencies, the influences of imperfections on the transducer stability will be checked. Two imperfections occur: the dielectric loss and the insulation resistance.

If a sine wave voltage is applied across a capacitor, the resulting current will be made up of a charging current and a loss current. The relative permittivity ε_r of the medium between the elec-trode plates is in fact a complex variable, which can be divided into a real part ε_r' that represents the storage and an imaginary part ε_r'' that represents the loss [92]. As already has been discussed in chapter 2, the angle of loss, $\tan \delta$, is the ratio of the energy lost to the energy stored:

$$tan\,\delta = \frac{\varepsilon_r''}{\varepsilon_r'} \tag{4.21}$$

Hewlett Packard [92] gives values for $\tan \delta$ at 3 GHz. From:

$$n = \sqrt{(\mu_r \varepsilon_r)} \tag{4.22}$$

and $\mu_r \cong 1$ (μ_r is the relative permeability of the medium), follows

$$\varepsilon_r = n^2 \tag{4.23}$$

when n is the refractive index of the medium. According to Froome and Essen [93], n holds for all frequencies below 40 GHz. For air, this gives $\tan \delta = 10^{-5}$. The power loss P_{loss} in a capacitor can then be calculated as follows:

$$P_{loss} = UI\,tan\,\delta = \frac{U^2}{Z}\,tan\,\delta = \frac{U_0^2}{2}\,j\omega C\,tan\,\delta \tag{4.24}$$

where U_0 is the amplitude of the alternating voltage signal. When $U_0 = 10$ V, $\omega = 10^6$ rad/s and $C = 10$ pF, the power loss is in the order of 10^{-8} W. This is, for instance, lower than the loss in the substrates which carry the transducer electrodes. For a 10x10x1.5 mm³ glass substrate, the capacitance C is 2 up to 10 pF and $\tan \delta = 10^{-3}$, resulting in a loss in the order of 10^{-6} W.

The dielectric solid substrate carrying the transducer electrodes must be a (very) good insulator. Unfortunately, dirt films and moisture on the insulator can decrease the insulation resistance due

to surface leakage currents. As a result, the sensitivity of the transducer to changes in the relative humidity of air will increase. However, because most of the nanopositioning applications work in a vacuum, there will be almost no dirt and moisture films on the electrodes. Therefore, the insulation resistance change is expected to be negligible.

4.5.2.6 Electrostatic forces

As a result of the electric field in a capacitor, an attractive electrostatic force works between the capacitor electrodes. If the plate distance d_0 and the maximum displacements x and y are small relative to the width $2a$ and length $2b$ of the overlapping area of the electrodes, the electrostatic force in a parallel plate capacitor can be approximated by:

$$F_z = 2\frac{\varepsilon_0 \varepsilon_r abU^2}{d^2} \tag{4.25}$$

With $U = U_0 \sin(\omega t)$ and

$$U^2 = \frac{U_0^2}{2}\left(1 - \cos(2\omega t)\right) \tag{4.26}$$

equation 4.25 can be rewritten as:

$$F_z = \frac{\varepsilon_0 \varepsilon_r ab}{d^2}U_0^2\left(1 - \cos(2\omega t)\right) \tag{4.27}$$

Suppose that in case of nanopositioning, the maximum overlapping area is 100 mm^2 and the minimum electrode distance is 0.1 mm. For a sine wave voltage, with $U_0 = 10$ V, the maximum electrostatic force in the Z direction is then $2.2 \cdot 10^{-6}$ N. As the nano stage stiffness in the direction of motion is expected to be in the order of 10^6 N/m, deformations of the nano stages will not exceed the picometer level and can therefore be neglected. The electrostatic forces will vary with a frequency of about 100 kHz. This frequency is much higher than the first resonance frequency of the nano stages and therefore electrostatic forces are expected to have no influence on the nano stage vibration amplitude in this particular case.

In case of stability control, the plate distance can be as small as 10 µm, increasing the electrostatic forces with a factor 400. Although, the frequency of the forces is much higher than the first resonance frequency of typical nano stages, an effect on the nano stage stability can not be excluded.

4.6   Capacitive transducers in a TEM: side effects

Interference of the electron beam or the magnetic field in-between the objective lens pole pieces and the capacitive transducers or vice versa was estimated to be very low. Like the piezo actuators, the electrodes of a capacitive transducer need to be connected to the capacitive measurement electronics by means of thin leads. In a magnetic field, the electrons in these leads experience a Lorentz force which can be calculated by means of equation 2.8.

This force has no netto effect on the current through the conductors of the capacitive transducer and consequently no effect on the transducer accuracy. The Lorentz force is proportional to the

detector current I_d through the conductors. According to equation 4.19, the maximum current is in the order of 10^{-6} A ($f = 100$ kHz, $C = 1$ pF and $U_0 = 10$ V). The force on a conductor with length l in a homogeneous magnetic field B is then equal to:

$$F_L = BI_d l \qquad (4.28)$$

With $l = 50$ mm, this force is not larger than 100 nN. It could cause vibrations at the 100 kHz sine wave frequency of the synchronous detector, which is again much higher than the first resonance frequency of the nano stage and thus the vibrations can be neglected.

The capacitive transducers can be electrically insulated, with relative ease, from the influence of the electron beam or the piezo actuators and vice versa by shielding and guarding.

5 Stability

5.1 Introduction

In a TEM, position stability of the specimen relative to the lower pole piece of the objective lens is very important with regard to the resolution of the image and the image drift. Stability is also important with regard to nanopositioning.

Figure 5.1 shows the nano stage concept once more. The nano stage table is the specimen holder and carries the specimen. The electrons collide with a small area of the specimen which is about a micrometer in diameter. A part of the specimen in this spot is imaged on the fluorescent screen or the CCD camera. It is this part of the specimen that must be positioned and kept stable relative to the lower pole piece.
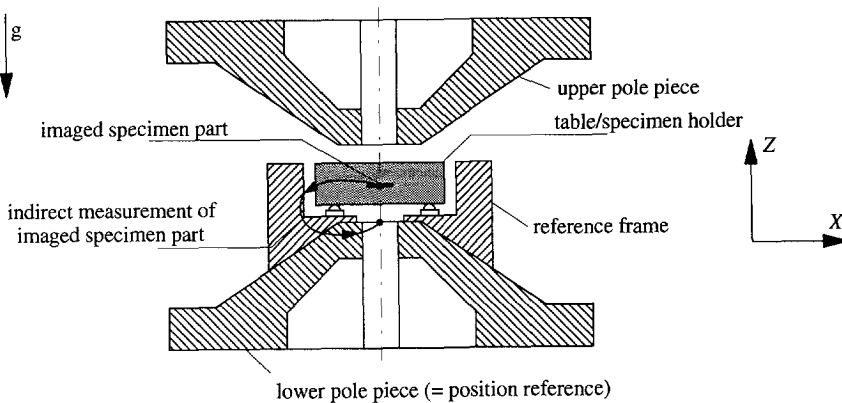
Fig. 5.1   Overview of the application of a nano stage as a specimen positioning device in a TEM. The nano stage table is the specimen holder. The position of the imaged specimen part should be compared as directly as possible to the lower pole piece.

The position stability of the table relative to the lower pole piece can be divided in two quantities: the drift rate and the vibration amplitude. The drift rate is a measure of the quasi-static, average table displacement per unit of time. The vibration amplitude over a certain frequency span is a measure of the maximum cyclic table displacements over that frequency span. The

amplitude of the table displacements depends on the nano stage frequency response to external vibrations.

The position stability of the table relative to the lower pole piece depends on different quasi-static and dynamic errors. Quasi-static errors are caused by quasi-static error sources which do not change or change very slowly in time. An important quasi-static error source is heat produced inside and outside the nano stage. This heat is transferred to or from the nano stage as a result of temperature differences. The heat transfer in the microscope is influenced by various heat sources and heat sinks inside and outside the microscope. In fact, as a result of a continuous change in the microscope's settings and the environmental circumstances thermal equilibrium is never obtained in an operational TEM. Other quasi-static error sources are creep and drift. They influence the stability of parts of the setup. The drift rate of the specimen strongly depends on the type of experiment it is used for and on the time between changes in the microscope's settings. It ranges from tenths up to tens of nanometers per minute for heating experiments [94]. Dynamic error sources are internal and external vibrations from different sources. They cause cyclic position changes of the table relative to the pole piece. The present magnitude of the vibration amplitude of the specimen (holder) relative to the lower pole piece is estimated to be in the order of 0.1 nm [95].

It should be noted that an important difference exists between the (environmental) conditions to which a nano stage in a TEM is exposed and the conditions to which the majority of the experimental nano stage setups tested in this and the next chapter was exposed. The main difference is the environmental pressure, which is, within the TEM, down to 10^{-4} Pa. In such a vacuum, heat transfer is different [96]. This aspect should be given serious attention because it may influence the quasi-static nano stage stability. However, there is no reason to assume that the vacuum environment has influence on the dynamic stability of the nano stage and the reference frame. Other differences are the presence of heat sources like the electromagnetic lenses and the electron beam. Almost all experiments on the nano stage setups presented in this chapter and in chapter 6 were performed in ambient air because doing experiments in a vacuum is much more complex and time consuming and because most of the setups did not require a vacuum to prove a certain behavior.

Before discussing the effect of quasi-static and dynamic error sources on the stability of a nano stage, three principally different ways to obtain high position stability are described (section 5.2). The requirements on the nano stage and on the vibration isolation system regarding the influence of vibrations are discussed in section 5.3. The influence of heat production in a nano stage and its environment on the table's position stability will be estimated in section 5.4. Creep will be discussed in section 5.5. The influence of drift and creep effects in the table supports and the piezo actuators on the nano stage stability will be investigated in sections 5.6 and 5.7 by means of some experiments.

5.2   Concepts to obtain stability

The discussion on the concepts to obtain table position stability distinguishes between the quasi-static and the dynamic table stability. Quasi-static and dynamic position stability at the picometer

level can in theory be obtained with a positioning device with high intrinsic position stability or by applying closed-loop displacement control. Quasi-static position stability can also be obtained by applying quasi-static position corrections based on knowledge about the table drift course directly after moving the table to a new position.

In order to obtain a high level of quasi-static position stability of the imaged part of the specimen by means of closed-loop control, the position of this part of the specimen should, ideally, be measured directly relative to the lower pole piece and not through intermediate elements or intermediate instruments. A way to achieve this is by using the specimen position information available from the image. Unfortunately, this option was classified as not (yet) useful (see chapter 1). A practical alternative is to use additional transducers, which, by definition, measure the position of the (imaged part of the) specimen relative to the lower pole piece *indirectly*. Still, it is important that such position transducers measure the specimen position as directly as possible relative to the center top part of the lower pole piece (see figure 5.1). In practice, however, this is often not possible, either because these places do not allow the presence of position transducers or because the position transducer needs a lot of space. Another reason may be that the number of degrees of freedom of the table does not allow direct measurement of the specimen position relative to the pole piece. Nevertheless, the number and size of intermediate elements or transducers, through which the position of the specimen is determined, must be as small as possible.

A practical approach to achieve a high quasi-static specimen stability by means of closed-loop control is to compare the specimen *holder*'s position instead of the specimen position to a position reference frame, which is attached to the lower pole piece. As a consequence of this approach, the repeatability and the stability of position measurements depend on the dimensional and form stability of both the reference frame and the specimen holder. This dimensional and form stability make demands on the choice of materials, on the construction of both the specimen holder and the reference frame, and on the mechanical and thermal loads applied. During this research, the dimensional and form stability of the nano stage table and the reference frame have not been investigated extensively. The approach was to use standard construction materials, to use the same material for both of them, and to keep changes in the mechanical and thermal loads low. Because of the expected difference in the first resonance frequencies of the reference frame and the piezo drives, the intrinsic stability of the reference frame is assumed to be higher than the intrinsic stability of the table. This suits application of such a frame as a position reference.

As far as the dynamic position stability is concerned, it is important to repeat that it is difficult to suppress vibrations with amplitudes in the subnanometer range by means of closed-loop control with capacitive transducers because of the low bandwidth of the capacitive displacement transducers at a large ratio of range and resolution. That is why a good dynamic stability of the nano stage table must be based on its low sensitivity to vibrations.

For a certain range of applications of specimen positioning in a TEM, a nano stage with a high intrinsic position stability of the table is given preference to a nano stage using closed-loop displacement control. This research has concentrated on maximizing the intrinsic position stability of the nano stage, on minimizing the settling time to reach picometer stability, and on obtaining knowledge on the table drift course after positioning. If the nano stage concept is used for specimen positioning in a TEM, high intrinsic position stability, dimensional stability and form stability are supported by:

- the vibration isolation system which suppresses the effect of floor vibrations on the column,
- a high first resonance frequency ω_0 of the nano stage in all directions, and
- the fact that a nano stage has no direct mechanical lead-through to the outside of the vacuum chamber.

Still, it is very important to realize that all methods to obtain stability are limited by the uncertainty about the stability of the elements between the part of the specimen that is observed and the mechanical parts of which the position is actually measured.

5.3   Dynamic stability

Vibrations influencing the nano stage table position stability originate from internal and external vibration sources like the nano stage piezoelectric drive, building vibrations, vibrations from microscope subsystems, acoustic vibrations, water coolant flow, and air flow from climate conditioners. In spite of the vibration isolation system, vibrations from sources outside the column (partly) enter the column. The effect of all these vibrations on the position stability of the table can be estimated by representing the nano stage by a mass-spring-damper system having resonance frequency ω_0 and relative damping coefficient β (see figure 5.2)
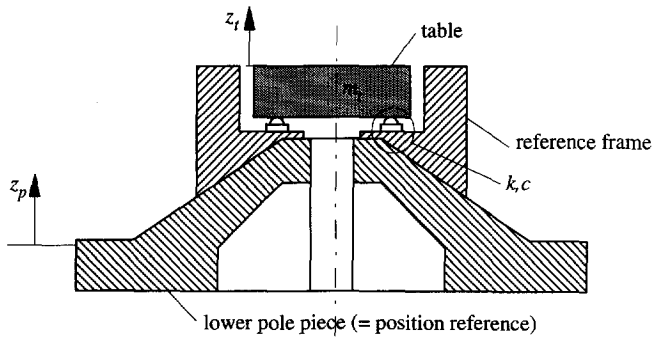
Fig. 5.2   The nano stage can be represented by a mass-spring-damper system having resonance frequency ω_0 and relative damping coefficient β. Vibrations of the pole piece are represented by z_p, vibrations of the table by z_t.

The idealized transfer function is given by:

$$
\frac{z_t}{z_p} = \sqrt{\frac{1 + \left(2\beta \frac{\omega}{\omega_0} \right)^2}{\left(1 - \frac{\omega^2}{\omega_0^2} \right)^2 + \left(2\beta \frac{\omega}{\omega_0} \right)^2}}
\tag{5.1}
$$

where $\omega_0 = 2\pi f_0 = \sqrt{\dfrac{k}{m_t}}$ and $\beta = \dfrac{c}{2m_t\omega_0}$.

Position changes or vibrations of the pole piece should be exactly followed by the table. This implies that the ratio z_t/z_p should be equal or close to 1. For $\omega/\omega_0 \leq 0.2$, the difference between the amplitude of the pole piece and the table is less than 5% ($\beta = 0.03$ [65]). In order to maximize the table position stability, the nano stage resonance frequency f_0 should be as high as possible.

The position error ε is defined as the difference between the position of the pole piece (z_p) and the table (z_t):

$$\varepsilon = z_t - z_p \tag{5.2}$$

If the pole piece vibration-acceleration level resulting from vibrations is given by:

$$a = \hat{a}\cos(\omega t) \tag{5.3}$$

the position error equals:

$$\varepsilon = \frac{\hat{a}}{\omega^2}\left\{ \sqrt{\frac{1+\left(2\beta\frac{\omega}{\omega_0}\right)^2}{\left(1-\frac{\omega^2}{\omega_0^2}\right)^2+\left(2\beta\frac{\omega}{\omega_0}\right)^2}} - 1 \right\} \tag{5.4}$$

Figure 5.3 shows the position error ε as a function of the pole piece vibrations, for three different resonance frequencies of the nano stage (0.5, 1 and 1.5 kHz) and for $\hat{a} = 10^{-4}$ m/s^2 ($\beta = 0.03$). This is the maximum allowable acceleration level on the TEM column specified by Philips. It is clear that the nano stage should not be exposed to pole piece vibrations close to the resonance frequency f_0 of the nano stage. Figure 5.3 shows that nano stage resonance frequencies in the order of 1.5 kHz and higher may be sufficient to make the nano stage table follow pole piece vibrations with a position error that is smaller than 20 picometer. In practice, the nano stage cannot be directly attached to the pole piece. It will be placed on an intermediate support, which should be considered as a part of the nano stage.

Fig. 5.3 *The table's position error ε as a function of pole piece vibrations (z_p) at $\hat{a} = 10^{-4}$ m/s^2 for different f_0 of the nano stage.*
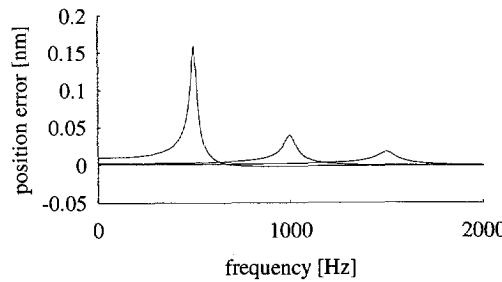
Internal nano stage dynamic errors originate from the piezoelectric drive. It causes impulse forces on the table which results in a vibration of the table after stepping. This vibration can be characterized by:

$$z_t \cong s_t \left(1 - \frac{1}{\sqrt{1-\beta^2}} e^{-\beta \omega_0 t} \cos\left(\sqrt{1-\beta^2}\, \omega_0 t\right) \right) \tag{5.5}$$

Typical step sizes of the table (s_t) are in the order of 50 nm. With $\beta = 0.03$ and $f_0 = 1.5$ kHz, the settling time to achieve picometer vibration amplitudes is in the order of one tenth of a second and can be neglected.

In the TEM situation, the level of pole piece accelerations is kept low by the specially designed vibration isolation system mentioned before. The efforts to obtain a high nano stage stability should not only concern the nano stage, but the vibration isolation system as well. This system, however, gives no protection to acoustic vibrations. These have to be suppressed by the TEM column and the nano stage itself.

5.4   Thermal stability

5.4.1   Introduction

Temperature disturbance is the most serious problem in the whole field of precision engineering. Changes in the heat production or heat transfer in nano stages or its environment can have a strong influence on the dimensional and form stability of the nano stage, its reference frame and the column. Extensive investigation of the heat production and the heat transfer in the microscope column and the microscope environment is beyond the scope of this research. It is assumed that the heat transfer from the column to the nano stage can be made low enough to assure sufficient specimen stability. Still, some remarks regarding the influence of heat sources in the column and the environment should be made.

The TEM is supposed to be in a temperature controlled room, where heat sources outside the column are expected to cause only slow temperature changes. An important advantage of a pole piece nano stage is that the influence of such heat sources is suppressed, because heat must first be transferred through the column to the vacuum chamber and the nano stage. Nevertheless, changes in the external heat production should be kept to a minimum.

The number of heat sources and heat sinks in the column and the amount of heat they produce or absorb is considerable. The main heat sources are the electromagnetic lenses. Although, they are cooled by a water coolant system, a part of the heat they produce is transferred to the column. In normal use, the magnetic lens currents and water coolant currents are never switched off in order to achieve a high level of thermal equilibrium. Besides that, the stability of the lens current is in the order of a few ppm. However, several actions disturb this 'equilibrium': switching on the electron beam, changing the electron beam settings, changing lens settings, moving the specimen to a new position, or changing specimens. During normal operation, these changes cannot be avoided. It is assumed that entire thermal equilibrium is never obtained in an operational TEM.

Therefore, depending on the expected amount of heat transfer, the nano stage should be thermally isolated from its environment. Before discussing the effect of heat sources in the nano stage, the ways of heat transfer should be considered.

5.4.2 Heat transfer

Heat can be transferred by conduction, by convection and by radiation. Often, all three types act in conjunction. Heat transfer by conduction depends on the heat conductivity coefficient λ of the materials involved and on the medium between them. The heat conductivity coefficient depends on the molecular structure of the materials or gasses involved. The conductive heat transfer rate $\dot{Q}_c$ in a bulk material between two surfaces of area A, temperature T and at distance δ_i is given by:

$$\dot{Q}_c = \frac{\lambda A(T_{high} - T_{low})}{\delta_i} = KA(T_{high} - T_{low}) \tag{5.6}$$

where K is the heat transfer coefficient. For a gas, the heat conductivity coefficient is determined by the density of gas molecules between two surfaces. The conductive heat transfer rate in a gas of pressure P (in Pa) is given by [96]:

$$\dot{Q}_{cg} = A\beta\Lambda(T_{high} - T_{low})P \tag{5.7}$$

where β is the molecular accommodation factor, and Λ is the free molecular thermal conductivity coefficient. On this basis, the conductive heat transfer rate in a vacuum of 10^{-4} Pa, with $\Lambda = 1.2$, $\beta = 0.5$, and a temperature difference of 0.1 K is only $6 \cdot 10^{-6}$ W/m^2 and can, as will be shown, be neglected. In the vacuum chamber of the TEM, this leaves conductive heat transfer through mechanical contacts, for instance, through the nano stage table and the support elements, through the piezo actuators and the base, and through the reference frame and the pole piece. Except for vacuum, conductive heat transfer in practice goes together with heat transfer through convection. In case of heat transfer through different homogeneous material layers in contact, the factor $1/KA$ can be approximated by:

$$\frac{1}{KA} = \frac{1}{\alpha_i A} + \sum_i \frac{\delta_i}{\lambda_i A} + \frac{1}{\alpha_a A} \tag{5.8}$$

where α_i and α_a are the heat transfer coefficients for convection on both sides of a plane wall. For free convection in gases, these heat transfer coefficients are in the order of 10 up to 20. The heat transfer rate through a stainless steel plate of 10 mm, having a temperature difference of 0.1 K is about $1.6 \cdot 10^2$ W/m^2. It should be noted that the factor $1/KA$ strongly depends on the size of the real contact area between materials.

The heat transfer rate for radiation can be calculated by:

$$\dot{Q}_r = CA(T_{high}^4 - T_{low}^4) \tag{5.9}$$

where C is a constant depending on the Kirchhoff emission factor, the Stefan-Boltzmann constant and the shapes and sizes of both the 'hot' and 'cold' area. In the most unfavorable situation of two black surfaces, the heat transfer rate for radiation at a temperature difference of 0.1 K is $4.6 \cdot 10^{-1}$ W/m^2.

In conclusion, the heat transfer in a 10^{-4} Pa vacuum can be described by conduction through materials in contact and by radiation. For the nano stage setups not used in vacuum, heat transfer is determined by a combination of conduction, convection, and radiation. In order to slow down conductive heat transfer between the pole piece and the nano stage, a material with a low heat conductivity can be used between the pole piece and the nano stage. In order to prevent radiative heat transfer to the nano stage, a reflective coating, like gold, can be used on the outer nano stage areas.

5.4.3   Heat sources in the nano stage

The thermal stability of a nano stage is directly affected by heat produced in the piezo drive and the capacitive transducers, and heat transferred from the electron beam, from the pole piece and from cooling or heating holders. Depending on the amount of heat produced in and transferred to the nano stage, the nano stage sensitivity to these influences should be correspondingly low. The heat production resulting from piezo actuators and capacitive transducers was estimated in chapters 2 and 4. The influence of this heat production and the influence of the electron beam on the nano stage and the specimen stability are discussed here. The influence of cooling and heating holders is omitted because this is a very special issue that should be subject of another research.

A piezo drive has two internal heat sources: heat production in the piezo actuators and heat production due to slip between the table and its supports. It is assumed that, the heat that is produced is completely stored in the piezo actuators and in the table. The amount of heat produced by dielectric loss in the piezo actuator can be estimated by means of equation 2.3. The total piezo capacitance C_p in a piezo drive is about 0.2 nF. The dielectric loss factor $tan\,\delta$ is about 0.015. An upper limit of the heat production rate can be estimated by assuming continuous motion at 500 Hz frequency and 100 V driving voltage. The heat production rate then is $1.5 \cdot 10^{-5}$ W. The heat produced due to slip depends on the maximum friction force $F_{f_{max}}$, the driving frequency f and the step size of the table s_t, assuming that the preload force is constant. The step size is multiplied by a factor η in order to compensate for multiple sliding phases during a single step; η is estimated to be 1.5. The heat production rate by sliding is estimated by:

$$\dot{Q}_s = \eta F_{f_{max}} f s_t = \eta \mu_d m_t g f s_t \qquad (5.10)$$

With $s_t = 50$ nm, $\mu_d = 0.15$ and $m_t = 0.03$ kg, the heat production rate due to slip is $1.7 \cdot 10^{-6}$ W. The total heat production rate is then in the order of $2 \cdot 10^{-5}$ W. Continuous heat storage in the piezo actuators causes a drift of the table relative to the lower pole piece. Assuming linear expansion, the magnitude of this drift can be estimated by:

$$\frac{\Delta w}{\Delta t} = w\alpha\frac{\Delta T}{\Delta t} = w\alpha\frac{\dot{Q}}{V\rho c} \qquad (5.11)$$

where w is a typical dimension of the piezo actuators, α is the linear expansion coefficient of the piezo actuators, $\dot{Q}$ is the heat production rate, V is the piezo actuator volume, ρ is the density, and c is the specific heat of the piezo ceramic. The maximum linear expansion rate is estimated to be in the order of $2 \cdot 10^{-12}$ m/s = 120 pm/min.

The heat production rate in a 10x10x1.5 mm^3 glass plate which carries the electrodes of a capacitive displacement transducer was estimated to be in the order of 10^{-6} W (see section 4.5.2.5). Assuming linear expansion and assuming $\alpha = 9.3 \cdot 10^{-6}$ K^{-1}, $\rho = 2.6 \cdot 10^3$ kg/m^3 and $c = 0.84 \cdot 10^3$ J/kg·K, the substrate expansion rate is calculated to be $4 \cdot 10^{-14}$ m/s. This effect can be neglected.

An important external heat source is the electron beam. Since a part of the electron energy is lost during specimen interaction, the specimen heats up. The electron beam current is in the order of 1 nA, the electron acceleration voltage is about 100 keV. Although a part of the electrons in the electron beam collides with different obstacles placed in the optical path, like apertures, most electrons reach the specimen. Due to specimen interaction, electrons lose about 0.02% of their energy. The heat production rate in the specimen is therefore about $2 \cdot 10^{-8}$ W. This heat will be stored in the specimen, the thin copper grid that supports the specimen and in the nano stage table. If it is assumed that all the heat produced by the electron beam is stored in the table, this would cause an expansion rate of the table of less than 0.1 picometer per second for a table with dimensions 5x5x1 mm^3. This effect can be neglected. In practice, the amount of heat transferred to the table depends on the size of the contact area between the grid and the table. This means that a part of the heat produced by the electron beam is stored in the specimen and the grid.

A TEM specimen is about 3 mm in diameter and about 50 nm in thickness. The copper grid is normally about 15 µm thick; between 25 and 60% of the grid area consists of bars. The heat produced by the electron beam is absorbed by the specimen and the copper grid. It is assumed that the thermal gradient in the specimen/grid configuration is low due to their high conductivity so that thermal equilibrium in the specimen and the grid is obtained fast. However, if all the heat produced by the electron beam is stored in the specimen and the grid, this can result in a drift rate in the order of 10 nm/min [97]. This means that image stability not only depends on the position stability of the stage table. In order to obtain low specimen drift fast, the heat transfer rate to the table should be high. The influence of thermal drift in the specimen and the grid was confirmed by Watt [98]. In chapter 6, an experiment is described in which the nano stage table position is compared to the image position recorded by the microscope's CCD camera.

Although the effect of the electron energy loss on the nano stage table stability is low, the specimen is not the only place where electron energy is converted into heat. Many electrons collide with the aperture holder between the specimen and the lower pole piece. This aperture holder therefore is an indirect heat source that can not be neglected. The amount of electrons that collides with the aperture holder can be up to 99% of the electrons of the electron beam.

5.5   Creep

An abrupt change in the mechanical load of an object results in an immediate elastic and partly plastic deformation response (initial strain) and a time dependent deformation. This time dependent deformation is called creep. Creep is defined as the relative change in the strain of an object under constant load, directly after loading and after a suitable chosen time interval. At this point, one should distinguish between object strain caused by creep and object strain caused by relaxation of internal material stresses. These internal material stresses often originate from the

manufacturing process. It is assumed that materials applied in nano stages are treated such that they do not suffer from this stress relaxation. This assumption is assumed to hold for all nano stage elements but the piezo actuators.

For many applications, creep becomes only important at elevated temperatures (~$0.4 \cdot T_{melt}$). However, as far as stability at the picometer level is concerned, creep effects at room temperature values should certainly be considered. Traditionally, the creep rate of an object is divided in three phases (see figure 5.4): I) the strain rate decreases, II) the strain rate is constant, and III) the strain rate increases. The course of the strain rate in time and the magnitude of the strain rate depend on the material temperature and the magnitude of the stresses. As far as nano stages are concerned, it is assumed that stresses and application temperatures are so low that phase III is not reached. Besides that, it is assumed that after a change of load, the table strain rate decreases resulting in a constant strain rate of zero (phase II).
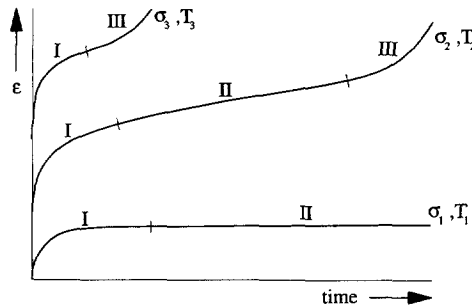
Fig 5.4   The creep rate of an object can be divided in a decreasing phase, a constant phase and an increasing phase. The appearance of these phases depends on the application temperature and the magnitude of the stresses.

According to Bethe [99], creep consists of two parts: thermoelastic creep and "anelasticity". Thermoelastic creep is explained by the fact that any adiabatic deformation of a solid object changes its volume resulting in a temperature change and a dimensional change ruled by the linear expansion coefficient of the object. The anelastic behavior is the result of an atomic redistribution in the deformed lattice. Two mechanisms of this redistribution exist: diffusion creep and dislocation creep [100]. Depending on the load situation, one of these mechanisms or a combination of these mechanisms occurs. In case of nano stages, creep will be ruled by diffusion. The magnitude of the creep effects depend on the type of material, its (metallurgical) constitution, and its dimensions (creep increases with decreasing body thickness). It can, for instance, be expected that a monocrystalline material will suffer less from creep than a polycrystalline material. Creep can be as high as 1% of the change in the initial strain. In case of the example of the contact between the ruby sphere and the table in chapter 3, this would imply table drifts in the order of 1 nm. This will be investigated in the next section. Bethe proved that creep can be minimized by the choice of materials. Quartz glass, copper-beryllium alloys and single crystallines like silicium, germanium or sapphire showed small creep, compared to for instance Zerodur.

5.6   Support stability

5.6.1   Introduction

Generally, a nano stage table is supported by support elements which guide the table in a limited number of degrees of freedom. The support stability directly influences the table stability. Therefore, the quasi-static support stability should be considered in the direction of motion and in the direction of the preload force. Figure 5.5 shows a schematic view of a table on support elements and the stability measurements that were performed. The settling time is the time required to reach a certain drift rate. In order to determine the amount of contact creep in the (or near the) supports, some experiments have been carried out. The test setups used for these experiments are described in section 5.6.3 and the experimental results in sections 5.6.4 and 5.6.5. During the experiments, it was found that the shape of the support elements was very important. In order to explain this, a partly new contact theory is presented in the next section.
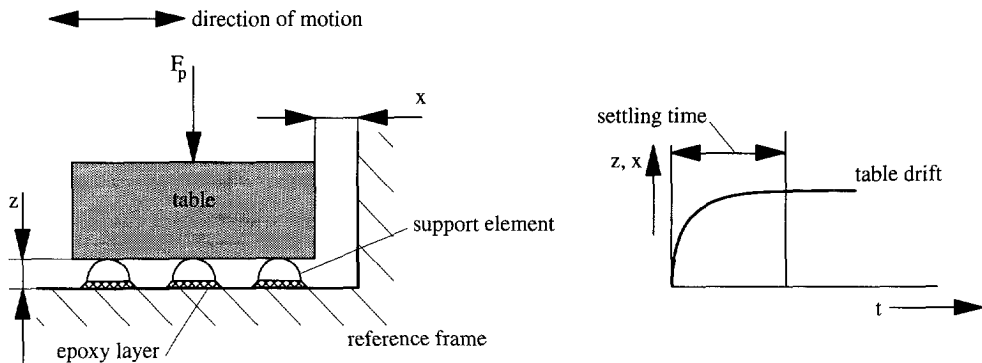
*Fig. 5.5   The nano stage table is supported by support elements. After moving the table, the position sta-
bility of the table can be measured in time relative to the reference frame, both in the direction
of motion and in the direction of the preload force F_p.*

5.6.2   A subnanometer contact theory

In the conventional theory on contact surfaces [69], the macroscopic contact area between two bodies is called the apparent contact area A_a. However, within this area a limited number of real contacts between sets of surface asperities of both surfaces exits, the junctions (see figure 3.10). The sum of the junction areas over the whole apparent contact area is called the real contact area A_r. As soon as the junctions are made, the position of the table relative to the support is stable at the micrometer level. This level of stability can be explained by the fact that the initial elastic and plastic deformations of the asperities, take place within fractions of a second. However, at the

nanometer level there is still drift in the direction of motion as well as in the direction of the preload force. This drift can be explained by creep in the junctions as a result of the preload force and as a result of small (residual) friction forces in the junctions in the direction of motion. The residual friction forces can be induced by table motion. It is assumed that the magnitude of these residual friction forces for instance depends on the time between stick of single junctions in the contact areas, on the magnitude of the maximum friction force F_{fmax} (and hence on the magnitude of the preload force), and on the stiffness of the surface asperities. The residual friction forces can cause a combination of stress relaxation and creep, resulting in drift of the table. However, according to the measurements presented later, the large position drift rates in the direction of the preload force occurring in supports with a large apparent contact area, cannot be explained by these effects only. The conventional contact theory must therefore be extended.

At the nanometer level, the table stability may not only be influenced by creep in the junctions and the magnitude of the preload force F_p, but also by the size of the apparent contact area A_a and by the presence and composition of layers of adsorbed molecules at the contact surfaces. These layers can be found at surfaces exposed to the atmosphere at moderate levels of humidity [96]. Generally, these layers consist of 50 up to 100 layers of molecules, which is equal to a thickness of tens of nanometers. When the surfaces of the table and the support element are brought into contact, the preload force is balanced by the rise in pressure in the layer of adsorbed molecules which is induced by the flow resistance of the adsorbed water layer. The rise in pressure causes a flow of the adsorbed molecules into the small gaps between the asperities of both surfaces (see figure 5.6). Consequently, the adsorbed layer between two closely approached asperities is partly pressed away. The flow of the water layer is time dependent. It is expected that the flow resistance depends on the gap configuration and on the composition of the layer of adsorbed molecules. It is expected that the gap configuration will, to a large extent, be determined by the shape of the support elements. It is expected that the size of the apparent contact area has a strong influence on the amount of drift. The smaller the apparent contact area, the smaller the number of potential junctions and the higher the local initial pressure in these junctions and in the adsorbed water layer. Consequently, the adsorbed layer is pressed away more easily, resulting in shorter settling times.
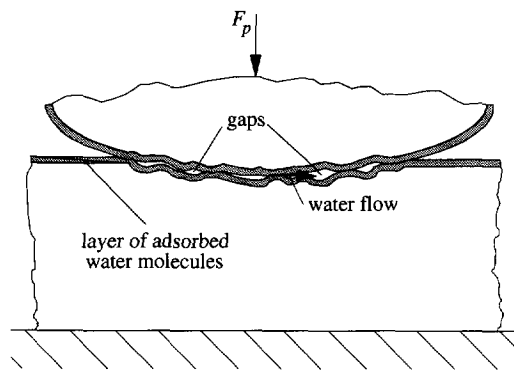

Fig. 5.6   Drift in the direction of the preload force of a support configuration can partly be explained by
          the layer of adsorbed water molecules.

In an environment with a certain level of humidity, the layer of adsorbed molecules will recover as soon as the connection is released. However, when the table slides over its supports as a result of a step with a piezo drive, the question arises as to whether the water layer will recover, and if so, to what extent. During such a step, the surface asperities slide over each other and, depending on the junction area size, form new junctions. As a result, water molecules on surface asperities are pushed away. Moreover, former water layers on surface asperities forming a junction have less chance to recover. Therefore, the table drift in the direction of the preload force after moving the table is expected to be smaller than after *initially* placing the table on the support elements.

The table drift rate may be influenced by the water layer on the surface and the composition of the gas molecules of the environment, both working as some sort of lubricant.

Many nano stages will be applied in vacuum. The number of adsorbed water molecules on a contact surface will then be much less, resulting in a different drift behavior of the table after it is moved to a new position. The experiments described in section 5.6.4 were performed both in vacuum and in air in order to prove this different behavior.

5.6.3   Experimental setups

Two setups were built in order to investigate the support stability both in the direction of the preload force and in the direction of motion.

The first setup is shown in figure 5.7. Two types of supports were investigated with this setup: a kinematic support and a nonkinematic support. The kinematic support consisted of three spherical support elements, having a small ratio of the apparent and the real contact area. It is expected that this support configuration has a short settling time. The nonkinematic support consisted of an extremely flat area, having a large ratio of the apparent and the real contact area. The table's position stability in the Z direction was considered for two different situations: after initially placing the table on the support and after a step in the X direction. The test setup consisted of a
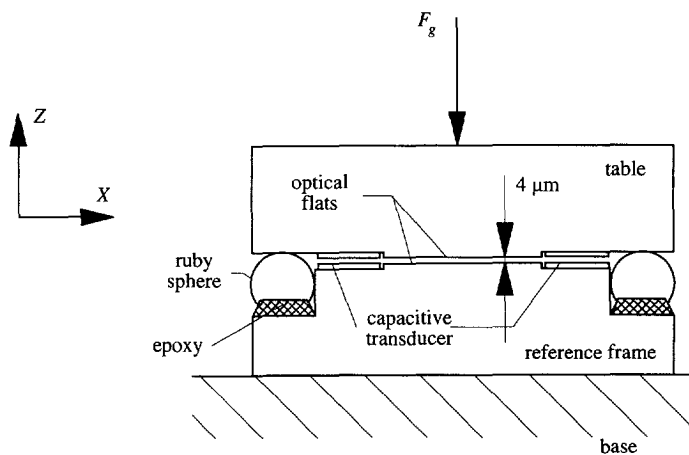

Fig. 5.7   The setup to investigate the support stability of two different supports in the direction of the preload force.

Zerodur [101] table and a Zerodur reference frame, which was attached to a base. Zerodur was used to minimize the influence of temperature changes. The support elements were preloaded by the gravity force F_g of the table in the Z direction; the X direction is the direction of motion. A step of the table in the X direction was made by applying a small impact force to the base. Both the reference frame and the table had a flat surface of 15x15 mm^2, with a flatness better than 300 nm and a roughness R_a = 50 nm. The table was either placed on the three ruby spheres or on the flat surface of the reference frame when the spheres were taken away. The spheres were fixed to the reference frame by surrounding the contact point of the spheres and the reference frame with an epoxy, leaving a 4 µm gap between both flat surfaces. The table dimensions and the reference frame outer dimensions were the same: 40x40x12 mm^3. The flat surfaces of the table and reference frame were surrounded by a 0.1 millimeter high step to provide a gap for a capacitive displacement transducer, which measured the table drift in the direction of the preload relative to the reference frame with a resolution of 15 pm at 2 Hz bandwidth. The influence of the table gravity force on the support stability was verified by attaching extra masses to the table. The influence of different table materials on the *kinematic* support stability was tested by applying three different table materials: Zerodur, aluminum and stainless steel coated with a 1 µm TiCN layer. The aluminum and stainless steel table were not provided with an optical flat. Like the Zerodur table, the aluminum and stainless steel tables were 0.08 kg.

In order to investigate the influence of the adsorbed layers of water molecules on the stability of the table, the thickness of this layer of water molecules was varied. The starting condition was ambient air, with approximately 50% humidity. Later on, the test setup was placed in a vacuum system to substantially decrease the water layer thickness. By evacuation to 10^{-4} Pa, desorption of the water molecules from all surfaces occurs. Although the pressure in the vacuum system is no direct measure of the adsorbed water layer thickness, it is generally expected that after 24 pumping hours and a pressure of 10^{-4} Pa, only one or two monolayers of water molecules are left on the surfaces [96]. During the third phase of the experiment, the vacuum system was filled with nitrogen gas instead of ambient air. Compared to the ambient air situation the composition
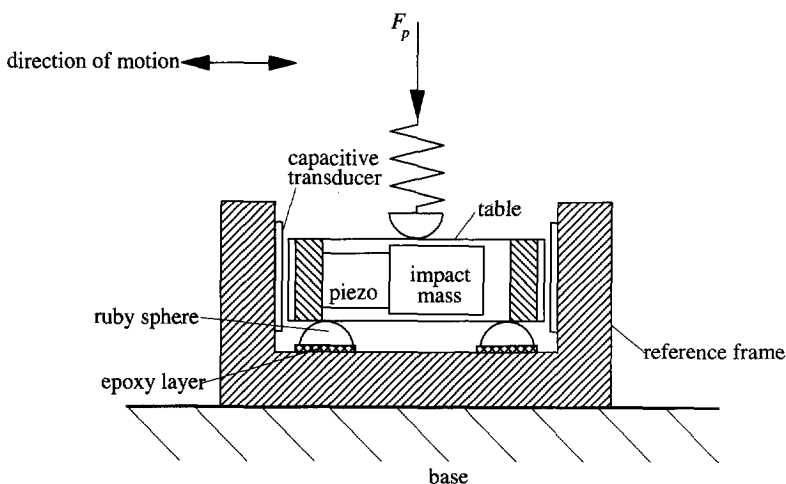

Fig. 5.8   The setup to verify the table's position stability after stepping in the direction of motion.

of the gas molecules in the vacuum system is then completely different. In the vacuum system, the table was placed on the support and periodically lifted from the support by means of a linear vacuum feed-through which served as a lift. The entire measurement setup was placed in a temperature and humidity controlled room. The test results of this first setup are given in section 5.6.4.

The second setup is shown in figure 5.8. It was used to test the table's position stability relative to the reference frame in the direction of motion after stepping. It consisted of an aluminum reference frame, three ruby spheres, a differential capacitive plate-distance transducer, and a table. The table was moved relative to the reference frame by means of IDM. The table was made of stainless steel coated with a TiCN layer. The table mass m_t was 0.03 kg. The table was preloaded by an adjustable force F_p (up to 8 N), in this way allowing motion in the direction parallel to the gravity field ($\mu_{st} \cong 0.15$). The displacement resolution of the capacitive transducer was 30 pm. The test results are given in section 5.6.5.

5.6.4 Support stability in the direction of the preload force

5.6.4.1 Kinematic support

Figure 5.9a shows typical results of the initial drift in the Z direction of the Zerodur table relative to the kinematic support formed by the three ruby spheres. The drift courses represent the table position stability in ambient air, in 10^{-4} Pa vacuum and in nitrogen gas, respectively. For all three situations, the table drifted a few nanometer towards the reference frame over 30 minutes. Drift rates in the order of 50 pm/min are reached within 15 minutes after initially placing the table on the spheres. The total amount of drift, the drift rates and the settling time were at least 20 times smaller than for the nonkinematic support, as will be shown in the next section. This difference was explained by the small apparent contact area and the high contact pressures when contact was made. In ambient air, the water layer was immediately pressed away and its influence on the table drift was small. Therefore, the table drift for the kinematic support in the direction of the preload force should be attributed to creep in the junctions of the contact area. Although the difference in the amount of drift between each of the three support conditions was less than 2
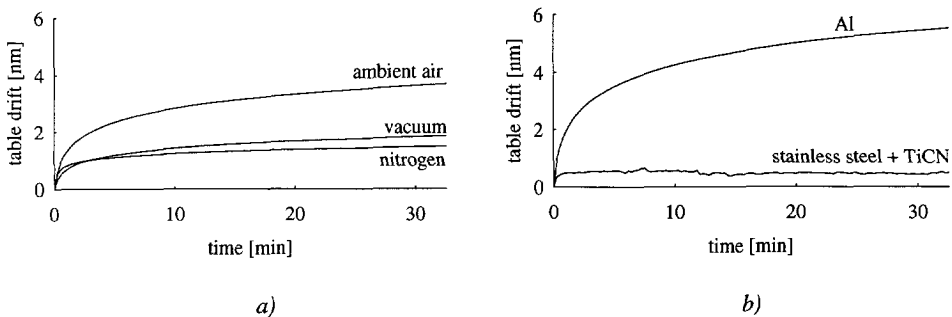
Fig. 5.9   a) Initial drift in the Z direction of the Zerodur table placed on a kinematic support in ambient air, in 10^{-4} Pa vacuum and in nitrogen gas. b) Initial drift courses of the aluminum table and the TiCN coated stainless steel table placed on the kinematic support in ambient air.

nanometers, the table drift under ambient air conditions was generally found larger than the table drift in vacuum and in the nitrogen gas situation. The latter was generally found to be the smallest.

Figure 5.9b shows the initial drift of the kinematically supported aluminum table and the TiCN coated stainless steel table under ambient air conditions. For the aluminum table, a 5 nanometer drift over 30 minutes was found. For the stainless steel table, the drift was much lower. The settling time to reach a drift rate of 100 pm/min was smaller than 1 minute. The relatively large amount of drift in the Zerodur table compared to the stainless steel coated table was in accordance with the large creep rates found for Zerodur by Bethe. Besides that, there seemed to be a relation between the amount of drift of the three tables in ambient air and their modulus of elasticity and surface hardness. Table 5.1 gives the modulus of elasticity and the Vickers hardness of the materials used in the experiments. Apparently, high contact pressures in materials or layers with a high modulus of elasticity and/or hardness cause less table drift. However, the ratio between the thickness of the TiCN coating and the approach δ between the ruby sphere and the table should also be taken into account ($\delta \cong 100$ nm). It is expected that table drift increases when this ratio decreases.

Material	Modulus of elasticity (10^9 N/m^2)	Vickers hardness (H_v)
Zerodur	90	600[b]
Ruby	320	20 000
Aluminum	72	80
Stainless steel	210	<250
TiCN	_[a]	3 000

[a] Equivalent modulus of elasticity depends on the bulk material and TiCN layer thickness.
[b] Reference [102].

Table 5.1   Modulus of elasticity and Vickers hardness of the materials used.

The influence of stepping in the X direction on the stability in the Z direction is shown in figure 5.10. Compared to initial placement, the drift in the Z direction after stepping was less. There was no significant difference in the drift after a single or after 10 steps. The settling time to

Fig. 5.10   Table drift in the Z direction after 10 steps of about 100 nm each in the X direction in ambient air.

obtain a drift rate of less than 100 pm/min was around 150 seconds for the Zerodur table and about 15 seconds for the TiCN coated stainless steel table.
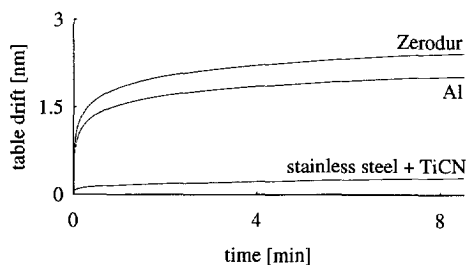
All the drift courses shown were average results of repeated measurements. The shape of the drift courses was remarkably constant and very smooth. They could be well described by a logarithmic curve. The spread in the total amount of drift over the measurement interval was up to ±30% of the values shown. A part of this spread can be explained by the spread in the starting point of the measurement after initially positioning and after stepping of the table.

With regard to the required drift rates and settling time in the TEM application, it can be concluded that kinematic supports become stable at the subnanometer level in the direction of the preload force within an acceptable settling time if special attention is paid to the material selection of the contact surfaces. Moreover, with regard to the kinematic support stability, it seems that the choice of materials is more important than the environmental conditions.

5.6.4.2 Nonkinematic support

The initial drift of the Zerodur table in the direction of the preload force after placing the flat surface of the table on the flat surface of the reference frame is shown in figure 5.11. It was experienced that, for this nonkinematic support, drift could be called initial when the table was lifted from the reference frame for at least two hours before it was placed back. This appeared to be the time interval for the contact surfaces to fully recover from a 30 minute contact period. Such a long recovery time cannot be explained by a slow recovery of the water layer on the contact surfaces, because the water layer was assumed to recover in a fraction of a second. It was assumed that creep played a part here. The total amount of table drift for the nonkinematic support was about a factor 20 larger compared to the kinematic support. Drift rates lower than 100 pm/min were not achieved within 30 minutes for all three conditions: ambient air, 10^{-4} Pa vacuum and nitrogen gas. However, there was a clear difference between them. The initial drift under ambient air conditions (~100 nm) was more than twice the initial drift under low vacuum conditions (~45 nm) and about four times the initial drift under nitrogen conditions (~25 nm). These results confirmed the influence of the adsorbed water molecules on the contact surfaces. Although, the table drift both under low vacuum and nitrogen gas conditions was smaller than under ambient air conditions, it was much larger compared to the table drift in case of the kinematic support. The remaining drift effect may be attributed to a large amount of creep in the
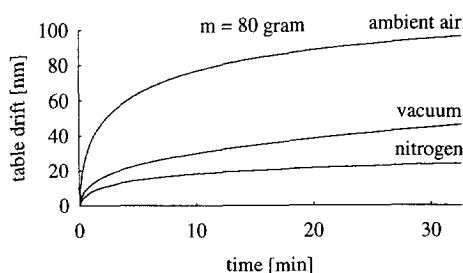

Fig. 5.11   *Initial drift of the nonkinematically supported Zerodur table over an interval of 30 minutes for three different environmental conditions.*

(relatively large number of) junctions. Nitrogen gas appeared to stimulate short settling times. The constancy of the drift course shape and its smoothness were even higher than for the kinematic support situation. The repeatability of the initial drift measurements was within 15%.

In order to test the effect of a short break in the contact between the table and the reference frame, four successive 30 minute drift measurements were carried out in vacuum. Between each drift measurement, the table was lifted for about 30 seconds. Figure 5.12a shows the set of drift curves. The first measurement (1) was an initial measurement. The total amount of drift decreased after each drift measurement. It appeared that 30 seconds was too short for the contact surfaces to fully recover from the 30 minute contact periods. From the third measurement on, a kind of drift "saturation" seemed to occur. Figure 5.12b shows the 30 minute drifts after connection breaks of 1, 2, 5, 15 and 60 minutes, following an initial measurement. As expected, drift increased with connection break time.

Two additional drift measurements were performed in ambient air with larger preload forces of 1.5 and 3.5 N, respectively. In agreement with the subnanometer contact theory, the amount of table drift and drift rate after 30 minutes was lower compared to initial measurements with a 0.8 N preload force.

After an initial 30 minute drift in ambient air, the table was moved about 200 nm in the X direction by applying a small impact force to the setup base. The successive 30 minute drift was about 20% of the initial amount of drift. However, the drift curve was not as smooth as all former curves, which may be an indication that different effects dominated the drift course.

a)   b)
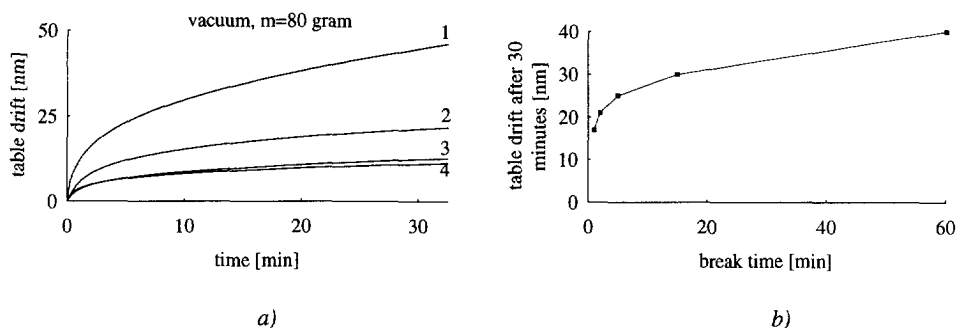
Fig. 5.12   a) Four (1-4) successive 30 minute drift courses with connection break times of about 30 seconds (measured in vacuum). b) Table drift, measured 30 minutes after connection breaks of 1, 2, 5, 15 and 60 minutes, following an initial measurement.

From the experiments in this section, it should be concluded that the stability of the nonkinematic support is lower than the stability of the kinematic support. It should also be concluded that the layer of adsorbed water molecules has a strong influence on this stability. Therefore, the kinematic support is the best solution in nano stages.

5.6.5   Support stability in the direction of motion

For the investigation of the support stability in the direction of motion, only kinematic table supports were considered. All further experiments were performed in ambient air, since the influ-

ence of a vacuum on the kinematic support stability was expected to be low and since it was technically more complex to perform experiments in vacuum.

During the experiments, especially the influence of the preload force on the table stability was considered. This is important with regard to the difference between stepping perpendicular and parallel to the gravity field. For motion perpendicular to the gravity field, there is normally no preload other than the table gravity force working on the spherical support elements. For motion parallel to the gravity field, the preload force must be increased about one order of magnitude. The time interval during which the table drift was measured was shortened to one minute, since the major drift occurred during this period after stepping. For the experiments, the setup of figure 5.8 was used.

Figure 5.13a shows a typical table drift course after a single, 67 nm IDM step for a preload force of 0.3 N (mass of the table only). After a considerable drift rate during the first few seconds, the drift rate decreased. The settling time to reach a drift rate of 100 pm/min was in the order of 12 seconds. Although the drift course was less smooth, the amount of table drift was very well comparable to the drift of the stainless steel table in the direction of the preload force, as was shown in figure 5.10. Since creep can only occur under load, table drift in the direction of motion could be explained by the presence of (residual) friction forces in the contact areas between table and support elements. This resulted in creep in these contact areas and in the epoxy layer between the support elements and the reference frame. The lower smoothness of the table drift course could be explained by the mutual influence of the friction forces in the junctions of the three contact areas.

a)   b)
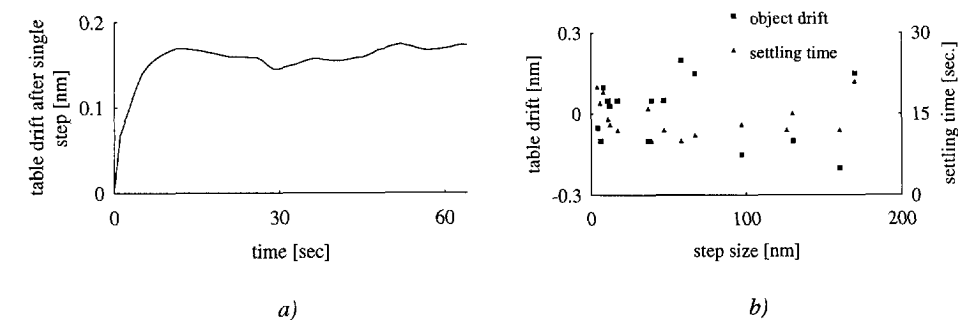
Fig. 5.13   a) Typical table drift course in the direction of motion after a single 67 nm IDM step at 0.3 N preload force. b) Table drift measured one minute after a single IDM step at 0.3 N preload force and the settling time needed to reach a drift rate of 100 pm/min.

Figure 5.13b shows the table drift one minute after a single IDM step in the direction perpendicular to the gravity field for different step sizes. The table drift was typically in the order of 0.15 nm and there seemed to be no relation between the step size and the amount of drift. It should be noted, however, that the direction of the table drift was unpredictable with respect to the stepping direction. The settling times to reach a drift rate of 100 pm/min varied between 5 and 20 seconds. It was also found that the number of steps had no significant effect on the amount of drift. This was in accordance with the assumption on the residual friction forces.
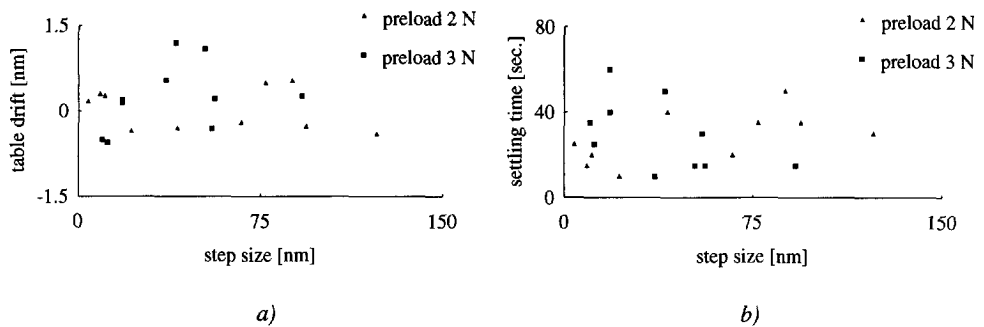
Fig. 5.14   a) Table drift measured one minute after a single IDM step for two different values of the preload force: 2 N and 3 N. b) Settling time needed to reach a drift rate of 100 pm/min.

Figure 5.14a and b show the table drift and the settling time one minute after a single IDM step for different step sizes and for two different values of the preload force: 2 N and 3 N. Compared to the 0.3 N preload force, both the drift and the settling time increased for most of the measurements. The spread in the amount of drift and in the settling time were considerably large. This was in agreement with the theory on the residual friction forces in the contact areas between the table and the supports, because it was expected that the magnitude of the creep effects would be proportional to the magnitude of the preload force. Like for the 0.3 N preload force, the direction of the drift appeared to be random and there appeared to be no relation between the step size and the amount of drift. Besides that, the smoothness of the drift courses was decreased further and the shape of the drift courses was far from constant. In order to investigate the effect of a constant gravity force on the table in the direction of motion, the setup of figure 5.8 was rotated 90 degrees. However, no significant effect on the table drift was found.

From the former experiments, it should be concluded that the settling time to reach a drift rate lower than 100 pm/min of a kinematically supported table in the direction of motion *can* be in the order of 10 seconds, as was specified in table 1.1, if the preload force on the table remains low. The assumption of the existence of residual forces can be used to explain the existence of table drift in the direction of motion by lack of an external force working on the table in that direction. It can also explain the spread in the amount of drift and the settling time and their dependence on the magnitude of the preload. As a result of this spread and the spread in the shape of the drift course, the table drift rate resulting from creep in its supports cannot be controlled on the basis of knowledge about the table drift course, but only by means of closed-loop control.

5.7   Piezo actuator stability

The piezo actuator stability is mainly determined by the piezo drift which follows a voltage change. As was explained in chapter 2, the amount of drift and the drift rate depends on the size of the voltage step or the voltage cycle, but also on the deformation history of the piezo actuator. As was concluded in chapter 3, piezo drift influences the table drift in piezo drives. In order to obtain a high table stability without applying closed-loop control, piezo drift must be minimized

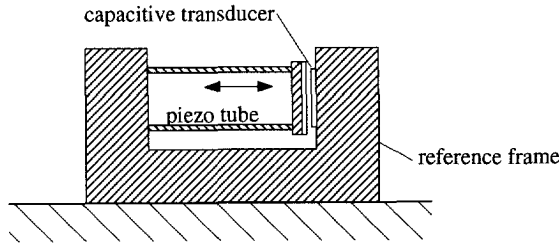*Fig. 5.15*   *Drift effects in a piezo actuator were investigated with a single tube actuator and a capaci-*
                tive transducer.

by using low driving voltages or it must be compensated by applying open-loop control. The latter may be achieved in two ways. Either by compensation based on knowledge of the piezo drift course or by making a single compensation voltage cycle as was discussed in chapter 2. Both methods can only be successful when the deformation history of the piezo actuator is simple and when its influence is well known. In practice, this means that the amplitude of the driving voltage and the shape of the voltage cycle in time should be reasonably constant. During the experiments, the simplicity of the piezo history was maintained by changing the magnitude of successive voltage cycles with a maximum of 10 V only. In order to investigate the benefit of both compensation methods, the setup of figure 5.15 was used. It consisted of a reference frame, a piezo tube, and a plate-distance capacitive transducer with a resolution of about 6 pm.

Figure 5.16 shows two typical drift courses of the piezo actuator after voltage cycles of 200 V amplitude with and without a compensation cycle of 30 V. For open-loop compensation based on knowledge about the piezo drift course, the drift courses without compensation cycle were considered first. Generally, these drift courses were very smooth. The amount of piezo drift was about 3% of the nominal piezo deformation during a voltage cycle. The repeatability of the amount of drift and the drift rate a certain time after the voltage cycle at constant amplitude was within 15%. This means that the piezo actuator drift rate can be decreased by at least a factor of five. It was found that this open-loop compensation method does not work for small voltages (< 40 V) because the piezo drift for these voltages is so small that a significant decrease of the drift rate was not perceptible. Figure 5.17a shows piezo drift rate values without compensation cycle as a function of the amplitude of the preceding voltage cycle and for three different time intervals after such a cycle: 20, 60 and 120 seconds. From figure 5.17a, it is clear that the drift rate decreased with time and that the drift rate increased with increasing voltage up to amplitudes of 100 V. Above this amplitude, the drift rate became independent of the voltage. The reason for this latter effect was not clear. It was also found that the piezo actuator drift rate increased as a function of the number of preceding cycles. This increase was about a factor of 1.2 when the number of cycles increased from one to ten and about a factor of two when the number of preceding cycles increased to 100. This increase may be partly subscribed to the heat production in the piezo actuator and partly to a shift of the hysteresis curve relative to its zero point during the first few curves. One should realize that the amount of drift and the drift rate of a piezo actuator can easily be much higher than the table drift and the table drift rate resulting from creep in a kinematic support.
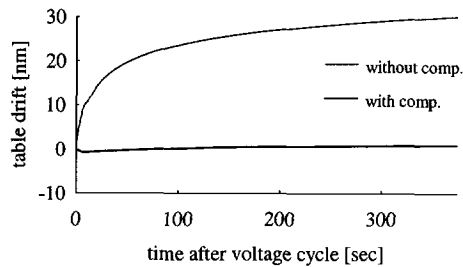
Fig. 5.16   Two typical drift courses of a piezo actuator with and without a compensation cycle of 30 V
            after a voltage cycle of 200 V amplitude.

In order to investigate the benefit of the compensation cycle method, figure 5.17b should be
compared with figure 5.17a. Figure 5.17b shows the piezo drift rate values after a compensation
cycle as a function of the amplitude of the preceding cycles. The amplitude of the compensation
cycle was optimized with regard to the amplitude of the preceding cycles. The amplitude of the
optimum compensation cycle ranges between 15 and 80% of the amplitude of the preceding
cycle; the larger the amplitude of the preceding cycle, the smaller the relative amplitude of the
compensation cycle. The reduction of the drift rates ranged from a factor of 1.5 for cycle ampli-
tudes of 20 V up to a factor of 100 for 200 V. The repeatability of the compensation cycle
method was found to be better than 10%. This implied that this compensation method was
slightly better than compensation by knowledge about the drift course. The concept of the com-
pensation cycle proved to work for voltage cycles with an amplitude larger than 40 V. Below this
voltage the drift of a piezo actuator is so small that a significant effect of the compensation cycle
was not perceptible. The effectiveness of the compensation cycle method was hardly affected by
the number of preceding steps.

a)   b)
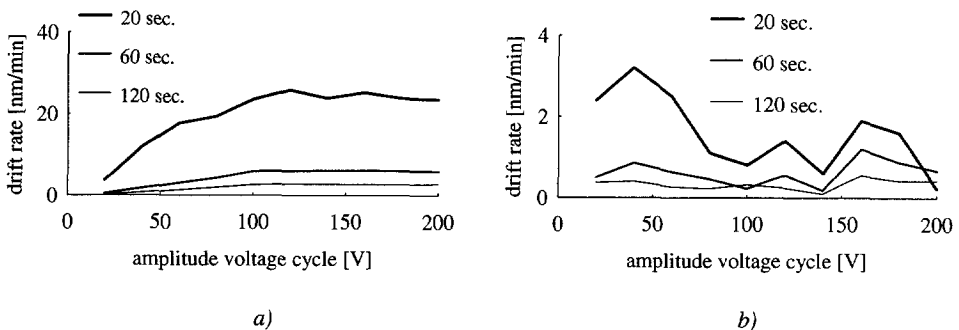
Fig. 5.17   a) Piezo drift rates for different values of the voltage cycle amplitude for three different
            intervals after the last cycle: 20, 60 and 120 seconds. b) Piezo drift rates after the same
            voltage cycles and an 'optimum' compensation cycle.

From the experiments in this section, it should be concluded that piezo drift can be reduced with
al least a factor of five by means of open-loop compensation methods. However, the success of

these open-loop compensation methods depends on the knowledge about the deformation history of the piezo actuators.

5.8   The choice of materials

In a nano stage, one can distinguish between three types of materials: the bulk materials for the table and the reference frame, the ceramic of the piezo actuators, and the materials in the contact zone between table and supports. As was shown in this chapter, they all influence the stability of the nano stage table. Detailed information on the choice of piezo actuator ceramics and contact zone materials was given in chapters 2 and 3. At this point, some general remarks on the choice of nano stage materials with regard to stability are made.

One of the major concerns with regard to table and specimen stability is the influence of overall or local temperature changes as a result of continuous changes in the heat transfer to the nano stage. As was discussed before, the effects of overall temperature changes can be partly compensated for by a symmetric nano stage design. In that case, changes in temperature will not affect the table position in first order. Another important measure is to use the same material for the table as well as for the reference frame. This minimizes table position changes due to differences in linear expansion coefficients. This may also be achieved by matching the linear expansion coefficients of the table and the reference frame in accordance with their dimensions. However, the large table strokes in a TEM make this compensation rather difficult. A last option to minimize sensitivity for varying thermal loads is to minimize the table stroke and to minimize the nano stage dimensions. The influence of local temperature changes can only be minimized by choosing a bulk material with a low linear expansion coefficient at room temperature, like Invar or Zerodur. However, the gain of using low expansion materials can be easily neutralized by the heat production and the resulting expansion of the piezoelectric ceramics of the piezo drives as was shown in section 5.4.3.

Material	ρ $[\cdot 10^3 \text{ kg/m}^3]$	$\alpha^{1)}$ $[\cdot 10^{-6} \text{ K}^{-1}]$	E $[\cdot 10^9 \text{ N/m}^2]$	$c^{1)}$ $[\cdot 10^3 \text{ J/kg·K}]$	$\lambda^{1)}$ $[\text{W/m·K}]$
Aluminum	2.7	23	70	0.95	237
Beryllium	1.9	12	300	1.78	170
Copper	8.9	17	120	0.39	390
Beryllium copper	8.9	18	120	n.a.	84
Stainless steel	7.8	10	210	0.5	16
Titanium	4.5	8.7	120	0.47	22
Invar	8.1	1	145	0.5	16
Zerodur$^{1)}$	2.5	0.05	90	0.8	1.5
Piezo ceramic	7.8	5	100	0.4	2.5

[1]   At 293 K.

Table 5.2   Material properties for some materials suitable for application in a nano stage.

The bulk material used for the tables and the reference frame should have a high ratio of the modulus of elasticity and the density (E/ρ), a low ratio of the linear expansion coefficient and the conductivity (α/λ) and a high thermal diffusivity ($\lambda/c\rho$). The bulk material must not be ferromagnetic or become partly ferromagnetic when it is machined. It must be possible to expose the bulk material to bake out temperatures of 150°C and high static magnetic fields of 2 T without significantly affecting their properties. With regard to charging effects by electrons from the electron beam, the bulk material should preferably be a conductor or otherwise should be coated with a conducting layer. As a matter of fact, coating the bulk material with a reflective coating may be useful in order to minimize radiative heat transfer. Table 5.2 gives properties of some materials suitable for application in a nano stage.

5.9   Concluding remarks

In this chapter, it was shown that there are three ways to obtain a high level of nano stage table stability: open-loop and closed-loop position control and control by means of knowledge about the table's drift course. A high level of the intrinsic stability of piezo drives is determined, among other things, by a high resonance frequency, by applying low driving voltages and by a low sensitivity of the piezo drive to thermal disturbances, especially in the critical directions.

Closed-loop compensation methods strongly depend on the stability of the elements between the object which position must be stabilized and the place where this position is actually measured. In order to obtain effective closed-loop positioning at the picometer level, all intermediate elements must have picometer stability. Just considering the heat production and the heat transfer in the nano stage, it becomes questionable whether closed-loop compensation at the picometer level will be useful.

Apart from insensitivity for quasi-static and dynamic internal and external disturbances, the nano stage should be well isolated from internal and external mechanical vibrations. This means that not only the specimen holder sensitivity to vibrations should be decreased but also that the performance of the vibration isolation system should be improved. Also, the nano stage should be isolated from or should have a low sensitivity for thermal and electrical disturbances.

Heat transfer in vacuum can be described by conduction through materials in contact and by radiation. Important heat sources that influence the nano stage table and specimen stability are the piezo drives and the electron beam. Heat production in the piezo drives can be minimized by applying low driving voltages and frequencies. The electron energy loss in the specimen can seriously affect the internal specimen stability.

The settling time of a kinematically supported nano stage table to reach a low drift rate after stepping can be in the order of 10 seconds if special attention is paid to the material selection of the contact surfaces. This settling time increases with increasing preload force. Besides that, the table drift course becomes less smooth which lowers the intrinsic nano stage stability. Therefore, preload forces should be kept as low as possible.

Open-loop compensation methods can reduce piezo drift with at least a factor of five if the deformation history of piezo actuators is well known.

6 Practical nano stage designs

6.1 Introduction

During this research, a number of different nano stage setups was built in order to study their positioning and stability performance. This chapter discusses the design and performance of four experimental nano stages on the basis of the theoretical aspects and design considerations given in chapters 2 to 5. The following setups are discussed: an XY stage, a Z stage, a one degree of freedom (DoF) rotor stage, and a TEM stage. Some parts of the stage designs and some parts of the discussions on the stage performance were presented previously [103,104,105,106].

6.2 The XY stage

6.2.1 Stage requirements

In order to gain knowledge on the performance and the design parameters of ISM drives for positioning in a plane perpendicular to the gravity field, the XY stage design had to meet the following requirements:

- the stage table position must be measured in the XY plane and the Z direction,
- the size of the stage table must be compatible with the space available in the TEM application,
- the stage table stroke in the X direction must be 1 mm,
- the position repeatability in the XY plane must be better than 10 nm, and
- the resolution of the displacement transducers in the Y and the Z direction must be about 20 pm.

6.2.2 The experimental setup

The experimental XY stage is shown in figure 6.1. It consisted of five main element groups: a reference frame, three piezoelectric tube actuators, three spherical table supports, a table, and three sets of differential plate-distance transducers. The piezo tubes, which had an outer electrode

segmented into four equal parts, were attached to the reference frame. The combination of the three piezo tubes made the XY stage in fact a six degree of freedom positioning device. Each tube had a ruby sphere attached to it by means of a thin (100 μm) epoxy layer. The segmented tubes were aligned such that their main deformation direction was parallel to the main axes of the capacitive transducers. For practical reasons, the piezo tube dimensions were chosen relatively large. They had a length L_t of 7.5 mm, an outer diameter d_{out} of 6.4 mm, and a wall thickness t of 0.6 mm. The sphere had a diameter d_s of 5 mm, half of which was sticking out of the tube. The table was a square, with outer dimensions 20x20x7 mm^3. The bottom of the table was a polished flat (R_a = 0.1 μm). It was placed on top of the spheres. The flat surface and the spheres formed a kinematic support, allowing ISM in the XY plane. ISM was obtained by applying a sawtooth voltage on a single segment of each piezo tube. This way, the opposite segment could be used as a transducer. The reference frame and the table were made from the same construction steel. In order to minimize wear caused by ISM, the table was coated with a 1 μm TiCN layer [107]. The mass of the table was $3.5 \cdot 10^{-3}$ kg, the mass of a tube was $4.5 \cdot 10^{-4}$ kg, and the mass of a sphere was $2.5 \cdot 10^{-4}$ kg.
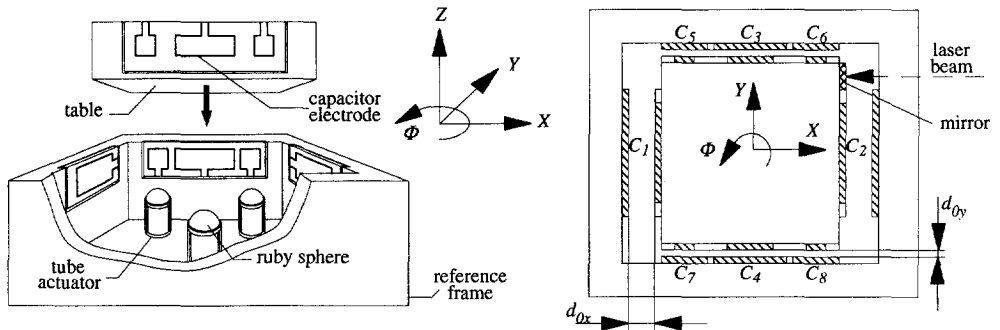
Fig. 6.1   The XY stage. The table can be positioned in the XY plane by means of ISM and capacitive displacement transducers.

The table position could be measured simultaneously in the X, the Y and the Φ direction. Eight glass plates were attached to the setup, which carried the electrode pattern of the capacitive transducers. The table's X position was measured by subtracting capacitances C_1 and C_2, the Y position by subtracting C_3 and C_4, and the Φ position by subtracting $C_5 + C_8$ and $C_6 + C_7$. The sensitivity of the capacitive transducers in the X and the Y direction was chosen different in order to investigate both the positioning repeatability of the table at the nanometer level and the position stability of the table at the picometer level. As a consequence, the stroke of the table in the X and the Y direction differed. Another capacitive plate-distance transducer (not shown in figure 6.1) was applied for measurement of the table position in the Z direction between the bottom of the table and the reference frame. The position of the table could also be measured in the X direction by means of a laser interferometer. The XY stage was attached to a base plate which was vibration isolated by three small tires placed on a heavy table. The complete setup was placed under a perspex box in order to minimize the influence of air turbulence on the setup.

The design of the experimental XY stage was not optimized for application as a highly stable and accurate nano stage. The XY stage was designed to prove the working of some principles and

verify some basic theoretical considerations. Nevertheless, it has provided an enormous amount of information and can be of value to further research.

6.2.3   Piezo actuators

It was not the intention of this research to extensively compare different piezo ceramics or to find the best type of piezo ceramic for a certain application. That should be a subject of another research. Throughout this research, the ceramic PIC155 was applied. Its properties are listed in table 2.1.

The XY stage was the first in a row of several nano stages. One of the objectives of these nano stages was to use different piezo actuators. For compact ISM drives, either shear or tube actuators can be applied, whereas for the XY stage stacked shear actuators are required. In order to illustrate a part of the design process of a nano stage, both actuator types will be compared with regard to application in the experimental XY stage.

Both actuator types can be compared by means of figures 2.10 and 2.11. For application in the XY stage, they require a high stiffness, a high resonance frequency, a small occupied space, a high sensitivity, and a low capacitance. The values for the stiffness and the resonance frequency of the shear and the tube actuators given in figures 2.10a and 2.11a should not be too decisive. Not just because these values are only theoretical values, but also because the resonance frequency of a piezo support in an ISM drive is also determined by the epoxy layers and the support elements. They can however give an indication of the difference in dynamic behavior between shear and tube actuators. The bending mode resonance frequency f_0 of a tube actuator for $L_t / d_{out} > 1$ can be approximated by:

$$f_0 = \frac{1}{2\pi}\sqrt{\frac{k}{m_{eff}}} = \frac{1}{2\pi}\sqrt{\frac{3k}{m_{tube}}} = \frac{3}{8\pi}\sqrt{\frac{E\left(d_{out}^2 + d_{in}^2\right)}{\rho L_t^4}} \qquad (6.1)$$

where E is the modulus of elasticity and ρ is the density of the ceramic.

As far as the occupied space of the shear actuators is concerned, the choice of their lateral dimensions is not tied to the standard manufacturing dimensions since they can be easily cut in smaller pieces. The lateral dimensions should preferably not be chosen smaller than about twice the actuator thickness because otherwise the assumption of shear deformation becomes questionable. The optimum lateral dimensions of a shear actuator can not be derived from figure 2.10 without making preferences to the value of either the stack's stiffness or the occupied space, and the capacitance. A simple criterion for the thickness is to use only catalogue values. A standard value is 1 mm. The sensitivity of the shear piezo is given by its charge constant d_{15}.

In order to minimize the occupied space of piezo tubes, their outer diameter d_{out} and their length L_t should be minimized. Like shear actuators, only standard dimensions were considered. The optimum outer diameter could be found by comparing the product of sensitivity and bending stiffness of standard tubes. This product had a maximum for $d_{out} = 3.2$ mm. The choice of the tube length was free up to 2.5 times the outer diameter, which was the maximum standard length. When determining the optimum tube length, one has to be aware of the fact that the tube deformation depends on the configuration of the piezo support. In case of the XY stage, the table displacement in the direction of motion is larger than the tube deformation. This is explained in fig-
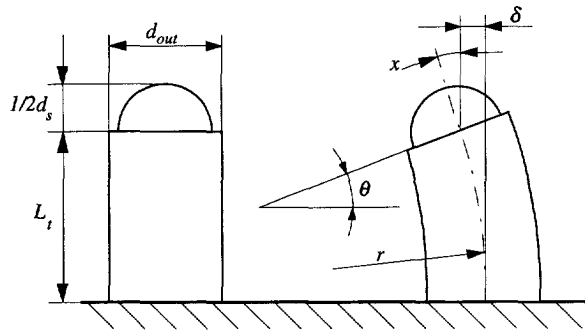
Fig. 6.2   The table displacement x_o is larger than the tube deformation δ. This is due to the rotation of the tube, which causes a roll off between table and sphere, resulting in an additional table displacement x.

ure 6.2. When a voltage is applied over one of the tube electrodes, the tube bends, and thus the end of the tube and the sphere rotate. The rotation of the sphere causes an additional table displacement $x = \theta d_s / 2$ due to roll off. According to Chen [42], the tube rotation θ can be calculated by:

$$\theta = \frac{L_t}{r} = \frac{4\sqrt{2}}{\pi} \frac{L_t}{d_{out}(d_{out} - d_{in})} d_{31} U_p \tag{6.2}$$

For a single electrode drive, the table displacement can subsequently be estimated by:

$$x_o = \delta + x = \frac{2\sqrt{2}}{\pi} \frac{L_t}{d_{out}(d_{out} - d_{in})} d_{31} U_p (L_t + d_s) \tag{6.3}$$

		sensitivity[1]	k_p[2]	f_0	occupied space	capacitance
		[nm/V]	[N/m]	[MHz]	[mm^3]	[nF]
stacked shear,	2x2x1 mm^3	0.45	$5.8 \cdot 10^7$	-	8	0.12
	3x3x1 mm^3	0.45	$1.3 \cdot 10^8$	-	18	0.27
	4x4x1 mm^3	0.45	$2.3 \cdot 10^8$	-	32	0.48
tube[3],	$L_t = 4$ mm	0.98	$1 \cdot 10^7$	0.08	30	1
	$L_t = 5$ mm	1.42	$5.1 \cdot 10^6$	0.05	36	1.25
	$L_t = 6$ mm	1.94	$3 \cdot 10^6$	0.03	42	1.5
tube[4],	$L_t = 7.5$ mm	2.3[5]	$1.8 \cdot 10^7$	0.05	240	3.4

[1]   Influence of table roll off was taken into account.

[2]   Static piezo actuator stiffness in the direction of the deformation.

[3] $d_{out} = 3.2$ mm, $d_{in} = 2.2$ mm.

[4] $d_{out} = 6.4$ mm, $d_{in} = 5.2$ mm.

[5]   For the charge constant d_{31}, the value found during experiments was used: $d_{31} = 175 \cdot 10^{-12}$ m/V (100 V_{pp}, 500 Hz), instead of the catalogue value.

Table 6.1   Parameter values of shear and tube actuators with standard dimensions.

Table 6.1 gives an overview of the values of the important actuator parameters for three stacked shear actuators of 2x2x1 mm^3, 3x3x1 mm^3 and 4x4x1 mm^3, and a tube actuator with d_{out} = 3.2 mm, d_{in} = 2.2 mm and L_t varying from 4 to 6 mm. It also gives these values for the tubes used in the XY stage.

According to the requirements made to the piezo actuators, it becomes clear from table 6.1 that stacked shear actuators score better on three of the parameters: the stiffness, the occupied space, and the capacitance. Also, the resonance frequency of the stacked shear actuators is expected not to be lower than the resonance frequency of the tubes. The tube actuators have a higher sensitivity. A difference of less importance is the number of electrical connections which is larger for a tube actuator. On this basis, shear actuators are preferred for application in ISM driven XY stages. This also applies for ISM drives for translations in one degree of freedom.

An advantage of piezo tubes in an experimental setup is the possibility to use them as an actuator and as a transducer at the same time. This can be achieved by using two of the four electrodes to position the table in the XY plane and to use the opposite electrode(s) as transducers. This way, tubes can be used to investigate the dynamic behavior of the XY stage during ISM in more detail by measuring the voltage over the transducer electrodes during and after stepping. After stepping, when the table and the tube are in rest, the voltage over the transducer's electrodes can also be used to measure the frequency and to estimate the level of table vibrations. The sensitivity of a transducer electrode to tube bending was measured to be $2.5 \cdot 10^{-3}$ V/nm.

6.2.4   Displacement transducers

Differential plate-distance transducers were chosen for position measurements in the X, the Y, and the Φ direction because they enable a symmetric XY stage design and because their sensitivity to parasitic motions is of second order. The table position in the three degrees of freedom was measured independently by three different ac-bridges having different sine wave frequencies (62, 96 and 125 kHz). A single plate-distance transducer was used to measure the table position in the Z direction. In that case, the ac-bridge was balanced by means of a variable precision capacitor.

From the setup requirements given, the electrode dimensions of the transducer were derived from the formula given in chapter 4. A minimum plate distance of 0.1 mm was taken into account, which resulted in a nominal plate distance d_0 in the X direction of 0.6 mm. In order to enable 10 nm position repeatability, the position resolution of the transducer should be about ten times higher: 1 nm. This meant that the ratio of range and resolution was $1 \cdot 10^6$. It was assumed that a 2 Hz transducer bandwidth was sufficient for accurate positioning at the nanometer level. At 2 Hz bandwidth, the resolution of the synchronous detector was $1 \cdot 10^{-6}$ pF, which resulted in a range to resolution ratio of $2 \cdot 10^7$, which was sufficient. The minimum overlapping area A in the X direction was calculated by means of equation 4.13: 21 mm^2.

The transducer range in the Y direction must be small enough to have about 20 pm position resolution. For a minimum plate distance of 0.1 mm, the minimum overlapping area A must be 29 mm^2. The same overlapping area was required for the Z transducer. The Z transducer must fit between the piezo supports of the table. The angular resolution of the Φ transducer must be sufficient to obtain 10 nm position repeatability of the table. The sum of the two overlapping areas

of the Φ transducer depended on the nominal distance d_{0y} and on the distance between these two areas. The latter depended on the width of the Y transducer electrodes.

In order to obtain a square table design, the Φ transducer was combined with the Y transducer, and the X transducer was combined with the mirror for the laser interferometer (see figure 6.1). The small current through the leads from the detector electrodes to the synchronous detector is extremely sensitive to deformation of this lead. In order to be able to fix the detector leads to the reference frame and the base plate, the detector electrodes were attached to the reference frame. The emitter electrodes were attached to the table. The width of the guard electrodes for all trans-ducers was taken equal to half the stroke of the table in the X direction: 0.5 mm. The distance between the detector electrodes of the Y and Φ transducer was also taken 0.5 mm. An overview of the final transducer characteristics is given in table 6.2.

	d_0 [mm]	C_0 [pF]	stroke [mm]/[rad]	resolution [nm]/[μrad]	A [mm^2]
X	0.6	1.1	1	0.27	75
Y	0.14	2.5	0.1	0.028	40
Z	0.15	4.1	0.001	0.018	70
Φ	0.14	2.5	0.01	0.01	40

Table 6.2   Characteristics of the capacitive transducers of the XY stage.

From the former overview, it can be concluded that the dimensions of the table are determined by the dimensions of the differential capacitive displacement transducers and not by the dimensions of the ISM drive.

6.2.5   Nanopositioning performance

6.2.5.1   Piezo drive control
The electronics for the piezo drive consisted of a computer controlled arbitrary waveform genera-tor [108] and a high voltage amplifier (HVA) [109]. The slew rate of the drive electronics was limited to 200 V/μs.

6.2.5.2   Computer simulation of the XY stage
In order to verify the accuracy of the analytic ISM model described in chapter 3, a computer simulation program based on this model was designed in VisSim® [110]. The validity of the model was tested by comparing the influence of the driving voltage and frequency on the table step size according to the computer simulation with the measured table step size of the XY stage.

6.2.5.3   Parameter measurement and estimation
In order to be able to implement the analytic ISM model into a computer simulation program and simulate the ISM performance of the XY stage, experiments and calculations were performed to estimate some stage and model parameters.

The stiffness k of the piezo support, defined in figure 3.8b, is a very important parameter with regard to the ISM performance. An approximation of this stiffness was determined by means of

FEA [67]. As an input, the thickness of the epoxy layer between the reference frame and the tube was measured. It varied between 5 and 10 μm. The stiffness k was calculated to be $6.4 \cdot 10^6$ N/m. It was found that the stiffness k was mainly determined by the stiffness of the epoxy layer between the reference frame and the piezo tube. The calculated epoxy layer stiffness was about a factor of two lower than the stiffness of the piezo tube ($2 \cdot 10^7$ N/m). The latter value corresponded very well with the theoretical value given in table 6.1.

The stiffness k was also deduced from a dynamic response measurement. (It would not be useful to measure the stiffness k statically by placing the table on its tube supports and applying a small force on the table in the X or the Y direction because the contact stiffness k_c between the table and the support would significantly influence the result.) Figure 6.3 shows the frequency response of one of the tube supports, determined by measuring the voltage on its transducer electrode. The resonance frequency of the support was about 20 kHz. Subsequently, k was calculated by means of equation 3.7 to be $4.5 \cdot 10^6$ N/m. This was about 25% smaller than the stiffness found by means of FEA. The difference can be explained by the uncertainty in the epoxy layer thickness. If the mass of the tube support is neglected compared to the table mass, the resonance frequency of the XY stage could be estimated from the measured stiffness and the table mass to be 3.1 kHz.
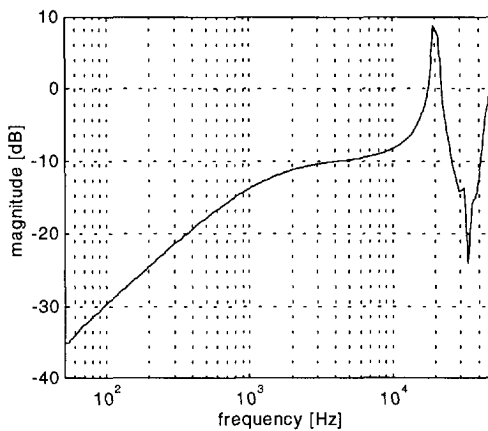
Fig. 6.3   Frequency response of one of the tube supports of the XY stage.

In order to determine the first resonance frequency of the XY stage in the Y direction, the table was placed on its tube supports. A sine wave voltage, swept in frequency, was applied to one of the Y electrodes of all three piezo tubes. As a result of the low amplitude of the driving voltage no significant slip occurred between the table and the tube supports. Figure 6.4 gives the frequency response of the XY stage table and of one of the piezo tubes. The response of the table was measured by means of the capacitive transducer. Both responses showed a peak value at 1.6 kHz, which was assumed to be the resonance frequency of the XY stage. This was substantially lower than the resonance frequency estimated from the stiffness k. The difference could to a large extent be explained by the contact stiffness k_c, which was assumed to be in the order of $2 \cdot 10^6$ N/m, as was calculated in chapter 3. Since this contact stiffness was about a factor five smaller than the stiffness of the epoxy layer between the tube and the reference frame, it could be
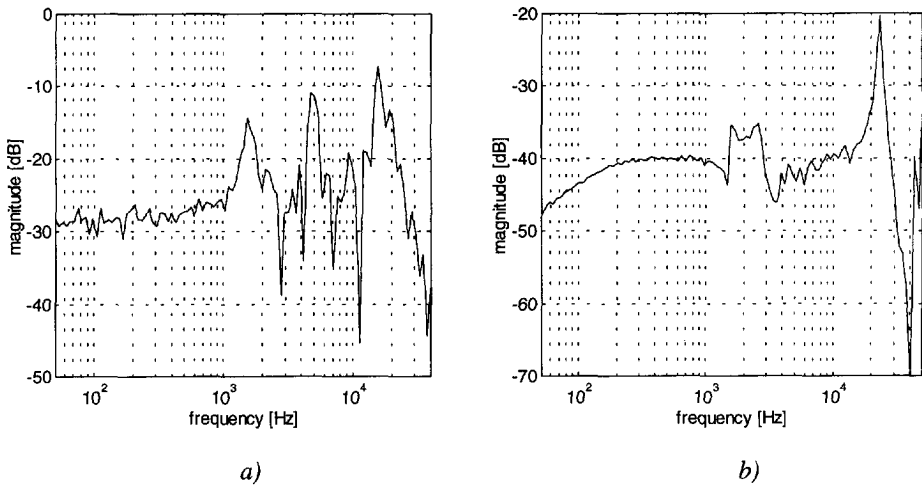
Fig. 6.4 a) Frequency response of the XY stage table. b) The frequency response of one of the tubes.

expected to dominate the response of the table. In that case, the resonance frequency of the stage was calculated by substituting $3k_c$ in equation 3.5 which resulted in a resonance frequency of 2.1 kHz. This was much closer to the measured value. The frequency peaks between 1.6 and 20 kHz were assumed to be superharmonic frequencies of the XY stage. The resonance peak at 24 kHz in figure 6.4b was higher than the resonance frequency of the piezo tube shown in figure 6.3. This can be explained by the fact that the tube was fixed at one end and supported at the other. Compared to the free end vibration mode, this resulted in a different vibration mode with a higher resonance frequency.

The coefficients of static and dynamic friction between the spherical supports and the table were difficult to predict because they depended on the materials in contact, the configuration of the contact area and the environmental conditions like temperature and relative humidity. Both coefficients of friction were estimated by slowly tilting the XY stage while continuously measuring the table position. The coefficient of static friction was estimated from the tangent of the tilt angle at which the table starts sliding. The coefficient of dynamic friction was estimated from the tangent of the tilt angle at which the table starts and keeps sliding after a small impulse force to the base. This resulted in $\mu_{st} = 0.17$ and $\mu_d = 0.14$. Alternatively, μ_d was estimated from the table acceleration during the slip period of an ISM step. As the friction force was the only force working on the table during the slip period, the coefficient of dynamic friction could also be estimated from the table acceleration during slip, since $\mu_d = \ddot{x}_o / g$. This resulted in $\mu_d = 0.15$.

The hysteresis loop of the piezo tube that was used in the computer simulation was determined by applying a 100 V_{pp} triangle, 100 Hz sine wave voltage to the tubes and measure the table position by the capacitive transducers. The measured hysteresis loop was fitted by a third order polynome and implemented in the model. The average stage sensitivity was 2.2 nm/V. This was in good accordance with the sensitivity value calculated in table 6.1.

A value for the velocity deadband $D_{\dot{x}}$, which defined the condition for stick, was derived from the maximum acceleration which can be applied to the table by friction forces. The velocity difference these friction forces could produce within one numerical integration step appeared to be a

useful value for the velocity deadband. This means that the velocity deadband changes with changing sliding conditions. For the XY stage, the velocity deadband $D_{\dot{x}_r}$ was chosen $1 \cdot 10^{-6}$ m/s. The numerical integration step size t_i must be optimized with respect to a short simulation time and accurate simulation results. A practical value for t_i was $1 \cdot 10^{-6}$ seconds.

6.2.5.4 Validation of the ISM model

Figure 6.5a shows the simulated and measured values of the table step size as a function of the amplitude of the driving voltage for single ISM steps. The simulated and measured values corresponded well. As expected, the step size increased with increasing driving voltage. Up to a certain minimum voltage, the table does not move. According to equation 3.30, the minimum drive voltage determined by the elastic buffer ($2\delta_t$=18 nm) was 4 V. According to equation 3.32, the minimum drive voltage determined by the slip condition was 5.8 V ($k = 4.5 \cdot 10^6$ N/m). These values are in good accordance with the simulated (5 V) and measured minimum driving voltage (6 V). It appeared that in this particular case the minimum driving voltage was determined by the support stiffness k and not by the elastic buffer. The minimum step size repeatedly obtained at 6 V was about 2 nm. The measured step size values were based on multiple measurements collected throughout this research. Generally, the deviation of the step size from the average step size given in figure 6.5a was about 10%.
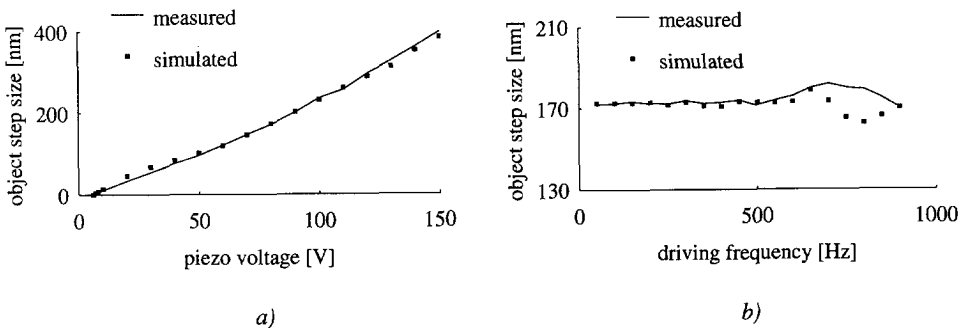
Fig. 6.5   a) The table step size for single ISM steps as a function of the amplitude of the sawtooth driving voltage. Both the measured and the simulated values are given. b) The table step size as a function of the frequency of the sawtooth voltage for a single ISM step.

Deviations from a linear relation between the step size and the applied voltage in figure 6.5a can be explained by the complex dynamic behavior of the system. As a result of the sudden start of the sawtooth slope, the combination of piezos and stage table started vibrating with a frequency close to the resonance frequency of the XY stage. During the slip period, the piezos slided forwards and backwards under the table at a frequency close to their resonance frequency. The step size was of course determined by the driving voltage applied, but also by the number of sliding phases and the moment of stick. According to the measured spread in step size at constant voltage, both these parameters seemed to be ruled by statistics, for instance due to local changes in the coefficients of friction.

In order to be able to compare different piezo drives, it may be useful to consider the ratio of the (measured) step size s_t and the nominal piezo deformation $\alpha d_{ij} U_p$. This ratio should be high to

obtain a high table velocity at given driving voltage. For the XY stage, the ratio of the step size and the piezo deformation increased from 0.15 for 6 V up to 1.15 for 150 V.

Figure 6.5b shows the simulated and measured table step size for different sawtooth frequencies at constant driving voltage (80 V) for a single ISM step. For frequencies up to 700 Hz, the simulated and measured step size values corresponded relatively well. An explanation for the difference at higher frequencies may be the appearance of slip during the start of the slow voltage rise (see figure 3.16).

From the above measurements and simulations, it can be concluded that the quality of both the analytic ISM model and the computer simulation is good for driving frequencies below 700 Hz. The simulation program was also used to predict the influence of several other parameters on the performance of ISM drives. However, one should be aware of the fact that the elastic buffer was not taken into account. Therefore, the simulation program cannot be used to accurately predict the performance of ISM drives around or below the minimum voltage determined by the elastic buffer.

6.2.5.5 Influence of other parameters on the XY stage performance
The influence of the coefficients of static and dynamic friction is shown in figure 6.6. It shows the simulated effect of a sweep of the coefficient of static friction μ_{st} from 0.1 to 0.25 (the ratio of the coefficients of the static and dynamic friction was kept constant) on the step size for three different amplitudes of the driving voltage. The results were not univocal. For some driving voltages, the step size increased, for other driving voltages it decreased. The influence of a change in the coefficient of friction was estimated to be relatively low because the difference in step size compared to the nominal simulated step size values given in figure 6.5 were less than 10%.
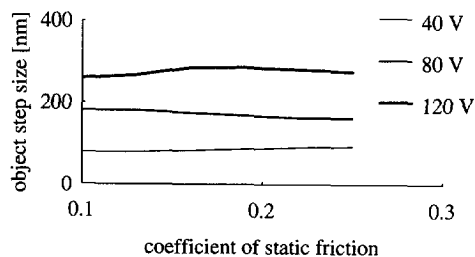
Fig. 6.6 The influence of changes in the coefficients of friction on the table step size.

The robustness of the simulations was tested by varying the velocity deadband value D_{x_r} and the integration step size t_i. A change in the nominal velocity deadband value ($D_{x_r} = 1 \cdot 10^{-6}$ m/s) of two orders of magnitude ($1 \cdot 10^{-5}$ - $1 \cdot 10^{-7}$) did not significantly influence the simulated step size. The simulated step size values did not vary for integration steps smaller than $2 \cdot 10^{-6}$ seconds. Above this value, the results became inaccurate.

6.2.5.6 Position repeatability

In order to prove the positioning repeatability of the XY stage at the nanometer level, closed-loop control of the table position was applied. The control loop consisted of three degrees of freedom position measurement by means of the capacitive transducers, a simple controller which generated a control signal to the driving electronics and the ISM drive. The table position was simultaneously measured in the X direction by means of a laser interferometer. The positioning repeatability was proven by moving the table between two positions at 0.1 mm distance in the X direction. Even with the simple controller, the position repeatability was better than 5 nanometer [111].

6.2.6 Stability performance

6.2.6.1 Intrinsic stability

The XY stage setup was designed as symmetric as possible, using the same material for the table and the reference frame, in order to compensate thermal disturbances. No special attention was paid to the choice of the reference frame and table material. Construction steel was chosen because of the excellent bonding properties of TiCN layers to it.

The intrinsic stability of the XY stage was determined by the table drift rate relative to the reference frame and by the table vibration amplitude a few minutes after positioning the table at a new position. The maximum short-term drift rate (< 3 min) was smaller than 50 pm/min. The middle long-term drift (< 60 min) was smaller than 0.5 nm. The vibration amplitude was estimated by measuring the piezo voltage noise on the tube actuators. The noise level was about $1 \cdot 10^{-4}$ V, which corresponded to a vibration amplitude of 40 pm.

The emitter electrodes on the table were connected to the ratio transformer by means of thin leads. The influence of these leads on the intrinsic table stability was negligible.

6.2.6.2 Stability in the direction of motion

The effect of ISM steps on the table drift in the direction of motion was measured for different amplitudes of the sawtooth voltage and for a different number of steps. Figure 6.7a shows the

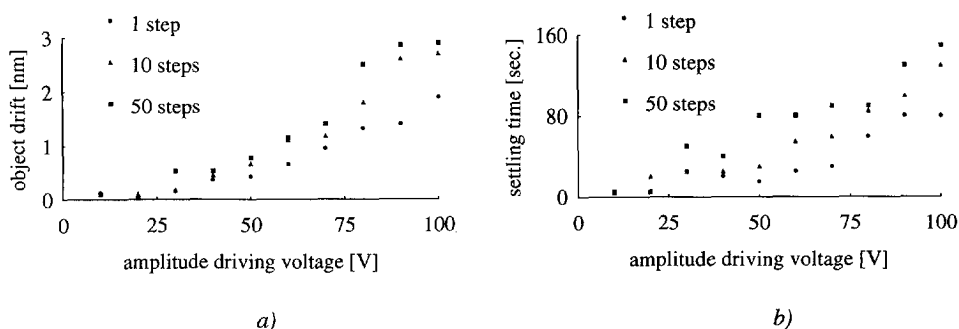a)   b)

Fig. 6.7 a) Table drift 3 minutes after 1, 10 and 50 ISM steps. b) Settling time needed to reach a drift rate smaller than 100 pm/min after 1, 10 and 50 ISM steps.

table drift 3 minutes after 1, 10 and 50 ISM steps and figure 6.7b shows the settling time needed to reach a drift rate smaller than 100 pm/min.

The drift, the drift rate and the settling time increased with increasing amplitude of the driving voltage, as could be expected from the theory on the piezo hysteresis. They also increased with the number of steps. This was not predicted by the theory on the piezo hysteresis. The increase may, however, be partly explained by heat production in the piezo and partly by a shift of the hysteresis curve relative to its zero point during the first few curves. Drift measurements, after a further increased number of steps at low driving voltages (10 - 30 V), showed that the drift, the drift rate and the settling time reached an asymptotic maximum that was only slightly higher than the values given for 50 ISM steps. The drift and settling time values of figure 6.7 were average values from five measurements. The spread in the drift and the settling time was up to 50% of the nominal values given. This spread mainly depended on the deformation history of the piezo tubes. The table drift for driving voltages above 30 V followed a logarithmic course in time in the direction opposite to the step direction, correspondent to the direction of the fast piezo deformation. Below this voltage, drift rates were small, but the direction and the shape of the drift course were less defined. This could be explained by the fact that table drift was ruled by a combination of piezo drift and creep in the contact areas.

For some TEM applications, it is important to have short settling times. It would also be advantageous to avoid closed-loop compensation of table drift. In case of the XY stage, the settling times for driving voltages of 10 and 20 V were short. For the TEM applications meant, the table drift at these driving voltages does not need to be compensated. A disadvantage of applying these driving voltages was the low maximum velocity of the table of about 20 µm/sec. For higher driving voltages, drift compensation is needed. Since the spread in the table drift and the table drift rate after stepping was considerable, compensation by means of knowledge about the drift course will not always be effective. Use of a compensation step resulted in drift rate reductions up to a factor of 20 for a driving voltage range up to 150 V and for up to 100 steps.

6.2.6.3 Stability in the Z direction

In order to determine the stability of the table in the Z direction, the table drift rate in this direction was measured after single and multiple ISM steps. On average, the amount of table drift in the Z direction was 20% smaller than the table drift in the direction of motion. This difference cannot be explained by the difference in the tube sensitivity in both direction, being about 2.5 nm/V for the Z direction and 2.3 nm/V for bending. However, for single electrode drive of the piezo tube, the piezo tube drift in the Z direction along a vertical line through the contact point between the ruby sphere and the table is smaller than the piezo tube drift in the Z direction along a vertical line through the electrode. For a double electrode drive, the piezo tube drift in the Z direction will probably be less for reasons of symmetry.

6.2.7 Additional experiments

One additional experiment was performed by means of a table with a V-shaped groove at the bottom. This V-shaped groove guided the table in the X direction. It was found that the step size of the table was reduced to about 50% compared to the step size of the table with the flat bottom. This effect was attributed to parasitic forces in the V-shape groove in the Y direction.

The reliability of the ISM drive of the XY stage was tested by continuously moving the table with the V-shaped groove from left to right in the X direction for 12 hours. During this period, the time to cross from left to right and backwards was measured. This cross time was 32 seconds on average with a standard deviation of 0.6 seconds. This experiment proved the reliability and the constancy of the stepping behavior of the ISM drive. Apparently, the combination of a ruby support and a TiCN coated stainless steel table showed such little wear that a 12 hours operation period was possible. However, this does not imply that this combination of contact materials is a suitable solution for (U)HV application.

6.3   The Z stage

6.3.1   Stage requirements

In order to gain knowledge on the performance of ISM drives and FSM drives for positioning parallel to the gravity field, a Z stage was designed. It had to meet the following requirements:

- the preload required to prevent the table from sliding downwards must be adjustable within reasonable limits and with a sufficient resolution,
- the dimensions of the table must be compatible with the space available in a TEM,
- the configuration of the Z stage must be such that both ISM and FSM can be investigated,
- piezoelectric shear actuators must be applied, and
- table displacements must be measured with a resolution of at least 20 pm.

6.3.2   The experimental setup

The experimental Z stage is shown in figure 6.8 [112]. It consisted of an aluminum reference frame, a cylindric table, six piezo supports, two spring systems to preload the table, and a single plate-distance transducer. Aluminum was chosen for the reference frame because, compared to construction steel, it has a high thermal diffusivity $(\lambda / c\rho)$, a low ratio of the linear expansion coefficient and the conductivity, and because it can be well machined. The piezo supports consisted of a piezoelectric shear actuator and a ruby half sphere with a radius of 2 mm. The piezo supports were split up in two sets: an upper and a lower set. Each set was placed around the table at angles of 120°. The preload force of the upper and the lower set of supports on the table was adjusted by means of a spring system. Four piezo supports were attached to the reference frame, the other two to the spring systems. The piezo supports were aligned such that their main deformation direction was the Z direction. The shear actuator dimensions were 4x4x1 mm³; the actuator material was PIC155. The table was an almost hollow, aluminum tube of 24 mm diameter, 25 mm length, 2 mm wall thickness and a mass of 0.015 kg. The mass of a piezo support was $2 \cdot 10^{-4}$ kg. The capacitive transducer configuration was equal to the Z transducer configuration of the XY stage. The sensitivity of the capacitive transducer was adjustable by adjusting the Z position of the table. During the experiments, the nominal plate distance d_0 was 125 μm, resulting in a transducer sensitivity of $5 \cdot 10^4$ pF/m. With a resolution of $1 \cdot 10^{-6}$ pF, table displacements of 20 pm could be detected. On top of the table, the emitter electrode of the capacitive transducer was

attached. The outer surface of the table was lapped ($R_a = 0.3$ µm) and anodized, resulting in a small surface layer of aluminum oxide to avoid wear. Because of their size, the spring systems were placed on opposite sides of the table. The spring systems were a combination of a leafspring and a flexible hinge, enabling adjustment of the preload force up to 8 N. All six shear piezo actuators could be driven separately. This enabled table motion either by ISM or by FSM. In order to test the influence of a different table material on the piezo drive performance, the aluminum table could also be replaced by a stainless steel table with a mass of 0.024 kg.
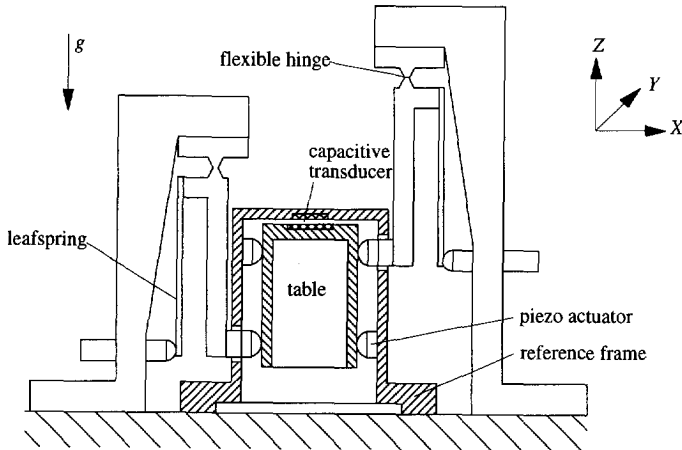
Fig. 6.8   The Z stage enables table motion parallel to the gravity field by means of ISM or FSM.

6.3.3   Nanopositioning performance

6.3.3.1 Piezo drive control
For the ISM drive of the Z stage, the same control setup as for the XY stage was used. For FSM drive, additional electronics were required to produce the special FSM drive signal. For instance, six instead of one HV amplifiers were used to drive each piezo support independently.

6.3.3.2 Parameter measurement and estimation
The sensitivity of the piezoelectric shear actuators was determined by applying a 500 Hz sine wave voltage to all six shear piezos and measure the displacement of the table. The shear piezo sensitivity at this frequency was 0.5 nm/V, assuming that the displacement of the table was equal to the shear piezo deformation ($f_0 \gg f_{sinewave}$). This sensitivity was well comparable to the

coefficient of friction ($F_p = 0.1$ N)	aluminum $d_s = 4$ mm	stainless steel $d_s = 4$ mm
μ_{st}	0.12	0.11
μ_d	0.1	0.09

Table 6.3   Coefficients of static and dynamic friction between the ruby spheres and the stainless steel or the aluminum table (measured values).

catalogue value of the charge constant d_{15} (0.45 nm/V).

The values measured for the coefficients of static and dynamic friction between the ruby support and the table are given in table 6.3.

Due to the cylindrical shape of the table, the contact area between the table and the supports was no longer a circle, but an ellipse. From Johnson [66] was found that for the given values of the principal radii of the table and the sphere, the ratio of the ellipse axes a and b was only 1.1. This implied that the elastic buffer and the maximum contact stiffness for the aluminum and the stainless steel table for different values of the preload force F_p could still, with high accuracy, be calculated from equations 3.8 to 3.12. The values are given in table 6.4.

preload	elastic buffer $2\delta_t$ [nm]		k_c [N/m]	
[N]	stainless steel	aluminum	stainless steel	aluminum
0.1	14	27	$2.3 \cdot 10^6$	$1.3 \cdot 10^6$
0.5	42	79	$3.9 \cdot 10^6$	$2.3 \cdot 10^6$
1.0	67	125	$4.9 \cdot 10^6$	$2.9 \cdot 10^6$
2.0	106	198	$6.2 \cdot 10^6$	$3.6 \cdot 10^6$
3.0	139	260	$7.1 \cdot 10^6$	$4.2 \cdot 10^6$

Table 6.4   *Values for the elastic buffer $2\delta_t$ and the contact stiffness k_c for the aluminum and the stainless steel table for different values of the preload force.*

The first resonance frequency of the aluminum table in the Z direction was determined by measuring the impulse response of the table. This response is shown in figure 6.9a for a preload force of 1 N. From this response, the resonance frequency of the table was deduced: 5.1 kHz. This meant that, when the mass of the piezo supports was neglected and the stiffness of all six supports was assumed to be equal, the stiffness of a single piezo support, including the contact stiffness k_c, was $2.6 \cdot 10^6$ N/m. This was slightly lower than the calculated contact stiffness, which confirmed the supposition that the contact stiffness is the dominant stiffness in nano stages.
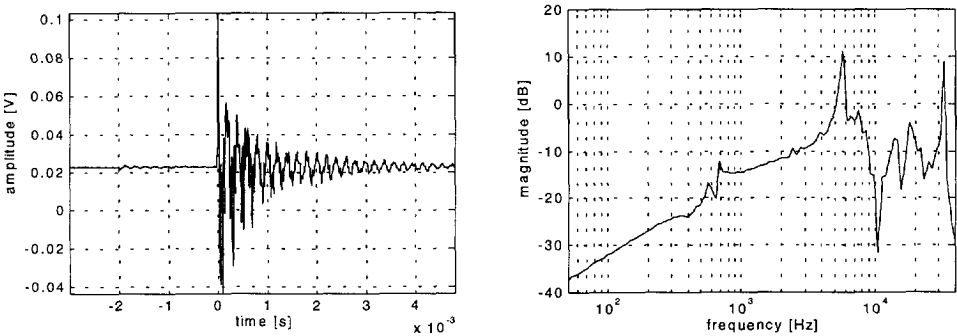

Fig. 6.9   *a) Impulse response of the aluminum table in the direction of motion. The resonance frequency was 5.1 kHz. b) Frequency response of one of the shear piezo actuators to a swept sine wave on the five other shear piezo actuators at 1 N preload force.*

Response measurements at higher preload forces showed an increase of the resonance frequency, which could be explained by the preload force dependence of the contact stiffness k_c.

In order to estimate the resonance frequency of a piezo support, a small sine wave voltage, swept in frequency, was applied to five of the six shear piezo actuators. The sixth shear piezo was used as a transducer. Figure 6.9b shows the frequency response of this shear actuator. The response shows a peak at 5.8 kHz, which was probably the first resonance frequency of the aluminum table. It was assumed that the peak at 31 kHz was the first, or one of the first resonance frequencies of the piezo support.

The static support stiffness k was estimated by means of the support model given in figure 3.8b. The epoxy layer thickness between the ruby sphere and the shear piezo and between the shear piezo and the base was measured to be about 10 μm. The modulus of elasticity of the epoxy layer was $4 \cdot 10^9$ N/m^2 [113]. Since the modulus of elasticity of the shear piezo was in the order of $70 \cdot 10^9$ N/m^2 (thickness 1 mm) and the modulus of elasticity of the ruby sphere was $320 \cdot 10^9$ N/m^2 (radius 2 mm), the stiffness of the piezo support was expected to be mainly determined by the shear piezo. Assuming linear deformation, the stiffness of the piezo support in the direction of motion could be estimated by:

$$k = \frac{12 E_p I_p}{t_p} \frac{1}{\left(4t_p^2 + 6t_p d_s + 3d_s^2\right)} \tag{6.4}$$

where t_p is the piezo thickness. From equation 6.4, the stiffness was estimated to be $1.3 \cdot 10^7$ N/m.

Compared to the first resonance frequency of the XY stage, the resonance frequency of the Z stage in the direction of motion was considerably higher. This was caused by a decrease of the table mass and by application of another type of piezo actuators. Still, the contact stiffness determined the resonance frequency to a large extent. An increase of the contact stiffness can be obtained by an increase of the preload. This is, however, unfavorable with regard to stability. Therefore, the contact stiffness should be maximized by optimization of the choice of materials and the shape of the contact area.

6.3.3.3 ISM performance
The ISM performance of the Z stage was investigated by measuring the upward table step size as a function of the amplitude of the driving voltage and the preload force. Figure 6.10 gives the
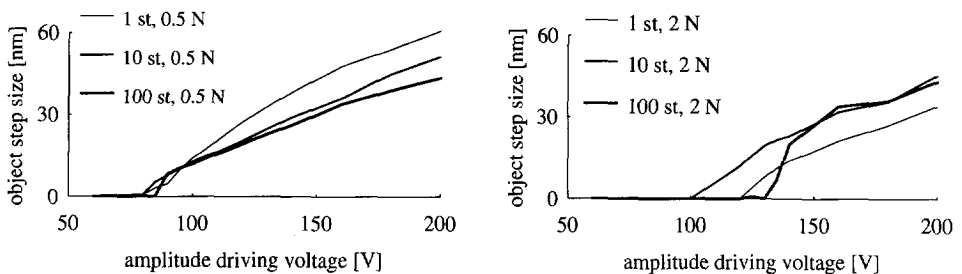

Fig. 6.10   *Upward step size of the aluminum table as a function of the amplitude of the driving voltage for two preload forces, 0.5 N and 2 N, and for different numbers of steps.*

table step size of the aluminum table for upward motion for two different preload forces, 0.5 and 2 N, and for different numbers of steps. As could be expected from the theory given in chapter 3, the minimum driving voltage increased with increasing preload force. Like for ISM motion perpendicular to the gravity field, there was a certain variation in the step size. This variation was about 20%. This was larger than the variation in the table step size of the XY stage. That could be explained by a difference in stage dynamics for single and multiple steps and by the 'cooperation' between the six piezo supports.

The initial tangential deformation δ_i of the aluminum table due to the gravity forces was calculated to be 12 nm for a 0.5 N preload force and 7 nm for a 2 N preload force. The minimum driving voltages at these preload forces for upward motion were estimated by means of equation 3.33: 103 and 208 V. As is shown in figure 6.10, these minimum driving voltages for a single step were 80 and 120 V respectively, which was much lower than predicted.

Figure 6.11 shows the upward and downward step sizes for the stainless steel table for preload forces of 1 N and 2 N. Since the stainless steel table had a larger mass, the minimum preload force required was 1 N. In spite of this higher minimum preload force, both minimum driving voltages measured (50 and 70 V, respectively) were clearly lower than the minimum driving voltages for the aluminum table for comparable preload forces. This was in accordance with the elastic buffer model. The initial deformation at preload forces of 1 and 2 N was 9 nm and 7 nm, respectively. The estimated minimum driving voltages for upward motion were 83 and 120 V (equation 3.33) and for downward motion 49 and 92 V (equation 3.34). This is clearly lower than for the aluminum table, but again much larger than the measured values.
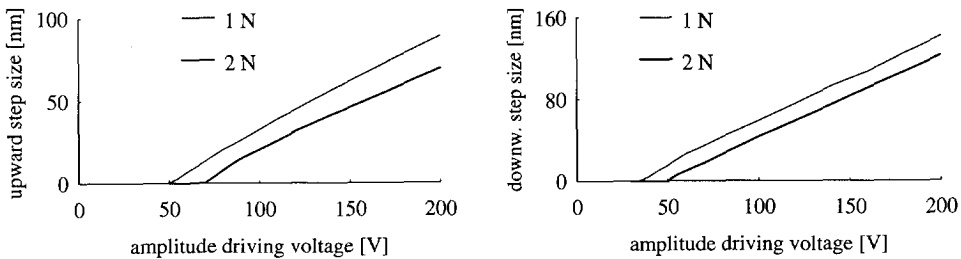
Fig. 6.11   Upward and downward step size of the stainless steel table at 1 and 2 N preload force as a function of the amplitude of the driving voltage.

The difference between the predicted minimum driving voltage and the measured values may be explained by the influence of the wear-resistant coatings on both tables which probably resulted in a higher equivalent modulus of elasticity for the contact area. For instance, the bulk modulus of elasticity of aluminum oxide is about $3 \cdot 10^{11}$ N/m^2. Then, the equivalent modulus of elasticity of the table surface may be about $1.4 \cdot 10^{11}$ N/m^2 instead of $7 \cdot 10^{10}$ N/m^2 for bulk aluminum. As a consequence, the predicted minimum driving voltages for upward motion would then be 65 and 140 V (instead of 103 and 208 V).

According to the condition for slip (equation 3.35), the minimum driving voltage was calculated from equation 3.36 to be 46 V. This confirmed the supposition that, in this case, the minimum

driving voltage was indeed determined by the elastic buffer. Efforts to minimize the minimum driving voltage should therefore concentrate on decreasing the elastic buffer.

The ratio of the step size and the piezo deformation of the Z stage for driving voltages up to 150 V was lower than for the XY stage. This ratio depended on the preload force and on the number of steps. The ratio of the step size and the piezo deformation could be increased by applying different preload forces for the upper and the lower set of piezo supports. If the preload force for the upper set was 1 N and for the lower set only 0.1 N, this ratio increased to 1.1 at a driving voltage of 200 V. This way, only the upper set of piezo supports moves the table; the lower set guides the table. The increased ratio of the step size and the piezo deformation was explained by the fact that the table experienced less parasitic forces of three instead of six piezo supports.

It was found that the table step size was almost independent of the frequency of the driving voltage. For a frequency range from 10 up to 1000 Hz, and for a preload force of 1 N and a driving voltage of 140 V, the deviation of the average table step size was only 5%.

6.3.3.4 FSM performance

The driving principle of frictional stepping motion (FSM) was explained in section 3.2.5. The FSM performance of the Z stage did not differ much from its ISM performance (see figure 6.12).
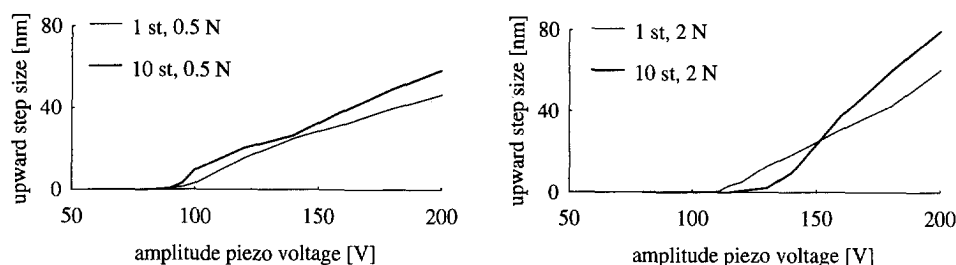
Fig. 6.12   Step size of the aluminum table for upward motion as a function of the amplitude of the driving voltage, for preload forces of 0.5 and 2 N.

The minimum driving voltages for the aluminum and the stainless steel table were about the same as those needed for ISM. However, the table step sizes for 'low' driving voltages were
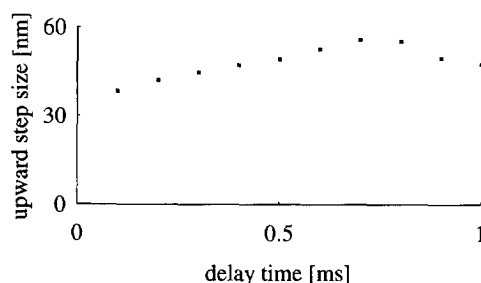
Fig. 6.13   Upward step size of the aluminum table as a function of the delay time t_d between the driving signals on the six piezo supports for a preload force of 0.5 N.

generally smaller. It was found that the table step size depended on the delay time t_d (see figure 6.13). This is the time between the mutual retraction of the piezo supports. An explanation for this effect can only be found in the dynamics of the FSM drive.

6.3.4   Stability performance

The quasi-static position stability of the stainless steel table relative to the reference frame was observed directly after stepping upwards for a driving voltage of 120 V and for different preload forces. Figure 6.14 gives typical results of the drift courses of the table at 1, 2 and 3 N preload force.
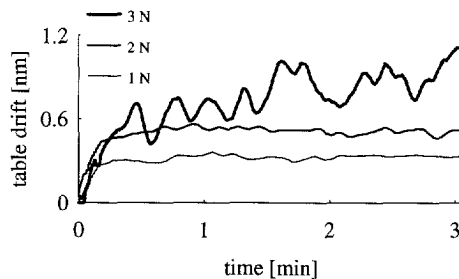
Fig. 6.14   *Table drift after stepping upwards with 120 V driving voltage for three different values of the preload force: 1, 2, and 3 N.*

Compared to the drift courses of the table of the XY stage, the drift courses of the table of the Z stage had a logarithmic shape but were much less smooth. The smoothness of the drift courses was decreased further when the preload force was increased. It was assumed that the logarithmic shape resulted from piezo drift, while the irregular character resulted from the residual friction forces in the contact area between table and supports. The settling time to reach a drift rate of 100 pm/min was generally between 10 and 80 seconds for preload forces of 1 and 2 N. For a 3 N preload force, the settling time increased drastically (>>200 seconds). The amount of drift, measured 3 minutes after stepping, increased with increasing driving voltage, ranging from 0.3 up to 2 nm for driving voltages ranging from 80 up to 170 V. Generally, the drift and the drift rate of the table of the Z stage were larger than the drift and the drift rate of the table of the experimental setup of figure 5.8. This could be explained by the increase of the number of object supports. This increase resulted in additional friction forces working on the table, in that way increasing the unpredictability of the table drift.

It should be concluded that in order to minimize the settling time of the table, the preload force and hence the mass of the table should be minimized. However, this is at the expense of the magnitude of the contact stiffness.

6.4   The piezo rotor

6.4.1   Stage requirements

In order to gain knowledge on the design and performance of piezo rotors, one of the piezo rotor designs of section 3.7 was tested. The requirements on the piezo rotor design were the following:

- the design should be such that its outer dimensions can be scaled down to a volume which is in accordance with the space between the objective lens pole pieces of a TEM, and
- it should be possible to measure the angular rotor speed.

6.4.2   The experimental setup

The piezo rotor configuration of figure 3.18 was chosen to be applied in the experimental setup. Two different ISM drive configurations were designed. They were called type 1 and type 2. The configuration of the type 1 piezo rotor is shown in figure 6.15a. The setup consisted of a rotor with ruby spheres attached to it at both ends and two piezo drives which rotated and supported the rotor. The piezo rotor was axially preloaded by a leaf spring. A piezo drive consisted of three piezoelectric shear actuators which were polarized tangentially to the center of the support. Simultaneous deformation of all six shear actuators of both piezo drives rotated the rotor. A disadvantage of the type 1 configuration was that each piezo needs its own connection to the drive electronics. An alternative configuration (type 2) is shown in figure. 6.15b. The shear actuators were attached under the support unit. An advantage of the type 2 configuration was that each drive needed only one connection to the drive electronics. This connection was attached to the

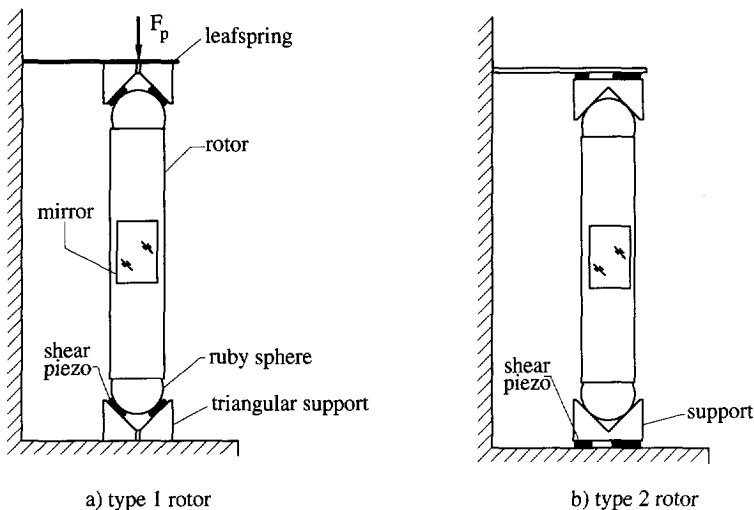a) type 1 rotor   b) type 2 rotor

Fig. 6.15   a) The configuration of the type 1 piezo rotor. There are two piezo drives, consisting of three piezoelectric shear actuators mounted on a triangular support that rotates the rotor. b) In the type 2 piezo rotor, the shear actuators are mounted under the triangular support.

conducting support. As a result, miniaturization of the latter configuration is easier than of the type 1 piezo rotor. A second advantage was the possibility to coat the support surfaces with a wear-resistant coating much easier. The type 2 piezo rotor was chosen to be tested without any further optimization of the design.

By applying a dc voltage to the shear actuators (PIC 155), very small rotations of the rotor in the order of 1 nrad were possible. Nearly continuous rotation was possible by using ISM. The support surface was polished and coated with a 1 μm TiCN layer. For this experimental setup, a stainless steel rotor of 20 mm length and 4 mm diameter was used. The diameter of the ruby spheres was 3.5 mm. On the rotor, a mirror was placed to measure the rotor's angular position with an autocollimator and the time needed for one revolution with an optical timer. Because it was easier to measure the rotor speed instead of the angular step size, the rotor performance was related to speed.

6.4.3   The rotor performance

By varying the amplitude and the frequency of the driving voltage, the angular step size and the angular rotor speed were varied. The smallest repeatable single ISM steps were measured at a driving voltage of 30 V_{pp}. They were as small as 1 μrad.

The angular rotor speed strongly depended on the frequency and the amplitude of the driving voltage and on the preload force. Figure 6.16 shows the rotor speed versus the frequency of the driving voltage. This curve was measured at a driving voltage of 100 V_{pp}. The maximum speed measured at this voltage was 0.5 rad/s. For driving frequencies up to 2 kHz, the speed was linearly progressive with increasing frequency. Above 2 kHz, the rotor speed was influenced by 'negative' slip during the slow voltage rise. It was also found that the rotor performance became less reliable at these frequencies. After a maximum at about 3 kHz, the speed started to drop. Both straight lines above and beneath the 100 V_{pp} curve give indications of the smooth parts of the rotor speed as a function of the driving frequency at 200 and 30 V_{pp}, respectively.
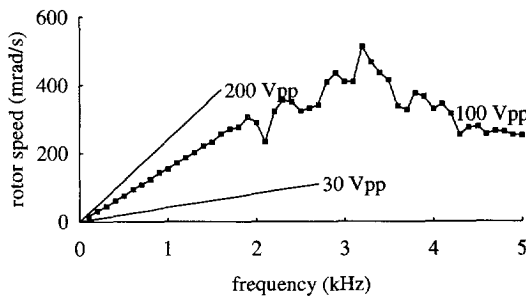
Fig. 6.16.   The rotor speed as a function of the driving frequency at 100 V_{pp}.

In order to test the reliability of the piezo rotor, two additional experiments were performed. During the first experiment, the rotor was driven continuously for 4 hours. During this time period, the rotor speed was measured. After a decrease of speed during the first hour, the rotor speed stayed nearly constant at 0.18 rad/s. During the second experiment, which took a two-week

period, the rotor was started each morning and driven for half an hour. The average rotor speed over this period was equal to the nominal rotor speed of 0.18 rad/s. From this experiment, it could be concluded that the piezo rotor worked in ambient conditions at any time, at the same driving voltage, and without cleaning or polishing the support nor the rotor.

6.5   The TEM stage

This section was based on a paper published in:

> **Proceedings American Society for Precision Engineering, Annual meeting, ASPE, Raleigh (NC), USA (1996), pp. 26-31.**

6.5.1   Stage requirements and research goals

The purpose of the TEM stage was to compare the stability of a simple nano stage applied as a specimen positioning device in a TEM to the specimen image stability. In order to achieve this, the following requirements were put on the TEM stage:

- it must be based on the nano stage concept and therefore it must be attached to the lower pole piece of the objective lens,
- the nano stage must at least have one degree of freedom in the XY plane, and
- the table position must be measured relative to the lower pole piece with a displacement resolution of 30 pm.

6.5.2   Experimental setup

The experimental setup is shown in figure 6.17. The TEM stage was placed on the lower pole piece of the objective lens in a Philips EM420 TEM. The TEM stage consisted of an aluminum reference frame, an ISM drive, consisting of three shear piezo actuators and three ruby half

Fig. 6.17   Configuration of the experimental TEM stage, based on the nano stage concept.

spheres, a stainless steel table and a set of differential capacitive plate-distance transducers. The dimensions of the shear actuators were 4x2x1 mm^3, the radius of the ruby spheres was 1 mm and the dimensions of the table were 14x14x6 mm^3. The bottom of the table consisted of a V-shaped groove and a small, flat surface, forming a kinematic support and allow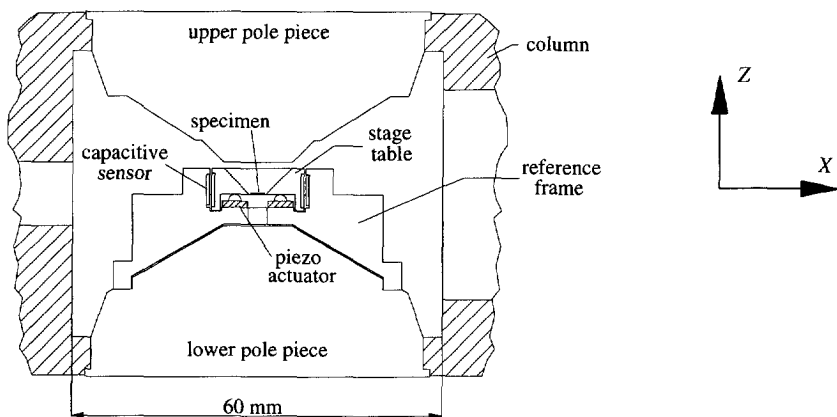ing table motion in the X direction only. The table was coated with a 1 μm TiCN layer. The stroke of the table in the X direction was 0.1 mm. The object position in the X direction could be measured with a resolution of 30 pm at 2 Hz bandwidth.

In order to be able to obtain a well defined position of the reference frame on the pole piece, a circular groove was machined into the pole piece far away from the top of the pole piece. The TEM stage was designed in such a way that the specimen, which was carried by the table, was exactly located in the middle between both pole pieces. The specimen was a 50 nm thick carbon foil which was illuminated by an electron beam of about 500 nm diameter ($I \cong 1$ nA). The specimen image was recorded by a slow scan CCD camera with 512x512 pixels. Converted to the specimen scale this meant 0.2 nm per pixel. By means of pixel interpolation [114], image shift measurement may be improved to the subpixel level. The CCD camera had a maximum recording rate of 1 Hz.

6.5.3   Nanopositioning performance

In order to obtain an impression of the difference in the ISM performance of nano stages in ambient air and in high vacuum, the table step size of the TEM stage was measured as a function of the applied driving voltage both in air and in high vacuum. The table step size in vacuum was, on average 15% lower for a driving voltage range up to 100 V_{pp}. Also, the minimum driving voltage in vacuum (28 V) was higher than the minimum voltage in ambient air (23 V). This means that a vacuum environment had some influence on the piezo drive performance, but not much. The higher minimum driving voltage in vacuum may be partly explained by a change in the coefficients of friction.

6.5.4   Stability performance

The intrinsic stability of the TEM stage was measured by monitoring the output of the balanced differential transducer. The drift rate of the table relative to the reference frame in vacuum was lower than 30 pm/min.
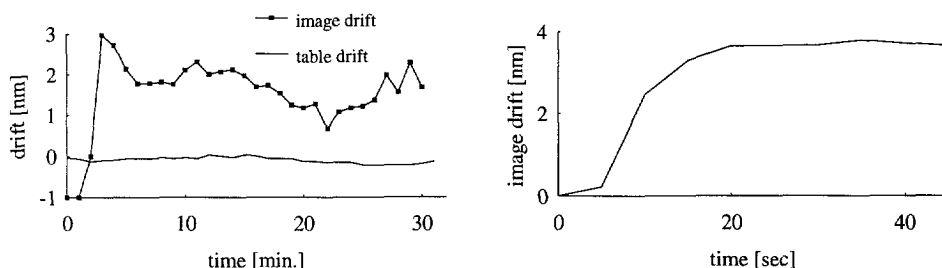

Fig. 6.18   a) Image and table drift after switching on the electron beam. b) Image drift after increasing the beam current with 20%.

Figure 6.18a shows the effect of switching on the electron beam on the stability of the table of the TEM stage and on the stability of the image. The table drift was recorded by the capacitive sensors and the image drift was recorded by the CCD camera. The recording rate of the CCD camera was adjusted at 1 image per minute. As a result of specimen heat up, a huge image drift occurred. During the first 60 seconds of the measurement, the image drift was so large that no correlation could be found between the first two images. The table position, however, was not affected at all. The same effect occurred when the table was moved to a new position over a distance with the same order of magnitude as the electron beam diameter. Figure 6.18b shows the effect of a forced, stepwise increase with 20% of the electron beam current on the image stability. Again, the table position was not affected, while there was a large image drift. This means that, in these cases, the image stability not depended on the table stability, but mainly on the internal specimen stability.

It must be noted from figure 6.18a that, after thermal equilibrium was obtained, the image stability still appeared to be low compared to the table stability. This can be partly explained by the fact that the peaks in the cross correlation functions calculated for two successive images showed large full width half maximum (FWHM) values due to a poor image resolution (1 nm). Therefore, the image resolution and the image contrast should be improved to be able to compare table drift and image drift at the subnanometer level.

6.6   Concluding remarks

Piezo actuators in combination with capacitive transducers have proven to be extremely suitable for positioning with nanometer resolution and repeatability with stroke to resolution ratios of up to 10^6 in air as well as in vacuum. They can also be applied in a TEM.

Each of the three piezo drives discussed showed to be able to rotate and translate perpendicular and parallel to the gravity field. There appeared to be only little difference in the performance of ISM drives in air and in high vacuum. The difference between the performance of ISM and FSM drives for equal table mass does not differ substantially.

The analytic ISM model proved to predict the behavior of ISM drives for motion perpendicular to the gravity field well. The contact stiffness k_c between the table and the supports plays an important role with regard to the resonance frequency of a piezo drive. The elastic buffer $2\delta_t$ determined to a large extent the minimum driving voltage of a piezo drive, especially as far as motion parallel to the gravity field was concerned.

The intrinsic stability of a nano stage can be at the picometer level. Nano stages can reach drift rates lower than 0.1 nm/min within 30 seconds settling time after moving the table to a new position if the driving voltage and the preload force are low. Open-loop methods for piezo drift compensation have proven to be able to decrease the piezo drift rates with at least a factor of five.

The image stability in a TEM depends not just on the nano stage stability, but also on the specimen (grid) stability.

7 Specimen stage configurations

7.1 Introduction

In chapters 1 to 5, a number of topics were discussed and investigated which contribute to positioning and position control of the table of a nano stage at the nanometer level and beyond. Throughout these chapters, the transmission electron microscope (TEM) was used as an application example of nano stages. It will be used as an example in this chapter as well. However, it is assumed that the discussion in this chapter on the transmission electron microscope example can be projected on other nano stage applications as well.

As was mentioned in chapter 1, the TEM can be used for an enormous range of applications and *in-situ* experiments. At the same time, this implies a large range of different sets of requirements on specimen positioning. These requirements regard the number and type of degrees of freedom in combination with the stroke, the positioning repeatability, the position stability, and the settling time to reach this stability level.

As far as specimen positioning in a TEM is concerned, three stage concepts for specimen positioning can be distinguished: the side-entry goniometer stage concept, the top-entry goniometer stage concept, and the nano stage concept. In addition to these concepts, some tools must be chosen which enable a high level of specimen positioning repeatability and position stability in order to meet the positioning requirements. Examples of these tools are:

- piezoelectric actuators and piezo drives for translations and rotations,
- open-loop compensation methods for piezo drift,
- feedback of image information to control the quasi-static image stability,
- capacitive transducers, and
- feedback control by means of position transducers, both to obtain a high level of positioning repeatability and position stability.

These tools can be globally grouped in five modules:

- an actuator module to obtain motion,
- a transducer module to measure displacements or position,
- a module to obtain a high level of positioning repeatability,
- a module to obtain a high level of position stability, and

- a module of additional topics.

The last module contains topics that do not match the other modules, like the concept of 'intrinsic stability' or the stacking order of the different degrees of freedom in a specimen stage. Another topic in this module is the choice of materials for specimen stages. These topics will be discussed in a separate section.

In this chapter, designers of specimen stages for a TEM are given some assistance in choosing the configuration of their specimen stage. In this respect, configuration means the combination of one of the specimen stage concepts and the tools from each module, which are required to obtain the desired positioning capabilities of the specimen stage. As an example, it is assumed that the positioning concept chosen is the *nano stage concept*.

As a result of the large number of different sets of requirements on specimen positioning, it is impossible to make general rules for the configuration of nano stages. Therefore, the assistance consists of the following three parts. The first part enumerates the different tools of each module and discusses their specifications (7.3). Besides that, feedback controlled drives are discussed (7.4). A feedback controlled drive is a combination of a tool from the actuator module and a tool from the transducer module which performs position control of a table or a specimen holder. In the second part, for reasons of demonstration, some examples of 'impossible' configurations of nano stages are given (7.5). The third part consists of a discussion on possible nano stage configurations for two different sets of positioning requirements (7.6) and gives a checklist by which a configuration can be analyzed (7.7). These two sets of requirements are given in section 7.2.

In the discussions on specimen stage configurations, it is almost impossible to be complete, because the number of possible configurations is very large. Moreover, a new or slightly different set of positioning requirements can result in completely different specimen stage configurations. Besides that, designer creativeness cannot be layed down in rules.

7.2   Examples of positioning requirements

7.2.1   Introduction

Before discussing specimen stage configurations, the set of positioning requirements should be carefully considered. It must be stressed that the slightest overkill in the set of requirements can result in an unnecessary complicated specimen stage configuration. Before making any decision on the specimen stage configuration, users and designers should together make a decision on the required number of degrees of freedom in combination with the stroke, on the required positioning repeatability, and/or on the required position stability in these degrees of freedom. Also, the amount of available space for specimen positioning in-between the objective lens pole pieces must be settled with. The next two sections give two examples of sets of positioning requirements for two different TEM applications.

7.2.2 Five degrees of freedom positioning

This example was previously considered in chapter 1. It indicates the required positioning capabilities of side-entry goniometer stages and was used as a starting point for the experimental set-ups of chapter 6. The set of positioning requirements for side-entry goniometer stages was already given in table 1.1. This set of requirements was agreed upon during conversations with the Philips Electron Optics department [23]. It is included in table 7.1, along with the positioning requirements of the next example.

7.2.3 The FANCIER

The FANCIER (Fabrication and Analysis of Nanostructures Combining Ion and Electron Regulation) is a particle beam instrument that is used in the NEXT (Nanoscale Experiments and Technology) project of the Delft University of Technology [115]. This project aims for the development of a system for nanometer scale fabrication in an all UHV environment and combines fabrication and analysis and in-situ measurements on nanostructures.

The FANCIER combines an ion beam and an electron beam on the same optical axis for fabrication and analysis of nanostructures [76]. The FANCIER consists of a scanning transmission electron microscope (STEM) equipped with a field emission gun (FEG). In order to be able to fabricate nanostructures with details in the order of a nanometer, researchers make high demands on the position stability of the specimen that contains the nanostructures. An example of these demands is included in table 7.1.

The number of degrees of freedom for the specimen stage of the FANCIER is low (positioning in the XY plane). The requirements on the position stability in the Z direction and on the stability of out of plane rotations are low compared to the requirements on specimen stability in the former example. However, the demands put on the quasi-static in plane specimen stage stability are very high.

	X,Y translation		Z translation		α, β tilt			
	5 DoF	FANCIER	5 DoF	FANCIER	5 DoF	FANCIER		
stroke	3	3	1	0	160	0	[mm]	or [°]
repeatability	50	50000	100	2	0.02	0.23	[nm]	or [°]
max. velocity	0.2	-[1]	0.05	-[1]	10	-	[mm/sec] or [°/sec]
min. velocity	0.5	-[1]	1	-[1]	0.1	-	[nm/sec] or [°/sec]
max. drift rate	0.1	0.05[2]	0.2	20[2]	-[3]	0.023[2]	[nm/min] or [°/min]
max. vibr. ampl.	0.01	0.05	0.02	20	-[3]	0.023	[nm]	or [°]

[1] For the FANCIER, there are no demands on velocity because the fabrication area of 50 x 50 μm^2 is covered by sweeping the electron beam.

[2] For the original side-entry configuration, Philips defined the tilt axis stability as 100 nm at 45°. As far as short term stability is concerned, the stability of the tilt axes must not compromise the stability in the X, Y and Z direction.

[3] The maximum drift rate for the FANCIER is given in nm/10 min or °/10 min.

Table 7.1   Positioning requirements for five degrees of freedom positioning and for the FANCIER.

7.3   TEM stage modules

7.3.1   Introduction

At a point on the route to a new TEM stage, it has to be decided which of the five modules have to be included in the specimen stage. The TEM stage configuration can consist of different combinations of modules and any combination of tools. This means that a configuration can consist of several tools from one module and that tools from another module can be absent. The choice for the actuators and the drive principles, and the choice for the displacement transducers will not be discussed. However, two remarks must be made.

As far as the nano stage concept is concerned, it is assumed that piezoelectric actuators will move the table of the drive modules. If the stroke of the table in a certain degree of freedom exceeds the maximum deformation of a single piezo actuator, a piezo drive can be applied to increase the stroke of the table. The choice for displacement transducers in practical TEM stages may be more complicated. Decisive parameters are the required space, the highest feasible resolution, the maximum ratio of range and resolution, and the required stability of the transducer. As far as their resolution is concerned, capacitive displacement transducers have shown to be unique. When position control at the subnanometer level is required, capacitive transducers are a logical alternative. For position control at the nanometer level, there are several alternatives [116]. However, in the discussions in this chapter, it is assumed that displacement measurements are performed by means of capacitive transducers.

Before considering the TEM stage configuration, the specimen positioning concept of the TEM stage must be chosen. One can either choose between the top-entry goniometer concept, the side-entry goniometer concept, or the nano stage concept. The choice for one of these concepts completely depends on the application. The advantages and disadvantages of the side-entry and the top-entry concept were shortly discussed in sections 1.4.2 and 1.4.3. For an extensive overview of their applications and their mutual advantages and disadvantages, it is recommended to read the literature referred to in chapter 1.

The advantage of the nano stage concept over both goniometer concepts is its compact design. This enables direct mounting of the nano stage on the lower pole piece as well as direct measurement of the specimen holder position relative to the lower pole piece in some degrees of freedom. Also, the nano stage has no direct mechanical connections to the outside of the vacuum chamber. The nano stage concept results in a high specimen stability due to a low sensitivity to (pole piece) vibrations and quasi-static changes in the environmental conditions. Due to the possible direct measurement of the specimen holder position to the lower pole piece, the nano stage concept also enables a high level of positioning repeatability.

The choice for a TEM stage positioning concept will not only depend on the expected performance of the particular concept but also on the type of objective lenses. As was already mentioned in chapter 1, it is important with regard to the resolution of the TEM to have a small gap

between both pole pieces. For commercial TEMs, several types of objective lenses exist which have different pole piece gaps. These gaps can be as small as 3 mm.

The choice for one of the specimen stage concepts also has consequences for the occupied space in the vacuum chamber. Both the side-entry and the top-entry concept consume less space of the vacuum chamber than the nano stage concept. Besides that, the number of possibilities to bring additional instruments close to the specimen decreases when the nano stage concept is used.

7.3.2   Overview of basic tools for specimen positioning

7.3.2.1   The specimen holder
The specimen holder carries the specimen and the specimen grid (if present). The dimensions of the specimen holder must be as small as possible to allow large tilts between the objective lens pole pieces. Generally, specimens have 3 mm diameter and are about 50 nm in thickness. It is assumed that the specimen holder has a minimum diameter of 3.5 mm and a minimum thickness of about 0.5 mm.

7.3.2.2   Piezo actuators and drive principles
Single piezo actuators
Single piezo actuators can be used for positioning with picometer resolution over a stroke of a few hundred nanometers. The open-loop positioning repeatability of piezo actuators depends on the piezo hysteresis and its deformation history. The position error will be typically 10 up to 20% of the nominal change of the open-loop motion. The quasi-static open-loop piezo actuator stability depends on the piezo hysteresis and the magnitude of the deformation change. It results in a drift which is in the order of 1% of the deformation change. The piezoelectric and electro-mechanical properties strongly depend on the nominal application temperature, on the driving voltage, and on the driving frequency.

Piezo drives
Piezo drives are used to overcome the small maximum deformation of piezo actuators. The maximum stroke of piezo drives depends on the configuration of the piezo drive and is either limited by the dimensions of the table or the dimensions of the support. The displacement resolution depends on the design and the configuration of the piezo drive, but can be equal to the displacement resolution of a single piezo actuator. Due to a variation in the step size up to 15%, the open-loop positioning repeatability of piezo drives is often not sufficient for most applications. The quasi-static open-loop stability of piezo drives is limited by the piezo drift or by creep in the support. The dynamic open-loop stability is determined by the level of external vibrations and the frequency response of the piezo drive. Piezo drives can be used to obtain translations perpendicular and parallel to the gravity field and to obtain rotations.

7.3.2.3   Capacitive displacement transducers
Capacitive displacement transducers are very well suitable for displacement measurement in a TEM. Their range to resolution ratio can be up to 10^7 depending on the maximum possible electrode area, the required bandwidth and the plate distance. Vibrations with amplitudes down to the (sub)nanometer level can not be detected by practical capacitive transducers. The minimum feasible resolution is determined by the flatness of the capacitor plates and the accuracy of the plate

alignment. It can be down to a few picometers. The main disadvantage of capacitive transducers is that the small plate distance needed for a high displacement resolution can limit the stroke of the specimen stage. This means that a combination of obtaining nanometer positioning repeatability over a stroke of a few millimeters and stability control down to the picometer level is not possible with a single capacitive transducer. The position stability and the positioning repeatability depend on the environmental stability, on the stability of the measurement electronics, on the stability of the mechanical parts of the measurement configuration, and on the measurement configuration used.

7.3.2.4   Open-loop control
Open-loop control methods can be applied for the compensation of specimen holder drift. They become useful when the drift behavior in time is well known. An example of an element that can cause specimen holder drift is a piezo actuator. The drift course of a piezo actuator is relatively well known when its (dynamic) deformation history is simple. This is often the case when changes in the driving voltage are constant and larger than 40 V. As far as piezo actuators are concerned, the open-loop control tool can help to decrease the drift rate with at least a factor of five. A second part of this tool is the use of a compensation cycle. This method is capable of decreasing the piezo drift rate with up to a factor of 20.

7.3.2.5   Feedback control
The application of additional sensors
This tool can be used in addition to the conventional side-entry and top-entry stages. It uses capacitive transducers (for instance combined with piezo actuators) placed inside the vacuum chamber of the TEM, which have a direct reference to the lower pole piece allowing control of the position of the specimen holder. The capacitive transducers can be used to improve the specimen holder positioning repeatability as well as to improve the quasi-static specimen holder stability. The main disadvantages of this feedback control tool are that direct measurement of the angular specimen position relative to the lower pole piece is often not possible and that application of this module can strongly limit the allowable stroke of the specimen holder.

Image feedback
This tool can be used in all three specimen stage concepts to compensate slow specimen drift. At the moment, the bandwidth of this tool is no larger than a few hertz. Besides that, the accuracy of this control tool depends on the dynamic stability of the specimen because this stability influences the image resolution and hence the accuracy of the cross-correlation calculations. Another disadvantage of this tool is that it cannot be used for all types of experiments in the TEM.

Feedback controlled drives
Feedback controlled drives combine a piezo drive and a set of capacitive transducers to perform position control of the piezo drive table relative to a reference frame. This tool can either be used to obtain a high level of positioning repeatability as well as a high level of quasi-static position stability. It can be used for translations as well as for rotations. As feedback controlled drives are the most important tools of nano stages, they will be discussed in more detail in section 7.4.

7.3.2.6 'Indirect' feedback control

This tool can be used to overcome the problem of the limited table or specimen holder stroke when capacitive displacement transducers are used for high resolution position control. An example of this tool is shown in figure 7.1. The main parts of this module are a piezo drive and a table, a *moveable* reference frame, and a set of capacitive transducers. In order to control the specimen holder position at the subnanometer level, the plate distance d_0 of the capacitive transducer must be small. This limits the stroke of the table (see figure 7.1a). By using a reference frame that can be moved relative to the pole piece by means of the specimen stage (see figure 7.1b), a high transducer resolution can be combined with a large table stroke. In the configuration of figure 7.1b, the reference frame is pushed by the table in the direction of motion. This method has two disadvantages. The table stability becomes dependent on the stability of the moveable reference frame relative to the pole piece and the necessary control to obtain a high level of positioning repeatability must be obtained by an additional set of displacement transducers.
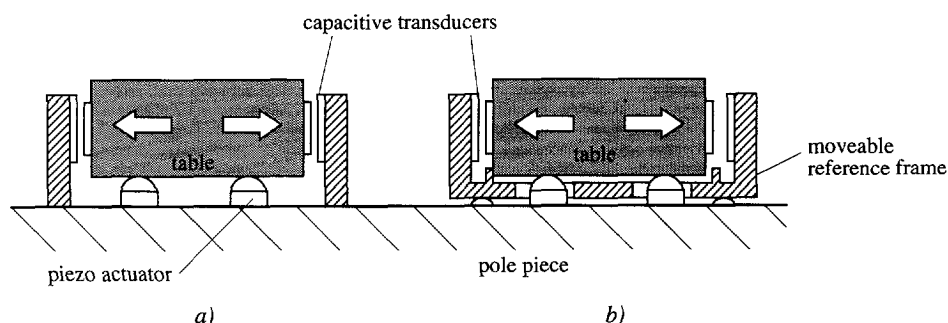
*Fig. 7.1   An example of 'indirect' feedback control by means of a stage that moves its reference frame. a)
The table stroke is limited by the small plate distance of the capacitive transducer. b) A move-
able reference frame is used to overcome this problem.*

7.3.3   Additional topics

7.3.3.1 Intrinsic stability

Intrinsic stability is the maximum stage stability that can be obtained without application of feedback control. It is not a tool but a (design) *concept* that can be used to obtain a high specimen holder stability. Intrinsic stability should be split in quasi-static intrinsic stability or minimum achievable drift rate of the specimen holder and dynamic intrinsic stability represented by the minimum vibration amplitude of the specimen. Quasi-static intrinsic stability is connected with the specimen stage sensitivity to slow environmental disturbances, with changes in the internal heat production in the specimen stage, with drift in piezo actuators, and with creep in the specimen holder supports. The choice of the specimen stage concept, of the specimen stage materials, of the design of the specimen stage, and of the way the specimen stage is driven influences the quasi-static intrinsic stability to a large extent. For a high intrinsic stability of the specimen holder, it is favorable to use low driving voltages in order to minimize piezo drift and to use small preload forces. The dynamic intrinsic stability is determined by the spectrum of vibrations subjected to the specimen stage and its frequency response. The parameters which determine the

dynamic intrinsic stability are the choice of the specimen stage concept, the vibration isolation system of the microscope, and the resonance frequency of the specimen stage.

7.3.3.2 Stacking of degrees of freedom

A very important topic with regard to the configuration of specimen stages is the stacking order of degrees of freedom. Stacking degrees of freedom means that the table and the actuators which perform motion in a certain degree of freedom are placed on a table that performs motion in a different degree of freedom. The upper table in the stack is the specimen holder. The stacking order has a considerably large influence on the positioning performance of a specimen stage as will be shown in section 7.6 for the nano stage concept. It influences the specimen holder stroke for tilting and the *eucentricity* of the specimen stage (eucentricity will be explained in section 7.4). Inherent to stacking drives with different degrees of freedom is that the positioning repeatability and the position stability of the specimen holder depends on the positioning repeatability and position stability of the tables of the lower drives, if the position of the specimen holder cannot be directly measured relative to the lower pole piece. This influence is called crosstalk. An option to minimize crosstalk is to clamp the table(s) of the lower drive module(s) firmly to their base. A problem of this method is that it requires a considerable clamping force which can reduce the quasi-static table stability as was investigated in section 5.6.

7.3.3.3 Choice of materials

Three different types of materials can be distinguished in a specimen stage:

- the bulk material for the specimen stage and the reference frames,
- the ceramic for the piezo actuators, and
- the materials for the contact zones between the stage table(s) and their supports.

The choice of specimen stage materials should be mainly based on the effect that a certain material has on the quasi-static and dynamic stability of the specimen stage.

7.4 Feedback controlled drives

7.4.1 Introduction

In this and the following sections of this chapter, it is assumed that the specimen stage concept chosen for specimen positioning in a TEM is the *nano stage concept*. Besides that, it is assumed that this concept is applied in a Philips EM420 using the TWIN objective lens configuration and with its optical axis parallel to the gravity field. The direction parallel to the optical axis is defined as the Z direction. The plane perpendicular to the optical axis is defined as the XY plane. This section discusses feedback controlled drives. These drives provide three basic types of controlled specimen motion:

- translation and rotation in a plane perpendicular to the gravity field (XY drive),
- translation and rotation in a plane not perpendicular to the gravity field (Z drive), and
- tilting ($\alpha\beta$ tilt drive).
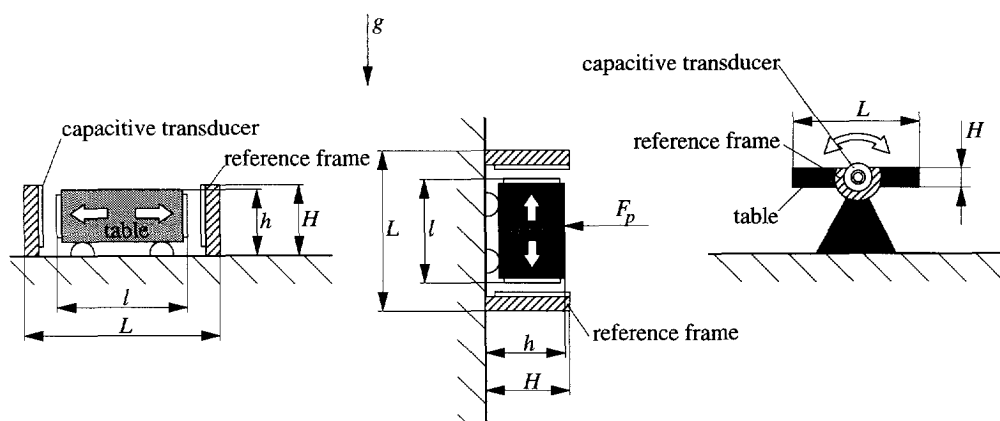
Fig. 7.2   Schematic representation of three types of feedback controlled drives: a) the XY drive, b) the Z drive, and c) the αβ tilt drive.

Feedback controlled drives are discussed here because they form a practical way to discuss the possible and impossible configurations of nano stages. Figure 7.2 shows the schematic representation of each drive including the way of position measurement. In this and the other schematic representations of nano stage configurations in this chapter, the piezo actuators are not shown because this would not add useful information. It is assumed that capacitive plate-distance transducers are used for the measurement of translations and small tilts and that capacitive in-plane transducers are used for the measurement of large rotations. It is also assumed that the maximum positioning repeatability of the table can be equal to five times the displacement resolution of the capacitive transducer. Section 7.4.3 discusses the minimum dimensions of the drive modules. Section 7.4.4 discusses some problems concerning stacking of drive modules. But first, the principle of eucentric tilt axes is explained in section 7.4.2.

7.4.2   Eucentricity

Eucentricity is explained in figure 7.3. A tilt axis is called eucentric when this axis and the elec-

Fig. 7.3   A tilt axis is eucentric when this axis and the electron beam cross each other in the specimen plane. As a result, the specimen remains focussed when it is tilted.

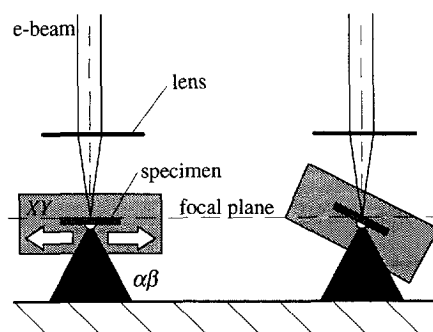tron beam cross each other in the specimen plane. As a result, the specimen remains focussed when it is tilted. Eucentricity can be achieved by placing the tilt drive(s) at the bottom of a stack of drives and is therefore strongly related to the stacking order of the drives.

If the $\alpha\beta$ tilt drive is not placed at the bottom of the stack, *pseudo-eucentricity* can be obtained by changing the specimen position in the X or the Y direction, and the Z direction (see figure 7.4). The table stroke in the Z direction must then be adjusted to the maximum allowable tilt angle.
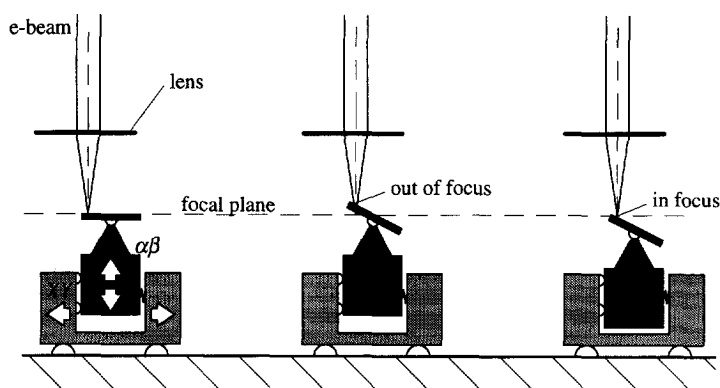
Fig. 7.4   If the $\alpha\beta$ tilt drive is not placed at the bottom of the stack, pseudo-eucentricity can be obtained by translating the specimen in the X or the Y direction, and the Z direction.

7.4.3   Minimum dimensions of the drives

7.4.3.1 Introduction

The minimum drive dimensions are important with regard to the limited space available in the vacuum chamber and with regard to the stacking order of the drives. The values for the minimum dimensions of the drives given in this section are first order approximations, partly based on calculations and partly on experience. The absolute minimum dimensions of the upper table in the stack, the specimen holder, are determined by the size of the specimen. It is assumed that closed-loop position control is required when the required positioning repeatability is smaller than 10% of the maximum table stroke. This is due to the maximum variation in the step size of a piezo drive.

7.4.3.2 The XY drive

The minimum space required by the XY drive depends on the required stroke, on the required level of positioning repeatability, on the size of the specimen, and on the minimum space required by the piezo drive. Differential capacitive transducer were assumed. The minimum dimensions of the detector area can be calculated by equation 4.13. Table 7.2 gives the estimated minimum dimensions of the XY drive for three different table strokes and for two different displacement resolutions. A minimum plate distance of 0.1 mm and a detector resolution of $1 \cdot 10^{-6}$ pF were assumed. The guard electrode width was taken equal to 0.6 times the table stroke.

stroke $X = Y$ [mm]	d_0 [mm]	occupied space l x w x h [mm³]		occupied space L x W x H [mm³]	
		Δx: 1 nm	10 nm	Δx: 1 nm	10 nm
0.1	0.16	8 x 8 x 3	8 x 8 x 3	10 x 10 x 3	10 x 10 x 3
1	0.6	8 x 8 x 3	8 x 8 x 3	11 x 11 x 3	11 x 11 x 3
3	1.6	21 x 21 x 9	10 x 10 x 4	25 x 25 x 9	15 x 15 x 4

Table 7.2   Estimated minimum space required by the XY drive for three values of the maximum table stroke and two values of the displacement resolution. The considerable increase of the occupied space for a table stroke of 3 mm is caused by the increase of the size of the electrodes of the capacitive transducer.

It is difficult to give a value for the minimum dimensions of the piezo drive of the XY drive because there is an enormous amount of piezo drive designs possible. It was assumed that for large table strokes the influence of the dimensions of the piezo drives on the minimum drive dimensions can be neglected. In that case, the dimensions of the piezo drives is mainly determined by the capacitive transducers. For small table strokes, the piezo drive dimensions will become more decisive. Table 7.2 distinguishes between the XY drive dimensions with and without the reference frame. This is done in view of the stacking of drive modules which is discussed later.

7.4.3.3 The Z drive

Besides the detector area of the capacitive transducer, the size of the specimen and the size of the piezo drive have to be taken into account when estimating the minimum dimensions of the Z drive. They are estimated in table 7.3 as a function of the table stroke and for application of either a single or a differential capacitive plate-distance transducer. The displacement resolution of the transducer was assumed to be 20 nm and the guard electrode width was assumed to be equal to 0.6 times the table stroke.

stroke Z [mm]	occupied space l x w x h [mm³]		occupied space L x W x H [mm³]	
	single	differential	single	differential
0.1	5 x 5 x 5	5 x 5 x 5	7 x 7 x 5	7 x 7 x 5
1	6 x 6 x 5	5 x 5 x 5	9 x 9 x 5	8 x 8 x 5
3	10 x 10 x 8	6 x 6 x 5	15 x 15 x 10	9 x 9 x 6

Table 7.3   Estimated minimum space required by the Z drive for three different values of the table stroke, for a displacement resolution of 20 nm and a measurement resolution of $1 \cdot 10^{-6}$ pF.

7.4.3.4 The $\alpha\beta$ tilt drive

Figure 7.5 shows a practical configuration of the $\alpha\beta$ tilt drive (double tilt). If only a single tilt is required, one drive can be omitted. The configuration of figure 7.5 allows tilt about the X and the Y axis. The minimum dimensions of this drive are determined by the size of the specimen, by the required maximum specimen tilt angle, by the required minimum space of the capacitive trans-
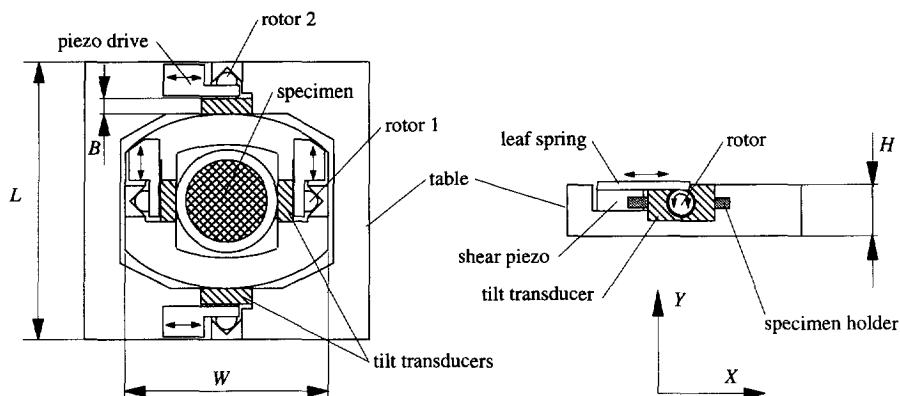
Fig. 7.5 A practical configuration of the $\alpha\beta$ tilt drive. Tilting is performed by means of the piezo rotor configuration of figure 3.20. The angular position of the rotor is measured by a capacitive in-plane transducer relative to the table.

ducer at a given required angular resolution, and by the required minimum space of the piezo rotor.

The minimum width b of a simple capacitive angular in-plane transducer can be estimated from equation 4.16 to be 0.07 mm for a resolution of 0.01° and a rotor diameter of 1 mm. The maximum transducer width is subsequently estimated to be 0.5 mm. The minimum amount of space required by the piezo drive is estimated to be 2x1x1 mm³. This piezo drive is, for instance, based on the leaf spring configuration discussed in section 3.8. Table 7.4 gives an overview of the estimated space required by the $\alpha\beta$ tilt drive for different values of the maximum tilt about the X and the Y axis for the configuration of figure 7.5.

α tilt [°]	β tilt [°]	occupied space $L \times W \times H$ [mm³]
30	0	8 x 7 x 3
90	0	8 x 7 x 4
90	30	10 x 8 x 4
90	60	10 x 8 x 7
90	90	10 x 8 x 8

Table 7.4 Estimated minimum space required by the $\alpha\beta$ tilt drive for different values of the maximum tilt about the X and the Y axis for the configuration of figure 7.5. Single tilt is assumed when the β tilt is equal to zero.

For double tilt, this results in an $\alpha\beta$ tilt drive which minimum dimensions in the X and Y direction are 8 up to 10 mm and which dimension in the Z direction is about 2 mm. The space required by the tilt drive increases when the specimen is actually tilted. These values are given in table 7.4. The maximum possible tilt angles are determined by the gap between the pole pieces.

7.4.4   Stacking of drives

Stacking of drives is used to increase the number of degrees of freedom of the specimen holder if the number of degrees of freedom of a single drive is not sufficient. In that case, the table of the upper drive module becomes the specimen holder. It is the position repeatability and the position stability of the specimen holder to which the set of positioning requirements refers to. Figure 7.6 shows two examples of a stack of an XY drive and a Z drive.

The configuration includes tools for feedback control of the specimen holder position in all three directions. It should be noted that, due to their configuration, the capacitive transducers can be made insensitive to parasitic motion. The configuration of figure 7.6a directly shows the former mentioned inherent problem of stacking drive modules. In order to obtain a high level of positioning repeatability of the specimen holder, the open-loop positioning repeatability of the specimen holder in the X and the Y direction, relative to the table of the XY drive and the open-loop positioning repeatability of the XY drive table in the Z direction must be as high as or better than the specimen holder positioning repeatability required in that direction. In case of a combination of three translations, this problem can be solved relatively simple by a change in the configuration, as is shown in figure 7.6b. The capacitive transducers used are all of the plate-distance type. The measurement of the specimen holder position in the X, the Y and the Z direction is now directly performed relative to the reference frame on the lower pole piece without limitations to the specimen holder strokes. Direct measurement of the specimen holder position becomes almost impossible when specimen holder translations and tilting have to be combined. Examples of 'impossible' configurations are discussed in the next section. Another disadvantage of stacking drives is the increase of the nano stage mass and the decrease of the specimen holder stiffness relative to the pole piece. This results in a lower resonance frequency and hence a lower intrinsic specimen holder stability as was discussed in chapter 5.

a)   b)
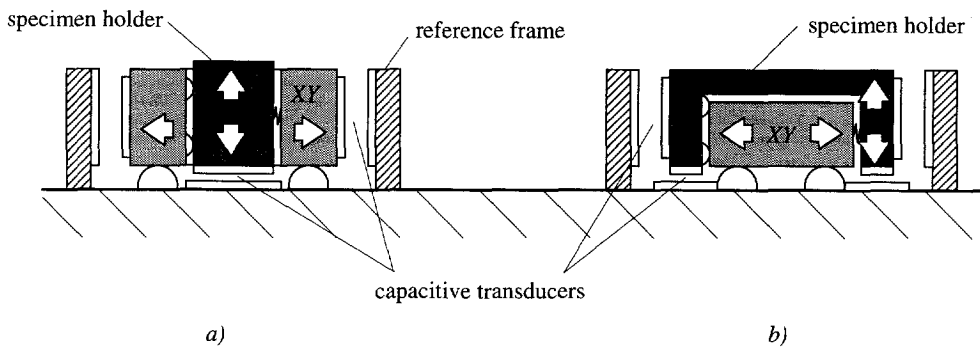
Fig. 7.6   Two configurations of a nano stage consisting of an XY drive and a Z drive. The Z drive is stacked on top of the XY drive. Both configurations include position control in all three degrees of freedom. a) Direct measurement of the specimen holder position in the X, the Y and the Z direction relative to the reference frame is not possible. b) Direct measurement of the specimen holder position in the X, the Y and the Z direction is possible without limitations to the strokes.

7.5   'Impossible' nano stage configurations

In order to show that a set of positioning requirements limits the number of possible nano stage configurations, two examples of 'impossible' configurations are given in this section. Figure 7.7a shows a stack of an XY drive and a tilt drive. The XY drive is placed on top of the tilt drive. If only small tilts are required, the position of the specimen holder can be directly measured relative to the reference frame on the lower pole piece. If large specimen tilts are required, the configuration of figure 7.7a can no longer be used due to the size of the XY drive and the configuration of the transducers. An alternative is shown in figure 7.7b; the tilt drive is placed on top of the XY drive. Using this configuration, it is impossible to measure the specimen holder position in the X and the Y direction directly to the reference frame on the lower pole piece. This means that the positioning repeatability and the intrinsic position stability of the tilt drive in the X and the Y direction and that the positioning repeatability and the position stability of the tilt of the table of the XY drive must be such that the specimen holder repeatability and stability are not compromised. In that respect, it may be useful to measure the tilt of the table of the XY drive relative to the reference frame on the lower pole piece (see figure 7.7c). Measurement of the XY position of the specimen holder relative to the table of the XY module is much more difficult with capacitive transducers.
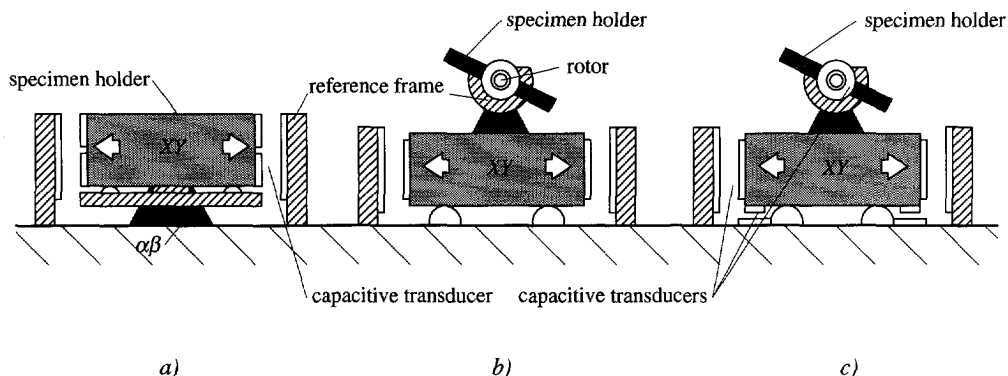
Fig. 7.7   Stack of an XY drive and a tilt drive. a) Direct measurement of the specimen holder position is only possible for small tilt angles. b) A change in the stacking order allows for large specimen tilts. c) Part of the problem may be solved by measuring the tilt angle of the table of the XY drive relative to the reference frame attached to the lower pole piece.

A second impossibility of the nano stage configuration of figure 7.7a is eucentric tilting. Besides that, obtaining pseudo-eucentric tilt is also impossible because of the absence of a Z drive.

Another impossible stage configuration is to combine a large table stroke (3 mm) and a high level of position stability obtained by using plate-distance transducers in the direction of motion. In order to obtain a large specimen holder stroke, the nominal plate distance of the capacitive plate-distance transducers used must be accordingly large (1.6 mm). However, in order to have subnanometer resolution to perform stability control, the nominal plate distance must be in the

order of 100 µm. Theoretically, there are two alternative configurations possible to solve this problem. In some applications, it may be possible to use a combination of in-plane and plate-distance capacitive transducers. A second solution is to use a moveable reference frame (see figure 7.1).

7.6 Possible configuration examples

7.6.1 Introduction

In this section, possible configuration examples are discussed for the two sets of positioning requirements given in table 7.1. Beforehand, it must be stated that these examples do not cover the whole range of possible configurations. This section gives some very likely configurations but does not claim to be complete. For both sets of requirements, application in a Philips EM420 with TWIN objective lenses is assumed. Figure 7.8 is a schematic to scale representation of the TWIN objective lens pole pieces, an aperture holder, and a backscattered electron detector. The nominal pole piece distance is 9 mm. However, the presence of the aperture holder decreases the available space to 8 mm. When the backscattered electron detector is used, the available space between the pole pieces is further reduced to 6.5 mm.
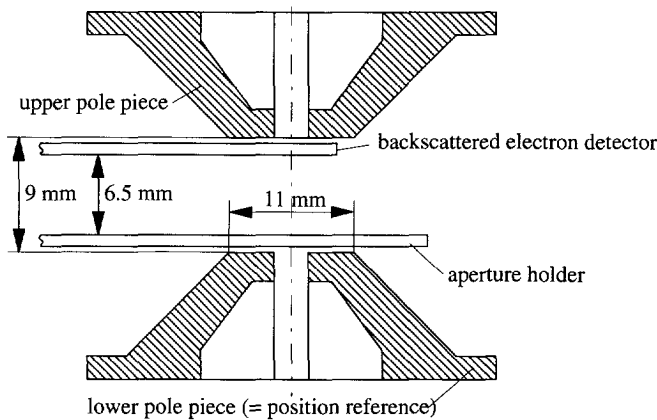
Fig. 7.8 Schematic to scale representation of the pole pieces of the TWIN objective lens of a Philips EM420, an aperture holder and a backscattered electron detector.

7.6.2 Five degrees of freedom positioning

From the set of requirements given in table 7.1, it is clear that the required levels of positioning repeatability must be obtained by feedback control. Besides that, it was chosen not to rely on feedback control tools to obtain low drift rates, but to use the intrinsic stability of the nano stage and the capabilities of the open-loop control tool to compensate for piezo drift. An optimum

configuration of a five degrees of freedom nano stage can be found by discussing various stacking orders of the required drives.

7.6.2.1 Stacking order of the $\alpha\beta$ tilt drive and the XY drive

In view of eucentricity, the XY drive is placed on top of the $\alpha\beta$ tilt drive. Because of the large tilts required, this implies that the reference frame of the XY drive has to be stacked on the tilt drive (minimum dimensions 15 x 15 x 4 mm^3, see table 7.2). It is clear that the maximum tilt about the X and the Y axis is limited by the dimensions of the XY drive (see figure 7.9a). For this configuration, the maximum possible α and β tilt is only about ± 15°. Another disadvantage of this stacking order is that, as a result of the gravity field, the forces on the specimen holder change with changing tilt angles. Furthermore, tilts change the function of the translations in the XY drive into translations which are no longer perpendicular to the gravity field. This means that the specimen holder must be preloaded which has a severe impact on the design and the performance of the drive.
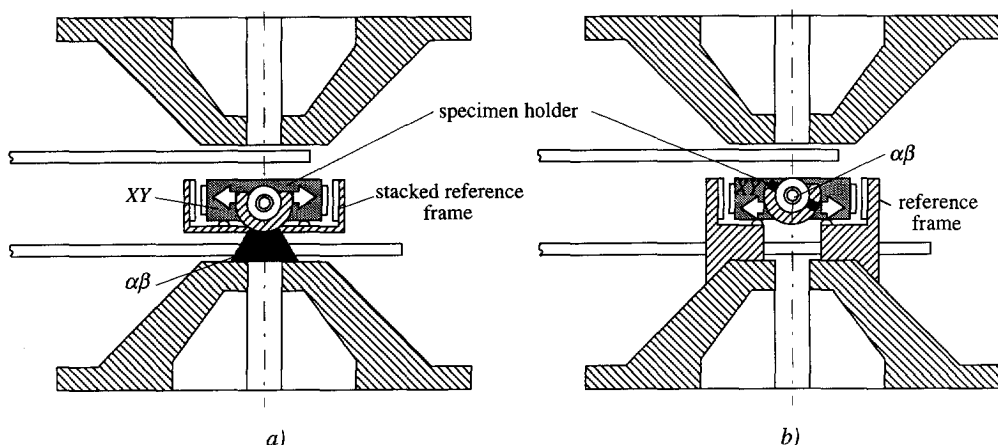
Fig 7.9   A stack of the $\alpha\beta$ tilt drive and the XY drive. a) The XY drive is placed on the $\alpha\beta$ tilt drive. b) The $\alpha\beta$ tilt drive is placed on the XY drive.

If the stacking order is changed, as shown in figure 7.9b, the maximum tilts of the specimen can be increased to ± 90° and ± 40° for the α tilt and the β tilt, respectively. This configuration does not have the problem of changing forces on the table of the XY drive. A disadvantage of this stacking order is that the tilt axes are no longer eucentric. Because pseudo-eucentricity of the tilt axes can be obtained by addition of the necessary Z drive, the stacking order of figure 7.9b is given preference to.

Although the proposed configuration of the $\alpha\beta$ tilt drive is in fact a stack of two drives (the configuration consists of two tables and two sets of piezo drives and position transducers), it is not useful to separate the α tilt and the β tilt over two different drives, unless one of the required tilt strokes is small.

7.6.2.2 Stacking order of the Z drive

As far as the stacking order of the XY drive and the Z drive is concerned (see figure 7.10), there are two parameters that influence this stacking order: the height of the Z drive and the specimen holder stroke in the Z direction. The set of requirements of table 7.1 assumes eucentric tilt. However, the 0.5 mm stroke for the translation in the Z direction is not enough if compared to the size of the specimen, the maximum tilt angles required and if pseudo-eucentricity is to be obtained. This means that the specimen holder stroke in the Z direction must be as large as 3 mm. In this respect, it may make sense to stack the XY drive on top of the Z drive, that way allowing the Z drive to consume more space. An important advantage of placing the Z drive on top is that the mass that must be moved in the Z direction is smaller. This means that the preload forces in the Z drive are minimized, which is advantageous with regard to stability after positioning. Table 7.3 gives the height of the Z drive as a function of the stroke of the table. If the specimen holder position can be directly measured to the reference frame on the pole piece, the dimensions of the Z drive are small enough to fit between the pole pieces (differential transducer). Therefore, the configuration of figure 7.10a is given preference to.
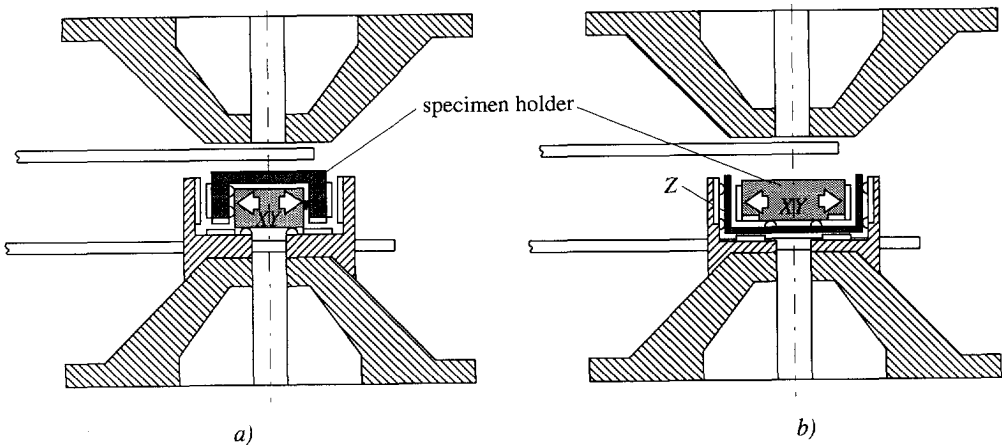
Fig. 7.10   Stack of an XY drive and a Z drive. a) The Z drive is placed on the XY drive. b) The XY drive is placed on the Z drive.

The $\alpha\beta$ tilt drive can either be placed between the XY drive and the Z drive (see figure 7.11a) or on top of the stack (see figure 7.11b). A disadvantage of the configuration of figure 7.11a is the reduction of the stroke in the Z direction at large tilt angles. Furthermore, placing the $\alpha\beta$ tilt drive between both translation drives has the disadvantage that the α and β tilt are limited and that the gravity force on the table of the Z drive changes with changing tilt angles α and β. Also, the tilt axes α and β are not eucentric. Therefore, the configuration of figure 7.11b seems the better alternative. Although the tilts α and β are not eucentric, the position of the Z drive table can be directly measured to the pole piece in the X, the Y, and the Z direction and the gravity force on all tables remains the same. However, the maximum tilt angles possible with the configuration of figure 7.11b are estimated to be smaller than the maximum tilt angles possible with the configuration of figure 7.9b. This is due to the stroke of the Z drive. One tilt with a maximum of $\pm$ 90° is still possible, the second tilt depends on the table stroke in the Z direction. The

stacking order of the XY drive and the Z drive has not much influence on the second maximum tilt angle possible.

a)   b)

Fig. 7.11   Two configurations for a stack of three drives. a) The αβ tilt drive is stacked between the
             XY drive and the Z drive. b) The αβ tilt drive is stacked on top of both the XY drive and the
             Z drive.

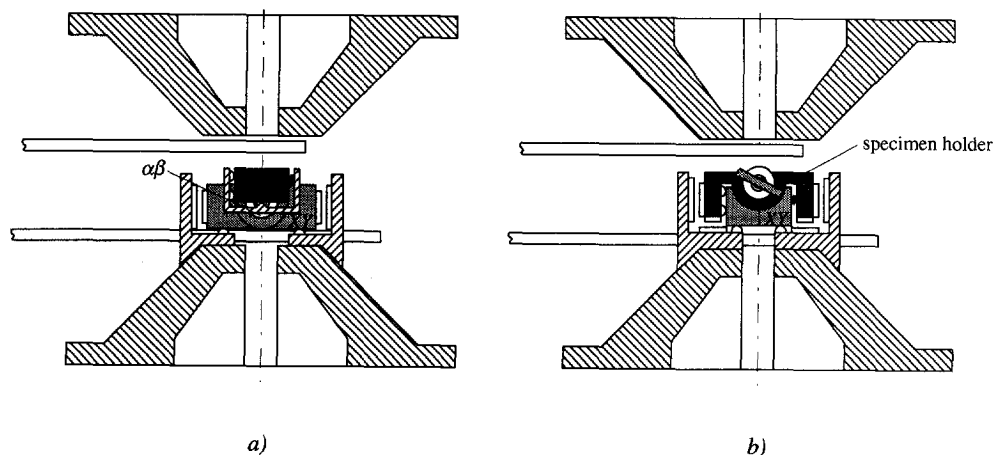The configuration of figure 7.11b is regarded to be the optimum configuration as far as the set of requirements for five degrees of freedom positioning is concerned. The final positioning repeatability of the specimen holder and the pseudo-eucentricity depend on the repeatability of the tilting motion, on the repeatability of the measurement of the specimen tilt, on the repeatability of the specimen position measurement in the X, Y, and Z direction, and on the accuracy of the calculation of the required position (corrections) in the X, Y, and Z direction. In order to get 50 nm overall positioning repeatability in the X and Y direction, it is assumed that the required angular resolution should be 10 nm/1.5 mm = $6.7 \cdot 10^{-6}$ rad. The repeatability of the position measurements completely depends on the transducer stability. The short term stability of a differential transducer with 1 pF nominal capacitance (10^{-5} pF over 3 min) is sufficient to achieve a repeatability of 50 nm over a 3 mm measurement range. To achieve this level of repeatability over a long time interval, bridge balancing is required. In that case, the repeatability of the bridge balancing method should be carefully considered. From the experiments during this research, it is known that this repeatability can be well within $5 \cdot 10^{-6}$. The accuracy of the calculation of the specimen holder position (corrections) depends on the accuracy of the mathematical relation between the transducer output and the specimen position. This relation needs to be calibrated, for instance by a laser interferometer. The specimen holder position stability is a combination of the stability of the stacked drives. The intrinsic specimen holder stability is lower than the intrinsic stability of a single drive. Although both the static and the dynamic specimen holder stability strongly depend on the final stage design and on the (environmental) conditions in each (TEM) application, it is expected from the scope of experiments that was performed that the specimen holder drift can be well below the 0.1 nm/min level and that the vibration amplitude can be below the 50 pm level.

7.6.3 The FANCIER

The FANCIER only asks for an XY drive. This means that the specimen holder position can be measured directly to the reference frame on the lower pole piece. The ratio of the required positioning repeatability and the stroke of the specimen holder asks for feedback control, although this control does not need to be very accurate. However, it is clear that it is the required quasi-static position stability and not the positioning repeatability that is the major concern of the FANCIER set of requirements. Although the demands put on the dynamic stability in the X and the Y direction are high, it is expected that they can be reached if the resonance frequency in these directions can be made high enough. The requirements on the position stability in the Z direction should be no problem.

Before discussing possible configurations, it must be stated that there will be a practical maximum drift rate level. This is independent of the configuration that is used and is due to the fact that there will always be (parts of) elements in the configuration between the specimen and the pole piece which position drift or deformation cannot be controlled. Examples of these elements are the specimen holder and the reference frame. The 50 pm/10 min drift rate level may be close to this maximum.

The combination of the 3 mm strokes of the specimen holder in the X and the Y direction, and a drift rate lower than 50 pm/10 min may be obtained by means of two different configurations (see figure 7.12. The main difference between these configurations is the application of either intrinsic stability and open-loop controlled tools or feedback control tools. Both configurations use an ISM drive. The configuration of figure 7.12a uses the intrinsic stability of the stage and the open-loop control tool to obtain the required drift rate level. Due to the low demands put on the position repeatability, the overlapping area of the capacitive plate-distance transducers used can be small. Besides that, the specimen holder only needs to carry the specimen. This can result in a very compact design and an accordingly high intrinsic stability.

a)   b)
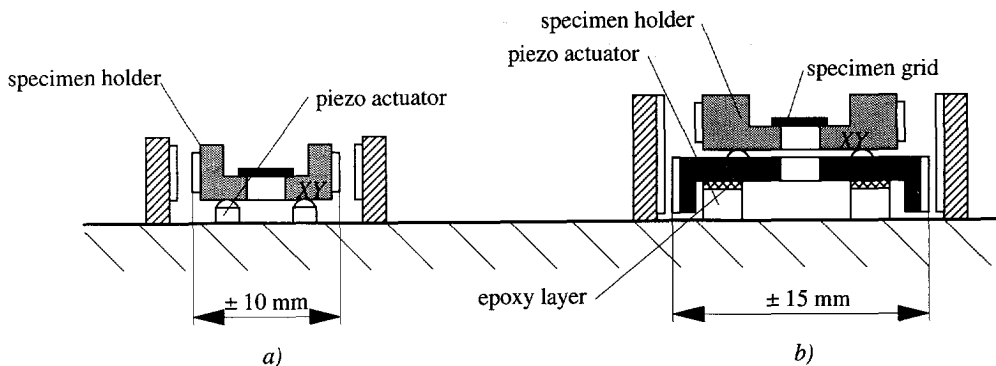
Fig. 7.12   Nano stages for the FANCIER consist of just an XY drive. Both specimen holders are moved by ISM. The configurations enable large specimen holder strokes and nanometer positioning repeatability. a) The stability of this configuration is based on its high intrinsic stability. b) A high specimen holder stability is obtained by means of indirect position measurements. The position of the specimen holder is controlled by measuring the position of the table relative to the reference frame with high resolution.

The configuration of figure 7.12b uses an indirect feedback control tool. The specimen holder is supported by a table that is attached to the piezo actuators by means of epoxy layers. Slip occurs between the specimen holder and this table. Two sets of plate-distance capacitive transducers are used. One set measures the position of the base relative to the reference frame with high resolution, the other set measures the specimen holder position relative to the reference frame with lower resolution. This way, the stroke of the specimen holder can be large and its position stability can be indirectly controlled by controlling the stability of the table. This is useful to compensate piezo drift. The position stability of the specimen holder of figure 7.12b depends on the position stability of the specimen holder relative to the table. Although the configuration of figure 7.12b will be less compact than the configuration of figure 7.12a, the configuration is still relatively small. As a result of the low level of position repeatability required, the set of capacitive transducers on the specimen holder has only a small overlapping area. Besides that, the specimen holder only needs to carry the specimen. The dimensions of the table are determined by the stroke of the specimen holder, the dimensions of the capacitive transducer, and the piezo actuators used. All together, the dimensions of this specimen stage will be around 15x15x6 mm^3 for 10 pm resolution and a plate distance of 0.1 mm. These small dimensions will result in a high resonance frequency and a low sensitivity to thermal load. However, one of the problems of the configuration of figure 7.12b is the mass of the table. Since this mass must be accelerated by the piezo actuators in order to obtain slip between the specimen holder and the table, the table mass must be small compared to the specimen holder mass.

A third solution for the FANCIER stage is to use a combination of plate-distance transducers and in-plane transducers as was proposed by De Jager [76]. The proposed configuration is sketched in figure 7.13a.

a)   b)
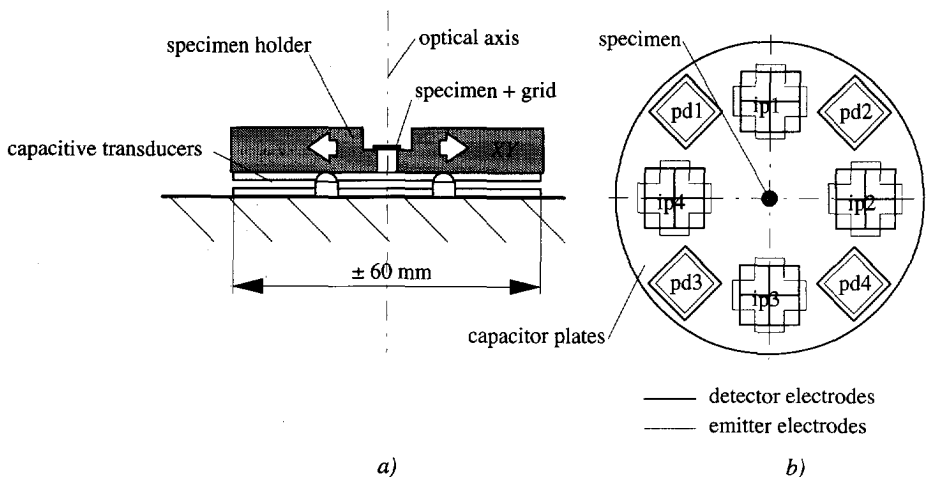
Fig. 7.13   a) Configuration of a feedback controlled FANCIER nano stage combining plate-distance and in-plane capacitive transducers to obtain a high displacement resolution and at the same time allowing large specimen holder strokes in the X and the Y direction (from [76]). b) The configuration of the in-plane (ip) and plate-distance (pd) capacitive transducers.

Compared to the former examples, the dimensions of this configuration are much larger. This means that the sensitivity of this specimen stage to vibrations is presumed to be higher than of the former examples. Besides that, the measurement loop between the specimen and the pole piece for this configuration is larger resulting in larger drift and creep effects in the components present in this measurement loop. Let's for instance consider the sensitivity of the configuration to thermal load. The specimen stage is symmetric relative to the optical axis and therefore is in first order compensated for changes in the overall thermal load. In practice, however, there will always be a position offset in the XY plane of the specimen holder relative to this optical axis, resulting in a capacitance difference in the in-plane transducers. A rise in the overall temperature changes this capacitance difference. This results in a difference in the real and the measured position drift of the specimen relative to the pole piece. If the position offset x_o is 1 mm and the thermal expansion coefficient α of the capacitor plates, the specimen holder and the reference frame is around $5 \cdot 10^{-6}$ per kelvin, the overall temperature change rate ΔT must be smaller than $\Delta x / 2\alpha x_o = 5$ mK per 10 min, for a drift rate Δx smaller than 50 pm/10 min. This is difficult to achieve.

An advantage of the configuration of figure 7.13 is that creep in the specimen holder supports can be compensated for.

7.7   Performance checklist

In order to be able to analyze a specimen stage configuration, a performance checklist was composed. This checklist is given below.

parameter	checkpoint
size	• what are the estimated minimum specimen stage dimensions?
	• does the specimen holder fit into the vacuum chamber?
	• does the specimen holder fit between the pole pieces?
stroke	• what are the maximum specimen holder strokes?
	• do they match the requirements?
	• if not, what measures can be taken to increase the specimen holder strokes?
	• what effect does this have on the specimen holder stability?
displ. resolution	• what are the maximum specimen holder displacement resolutions?
	• do they match the requirements?
intrinsic stability	• what is the expected level of quasi-static and dynamic intrinsic stability in the different degrees of freedom?
	• do they match the requirements?
	• what are the main parameters that limit the quasi-static and dynamic intrinsic stability?
settling time	• what is the expected settling time to reach a certain drift rate level?
	• does it match the requirements?
	• can the settling time be decreased by application of feedback or open-loop control?

direct feedback control	•	is it possible to perform direct measurement of the specimen holder position to the lower pole piece in all the required degrees of freedom?
	•	is it possible to change the specimen stage configuration to achieve this?
	•	does feedback control limit the opportunity to apply other forms or levels of control?
	•	what is the effect on the positioning repeatability and position stability of the specimen holder if its position can only be measured indirectly relative to the pole piece?
	•	if feedback control is applied, does it limit the stroke of the specimen holder in a degree of freedom and is that allowed?
indirect feedback control	•	is it useful or possible to extend the specimen holder stroke by application of a moveable reference frame?
	•	what is the effect of a moveable reference frame on the stability of this reference frame relative to the lower pole piece?
repeatability	•	what is the level of positioning repeatability in the various degrees of freedom?
	•	does it match the requirements?
	•	does the level of positioning repeatability limit the stroke or the quasi-static position stability of the specimen holder?
open-loop control	•	is the application of open-loop position control useful for this configuration?
eucentricity	•	is eucentric tilting required?
	•	does the configuration allow for eucentric tilting of the specimen about one or two axes?
	•	is it possible to establish pseudo-eucentricity?
velocity	•	what is the minimum and what is the maximum obtainable specimen holder velocity?
	•	does it match the requirements?
heat production	•	what is the expected amount of heat production in the specimen stage?
	•	does it affect the specimen holder stability?
	•	what is the influence of external heat transfer to or from the specimen stage?
insertion of specimens	•	is it possible to insert a specimen into the specimen holder from outside the vacuum?
	•	does the specimen insertion method compromise the specimen stage performance?
crosstalk	•	what is the expected level of crosstalk between the various specimen holder degrees of freedom?
	•	is it possible to decrease crosstalk by choosing another specimen stage configuration?
choice of materials	•	what is the influence of the choice of a certain material on the specimen stage performance?
	•	are the materials chosen vacuum compatible?
	•	are the material properties influenced by a high magnetic field or bake out at 150°C?
image	•	what is the expected time needed to obtain a suitable image by means of this specimen stage configuration?
manufacturing problems	•	is there any manufacturing problem to be expected for the specimen stage configuration under consideration?

7.8   Concluding remarks

From the former overview, it should be clear that there are many possible configurations for specimen stages in a TEM. The choice for one of the three specimen stage concepts is determined by the application and by the set of positioning requirements. The choice for a combination of modules and tools is strongly correlated with this choice for a specimen stage concept. By means of two examples of positioning requirements for specimen stages in a TEM, the important tools for (specimen) positioning at the nanometer level were discussed. These examples showed that there are two ways to combine a high specimen holder stability and a large stroke in a degree of freedom. One is to use the intrinsic stability of a nano stage, the other is to use a movable reference frame in combination with closed-loop position control. Despite this closed-loop control, the latter option still depends on the intrinsic stability of the movable frame relative to the pole piece. The intrinsic nano stage stability is also very important in a nano stage with many degrees of freedom, especially when large rotations are involved. In that case, the final specimen holder stability depends, at least in some degrees of freedom, on the intrinsic stage stability in that direction. When four or five degrees of freedom are required, the optimum nano stage configuration has its tilt drives on top of the stack and the drive for motion parallel to the gravity field as high as possible in the stack. The specimen stage configuration chosen can be analyzed by means of the performance checklist given. As a consequence of the result of this performance check, the configuration of the specimen stage can be changed by replacing, adding or omitting tools.

8 Conclusions and recommendations

8.1 Conclusions

This thesis describes theoretical aspects and practical design considerations of tools that can be used to build compact designed stages for positioning at the nanometer and subnanometer level as well as examples of practical nano stages which have been designed, realized and tested with success. As an example of the application of nano stages, a new concept for specimen positioning in a transmission electron microscope has been investigated and successfully tested by means of several experimental setups: *the nano stage concept*. The nano stage concept has proven to be a serious alternative for the traditional side-entry and top-entry specimen stages, especially when many degrees of freedom and large travel ranges of the stage table have to be combined with an extremely high position stability of the stage table. The compact design of the nano stages resulted in a high level of intrinsic stability of the nano stage table.

Piezoelectric actuators and capacitive transducers were essential components during the investigation of the nano stage concept and will be important components for the realization of future nano stages due to their compactness, their subnanometer positioning and measurement resolution, and their design flexibility. As far as nano stages are concerned, the choice for a type of piezo actuator and a type of piezo ceramic will always be a compromise between conflicting interest of (mutual) the piezoelectric, the mechanical, and the thermal properties of the actuator and the ceramic material. In most applications, the piezoelectric shear actuator will be the best type of piezo actuator. The stability of a piezo actuator after a change in voltage depends on and can be explained by the piezoelectric hysteresis curve.

Piezoelectric actuators have proven to be extremely suitable for application in nano stages. However, their maximum deformation is generally not sufficient to cover the required stroke of a nano stage. This problem can be overcome by using piezo drives which allow for translations both perpendicular and parallel to the gravity field as well as for rotations. Four types of piezo drives have been investigated during this work: clamp step motion (CSM) drives, inertial sliding motion (ISM) drives, impact drive motion (IDM) drives and frictional stepping motion (FSM) drives. Except for clamp step motion drives, a major feature of piezo-driven stages is that they do not require many precisely machined parts. All four piezo drives use a repeated motion or stepping cycle which makes their stroke in theory infinite. In practice however, the travel range of the

piezo-driven nano stage table is limited by the dimensions of the capacitive transducers in combination with the available space in the application. Due to the random variation in the size of the repeated motion cycles, a piezo drive and thus a nano stage requires position control to obtain nanometer positioning repeatability. It does however not require sophisticated methods of control to obtain nanometer positioning repeatability over millimeter strokes. The difference between especially the ISM, the IDM, and the FSM drives is so small that the choice for one of these drives strongly depends on the application.

The analytic, electromechanical model that has been developed for piezo drives helped to understand the behavior of these drives and resulted in some design considerations concerning drive optimization for a minimum driving voltage. Experiments proved that the model for ISM drives predicted the performance of such drives well. One of the submodels which described the contact between the table and its supports predicted a major influence of the (tangential) contact stiffness and the so called elastic buffer on the performance of piezo drives. Experiments and calculations together showed that the (tangential) contact stiffness in the direction of motion limits, to a large extent, the resonance frequency of a piezo drive and thus that of the stage table. This indirectly limits this intrinsic stability of the nano stage. The contact stiffness can best be maximized by optimization of the shape of the contact area between table and supports, and by the selection of the contact materials. At the same time, the minimum driving voltage of a piezo drive and the difference in the step size for upward and downward motion in the direction parallel to the gravity field can, to a large extent, be explained by the presence of the elastic buffer. During this research, piezo drives have proven to be reliable and robust in air as well as in vacuum.

Capacitive transducers were successfully applied for position measurement at the nanometer level and for monitoring the quasi-static position stability of the nano stage table at the picometer level. Unfortunately, capacitive transducers can not be applied for active vibration isolation since their bandwidth for large dynamic ranges is limited. Therefore, the dynamic stability of the nano stage will be completely dependent on passive isolation methods. The resolution of practical capacitive displacement transducers is limited by the flatness of the capacitor plates and the accuracy of the plate alignment and is generally in the order of a few picometer. Two types of capacitive displacement transducers can be distinguished: plate-distance transducers and in-plane transducers. In a nano stage, capacitive plate-distance transducers can best be applied for the measurement of translations and small parasitic rotations or tilts. For large rotations or tilts capacitive in-plane transducers should be applied. Capacitive transducers do not require large guarding electrodes for positioning with nanometer repeatability.

Alternating current bridges were successfully applied to measure very small changes in the transducer capacitance. The alternating current bridge in combination with the mechanical configuration of the capacitive transducers applied in this research have proven to be stable enough to perform reliable stability measurements at the picometer level if zero-point measurements were performed.

The nano stage stability is disturbed by various quasi-static and dynamic error sources. The influence of internal and external dynamic error sources (vibrations) on the nano stage stability can be minimized by passive means only. This requires a high quality vibration isolation system and a high first resonance frequency of the nano stage table relative to the lower pole piece. One of the major quasi-static error sources are heat production in the nano stage and heat transfer to the

nano stage. Heat production in the nano stage is induced by the piezo actuators during specimen positioning and by the electron beam. Experiments have shown that the stability of the image in a transmission electron microscope not only depends on the stability of the nano stage table relative to the lower pole piece of the objective lens, but also on the intrinsic specimen stability, which is strongly influenced by the heat production in the specimen by the electron beam. Other quasi-static error sources are creep and drift. The quasi-static stability of a nano stage can either be based on its intrinsic stability, on open-loop compensation or on feedback control. The latter method is limited by the uncertainty about the stability of the elements between the illuminated spot on the specimen and the mechanical parts of which the position is actually measured. This makes the use of position control of many configurations at the picometer level questionable. Open-loop compensation methods have proven to be successful in minimizing the effect of piezo drift. The intrinsic stability of compact nano stages can be down to the picometer level.

A theory was developed on the effect of the size of the contact points between the nano stage table and its supports and their influence on the nano stage table stability. This theory was successfully supported by experiments which showed that a support with a small ratio of the real and the apparent contact area is more stable than a support with a large ratio of the real and the apparent contact area. Another important parameter leading to a high intrinsic stability of the table is a low preload force on the support and thus a low table mass.

The configuration of a nano stage strongly depends on the set of positioning requirements made up for a particular application. One of the most important aspects of a nano stage configuration is the stacking order of the (piezo) drives when many degrees of freedom are required in an application. Especially specimen tilting influences the stacking order and the performance of a nano stage. When specimen tilting is required, the specimen holder stability always depends on the stability of a part of the nano stage. The only way to combine nanometer positioning repeatability and subnanometer positioning stability over large strokes is to rely on the intrinsic stability of the nano stage or to use a moveable reference frame and to rely on its intrinsic stability relative to its base. In case of positioning in many degrees of freedom, the (piezo) drive for motion parallel to the gravity field should be placed as high as possible in the stack. The tilt drives should be placed on top.

8.2 Recommendations

Given the limited space between the pole pieces, a problem of the nano stage concept is the insertion of specimens. This should be given thorough attention when a practical TEM nano stage is designed. Solutions to this problem may be to use specimen transfer systems comparable to the systems used in top-entry and side-entry goniometer stages.

The application of the nano stage concept can be extended considerably if the concept can be made suitable to perform *in situ* heating and cooling experiments, while maintaining a high stability of the stage table. In this respect as well, the compact design of the nano stage concept is a major advantage over traditional goniometer stage concepts.

In order to minimize creep, in order to minimize the elastic buffer, and in order to maximize the contact stiffness in the contact area between the nano stage table and its supports, the influence of bulk material and coatings should be subject of another research.

In order to prove the nano stage table stability through the image stability in the transmission electron microscope, a special designed specimen with a low thermal sensitivity should be used. One of the options for such a specimen may be to use thin, pre-stressed wires. It is also important to use a nano stage which allows specimen translation in the Z direction. This, to optimize the electron beam alignment and increase the image resolution.

With regard to image drift compensation, it would be advantageous to increase the speed of the cross-correlation calculations between images.

Besides that the results of this work can be directly used to support the design of nanopositioning devices in various high resolution microscopes, they may be applied for the design of low velocity, low force positioning devices with (sub)nanometer positioning resolution for use in other microscopes, in medical applications, in robotics, and in high precision manufacturing machines.

9 References

[1]   S.T. Smith and D.G. Chetwynd, *Foundations of Ultraprecision Mechanism Design*, Developments in Nanotechnology Vol. 2, Gordon and Breach Science Publishers, Switserland 1994, ISBN 2-88449-001-9.

[2]   A. H. Slocum, *Precision Machine Design*, Prentice Hall, New Yersey, USA 1992, ISBN 0-13-690918-3.

[3]   M. Bonis, Y. Alayli, P. Revel, P.A. McKeown, and J. Corbett, *International Progress in Precision Engineering*, Proceedings of the 8th International Precision Engineering Seminar, Compiègne, France 1995, ISBN 0-444-10000-8.

[4]   T. Higuchi, Y. Yamagata, K. Furutani, and K. Kudoh, Proceedings IEEE Micro Electro Mechanical Systems, Napa Valley, USA 1990.

[5]   C. Bai, *Scanning Tunneling Microscopy and its Application*, Springer Verlag, Berlin, Germany 1995, ISBN 3-540-59346-2.

[6]   G. Binnig, H. Rohrer, Ch. Gerber, and E. Weibel, Appl. Phys. Lett. **40** (1982), p. 178.

[7]   D.W. Pohl, Rev.Sci.Instr. **58** (1987), p. 54-57.

[8]   T. Higuchi, Y. Yusof, and M. Watanabe, Proceedings of the IEEE Micro Robots and Teleoperators Workshop, Hyannis, Massachusetts, USA 1987.

[9]   L. de Broglie, Phil. Mag. **47** (1924), p. 446.

[10]   H. Busch, Ann. d. Physik **81** (1926), p. 974.

[11]   M. Knoll and E. Ruska, Ann. d. Physik **12** (1932), p. 607.

[12]   JEOL high resolution TEM, JEOL JEM 1010, 40-100 keV, 0.45 nm resolution, JEOL Ltd.

[13]   A.M. Glauert (ed.), *Practical methods in electron microscopy*, North-Holland publishing company, the Netherlands 1981, ISBN 0-7204-4250-8.

[14]   L. Reimer, *Transmission electron microscopy, physics of image formation and microanalysis*, Springer Verlag, Berlin, Germany 1993, ISBN 3-540-56849-2.

[15]   J.A. Eades, J. of Phys. E: Sci. Instrum. **15** (1982), p. 184-186.

[16]   H.G. Heide, Ultramicroscopy **6** (1980), p.115-124.

[17]   T. Imura, *High Voltage Electron Microscopy*, Proceedings of the 3rd Int. Conf., edited by P.R. Swann, Academic Press London 1974, p.179, ISBN 0-12-678750-6.

[18]   H. Fujita (ed.), *History of Electron Microscopes*, 11th Int. Congr. on Electron Micrscopy, Kyoto 1986.

[19]   T. Mulvey and C.J.R. Sheppard (eds.), *Advances in optical and electron microscopy (Vol 11)*, Academic Press London, UK 1989.

[20]   K. Heinemann and H. Poppa, J. Vac. Sci. Technol. **A4** (1986), p. 127-136.

[21]   P.E.S.J. Asselbergs *et al*, Electron Optics Bulletin **133** (1994), p. 1-12.

[22] E.D. Boyes, Inst. Phys. Conf. Ser. **119** (1991), p. 539-542.

[23] P.E.S.J. Asselbergs, Philips Electron Optics, internal communication.

[24] W.G. Cady, *Piezoelectricity, an introduction to the theory and applications of electrome-chanical phenomena in crystals*, McGraw-Hill, New York, USA 1946.

[25] B. Jaffe, W.R. Cook, and H. Jaffe, *Piezoelectric Ceramics*, Academic Press, London and New York, UK 1971, ISBN 0-12-379550-8.

[26] Physik Instrumente Catalogue, Products for Micropositioning, Physik Instrumente GmbH & Co. Waldbronn, Germany.

[27] Philips Components, Piezoelectric Ceramics, Eindhoven, the Netherlands 1989.

[28] R.W. Basedow and T.D. Cocks, J. Phys. E:Sci. Instrum. **13** (1980), p. 840-844.

[29] A.E. Holman, *A novel scanning tunneling microscope with inherent scan linearization*, Ph.D. thesis, Delft University of Technology, Delft, the Netherlands 1996, ISBN 90-75698-04-6.

[30] S.M. Hues *et al.*, Rev.Sci.Instrum. **65** (1994), p. 1561-1565.

[31] L.E.C. van de Leemput *et al.*, Rev.Sci.Instrum. **62** (1991), p. 989.

[32] CICE S.A., Piezoceramics, Montreuil, France 1991.

[33] Vernitron Piezoelectric Division, Bedford, Ohio USA.

[34] EBL Company, East Hartford, Conneticut USA.

[35] D.G. Chetwynd, Prec. Eng. **9** (1987), p. 3-6.

[36] D.G. Chetwynd, Prec. Eng. **11** (1987), p. 203-209.

[37] J.W.G. Wildoër, *Low temperature scanning tunneling microscopy on mesoscopic systems*, Ph.D. thesis, Katholieke Universiteit Nijmegen, Nijmegen, the Netherlands 1996, ISBN 90-9009573-x.

[38] D.E. Grupp and A.M. Goldman, Science **276** (1997), p. 392-394.

[39] J. van Randeraat and R.E. Setterington, *Piezoelectric Ceramics*, Mullard Limited, London, UK 1974, ISBN 0-901232-75-0.

[40] G. Borchardt, E. Wehrsdorfer, and P.Pertsch, Proc. 4th Intern. Conf. on New Actuators, AXON Techn. Consult GmbH, Bremen, Germany 1994.

[41] G. Binnig and D.P.E. Smith, Rev. Sci. Instrum. **57** (1987), p. 1688.

[42] C.J. Chen, Appl. Phys. Lett. **60** (1992), p. 132.

[43] Burleigh Inchworm, Burleigh Instruments, Inc., Fisher, New York.

[44] T. Higuchi, Y. Yusof, and M. Watanabe, Proceedings of the IEEE Micro Robots and Teleoperators Workshop, Hyannis, Massachusetts, USA 1987.

[45] S. Behler, *Rastertunnelmikroskopie an Supraleitern und Fulleren bei tiefen Temperaturen*, Ph.D. thesis, University of Basel, Basel, Switserland 1994 (in German).

[46] H.J. Mamin, D.W. Abraham, E. Ganz, and J. Clarke, Rev.Sci.Instr. **56** (1985), p. 2168-2170.

[47] G. Binnig and C. Gerber, IBM Technical Disclosure Bulletin **23** (1980), p. 3369-3370.

[48] T. Tojo and K.Sugihara, Bull. Japanese Soc. of Prec. Eng. **19** (1985), p. 135-137.

[49] D.J. Peters and B.L. Blackford, Rev.Sci.Instr. **60** (1989), p. 138-140.

[50] K. Ikuta, S. Aritomi, and T. Kabashima, IEEE MEMS'92.

[51] N. Shimizu *et al.*, J. Vac. Sci. Techn. **A8** (1990), p. 333-335.

[52] T. Hatsuzawa *et al.*, Rev.Sci.Instr. **57** (1986), p. 3110-3113.

[53] M.P. Koster and A. Visscher, Mikroniek **6** (1993), p. 183-186 (in Dutch).

[54] Ch. Renner *et al.*, Rev.Sci.Instr. **61** (1990), p. 965-967.

[55] B.L. Blackford and M.H. Jericho, Rev. Sci. Instrum. **61** (1990), p. 182-184.

[56] J.W. Lyding *et al.*, Rev. Sci. Instrum. **59** (1988), p. 1897-1902.

[57] Ph. Niedermann, R. Emch and P. Descouts, Rev.Sci.Instr. **59** (1988), p. 368-369.

[58] K.H. Besocke, Surf. Sci. **181** (1987), p. 145-153.

[59] L. Howald, H. Rudin and H.-J. Güntherodt, Rev. Sci. Instrum. **63** (1992), p. 3909-3912.

[60] B.L. Blackford, Rev. Sci. Instrum. **64** (1993), p. 1360-1361.

[61] I.B. Altfeder and A.P. Volodin, Rev. Sci. Instrum. **64** (1993), p. 3157.

[62] P. Ge and M. Jouaneh, Proc. of the 11th annual meeting of the ASPE, Monterey, California, USA 1996, p. 396.

[63] B. Armstrong-Hélouvry, P. Dupont, and C.C. de Wit, Automatica **30** (1994), p. 1083-1138.

[64] D. Karnopp, ASME J. of Dyn. Syst., Meas. and Control **107** (1985), p. 100-103.

[65] P. Meijers, *Dynamica van machines*, Department of Mechanical Engineering, Delft University of Technology, Delft, the Netherlands 1994 (in Dutch).

[66] K.L. Johnson, *Contact mechanics*, Cambridge University Press, Cambridge, UK 1985, ISBN 0-521-25576-7.

[67] Algor, Algor Inc., Pittsburgh, USA.

[68] J.C. van der Schaft, *De tangentiële contactstijfheid van wrijvingswielen*, Eindhoven University of Technology, Eindhoven, the Netherlands 1989 (in Dutch).

[69] D. Landheer and A.W.J. de Gee, *Tribotechniek*, Delft University of Technology, Delft, the Netherlands 1989 (in Dutch).

[70] J.W.G. Wildoër *et al.*, Rev. Sci. Instrum. **65** (1994), p. 2849.

[71] B.L. Blackford, M.H. Jerico, and M.G. Boudreau, Rev. Sci. Instrum. **63** (1992), p. 2206.

[72] T. Higuchi, Y. Yamagata, K. Kudoh, and K. Iwasaki, Robotics Research; The Fifth International Symposium, MIT Press, Cambridge, Massachusetts, USA 1990.

[73] private communication.

[74] K.E. Drexler, *Nanosystems,molecular machining, manufacturing and computation*, John Wiley and sons Inc., New York, USA 1992, ISBN 0-471-57518-6.

[75] J.S. Faber, *Instrumentation for parallel-parallel coincidence electron spectroscopy*, Ph.D. thesis, Delft University of Technology, Delft, the Netherlands 1996, ISBN 90-9009862-3.

[76] P.W.H. de Jager, *Design of the "Fancier", an instrument for Fabrication and Analysis of Nanostructures Combining Ion and Electron Regulation*, Ph.D. thesis, Delft University of Technology, Delft, the Netherlands 1997, ISBN 90-407-1478-9.

[77] J.C. Maxwell, *A treatise on electricity and magnetism*, Clarendon, Oxford, UK 1873.

[78] R.V. Jones and J.C.S. Richards, J. Phys. E: Sci. Instrum. **6** (1973), p. 589-600.

[79] W.Chr. Heerens, J. Phys. E: Sci. Instrum. **19** (1986), p. 897-906.

[80] M.H.W. Bonse, *Capacitive Position Transducers; Theoretical Aspects and Practical Applications*, Ph.D. thesis, Delft University of Technology, Delft, the Netherlands 1995.

[81] X. Zhao, *Hochauflösende dreidimensionale Positionierungsbestimmung bei Rastersondenmikroskopen mittels kapazitiver Aufnehmer*, Ph. D thesis, Technische Universität Braunschweig, Braunschweig, Germany 1995, ISBN 3-89429-663-1.

[82] J.E. Griffith and D.A. Grigg, J.Appl.Phys. **74** (1993), p. R83-R109.

[83] Ansoft Corporation, Fout State Square, Suite 600, Pittsburgh (USA). Maxwell Software: User's Reference Guide, 1.0 edition, 1994.

[84] W.Chr. Heerens, Proceedings of the International Seminar on Quantitative Microscopy, PTB-Bericht **F-21** (1995), p. 46-50, ISBN 3-89429-921-5.

[85] F. Zhu, *Development of Capacitive Position Transducers through a Mechatronic Approach*, Ph.D. thesis, Delft University of Technology, Delft, the Netherlands 1992, ISBN 90-9005114-7.

[86] G. de Jong, *Smart Capacitive Sensors; physical, geometrical and electronical aspects*, Ph.D. thesis, Delft University of Technology, Delft, the Netherlands 1994.

[87] S. Huang, R.G. Green, A Plaskowski, and M.S. Beck, IEEE Transactions on Instrumentation and Measurement **37** (1988), p. 368-373.

[88] I.J. Walker and A.D. Stroobant, Jaeu **4** (1972), p. 32-37.

[89] B. Hague and T.R. Foord. *Alternating Current Bridge Methods*, Pitman Publishing, London, UK 1971.

[90] Ingenieursbureau Senstech, Oegstgeest, the Netherlands.

[91] General Radio Company.

[92] Hewlett-Packard, *Dielectric materials measurement forum, measurement fundamentals*, Hewlett-Packard, 1993.

[93] K.D. Froome and L. Essen, *The Velocity of Light and Radio Waves*, Academic Press, London, UK 1969.

[94] A.M. Glauert (ed.), Practical methods in electron microscopy, North-Holland publishing company, the Netherlands 1981, ISBN 0-7204-4250-8.

[95] P.E.S.J. Asselbergs, Philips Electron Optics, internal communication.

[96] W.C. Bigelow, *Vacuum methods in Electron Microscopy*, Practical Methods in Electron Microscopy Vol. **15**, Portland Press, London, UK 1994, ISBN 1-85578-052-6.

[97] H. van der Wulp, H.F. van Beek, and B.M. Mertens: *A Piezo-driven TEM-stage with sub-nanometer position stability*, Proceedings American Society for Precision Engineering, Annual meeting, ASPE, Raleigh (NC), USA 1996, p. 26-31.

[98] I.M. Watt, *The principles and practice of electron microscopy*, Cambridge University Press, Cambridge, UK 1997, ISBN 0-521-43456-4.

[99] K. Bethe, Sensors and Actuators **A21-A23** (1990), p. 844-849.

[100] R.W. Evans and B. Wilshire, *Introduction to creep*, Institute of Materials, London, UK 1993, ISBN 0-901462-64-0.

[101] Zerodur is a trademark of Schott Glaswerke, Mainz, Germany.

[102] Dengel, J. of Mater. Technol. **4** (1973), p. 386.

[103] H. van der Wulp *et al.*, Rev. Sci. Instrum. **66** (1995), p. 5339.

[104] H. van der Wulp and R. van Dalen, Proc. 8th Intern. Prec. Eng. Seminar, Compiègne, France 1995, p. 179-182.

[105] H. van der Wulp, M. Hoogteijling and P.V. Pistecky, Conference Proceedings 5th International Conference on new Actuators, AXON Technology Consult GmbH, Bremen, Germany 1996, p.196-199.

[106] H. van der Wulp, H.F. van Beek, and B.M. Mertens: *A Piezo-driven TEM-stage with sub-nanometer position stability*, Proceedings American Society for Precision Engineering, Annual meeting, ASPE, Raleigh (NC), USA 1996, p. 26-31.

[107] The titanium carbo nitride layer was deposited by Gimex technische keramiek b.v., Geldermalsen, the Netherlands.

[108] The Model 75A Arbitrary Waveform Generator from Wavetek San Diego was used.

[109] A home made high voltage amplifier was used, designed by the Centrale Elektronische Dienst of the Delft University of Technology.

[110] VisSim, Visual Solutions Inc., Westford, USA.

[111] R. van Dalen, *Positioneertafel met millimeter slag en nanometer reproduceerbaarheid*, Lab. for Micro Eng., Delft University of Technology, Delft, the Netherlands 1995 (in Dutch).

[112] B.C.T. van Bree, *Piëzo-aandrijving met nanometer reproduceerbaarheid voor verticale bewegingen*, Lab. for Micro Eng., Delft University of Technology, Delft, the Netherlands 1997 (in Dutch).

[113] Grace n.v., Westerlo, Belgium.

[114] W.J. de Ruiter, Ph.D. thesis, chapter 6, Delft University Press, Delft, the Netherlands 1992.

[115] S. Radelaar, *Nanofabrication by maskless techniques: towards new realms in mesoscopic physics*, Proposal International Apparatuur Schema, 1994.

[116] E.H. Zaaijer, *Nanosensoren*, Lab. for Micro Eng., Delft University of Technology, Delft, the Netherlands 1996 (in Dutch).

Summary

The aim of the work described in this thesis was to improve knowledge on the design and realization of nanopositioning stages being applicable in several fields of application, like scientific instruments and commercial equipment. Important applications of piezo-driven nano stages are found in high resolution microscopes, like scanning probe microscopes and electron microscopes. Improved resolution, higher stability and more compact design are properties that one would like to see in future nano stages.

This thesis describes theoretical aspects and practical design considerations of tools that can be used to build piezo-driven stages for positioning at the nanometer level as they have been developed throughout this work, starting from the state of the art knowledge from literature and private communications.

Chapter 1 gives a short introduction to nanopositioning and describes the aim of this work in more detail. Throughout this work, a transmission electron microscope (TEM) is used as an example of the application of nano stages. The working of the TEM as well as the new nano stage concept for specimen positioning are described. The use of the nano stage concept is an alternative for the use of the conventional top-entry and side-entry goniometer stages. The most characteristic property of the nano stage concept is a high level of intrinsic stability of the nano stage table. It is supported by a compact stage design and by the fact that the nano stage can be placed inside the small vacuum chamber of the TEM where it can be mounted directly on the lower pole piece. At the end of chapter 1, the choice for the use of piezoelectric actuators and capacitive transducers is explained and a first order design of a nano stage is given to focus on the design problems.

Chapter 2 treats the characteristic properties of piezoelectric actuators and piezoelectric ceramic materials. The characteristic hysteresis of piezo actuators is described from a different viewpoint as is common in literature and a way of compensating piezo drift is introduced. A comparison is made between several piezoelectric ceramic materials and several types of piezoelectric actuators. When choosing a piezoelectric ceramic and a type of piezo actuator, one has to deal with the conflicting interests of their mechanical, piezoelectric and thermal properties like the piezo sensitivity, the amount of hysteresis, the ratio of the modulus of elasticity and the density, the Curie point and the heat production in the piezo actuator.

As far as the application in a nano stage is concerned, piezo actuators have two important disadvantages. The maximum deformation of a single bulk piezo is insufficient to obtain nanopositioning over strokes as large as a few millimeter or a few radian and piezo actuators suffer from

hysteresis which causes piezo drift after any voltage change. The limited maximum deformation of piezo actuators can be overcome by using piezo drives. Piezo drift can be compensated for in various ways.

Chapter 3 describes theoretical aspects and practical design considerations of piezo drives that are important with regard to the application in nano stages. Four different drive mechanisms are distinguished: clamp step motion (CSM), inertial sliding motion (ISM), impact drive motion (IDM), and frictional stepping motion (FSM). An overview is given of piezo-driven stages using these drive mechanisms for both translation and rotation. They are mutually compared, taking into account their resolution, step size, intrinsic stability, resonance frequency, and occupied space. The differences between the four drive mechanisms are small and therefore the choice for the best suitable principle should be based on the application. An electromechanical model for inertial sliding motion and impact drive motion has been developed as well as models for piezo hysteresis, for friction and for the properties of the contact area between the table and its supports. These models help to understand the working of piezo drives and can be a support in the design process of practical nano stages. An important disadvantage of all piezo drives is that they require position control to obtain nanometer positioning repeatability of the table.

Chapter 4 discusses capacitive displacement transducers. They are used throughout this work to perform position measurements in order to control and verify the position or the stability of the nano stage table. Two different types of capacitive displacement transducers are distinguished: plate-distance transducers and in-plane transducers. They are compared with regard to application in a TEM nano stage. From this comparison, it was concluded that plate-distance transducers are the best solution for measurement of translations and small (parasitic) rotations. In-plane transducers must be used to measure large translations and rotations. Part of the comparison was the investigation of the influence of guard electrodes on the transducer performance. Some analytic and numerical calculations proved that guard electrodes are not required to obtain a high level of positioning repeatability, but have to be used to decrease crosstalk between transducers.

As a next step, the alternating current bridge (ac-bridge) in combination with synchronous detection is considered. The ac-bridge is the electronic measurement system used to measure the capacitance of the capacitive transducers. The stability of this measurement system is high enough to perform stability measurements at the picometer level, if zero-point measurements are performed. However, the bandwidth of the synchronous detector for high resolution measurements, which is in the order of a few hertz, is not sufficient to accurately measure table vibrations with subnanometer amplitudes. Therefore, the dynamic stability of a nano stage can not be improved by means of closed-loop control. The stability of practical transducers was investigated by means of experiments.

Chapter 5 considers the position stability of the nano stage table in both a theoretical and a practical way. This stability is disturbed by various quasi-static and dynamic error sources. The most important error sources are vibrations, heat production in and heat transfer to the nano stage and the specimen, creep in the contact area between table and supports, and piezo drift. Since the dynamic stability of the nano stage table can only be made high by passive means, the resonance frequency of the nano stage should be as high as possible. It was proven during this work by a combination of experiments that the quasi-static stability can be increased by application of

either closed-loop or open-loop control methods, or by using the high intrinsic stability of the nano stage.

Special attention is paid to the influence of the supports and the piezo drift on the quasi-static stability of the stage table. A new theory is presented on the behavior of the contact area between the table and its supports. Experiments supported this theory and showed that the stability of the contact area depends on the support configuration, on the layer of adsorbed water molecules, on the materials applied, and on the magnitude of the preload forces. In case of a support with a large apparent contact area, the table drift rate after positioning the table is much higher than for a support configuration with a small apparent contact area. This is, among other things, due to the layer of adsorbed water molecules on the contact surfaces. The stability of the supports with a small apparent contact area is assumed to be mainly influenced by friction forces which cause creep. This assumption was supported by the random direction of the table drift that was found and by the settling time dependence on the magnitude of the preload forces.

Piezo drift can be minimized by using open-loop and closed-loop position control. For small differences in the driving voltages, it was shown that piezo drift can be neglected. Experiments have shown that the two open-loop control methods that were tested can result in a drift rate decrease of a factor of five up to a factor of 20.

In chapter 6, the nano stage concept is investigated by means of four test setups: an XY stage, a Z stage, a piezo rotor and a TEM stage. It was proven that:

- piezo actuators and capacitive transducers suit application in nano stages very well,
- piezo drives perform reliable in air as well as in vacuum,
- 5 nm positioning repeatability can be obtained over a 1 mm travel range,
- the ISM model predicts the performance of ISM drives for motion perpendicular to the gravity field well,
- the vibration amplitude of a typical nano stage can be as small as 40 pm,
- the minimum drift rates of a typical nano stage table can be smaller than 50 pm/min,
- settling times to reach a drift rate of less than 0.1 nm/min without applying closed-loop control can be smaller than 30 seconds for low driving voltages and a low preload force,
- open-loop compensation methods can be applied with success on practical nano stages to compensate piezo drift,
- the resonance frequency of a nano stage strongly depends on the tangential contact stiffness in the direction of motion and is typically in the order of 1 up to 3 kHz,
- the elastic buffer determines the minimum driving voltage of piezo drives for motion parallel to the gravity field,
- minimum driving voltages for motion perpendicular to the gravity field are in the order of a few volt, while minimum driving voltages for upward motion parallel to the gravity field are about one order of magnitude higher,
- during the design process of the piezo drive and during actual positioning, one has to deal with the opposite interests between velocity and open-loop stability, between minimum driving voltage and tangential contact stiffness, and between a high piezo sensitivity and a high resonance frequency, and
- the image stability in a TEM not just depends on the stability of the specimen stage, but also on the specimen stability if settling times in the order of tens of seconds are required.

As a result of the large amount of different sets of positioning requirements, it is impossible to develop general design rules for the configuration of a specimen stage in a TEM. Therefore, in chapter 7, some assistance is given in choosing the best configuration of a nano stage. An overview of available tools is given that enable and support nanopositioning, together with some examples of 'impossible' configurations and examples of possible configurations for two different applications of a TEM nano stage.

It is shown that:

- the dimensions as well as the stacking order of feedback controlled (piezo) drives have a strong influence on the performance of a certain nano stage configuration,
- especially the requirement of large specimen rotations has a strong influence on the performance and the configuration of a nano stage,
- the minimum dimensions of a nano stage are, to a large extent, determined by the dimensions of the capacitive transducers,
- a combination of a large stroke and position control at the subnanometer level can be obtained by limiting the number of degrees of freedom of the stage table or by using a moveable reference frame,
- in case of many degrees of freedom, the stability of the nano stage table depends on the intrinsic stability of a part of the nano stage in at least some degrees of freedom,
- the most favorable position of a tilt module is on top of a stack of feedback controlled (piezo) drives,
- the drive that performs motion parallel to the gravity field should be placed as high as possible in the stack, and
- pseudo-eucentric tilt should be obtained by means of advanced computer control of the specimen position.

In chapter 8, general conclusions are drawn and several recommendations are given for further research.

Samenvatting

Het doel van het in dit proefschrift beschreven onderzoek was het uitbreiden van de kennis met betrekking tot het ontwerpen en realiseren van objecttafels waarmee kan worden gepositioneerd in het nanometergebied (nanopositioning). Dit soort objecttafels (nano stages) zijn zowel toepasbaar in wetenschappelijke als in commerciële instrumenten. Belangrijke toepassingen van nano stages zijn preparaathouders in hoge resolutie microscopen zoals scanning probe microscopen en electronenmicroscopen. Wenselijke eigenschappen van toekomstige (piezo aangedreven) preparaathouders ten opzicht van de huidige preparaathouders zijn een hogere positieresolutie, een hogere positiestabiliteit en een compacter ontwerp.

Dit proefschrift geeft een beschrijving van theoretische aspecten en praktische ontwerpen van gereedschappen die kunnen worden gebruikt voor de bouw van piezo aangedreven objecttafels voor het positioneren in het nanometergebied. Uitgangspunten van dit onderzoek vormden de state of the art op dit gebied zoals beschreven in de literatuur en enkele persoonlijke gesprekken.

Hoofdstuk 1 gaat in het kort in op het begrip nanopositioning en geeft een gedetailleerde beschrijving van het doel van het onderzoek. Het geeft een voorbeeld van een instrument waarin nano stages kunnen worden toegepast: een transmissie electronen microscoop (TEM). Dit instrument is gedurende het gehele onderzoek als voorbeeld gebruikt. De werking van de TEM en het nieuwe nano stage concept voor preparaatpositionering worden in hoofdstuk 1 beschreven.

Het gebruik van het nano stage concept in een TEM is een alternatief voor het gebruik van de conventionele top-entry en side-entry goniometer stages. De meest karakteristieke eigenschap van het nano stage concept is het hoge intrinsieke stabiliteitsniveau van de nano stage tafel. Deze wordt ondersteund door het compacte ontwerp van de nano stage en door het feit dat de nano stage geheel in de kleine vacuumkamer van de TEM kan worden geplaatst waar de stage direct gemonteerd kan worden op de onderste poolschoen. Aan het eind van hoofdstuk 1 wordt de keuze voor het gebruik van piezo actuatoren en capacitieve sensoren uitgelegd. Daarnaast wordt een eerste ontwerp van een nano stage geschetst om een idee te geven van de ontwerpproblemen.

Hoofdstuk 2 behandelt de karakteristieke eigenschappen van piezoelektrische actuatoren en van piezoelektrische keramische materialen. De voor piezo actuatoren karakteristieke hysteresis is beschreven vanuit een enigszins ander oogpunt dan gebruikelijk. Daarnaast wordt een manier geïntroduceerd om piezo drift te compenseren. Er is een vergelijking gemaakt tussen verschillende piezoelektrische keramische materialen en verschillende typen piezoelektrische actuatoren. Uit deze vergelijking kwam naar voren dat bij de keuze van een piezoelektrisch keramisch materiaal en een piezo actuator rekening moet worden gehouden met de tegenstrijdige belangen wat

betreft de gevoeligheid van een piezo, de grootte van de hysteresis, de verhouding van de elasticitietsmodulus en de dichtheid van het keramiek, het Curie punt en de warmteproduktie in de piezo actuator.

Piezo actuatoren hebben twee nadelen als het gaat om toepassing in nano stages. De maximum deformatie van een enkele piezo is onvoldoende om te kunnen positioneren over een bereik van enkele millimeters of enkele radialen en de hysteresis van de piezo actuatoren veroorzaakt drift na iedere verandering in de aangebrachte spanning over de piezo. De beperkte maximale deformatie van piezo actuatoren kan worden opgevangen door gebruik te maken van zogenaamde piezo aandrijvingen. Piezo drift kan op verschillende manieren worden gecompenseerd.

Hoofdstuk 3 beschrijft theoretische aspecten en praktische overwegingen die van belang zijn voor het ontwerpen van piezo aandrijvingen voor toepassing in nano stages. Er is onderscheid gemaakt tussen vier verschillende aandrijfmechanismen: clamp step motion (CSM), inertial sliding motion (ISM), impact drive motion (IDM) en frictional stepping motion (FSM). Verder is een overzicht gegeven van piezo aangedreven stages die deze mechanismen gebruiken voor zowel rotaties als translaties. De onderlinge resolutie, stapgrootte, intrinsieke stabiliteit, resonantie frequentie en gebruikt volume van deze mechanismen zijn vergeleken. Omdat de verschillen tussen de vier mechanismen klein blijken te zijn, hangt de keuze voor het best toepasbare mechanisme af van de toepassing. Ook is een elektromechanisch model ontwikkeld om inertial sliding motion en impact drive motion te beschrijven, evenals modellen die een beschrijving geven van piezo hysteresis, van wrijving en van de eigenschappen van het contactvlak tussen de tafel en zijn oplegpunten. Deze modellen helpen de werking van piezo aandrijvingen beter te begrijpen en kunnen het ontwerpproces van nano stages ondersteunen. Een belangrijk nadeel van piezo aandrijvingen is de noodzaak van positieterugkoppeling voor het verkrijgen van positiereproduceerbaarheid in het nanometergebied.

Hoofdstuk 4 beschrijft capacitieve verplaatsingsopnemers. Deze zijn gedurende dit onderzoek gebruikt voor het meten van de positie en voor het regelen en verifiëren van de stabiliteit van nano stage tafels. Er is onderscheid gemaakt tussen twee verschillende capacitieve verplaatsingsopnemers: plaat-afstand opnemers en in-het-vlak opnemers. Zij zijn vergeleken aan de hand van toepassing in een TEM nano stage. De vergelijking toonde aan dat plaat-afstand opnemers de beste oplossing vormen voor het meten van translaties en kleine (parasitaire) rotaties. Voor het meten van grote translaties en rotaties moeten in-het-vlak opnemers worden gebruikt. Een deel van de vergelijking bestond uit het bestuderen van de invloed van guard elektroden op de prestaties van de opnemers. Met behulp van enkele analytische en numerieke berekeningen is aangetoond dat guard elektroden niet nodig zijn voor het realiseren van een hoge positiereproduceerbaarheid, maar wel voor het verlagen van overspraak tussen opnemers.

Vervolgens is de combinatie van een wisselstroombrug en een synchrone detector bekeken. De wisselstroombrug is het electronische meetsysteem dat is gebruikt voor het meten van de capaciteit van de capacitieve opnemers. De stabiliteit van dit meetsysteem is zodanig dat stabiliteitsmetingen in het picometergebied verricht kunnen worden, mits dit nulpuntsmetingen zijn. De bandbreedte van de synchrone detector bij picometer resolutie is enkele hertz. Dit is onvoldoende om de trillingen van de tafel van de nano stage, die amplitudes hebben in het subnanometergebied, nauwkeurig te kunnen bepalen. Daarom kan de dynamische stabiliteit van een

nano stage niet worden verbeterd met behulp van closed-loop regelingen. De stabiliteit van prak-
tische capacitive opnemers is onderzocht aan de hand van experimenten.

In hoofdstuk 5 is de positiestabiliteit van de nano stage tafel op theoretische en praktische wijze
bekeken. De positiestabiliteit wordt door verschillende quasi-statische en dynamische stoorbron-
nen verstoord. De belangrijkste stoorbronnen zijn trillingen, warmteproduktie in en warmtetrans-
port naar de nano stage en het preparaat, kruip in de contactpunten tussen de tafel en de opleg-
punten en piezo drift. Omdat de dynamische stabiliteit van de nano stage tafel alleen op passieve
wijze kan worden verhoogd is het van belang dat de resonantiefrequentie van de nano stage zo
hoog mogelijk is. Een combinatie van experimenten heeft bewezen dat de quasi-statische sta-
biliteit van de nano stage tafel kan worden verhoogd door middel van closed-loop of open-loop
regelalgorithmen, of door middel van een hoge intrinsieke stabiliteit van de nano stage.

In hoofdstuk 5 is verder speciale aandacht besteed aan de invloed van de oplegpunten en de piezo
drift op de quasi-statische stabiliteit van de nano stage tafel. Daartoe is een nieuwe theorie gepre-
senteerd met betrekking tot het gedrag van het contactvlak tussen de tafel en de oplegpunten.
Experimenten ondersteunden deze theorie. Ze toonden aan dat de stabiliteit van het contactvlak
afhangt van de configuratie van de oplegpunten, van de laag geadsorbeerde water moleculen, van
de gebruikte materialen en van de grootte van de voorspankrachten. De driftsnelheid van een
tafel met oplegpunten met een groot schijnbaar contactoppervlak was veel groter dan voor opleg-
punten met een klein schijnbaar contactoppervlak. Dit komt onder andere door de laag geadsor-
beerde water moleculen op de contactoppervlakken. De stabiliteit van de oplegpunten met een
klein schijnbaar contactoppervlak wordt verondersteld met name te worden beïnvloed door
wrijvingskrachten die op hun beurt kruip induceren. Deze aanname is gestaafd door de
willekeurige richting van de gevonden tafel drift en door de afhankelijkheid van de inschakeltijd
van de grootte van de voorspankrachten.

Piezo drift kan worden geminimaliseerd door middel van open-loop en closed-loop positierege-
lingen. Hoofdstuk 5 laat zien dat piezo drift kan worden verwaarloosd wanneer de verandering in
de piezo spanning klein is. Experimenten toonden aan dat de twee geteste open-loop compensa-
tiemethoden resulteerden in een verlaging van de driftsnelheid van de tafel met een factor vijf tot
20.

In hoofdstuk 6 is het nano stage concept onderzocht aan de hand van vier testopstellingen: een
XY stage, een Z stage, een piezo rotor en een TEM stage. Experimenten toonden het volgende
aan:

- piezo actuatoren en capacitieve sensoren zijn zeer geschikt voor toepassing in nano stages,
- piezo aandrijvingen zijn betrouwbaar, zowel in lucht als in vacuum,
- 5 nm positie reproduceerbaarheid over een bereik van 1 mm is mogelijk,
- het ISM model voorspelt de werking van ISM aandrijvingen voor bewegingen loodrecht op
  het zwaartekrachtveld goed,
- de trillingsamplitude van een nano stage kan kleiner zijn dan 40 pm,
- de minimale driftsnelheid van een nano stage tafel kan kleiner zijn dan 50 pm/min,
- de inschakeltijden om driftsnelheden kleiner dan 0.1 nm/min te bereiken zonder gebruik te
  maken van closed-loop regelingen kunnen kleiner zijn dan 30 seconden wanneer gebruik
  wordt gemaakt van kleine piezo spanningen en kleine voorspankrachten,

- open-loop compensatie methoden kunnen met succes worden toegepast in nano stages om piezo drift te compenseren,
- de resonantiefrequentie van een nano stage, welke gemiddeld 1 tot 3 kHz is, hangt sterk af van de tangentiële contactstijfheid in de bewegingsrichting,
- de elastische buffer bepaalt de minimale spanning op de piezo aandrijving wanneer de beweging parallel is aan het zwaartekrachtveld,
- de minimaal benodigde spanning over de piezo voor een beweging loodrecht op het zwaartekrachtveld is een paar volt; de minimale spanning over de piezo voor een omhooggaande beweging parallel aan het zwaartekrachtveld is ongeveer één orde groter,
- gedurende het ontwerpproces van een piezo aandrijving moet rekening worden gehouden met de conflicterende belangen van snelheid en open-loop stabiliteit, van het minimum aandrijf voltage en de tangentiële contactstijfheid en van een hoge piezo gevoeligheid en een hoge resonantiefrequentie, en
- wanneer inschakeltijden voor de beeldstabiliteit in een TEM van enkele tientallen seconden noodzakelijk zijn dan is niet alleen de stabiliteit van de preparaathouder van belang, maar ook de interne preparaat stabiliteit.

Door de enorme hoeveelheid verschillende eisenpakketten ten aanzien van positioneren was het niet mogelijk algemene regels op te stellen voor de configuratie van nano stages in een TEM. Daarom geeft hoofdstuk 7 enige ondersteuning bij het kiezen van de beste configuratie van een nano stage. Het geeft een overzicht van de beschikbare instrumenten die het positioneren in het nanometergebied ondersteunen en mogelijk maken. Daarnaast zijn aan de hand van twee verschillende toepassingen van TEM nano stages enkele voorbeelden gegeven van mogelijke en 'onmogelijke' configurations. Belangrijke bevindingen uit hoofdstuk 7 zijn:

- de afmetingen en de stapelvolgorde van closed-loop geregelde (piezo) aandrijvingen hebben grote invloed op de werking van een bepaalde nano stage configuratie,
- met name de noodzaak tot grote rotaties heeft een belangrijke invloed op de prestatie en de configuratie van een nano stage,
- de minimale afmetingen van een nano stage worden in belangrijke mate bepaald door de afmetingen van de capacitieve opnemers,
- een combinatie van lange slag en positieregeling op subnanometer niveau kan alleen worden verkregen door het aantal vrijheidsgraden van de nano stage tafel te reduceren of door gebruik te maken van een beweegbaar referentieframe,
- de stabiliteit van een nano stage met veel vrijheidsgraden hangt af van de intrinsieke stabiliteit van een deel van de nano stage in tenminste een deel van de vrijheidsgraden,
- de beste positie van een tilt module is bovenaan de stapeling van een closed-loop geregelde (piezo) aandrijvingen,
- de aandrijving die zorgt voor de beweging parallel aan het zwaartekrachtveld moet zo hoog mogelijk in de stapeling worden geplaatst, en
- pseudo-eucentrische tilt kan worden gerealiseerd door geavanceerde positieregelingen.

In hoofdstuk 8 zijn algemene conclusies getrokken en zijn verscheidene aanbevelingen gedaan voor verder onderzoek.

Acknowledgements

The work presented in this thesis has had many contributors. Hereby, I would like to thank them all.

Some people deserve special credit:

Adriënne, your contribution can never be overestimated,

my parents for their support through the years, and

Jan and Anny for doing much inevitable work.

I also want to thank:

professor H.F. van Beek and professor P. Kruit for making this research possible, for their coaching, and for their critical remarks during the last stages,

Peter Pistecky for the 'smooth' cooperation, for the technical input and for the to-the-point discussions,

all students that joined the nanopositioning team: Berry de With, Rob van Dalen, Youri Piepers and Marcel Hoogteijling,

Bas Mertens for the time we spent on the TEM setups, and

Erik Zaaijer for the computer support and for carefully proofreading the manuscript.

Curriculum vitae

The author was born in Middelburg, the Netherlands on December 23rd 1968. He received primary school in Middelburg and Zevenbergen. In 1981, he attended secondary school at the Thomas More College in Oudenbosch before he started, in 1987, his studies in mechanical engineering at the Delft University of Technology. After a five years study and a half year practical period at the Philips Centre for Manufacturing Technology (CFT), the author graduated on a NASA research project at the Laboratory for Micro Engineering. Next, he worked for three months to build together the device that was designed during his graduation project. By then, he was given the opportunity to develop his mechatronics skills in a four years research project concerning nanopositioning at the Laboratory for Micro Engineering. At the moment, he is working for the Woodward Governor Company in Hoofddorp, the Netherlands.